MULTIPLEXED SEPARATIONS FOR NEW ADVANCES IN BIOMARKER DISCOVERY AND TISSUE METABOLOMIC STUDIES

MULTIPLEXED SEPARATIONS FOR NEW ADVANCES IN BIOMARKER DISCOVERY AND TISSUE METABOLOMIC STUDIES

By MICHELLE SAOI, B.Sc.

A Thesis Submitted to the School of Graduate Studies in Partial Fulfillment of the Requirements of the Degree

Doctor of Philosophy

June 2019

DOCTOR OF PHILOSOPHY (2019) McMaster University

(Chemistry and Chemical Biology) Hamilton, ON

TITLE: Multiplexed Separations for New Advances in Biomarker Discovery and Tissue Metabolomic Studies

AUTHOR: Michelle Saoi, B.Sc. (McMaster University)

SUPERVISOR: Professor Philip Britz-McKibbin

PAGES: xxii, 234

Abstract

Metabolomics offers a systemic approach to discover clinical biomarkers for early detection of chronic diseases while also revealing underlying mechanisms relevant to human disorders of complex aetiology. Metabolomic studies in support of chronic disease prevention have focused primarily on surrogate biofluids (*e.g.,* serum, plasma) for analysis due to their routine and less invasive sample collection in a clinical setting. However, biofluids are non-organ specific and thus are reflective of confounding biochemical processes within the body that are often difficult to interpret. As a result, it is necessary to assess metabolite changes localized within tissues since they are the direct site of pathogenic processes, in order to obtain more robust and specific biomarkers. This thesis aims to contribute to new advances in biomarker discovery and tissue metabolomic studies using multiplexed separations together with innovative data workflows based on multisegment injection-capillary electrophoresis-mass spectrometry (MSI-CE-MS). *Chapter II* introduces a high throughput yet targeted screening method for accurate quantification of serum γ-glutamyl dipeptides from a cohort of overweight Japanese non-alcoholic steatohepatitis (NASH) patients that may allow for better risk assessment of long-term survivorship complementary to histopathology. *Chapter III* introduces a non-targeted metabolite profiling strategy for fasting plasma samples from prediabetic, older adults undergoing short-term step reduction (<1000 steps/day) in order to identify adaptive metabolic responses to abrupt changes in physical inactivity for early detection of sarcopenia in high-risk older persons. *Chapter IV* describes the first metabolomics study to characterize the human skeletal muscle metabolome from mass-restricted tissue biopsies together with matching plasma samples, which identified novel metabolic signatures associated with strenuous interval exercise, as well as treatment effects from high-dose bicarbonate pretreatment that delays the onset of muscle fatigue. Lastly, in *Chapter V*, metabolite coverage was expanded to include fatty acids for comprehensive characterization of murine placental tissue metabolome, which

revealed sex-specific metabolic adaptations during gestation from maternal dams fed a standardized diet. In summary, this thesis contributes to new innovations in metabolomics for the discovery of novel biomarkers from blood and/or tissue specimens as required for early detection of chronic diseases relevant to population health, which were also used to validate the efficacy of therapeutic interventions based on physical activity to support healthy ageing.

Acknowledgements

Firstly, I would like to thank my supervisor, Dr. Philip Britz-McKibbin, for his continuous support and encouragement during my undergraduate and graduate studies. Through joining his research group, I have had many opportunities to expand my knowledge beyond analytical chemistry that have equipped me with a wide array of tools in my arsenal to be a well-rounded scientist. I am extremely grateful for his guidance, time and critical feedback during my studies, while also allowing me to develop new ideas in my research. Most importantly, I am appreciative for his enthusiasm and optimism whenever I felt discouraged. He would always reassure me that things would work out (even if it wasn't how I had initially planned).

I would also like to thank my committee members, Dr. Giuseppe Melacini, Dr. Martin Gibala and Dr. Deb Sloboda for their expertise, constructive feedback and valuable suggestions during committee meetings that forced me to think outside the box during my graduate studies. Furthermore, I would also like to thank all the collaborators involved in the studies described in this thesis – your time, advice and ideas were instrumental to this research.

I would like to thank past members of the Britz lab, Adriana Nori de Macedo, Alicia DiBattista, Karen Lam and Mai Yamamoto, for their mentorship, advice and guidance, especially during thesis writing. I would also like to thank my labmates, Meera Shanmuganathan, Nadine Wellington, Stellena Mathiaparanam, Ritchie Ly, Sandi Azab, Biban Gill, Erick Helmeczi, Jordan Holzschuher, Alice Li, Harry Lu, Zach Kroezen, and Sabrina Macklai. It has been a privilege to have had many supportive, charismatic and hardworking labmates that have made my Ph.D. enjoyable. I am extremely fortunate to have you all in my life and will dearly miss you all.

To my closest and dearest friends, Jen, Joy and Shalini, thank you for always supporting me and cheering me up whenever I was faced with obstacles or self-doubt throughout this journey. I could always count on anyone of you whenever I needed a shoulder to cry on or simply a break from the lab, data processing or writing.

I would like to express my deepest gratitude to my parents and my brother for their endless love, guidance and comfort during this journey. Mom, thank you for being a strong, female role model throughout my life and for continuously encouraging me to do the best I can. Dad, thank you for teaching me the importance of hard work and perseverance in life. Without the many sacrifices both of you have made, I would not have had the opportunity to purse my Ph.D. Finally, I would like to thank my partner, Ray, for the constant love, support and encouragement to overcome the numerous challenges I faced in this journey. You continue to be my number one supporter and for that, I am truly thankful to have you by my side each and everyday.

Table of Contents

List of Figures

Supporting Figures

List of Tables

Supporting Tables

List of Abbreviations and Symbols

[M + H]-	Deprotonated molecular ion
$[M + H]^+$	Protonated molecular ion
$[M + Na]^+$	Sodiated molecular ion
ALT	Alanine aminotransferase
ANCOVA	Analysis of Covariance
ANOVA	Analysis of Variance
APCI	Atmospheric-pressure chemical ionization
AST	Aspartate aminotransferase
ATP	Adenosine triphosphate
BBOX	γ-butyrobetaine hydrolase
BGE	Background electrolyte
BMI	Body mass index
C0	Carnitine
C2	Acetylcarnitine
C5	Valerylcarnitine
C6	Hexanoylcarnitine
C6-OH	Hydroxyhexanoylcarnitine
C7	Hepatonylcarnitine
C8	Octanoylcarnitine
C12	Dodecanoylcarnitine
C14	Tetradecanoylcarnitine
C16	Hexadecanoylcarnitine
C16:1	Hexadecenylcarnitine
C18	Octadecanoylcarnitine
cAMP	Cyclic AMP
CAPS	3-cyclohexylamino-1-propanesulfonic acid
ccRCC	Clear cell renal cell carcinoma
CE	Capillary electrophoresis
CID	Collisional induced dissociation
Cl-Tyr	3-chloro-*L*-tyrosine
CNB	Core needle biopsy
COW	Correlation optimized warping
CRC	Colorectal cancer
CV	Coefficient of variation
CysGly-CySS	Cysteinylglycine-cystine

DESI-MS	Desorption electrospray ionization-mass spectrometry
DI-MS	Direct injection-mass spectometry
DNA	Deoxyribonucleic acid
DTT	Dithiothreitol
DTW	Dynamic time warping
DXA	Dual X-ray absorptiometry
EDTA	Ethylenediaminetetraacetic acid
EI	Electron ionization
EOF	Electroosmotic flow
ESI	Electrospray ionization
F-Phe	4-fluorophenylalanine
FC	Fold change
FDR	False discovery rate
FNAB	Fine needle-aspiration biopsy
FTICR	Fourier-transform ion cyclotron resonance
FWER	Family wise error rate
GC	Gas chromatography
GGT	γ−glutamyl transferase
GSH-OEt	Reduced glutathione ethyl ester
GSH	Reduced glutathione
GSH	Reduced glutathione
GSH-Cys-SS	Glutathione-cysteine-disulfide
GSSG	Oxidized glutathione
H&E	Hematoxylin & Eosin
HCA	Hierarchical clustering analysis
HCC	Hepatocellular carcinoma
HILIC	Hydrophilic interaction
HMDB	Human metabolome database
HP-921	Hexakis (2,2,3,3-tetrafluoropropoxy)phosphazine
HRMAS	High resolution magic angle spectroscopy
HR_{max}	Maximal heart rate
IDC	Invasive ductal carcinoma
IL-6	Interleukin 6
K-S	Kolmogorov-Smirnov
KEGG	Kyoto encyclopedia of genes and genomes
KNN	*k*-nearest neighbour
LAESI-MS	Laser ablation electrospray ionization-mass spectrometry
LC	Liquid chromatography

LC-MS/MS	Liquid chromatography-tandem mass spectrometry
LSD	Least significant difference
m/z	mass to charge ratio
MALDI-MS	Matrix assisted desoprtion ionization-mass spectrometry
MCT	monocarboxylate transporters
mPLS-DA	multilevel partial least squares discriminant analysis
MRM	Multiple reaction monitoring
MS	Mass spctrometry
MS/MS	Tandem mass spectrometry
MSI-CE-MS	Multisegment injection-capillary electrophoresis-mass spectrometry
MSI-CE-MS/MS	Multisegment injection-capillary electrophoresis-tandem mass spectrometry
MSI-NACE-MS	Multisegment injection-nonaqeuous capillary electrophoresis-mass spectrometry
MT	Migration time
MUFA	Monounsaturated fatty acids
MWCO	Molecular weight cut off
NAFL	Non-alcoholic fatty liver
NAFLD	Non-alcoholic fatty liver disease
NAS	NAFLD activity score
NASH CRN	NASH clinical research network
NDS	Naphthalene disulfonate
NIST	National Institute of Standards and Technology
NMR	Nuclear magnetic resonance
NMS	2-napthalenesulfonic acid
NTS	Naphthalene trisulfonate
oPLS-DA	Orthogonal partial least squares-discriminant analysis
PARAFAC	Parallel factor analysis
PBS	Phosphate-buffered-saline
PCA	Principal component analysis
PCr	Phosphocreatine
PDCL	Personal Compound Database and Library
PESI-MS	Probe electrospray ionization-mass spectrometry
PLS-DA	Partial least squares-discriminant analysis
PO_4^{3-}	Inorganic phosphate
PUFA	Polyunsaturated fatty acids
QA	Quality assurance

QC	Quality control
QTOF	Quadrupole time-of-flight
RAFFT	Recursive alignment by fast Fourier transform
REIMS	Rapid evaporated ionization mass spectrometry
RF	Random forests
RMT	Relative migration time
RNA	Ribonucleic acid
ROC	Receiver operating characteristic
RP	Reverse-phase
RPA	Relative peak area
RT	Retention time
S-W	Shapiro-Wilk
S/N	Signal-to-noise ratio
SFA	Short chain fatty acids
SOM	Self organization mapping
SVM	Support vector machine learning
TAD	Thiomorpholinoacetic acid-1,1'-dioxide
TNF-α	Tumor necrosis factor - alpha
TOF	Time-of-flight
UHPLC	Ultrahigh performance liquid chromatography
UPLC-MS	Ultra performance liquid chromatography-mass spectrometry
UV	Ultraviolet
VIP	Variables of importance in projection
XDH	Xanthine dehydrogenase
XO	Xanthine oxidase

Declaration of Academic Achievement

The following material has been previously published and is reprinted with written permission:

Chapter IV. Reprinted and adapted from Saoi, M.; Percival, M.; Nemr, C.; Li, A.; Gibala, M.; and Britz-McKibbin, P. Characterization of the Human Skeletal Muscle Metabolome for Elucidating the Mechanisms of Bicarbonate Ingestion on Strenuous Interval Exercise. *Anal Chem*. **91**, 4709-4718, 2019. Copyright (2019) American Chemical Society

Chapter I
Introduction: A Review of Tissue Metabolomic Studies in Clinical Research

Chapter I: A Review of Tissue Metabolomic Studies in Clinical Research

1.1 Historical overview of tissue biopsies: from histology to systems biology

Renowned French pathologist and founder of modern histology, Marie François Xavier Bichat, first defined the term "tissue" as fundamental structural units of organs within the human body that comprised of interlaced vessels and fibers, resembling a woven structure (Bichat 1977). Bichat's tissue doctrine of general anatomy stated that in order to advance understanding of disease origins and improve therapeutic interventions, one must directly analyze the specific sites of disease progression within the organs (*i.e.,* tissues) (Bichat 1977; Haigh 1984). Through his contributions, the inception of histology emerged as the systematic study of tissue specimens using microscopy. Typically, specimens for histology are obtained using tissue biopsy techniques. In 1847, Kün was the first to employ a needle-biopsy technique for extracting tumor tissue for microscopy (Kun 1847). Thereafter, Sir James Paget and Erichsen used a needle-aspiration biopsy method for histological analysis of breast tumours in 1853 (Rosa 2008; Webb 2001). The needle biopsy technique was further developed as a diagnostic tool for assessing tumours in the 20th century. In the mid-1920s, the needle aspiration biopsy technique became routine clinical practice at the Memorial Center in New York where 2,500 tumors were assessed using the method over three years (Martin and Ellis 1930; Rosa 2008). Despite promising evidence for its utility of tissue biopsies for tumour diagnosis, the technique faced early criticisms from clinicians deeming the technique as inaccurate due to the small amount of tissue specimens obtained while others feared of potential adverse effects (*e.g*., metastasis) resulting after the procedure. Furthermore, employing this technique into clinical practice would require trained specialists to perform and interpret the results, placing a burden on medical resources (Rosa 2008). While being widely rejected in the US, the needle-aspiration biopsy technique continued to be used across Europe during the Second World War (Webb 2001). Ultimately, within the latter half of the 20th century,

further developments in the technique led to its widespread use in other developed countries worldwide (Rosa 2008).

At present, tissue biopsies are routinely used in histology and cytology for disease diagnosis of benign and malignant tumours. Tissue processing for histopathology involves a number of key steps: fixation, staining, processing, embedding and sectioning (Titford 2014). Fixation involves preserving the tissue cellular structure while minimizing decay due to autolysis, through a chemical process (Comanescu et al. 2012). Formalin represents the most common fixative used in histology that preserves secondary and tertiary protein structures. Other fixatives include paraffin-formalin for immunohistochemistry and bouin fixative for soft and/or delicate tissue (*e.g.*, brain) (Alturkistani et al. 2015). After fixation, histological staining is performed to help enhance important features within the tissue for visualization under a light microscope. A combination of two dyes, hematoxylin and eosin (H&E), is the most widely used staining procedure in histology. Hematoxylin consists of a blue dye that stains nuclei by binding to basophilic components such as DNA and RNA within the nucleus. In contrast, eosin is a pink dye that stains components within the cytoplasm by binding to acidophilic substances such as charged amino acid side chains. Recent advancements in stains for more specialized features include Masson's stain for connective tissue and Golgi stain for neuronal fibres (Alturkistani et al. 2015). Thereafter, further processing such as dehydration is completed in order to facilitate removal of water for solidification, followed by embedding in paraffin wax and sectioning onto a microscope slide for examination (Alturkistani et al. 2015). These steps are crucial in order to preserve clinically relevant pathological information while minimizing perturbations in intact cellular and structural components to make an accurate diagnosis (Comanescu et al. 2012). Despite the widespread use of histology by pathologists for clinical decision making, the method is prone to observer bias that stem from visual (*e.g.,* differences in illusion of size, brightness, colour hues) and

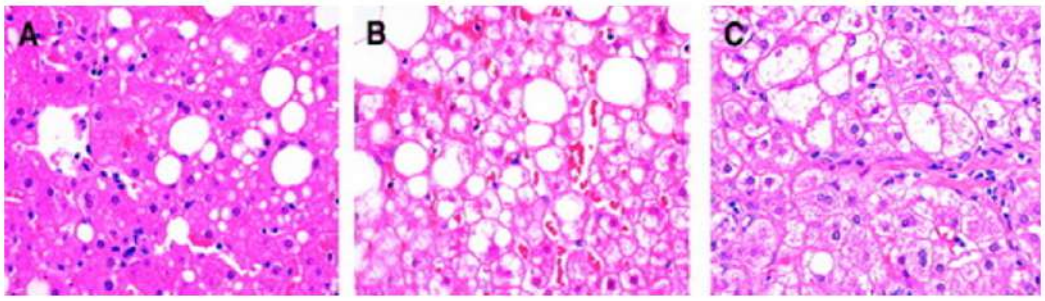

Figure 1.1: Photomicrographs of hepatocyte scoring of ballooning injury. (A) Score = 0; no ballooning evident in presence of mild steatosis (white cell deposits). (B) Score = +1; few balloon cells shown surrounding steatotic hepatocytes. (C) Score = +2; ballooning injury prominent, with few steatotic hepatocytes. Hematoxylin and eosin; original magnification x600. Reproduced from Kleiner *et al*. 2005 with permission (Kleiner et al. 2005).

cognitive biases (*e.g.,* confirmation and/or context bias) that may lead to subjective interpretation and grading using semi-quantitative scoring systems (Aeffner et al. 2017). For instance, Kleiner *et al.,* previously performed a study to examine inter and intra-observer variability in histopathology scoring of liver specimens (n = 50) obtained from patients with non-alcoholic fatty acid liver disease (NAFLD). While all pathologists showed high agreement in steatosis and fibrosis scoring among adult cases, there were lower levels of agreement in pediatric cases, especially in evaluating the presence of microvesicular steatosis, pigmented macrophages and ballooning (Kleiner et al. 2005). **Figure 1.1.** illustrates photomicrographs representing the scoring of ballooning injury in hepatocytes that range from 0, with no presence of ballooning, to +1 showing few balloon cells and finally to +2, where prominent ballooning is evident. Interestingly, the intermediate case of ballooning (*i.e.,* score = +1) showed higher inter-observer variability among the pathologists. The authors reported that the photomicrograph of the intermediate cases showed balloon cells that were surrounded by steatotic hepatocytes of similar size, making it more difficult for pathologists to differentiate these features from one another, compared to other extreme cases of fewer (*i.e.,* score = 0) to multiple (*i.e.,* score = 2) ballooning (Kleiner et al. 2005). While histopathology and semi-quantitative grading is clinically useful for patient stratification in diseases such as NAFLD, it

is imperative to understand the potential visual and cognitive biases that may lead to subjective interpretation among pathologists. Evidently, there is a need for more objective biochemical tests to facilitate clinical decision making while supporting histopathological findings.

In recent years, tissue biopsies have emerged as a specimen of interest in systems biology "-omics" approaches, including genomics, epigenomics, transcriptomics, proteomics and metabolomics **(Figure 1.2)**. Metabolomics aims to characterize and quantify low molecular weight metabolites (< 1.5 kDa) within complex biological specimen, such as biofluids, single cells, and tissue specimens (Goodacre 2005). Metabolites are clinically relevant proxies of biochemical activity that are strongly associated with molecular phenotype due to its sensitivity to environmental exposures and physiological changes (Alonso et al. 2015). Metabolomics not only can be used to discover biomarkers for early detection of treatable diseases of unknown etiology, but can also reveal the underlying mechanisms of therapeutic interventions based on pharmacological agents, exercise training and/or nutritional supplementation (C. H. Johnson et al. 2016; Patti et al. 2012). Traditionally, most metabolomics studies rely on a surrogate biofluids (*e.g.,* urine, plasma, stool) due to its less invasive sample collection, especially for biomonitoring applications in large population cohorts. However, biofluids are non-organ specific and are reflective of many biochemical processes occurring over numerous tissues and cell types within the body (Zukunft et al. 2018). As a result, it is imperative to analyze tissues directly as they are the direct and localized site of most disease processes that can be measured at early stages of development. Furthermore, they may provide more robust biomarkers in the context of disease screening, diagnosis or prognosis as compared to blood or urine specimens (Gonzalez-Riano et al. 2016). In 2002, Watkins and colleagues reported one of the first comprehensive tissue metabolomics studies in murine heart and liver

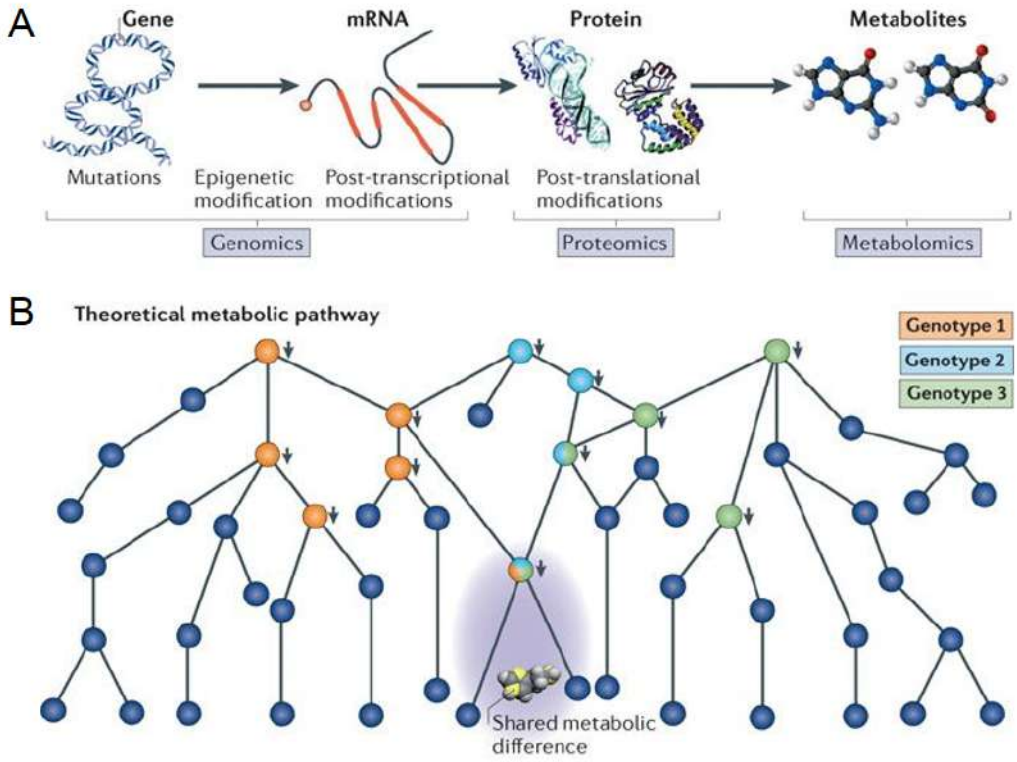

Figure 1.2: (A) The "omics" cascade used in systems biology illustrating interactions between genomics, transcriptomics, proteomics and metabolomics. Unlike genes and proteins that undergo a number of epigenetic and post-transcriptional modifications, metabolites are downstream end products of these interactions that can be linked to the observed phenotype. (B) A schematic of a metabolic pathway illustrating enzymatic alterations elicited by a single or multiple genotypes that lead to a myriad of metabolic perturbations that can be used to correlate with the phenotype. Reproduced from Patti *et al*. 2012 with permission (Patti et al. 2012).

tissues to examine the effects of rosiglitazone on lipid metabolism in type 2 diabetes (German et al. 2002). Within the last two decades, there has been a rapid increase in tissue metabolomics studies with new advances in sample preparation techniques, as well as instrumentation and bioinformatics to expand the detection and identification of metabolites from minimal amounts of tissue (Veenstra and Zhou 2009). In a recent PubMed search using the terms "tissue metabolomics," over 1100 studies have been reported for mammalian tissue specimens from 2002 to March 2019, with a majority of studies performed from 2015 onwards as depicted in **Figure 1.3 (A)**. Moreover, a diverse range of tissue specimens have been

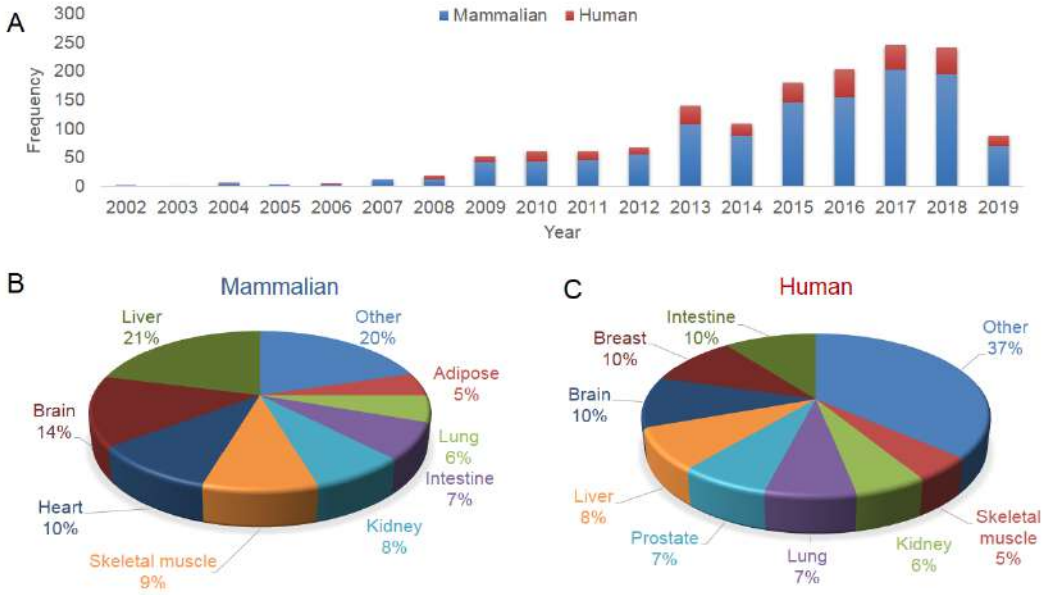

Figure 1.3: (A) An overview of published research articles in the field of tissue metabolomics from 2002 to March 2019 based on a PubMed search with the terms "tissue metabolomics." Only original research articles were reported (excluding comprehensive reviews, book chapters, commentaries, conference abstracts) based on mammalian species (blue). Approximately 20% of these studies were based on human tissue specimens (red**).** Pie chart distributions of various (B) mammalian and **(c)** human tissue specimens analyzed in these published studies.

analyzed in these published reports with liver (21%), brain (14%), heart (10%), skeletal muscle (9%) and kidney (8%) tissues comprising of the top five organs mainly analyzed from mammals as depicted in **Figure 1.3 (B)**. Other mammalian tissues less frequently explored include adipose, pancreas and bladder tissue. Approximately 20% of these studies involved human tissue specimens – the most common being brain (10%), intestine (10%), breast (10%), liver (8%) and prostate (10%) tissues as illustrated in **Figure 1.3 (C)**. A majority of these studies employed nontargeted metabolomics approaches for differentiating tumour-related metabolite markers in cancerous *vs.* noncancerous tissue, including hepatocellular carcinoma (HCC), colorectal cancer (CRC), and breast cancer, whereas brain tissue metabolomic studies focus on neurodegenerative diseases such as Alzheimer's

disease. Evidently, tissue metabolomics is a rapidly evolving field that shows promise in a wide array of clinical applications from biomarker discovery to drug development in order to develop more efficacious yet safe interventions for the prevention or treatment of chronic human diseases.

1.2 Overview of tissue metabolomics workflows

To date, two complementary strategies have been adopted for tissue metabolomics studies, namely targeted (hypothesis-driven) analysis of known metabolites and/or non-targeted (hypothesis-generating) analysis of all detectable metabolites when using one or more instrument platforms. Targeted metabolomics focuses on measuring a small subset of metabolites within one or more metabolic pathways of interest in order to answer a defined biochemical question (D. Broadhurst et al. 2018; Patti et al. 2012). In this case, absolute quantification of the metabolites can be achieved using stable-isotope dilution mass spectrometry (MS) methods and authentic chemical standards, where data preprocessing, statistical analyses and biochemical interpretation is far more routine than nontargeted metabolite profiling (D. Broadhurst et al. 2018; Yi et al. 2016). However, a major drawback of targeted approaches is the limited coverage when characterizing the metabolic phenotype of a tissue that is unsuitable for discovery-based studies required for understanding complex disease processes of unknown etiology. In contrast, nontargeted metabolomics is a global approach that aims to measure a far wider range of metabolites within a tissue specimen, including the identification of unknown metabolites of biological or clinical significance. In contrast to targeted approaches, nontargeted metabolomic studies aim to filter, authenticate and annotate metabolites from potentially thousands of molecular features measured when using full-scan high resolution MS methods whose chemical structures are unknown *a priori* (Patti et al. 2012). Indeed, only a small fraction of total detectable signals generated in ESI-MS represent reliable and authentic metabolites from tissue samples, whereas a majority of molecular features are derived from spurious

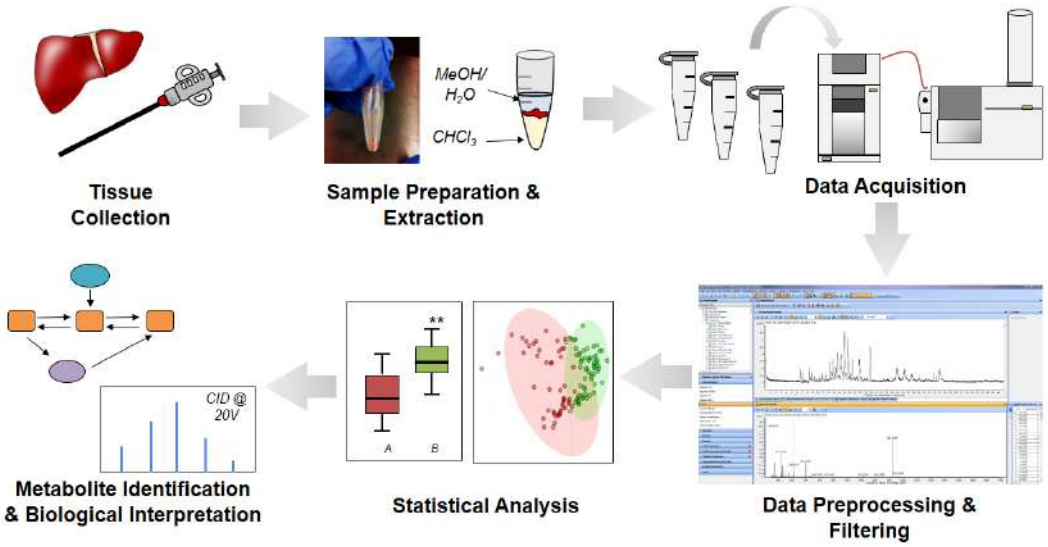

Figure 1.4: Overview of workflow for MS-based tissue metabolite profiling studies. Tissue collection via biopsy or autopsy by a trained physician represents the first key step in the workflow. Thereafter, tissues undergo several steps of sample preparation (*e.g.,* lyophilization, homogenization etc.) prior to metabolite extraction. Following rigorous sample preparation methods, metabolite profiling is performed using a suitable analytical platform of choice such as NMR or hyphenated MS-based analytical platforms (*e.g.* GC-, LC-, CE-MS). Data preprocessing and filtering are then applied to the complex metabolite data acquired to obtain a clean data matrix for statistical analysis, metabolite identification and biological interpretation.

signals, background adducts and contaminants that need to be rigorously filtered from data (Jankevics et al. 2012). As a result, since chemical standards and stable-isotope internal standards are often not available, only semi-quantitative or relative quantification is feasible in discovery-based tissue metabolomic studies involving high dimensional data sets requiring multivariate statistical approaches for improved data visualization, pattern recognition, group classification and metabolite ranking (Yi et al. 2016). As a result, numerous steps are involved in tissue metabolomic workflows **(Figure 1.4)** in order to obtain high data quality while reducing bias and false discoveries (Want et al. 2013), including structural elucidation of unknown compounds when using MS/MS from their most likely molecular formula (Dunn et al. 2013). These steps will be outlined in detail in the proceeding sections.

1.2.1 Tissue collection and sample preparation

Tissue collection and sample preparation is one of the outstanding challenges that remains a major bottleneck and source of bias in tissue metabolomic workflows. Typically, tissue collection is performed under anesthesia through a biopsy, surgical procedure or an autopsy by a trained physician. Depending on the tissue of interest, a number of microsampling biopsy procedures can be used for tissue collection. However, the most common procedures include fine needle-aspiration biopsy (FNAB) and core needle biopsy (CNB). FNAB is a minimally invasive, low cost and simple biopsy technique that requires no anesthesia to obtain small amounts of tissue using a small, fine needle (Łukasiewicz et al. 2017). FNAB has been used in breast (Ly et al. 2016), thyroid (Gharib et al. 1993) and pancreatic tissue (Gress et al. 2001) for disease diagnosis and/or tumour progression. CNB is routinely used in clinical and/or research settings that employs a larger needle to obtain "core" intact tissues for examination. In contrast to FNAB, this technique requires local anesthesia and is prone to slightly more complications (*e.g.,* pain, discomfort, infection) (Nassar 2011). **Figure 1.5** illustrates an example of a CNB technique (*i.e.,* Bergstrom muscle biopsy) introduced by Tarnopolsky *et al.,* for obtaining skeletal muscle tissue. After local anaesthesia is applied, the biopsy needle is inserted through the subcutaneous tissue, fascia and into the muscle, where suction is applied to obtain the tissue (~150-200 mg). The tissues are subsequently inspected for adequacy and quality, and sectioned for analysis (Tarnopolsky et al. 2011). Similar CNB techniques have been utilized for other tissues including liver (Padia et al. 2009), breast (Meyer et al. 1999) and lymphatic tissues (Ben-Yehuda et al. 1996).

There are numerous other precautions one should take for collecting tissues for non-targeted metabolomics studies as summarized in **Table 1.1**. For instance, after tissue collection via biopsy or surgical procedures, tissues should be removed of fat/connective tissue as well as potential contaminants such as anesthetics used

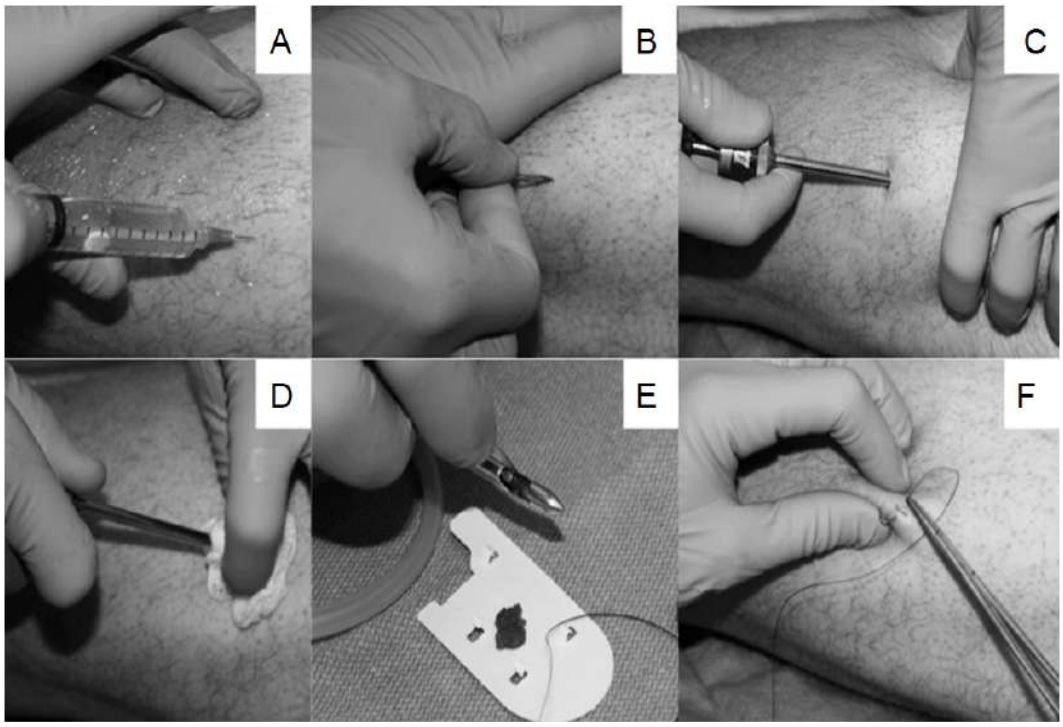

Figure 1.5: Schematic of a suction-modified Bergström muscle biopsy technique. (A) Lidocaine is first applied to the skin and subcutaneous tissue. (B) An incision is made though the subcutaneous tissue into the fascia to help guide the biopsy needle (C) into the muscle, where suction is applied to obtain the tissue specimen. (D) Removal of the needle is facilitated using counterpressure and twisting motion. (E) The specimen are examined for adequacy and aliquoted to smaller pieces for analysis. (F) The incision is closed using a 3.0 silk suture. Reproduced from Tarnopolsky *et al*. 2011 with permission. (Tarnopolsky et al. 2011).

during the collection procedure or blood from the specimen, in order to obtain an accurate, metabolite profile representative of the tissue. Moreover, it is imperative to immediately freeze tissues after collection (*i.e.,* flash-freezing) and store the specimens at low temperatures (-80°C) (Gonzalez-Riano et al. 2016; Want et al. 2013) in order to halt metabolism and ensure metabolites within the tissues remain stable following sample collection and long-term storage (Want et al. 2013). This is crucial for labile metabolites such as major phosphagens (*e.g.,* ATP) and thiols (*e.g.,* GSH) that are prone to hydrolysis and oxidation artifacts, respectively.

Table 1.1: Guidelines for tissue collection in animals and human tissues for nontargeted MS-based metabolomics. Adapted from Want *et al*. (Want et al. 2013)

Tissue collection recommendations for nontargeted hyphenated-MS metabolomics studies	
General Concerns:	- Ensure timing of tissue collection is randomized for the entire study cohort - Be cautious of contaminants due to collection procedure (*i.e*., anesthetics, surgical instrument cleaning solutions) - Large tissue samples should be divided and aliquoted into smaller pieces for freezing and storing to i) accelerate the freezing process and ii) minimize number of freeze-thaw cycles
Sampling from human patients	- Small biopsies are typically obtained - Ensure samples are snap-frozen immediately - Ensure blood is removed using deionized water or PBS from samples to minimize contamination
Sampling from animals	- Whole organ samples are typically obtained - Subdivide and aliquot the whole organ and snap-freeze them; if this is not possible, freeze the whole organ - In rodents, the exsanguination process should be performed first before tissue removal in order to minimize contamination of blood on tissue

After collection, tissues can either be lyophilized (*i.e.,* freeze-dried) or remain wet prior to various sample workup protocols that are critical for subsequent metabolomic analysis, such as tissue disruption, liquid extraction, sample deproteinization and/or chemical derivatization. However, lyophilizing tissues is often preferred as a means to quench any residual enzymatic activity and eliminate excess water from the sample while minimizing biological variance by more accurately weighing out dried tissue speicmens prior to extraction (Gonzalez-Riano et al. 2016). Thereafter, the tissues are further subjected to grinding with a nitrogen cooled mortar and pestle or homogenization to break the tissues further. Manually grinding the tissue using a cooled mortar and pestle remains the gold standard; however, it is extremely labour intensive and low throughput. Tissue homogenization consists of physically disrupting the tissue using a homogenizer (*i.e*., Quiagen Tissuelyser, Precelly's 24 bead-based homogenizer) (Geier et al.

2011; Masson et al. 2010, 2011; Römisch-Margl et al. 2011) to ensure a consistent, homogenous solution results upon addition of the extraction solvents. Furthermore, many homogenizers to date, such as the Precelly's 24 homogenizer, are capable of sampling up to 24 samples, significantly increasing throughput with bettter reproducibility due to automation (Römisch-Margl et al. 2011). While homogenization is evidently less labour intensive, it is impractical for smaller tissue quantities (C. Y. Lin et al. 2007). Therefore, several factors such as minimum tissue quantity available, number of samples and available infrastructure must be considered when choosing an appropriate method for homogenization of tissue specimens prior to metabolite extraction.

To date, numerous metabolite extraction methods have been reported for various tissue specimens from animals and humans; this stems from the chemically diverse range of metabolites present within tissue metabolomes that span a wide dynamic range having different solubilities and chemical stabilities. As a result, there is no single global extraction procedure when performing nontargeted tissue metabolomics studies that can simultaneously extract the entire metabolome with high efficiency (Beltran et al. 2012; C. Y. Lin et al. 2007). In general, the optimal extraction method to employ in tissue metabolomics studies should be nonselective, reproducible, simple and produce high metabolite yields with good long-term stability (Gonzalez-Riano et al. 2016; C. Y. Lin et al. 2007). In 2007, Lin *et al*., first sought out to determine a simple, reproducible extraction method for muscle and liver tissues using NMR metabolomics. Various extraction solvents were compared in this study including, perchloric acid, as well as polar organic solvents (*i.e.,* methanol, ethanol, acetonitrile) mixed with water and/or chloroform. Overall, the methanol/chloroform/water solvent system based on the classic Bligh-Dyer extraction procedure was ideal for the tissue samples due to its efficiency in obtaining both hydrophilic and hydrophobic metabolites distributed across two immiscible solvent layers with high efficiency and reproducibility (C. Y. Lin et al.

2007). In addition, Wu *et al.* also concluded that a two-step Bligh-Dyer extraction procedure with the addition of extra water and a 10 min equilibration time resulted in high metabolite extraction yields and good reproducibility while minimizing metabolic decay (Wu et al. 2008). Many studies to date have made advances in overcoming the low throughput in tissue metabolite extraction procedures that can be implemented in multiplatform approaches (Römisch-Margl et al. 2011; Zukunft et al. 2018). Furthermore, there have been efforts made to establish standard extraction procedures for various tissue types (*e.g.*, liver kidney, skeletal muscle etc.) in murine tissues (Zukunft et al. 2018).

1.2.2 Analytical techniques for tissue metabolomics

Global metabolome analysis of complex and heterogeneous tissue specimens with high data fidelity is a persistent challenge in metabolomics (Dunn and Ellis 2005; Y. Wang et al. 2015). In most cases, orthogonal extraction and/or analytical platforms are required to achieve broad metabolome coverage for a diverse range of metabolites ranging from abundant electrolytes/osmolytes to low abundance polar metabolites and unknown intact lipids. Recent technological advances in both nuclear magnetic resonance (NMR) and mass spectrometry (MS)-based analytical platforms, especially when coupled to high efficiency separations such as gas chromatography (GC), liquid chromatography (LC) and capillary electrophoresis (CE), have enabled the identification and quantification of a wide array of metabolites from tissue extracts (Zhang et al. 2012).

NMR spectroscopy presents a fast and reproducible platform for metabolite profiling and metabolic flux analysis (Bothwell and Griffin 2011) while allowing for quantitative and qualitative determination of metabolites with excellent long-term stability (Alonso et al. 2015; Zhang et al. 2012). Moreover, minimal sample preparation is required allowing intact metabolites to be measured non-destructively in complex, biological samples within minutes (*i.e.*, 2-3 min per

sample) depending on spectral acquisition settings. However, NMR requires large sample volumes (*i.e.*, 100- 200 μL) while also being prone to spectral overlap and low sensitivity that prevents detection of sub-micromolar concentrations of metabolites as compared to MS-based techniques (Alonso et al. 2015; Wishart 2016; Zhang et al. 2012). The advent of High Resolution Magic Angle Spectroscopy (HRMAS)-NMR, first introduced by Cheng *et. al.* (Cheng et al. 1996), allows for intact tissue analysis from minimal amounts of tissue (*i.e.*, 10–20 mg) while achieving highly resolved spectra (Burns et al. 2004; Dinges et al. 2019; Tsang et al. 2005). More importantly, since the tissue remains unaltered during analysis, other tests can be performed on the same tissue by trained physicians and/or pathologists (*e.g.*, histopathology). Tate and colleagues first demonstrated the utility of HRMAS-NMR as a metabolomics platform to decipher metabolic differences between cancerous kidney tissue from normal/non-cancerous tissue in human clear cell renal cell carcinoma (ccRCC) patients (Tate et al. 2000). Since 2004, HRMAS-NMR has been successfully used for intact tissue metabolomics analysis in various tissue types including brain, breast, lung, and pancreas (Dinges et al. 2019). In particular, HRMAS-NMR has been for examining differences in metabolite profiles between cancerous and adjacent, noncancerous tissue and monitoring disease progression (Chen et al. 2017; Haukaas et al. 2016; Vandergrift et al. 2018). For instance, Bathen *et al.* applied HRMAS-NMR on over 300 breast tissue samples to differentiate between tumour and non-cancerous, adjacent tissue. Based on the metabolite profiles depicted in **Figure 1.6,** choline metabolites (*e.g.,* choline, phosphocholine), glycine and taurine were elevated in tumour tissue compared to the normal, adjacent tissue (Bathen et al. 2013). However, the high infrastructure and operating costs of NMR, as well as its complicated spectral processing steps prevent its widespread applicability in tissue metabolomic studies in non-specialized laboratories.

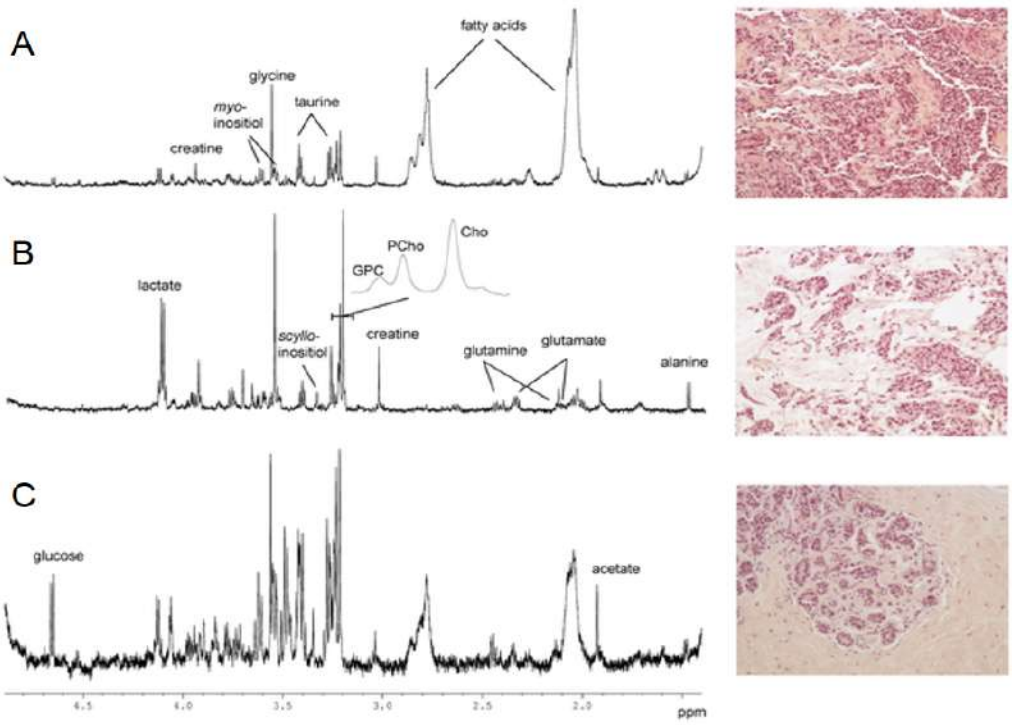

Figure 1.6: Representative HRMAS-NMR spectra and corresponding histopathology images of cancerous breast tissues of patients diagnosed with (A) invasive ductal carcinoma (80% tumour cells) and (B) invasive mucinous carcinoma with (60% tumour cells). Elevations in choline-derived metabolites, glycine and taurine were characteristic in tumour tissues compared to (C) non-cancerous, adjacent tissues (0% tumour cells). Reproduced by Bathen et al. 2013 with permission. (Bathen et al. 2013)

In contrast, MS-based techniques have been more widely applied in tissue metabolomics studies due to its higher sensitivity that can measure a wider range of metabolites as compared to NMR. Moreover, recent advances in high resolution MS with higher resolving power and mass accuracy together with faster scan rates have greatly improved analytical performance to reduce isobaric interferences while allowing for the identification for unknown metabolites (Fuhrer and Zamboni 2015; Wishart 2016; Zhang et al. 2012). Moreover, different ion sources (*e.g.,* ESI, APCI, and EI) and mass analyzers (*e.g.,* TOF, QTOF, Orbitrap, FTICR) can be used in tandem with suitable separation methods in tissue metabolomics studies depending on the metabolites of interest. Direct injection-mass spectrometry (DI-MS) of tissue extracts offers a "separation-free" platform for high throughput

metabolite profiling making it an attractive technique for large-scale metabolomic studies, such as shot-gun lipidomics (Y. Wang et al. 2015). However, DI-MS is prone to ion suppression due to matrix effects as well as lower specificity due to lack of resolution of isobaric ions that can contribute to false discoveries without stable-isotope internal standards; additionally unknown identification is challenging due to convoluted MS/MS spectra when compared to reference spectral databases without orthogonal retention/migration time information (Holmes et al. 2015; Zhang et al. 2012).

Alternatively, ambient ionization MS is a rapid technique for the analysis of samples requiring minimal sample preparation for *in situ* metabolic profiling without separation (Y. Wang et al. 2015). In recent years, the use of ambient MS-based techniques have increased for tissue metabolomics (Clendinen et al. 2017). Desorption electrospray ionization (DESI)–MS, first introduced by Cooks and colleagues (Takáts et al. 2004), enables the direct analysis of metabolites from intact tissue specimens by applying a fine spray of charged droplets to extract metabolites from the sample surface while facilitating droplet formation and collision prior to analysis via mass spectrometry (Clendinen et al. 2017). Importantly, DESI-MS also allow for mass spectral imaging of tissue that retains the underlying spatial distribution of metabolite concentrations lost with conventional metabolomic methods relying on tissue disruption, homogenization and extraction processes. DESI-MS has demonstrated its utility for providing intraoperative tissue characterization for disease diagnosis. For instance, Eberlin *et al.* (Eberlin et al. 2013), first developed a DESI-MS technique combined with machine learning methods (*i.e.*, SVM) for brain tumour classification based on lipidomic profiling, which coincided with histopathology diagnosis in 32 surgical specimens (n =5). As seen in **Figure 1.7**, DESI-MS imaging of meningioma brain tissue samples revealed elevations in characteristic lipids, *m/z* 788.3 and *m/z* 885.3. Interestingly, the regional distribution of these lipids shown in the DESI-MS images

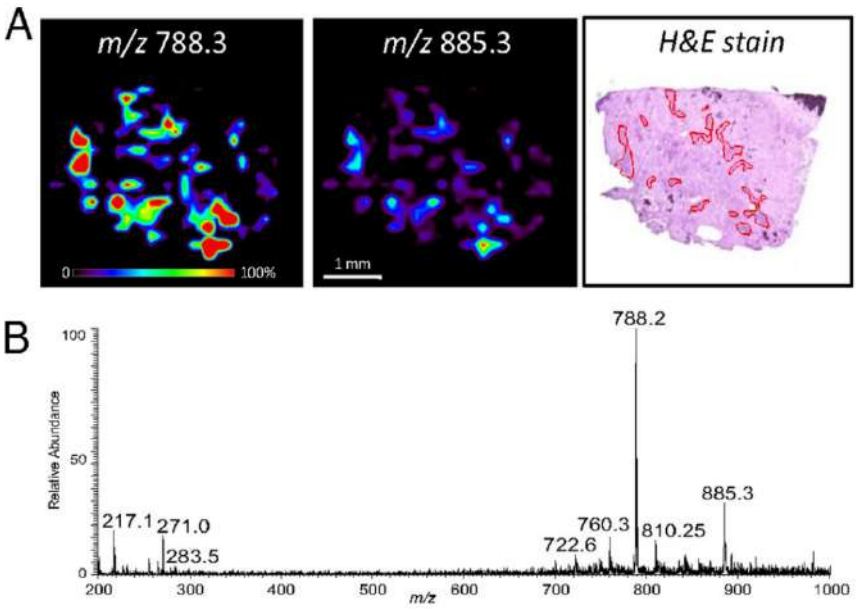

Figure 1.7: (A) DESI-MS imaging of brain tissue obtained from a case of meningioma with characteristic abundances of lipid species m/z 788.3 and m/z 885.3. The regional distribution of these species coincided with the distribution of meningioma cells based on histopathology results. (B) Mass spectrum of meningioma regions within the brain tissue specimen analyzed. Reproduced from Eberlin et al. 2013 with permission (Eberlin et al. 2013).

were highly correlated with the distribution of meningioma cells as observed via histopathology of the same brain tissue specimen. The study demonstrated the utility of DESI-MS as an alternative, promising ambient MS technique to provide accurate diagnosis based on tissue characterization in tumours that coincided with gold standard techniques (*e.g.,* histopathology) currently implemented within clinical settings. Probe electrospray ionization (PESI)-MS has also emerged as an ambient MS technique for real time, *in vivo* analysis for tissue specimens. The mechanism of ionization is achieved through insertion of an acupuncture needle into the sample of interest where water content enables ionization to occur upon application of high voltage (Clendinen et al. 2017; Hiraoka et al. 2007). Yoshimura *et al*., used PESI-MS as a minimally invasive technique for revealing differences in triglyceride expression among cancerous and non-cancerous kidney tissue ccRCC patients, signifying its potential for cancer diagnosis (Yoshimura et al. 2012). The

advent of laser ablation electrospray ionization (LAESI)-MS by Nemes and Vertes (Nemes and Vertes 2007), allowed both *in situ* and *in vivo* tissue analysis with no sample preparation over a wide mass range (up to 60 kDa). Using the native water content of the sample, a mid-infrared laser is focused on the sample matrix facilitating ablation followed by ionization (Clendinen et al. 2017; Y. Wang et al. 2015). LAESI-MS has been applied to various biological specimens, most notably in brain tissue and single cells. One of the first applications of LAESI-MS for direct tissue analysis was performed by Shrestha *et al*., in which several metabolites and lipids were characterized in mouse brain tissue. This study showed the potential of LAESI-MS as well as other novel ambient MS-techniques for *ex vivo* analysis of specimens, where physiological and metabolic processes reflect closely those in their native state without any artifactual changes in biochemical activity due to extensive sample pretreatment (Shrestha et al. 2010). Rapid Evaporative Ionization Mass Spectrometry (REIMS) or "iknife" was recently introduced as an ambient ionization technique that allows for *in situ* tissue sampling for real time characterization of human tissue to guide surgical operations/procedures while facilitating rapid data analysis for patient diagnosis (Balog et al. 2013). A schematic of the REIMS instrumentation setup during intraoperative procedures is depicted in **Figure 1.8**. During surgery, a high frequency current is applied to the surgical blades to facilitate tissue plume formation in order to produce charged species that are subsequently removed by suction from the surgical site to the mass spectrometer for data analysis (Clendinen et al. 2017). Intriguing results obtained by Balog *et al*., revealed that the intraoperative REIMS technique coincided with postoperative histopathology results in 96.2% of the cases (n = 81), demonstrating the potential of iknife technology to be translated for routine clinical use during surgical procedures while accelerating decision making to improve patient outcomes (Balog et al. 2013). While the use of ambient MS-techniques in tissue metabolomics is steadily increasing due to its ability to directly analyze intact tissue samples in real time, these techniques are prone to ion suppression and matrix effects, as well as

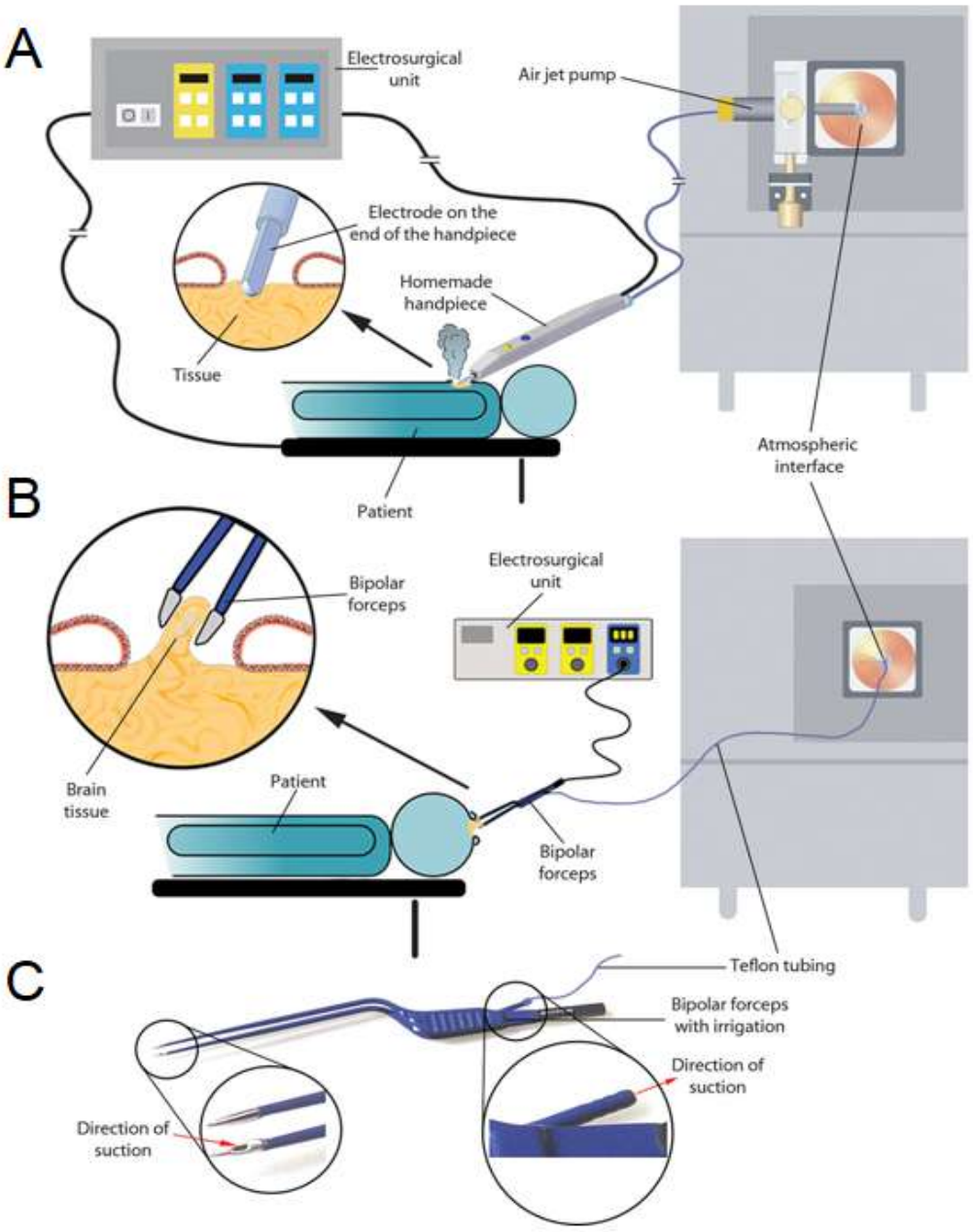

Figure 1.8: Schematic of the REMIS (iknife) instrumentation used for (A) monopolar and (B) bipolar electrosurgery for guiding surgical procedures while facilitating rapid data analysis and patient diagnosis. (C) Commercially available bipolar forceps used during electrosurgery to facilitate aerosol aspiration for MS data analysis. Reproduced from Balog *et al*. 2013 with permission (Balog et al. 2013).

isobaric/isomeric interferences due to lack of high efficiency separation methods prior to ionization, that can contribute to bias and false discoveries (Clendinen et al. 2017).

A majority of tissue metabolomics studies still rely on hyphenated analytical platforms that couple different separation methods to MS in order improve selectivity and expand metabolome coverage despite longer total analysis times as a way to improve the resolution of isomeric and isobaric ions, enhance MS/MS spectral quality for metabolite identification, as well as reduce ion suppression effects between samples (Alonso et al. 2015; Y. Wang et al. 2015). **Table 1.2** summarizes key hyphenated-MS platforms that are commonly employed in tissue metabolomics studies. Within recent years, tissue metabolomics studies have used various instrumental configurations for targeted and nontargeted approaches **(Figure 1.9)**. Overall, LC-MS is the most commonly used platform for tissue metabolomic studies to date (39%) due to the fact that complementary retention mechanisms can be used to resolve chemically diverse classes of metabolites when using reversed-phase (RP), hydrophilic interaction (HILIC) and/or ion-exchange column types in conjunction with optimal gradient elution programs. RP columns are the most column types employed in a majority of tissue metabolomics studies. However HILIC columns have been also gaining widespread use within recent years. As a result, the broad selectivity of LC-MS enhances metabolome coverage with high sensitivity, small sample requirements and ease of compatibility with various mass analyzers (Holmes et al. 2015; Wishart 2016). GC-MS is followed as the second most widely used analytical platform (23%) in tissue metabolomics studies, with ~14% of these studies utilizing both LC-MS and GC-MS to increase metabolome coverage of the tissue specimens analyzed (Garvey et al. 2014; Gonzalez-Riano et al. 2017; Lieblein-Boff et al. 2015; Meller et al. 2015). Both NMR and HRMAS-NMR together comprised of ~24% of methods applied for tissue metabolomic studies primarily due to its less destructive sample preparation

methods as compared to MS-based platforms that allows for direct measurement of metabolites within intact tissue (Alonso et al. 2015; Wishart 2016). Interestingly, while CE-MS is a high efficiency separation platform that is ideal for analysis of mass-restricted tissue specimens, it remains an underutilized technique in tissue metabolomics studies (4%) in comparison to other hyphenated-MS based platforms (Hatazawa et al. 2015; Satoh et al. 2017; Tang et al. 2018). Furthermore, DI-MS and FIA-MS are also underrepresented analytical platforms in tissue metabolomics studies (2%) due to the low specificity and issues with ion suppression and matrix effects, limiting their utility to largely targeted-based studies (Bijkerk et al. 2019; Singhal et al. 2017). Other analytical techniques have also been over recent years in tissue metabolomics studies include multidimensional separation techniques (*e.g.* GCxGC-MS), ambient ionization-MS techniques (*e.g.,* DESI-MS, LAESI-MS),(Guenther et al. 2015; Paine et al. 2016) and imaging techniques such as matrix assisted desorption ionization (MALDI)-MS imaging (Jung et al. 2016; Zhao et al. 2018).

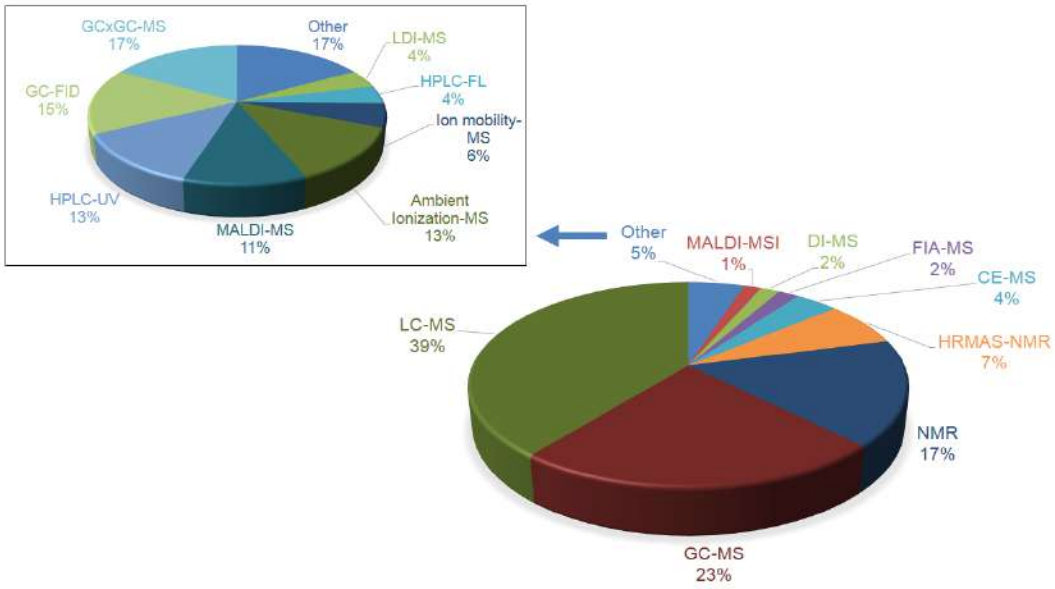

Figure 1.9: Representative pie chart summarizing the most common analytical platforms used in tissue metabolomics studies from 2002 – March 2019. The inset depicts the distribution of other, less frequently used analytical platforms (*i.e.,* GCxGC-MS, Ambient ionization-MS, ion mobility-MS etc.) encompassed in the published metabolomics studies.

Table 1.2: Summary of hyphenated separation techniques coupled to MS for tissue metabolomics studies. Adapted from Wishart *et al*. (Wishart 2016), Holmes *et al*. (Holmes et al. 2015), and Kuehnbaum *et al.* (Kuehnbaum and Britz-McKibbin 2013).

Platform	Advantages	Disadvantages
Gas chromatography – mass spectrometry (GC-MS)	- Highly sensitive and reproducible - Modest sample volume requirements (100 -200 µL) - Widely available EI-MS spectral databases for metabolite ID - High resolution separations, including GC X GC - Robust and mature platform - Can be automated	- Extensive sample pretreatment (*i.e.*, sample derivatization) - Limited to volatile & thermally stable compounds - Long analysis times and low sample throughput - Limited column types as compared to LC
Liquid chromatography – mass spectrometry (LC-MS)	- Highly sensitive - Small sample volume requirements (10 – 100 µL) - Simple sample preparation - Broad selectivity due to variety of columns available - Core shell or UHPLC for high efficiency separations, including LC X LC - Can be automated	- Standardization difficult with various columns and gradient elution programs - Prone to ion suppression due to ESI-MS - Limited MS/MS spectral databases for metabolite ID - Prone to batch effects due to instrumental drift - Poor precision (HILIC)
Capillary electrophoresis-mass spectrometry (CE-MS)	- High efficiency separation for polar/ionic compounds - Minimal sample volume requirements (< 20 µL) - Simple sample preparation - Minimal ion suppression - Accurate prediction of ion mobility for identification - Multiplexed separations for higher sample throughput	- Moderate sensitivity with sheath liquid interface - Bias to charged compounds in ESI-MS - Limited databases for metabolite identification - Poor migration time reproducibility due to changes in EOF

1.2.3 Pre-analytical QA/QC considerations to reduce false discoveries in tissue metabolomics

In order to achieve reproducible research findings with high data quality in nontargeted metabolomics studies, care must be taken in the pre-analytical phase in the workflow to minimize false discoveries. Inadequate study power is a major limitation in tissue metabolomics studies due to limited sample sizes and small effect sizes compared to the large inherent biological variance in the study cohort (D. I. Broadhurst and Kell 2006; Ioannidis 2007). In order to reduce false discoveries, well-controlled observational studies should be performed where comparison groups are closely matched in terms of anthropometric and clinical characteristics (*i.e.,* sex, age, BMI), especially when measuring small to modest effect sizes in the metabolome (Dunn, Broadhurst, Atherton, et al. 2011). Furthermore, it is crucial to implement stringent quality assurance (QA) and quality control (QC) practices in the experimental workflow to minimize bias and false findings. Quality assurance is defined as systematic practices that are routinely implemented prior to sample processing and data acquisition in order to successfully obtain high quality yet reproducible data that is likely free of bias. For instance, protocols that include addition of recovery standards (*i.e.,* added before sample preprocessing) and internal standards (*i.e.,* added to samples before data acquisition) is a crucial QA practice in order to assess and correct for variations associated with sample preprocessing and data acquisition, respectively (D. Broadhurst et al. 2018; Dudzik et al. 2018). Other examples of QA practices include the implementation of standardized operating procedures (SOP) with rigorous staff training in all aspects of the metabolomics workflow, including sample collection/storage, sample workup, instrument calibration and operation, preventative instrument maintenance, as well as data preprocessing steps (D. Broadhurst et al. 2018). Additionally, implementing QC samples in nontargeted metabolomics workflows has been emphasized within the last decade in the metabolomics community given lessons learnt from instrumental bias and false

discoveries in cancer biomarker studies in proteomics which have largely failed to reach the clinic (D. Broadhurst et al. 2018; Diamandis 2012; Dudzik et al. 2018; Dunn et al. 2012; Dunn, Broadhurst, Begley, et al. 2011; Lewis et al. 2016; Sangster et al. 2006) QC samples are implemented in workflows for multiple purposes: (1) to assess system stability and performance, (2) to evaluate technical precision and detect systematic bias and (3) to correct for within and between batch variations associated with long-term signal drift over time during data acquisition. QC samples should resemble the metabolite composition of the tissue specimen analyzed in a given study, such as a standard reference material (NIST) or a representative pooled sample from cohort under investigation (Dunn, Broadhurst, Begley, et al. 2011).

QC practices are utilized to ensure QA practices have been fulfilled to achieve high data quality before and after data acquisition (D. Broadhurst et al. 2018). During data acquisition, multiple steps should be implemented in metabolomics workflows to assess system suitability. At the start of analysis, blank samples are run to assess potential contamination of the column or capillary. Additionally, blank samples can also be injected intermittently between sequences of study samples to determine if sample carryover is observed; if a peak in the blank signal appears, the signal can be flagged and subsequently removed if its intensity is greater than a predefined threshold. Moreover, blank samples can be useful in the data preprocessing step of peak filtering where signals derived from solvents, sample collection and/or handling can be identified and removed from the final data matrix. After injecting blank samples at the start of the analysis, a mixture of authentic chemical standards is subsequently run to assess instrumental performance (*i.e.,* accuracy and precision) prior to the analysis of the study samples. Ideally, the standards should cover a wide *m/z* range and RT or MT range in order to assess if performance factors such as sensitivity, RT/MT, and peak shape fulfill pre-determined acceptance criteria, such as a mean CV for metabolite RT < 2%

from QC samples with no evidence of peak splitting or ion suppression. If the standards do not fulfill the criteria, corrective maintenance measures should be performed, such as rigorous cleaning of the ion source, mass tuning etc. (D. Broadhurst et al. 2018). However, if such criteria are satisfied, pooled QC samples should be injected immediately after the standards in order to equilibrate the system, which will assist in minimizing variability in RT or MTs and stabilizing the response of the detector (Zelena et al. 2009). Once good system suitability has been evaluated following repeat analysis of QC samples, the study samples are fully randomized and subsequently analyzed in batches while analyzing intermittent pooled QC samples after every 5 to 10 samples to monitor for signal drift with sufficient temporal resolution (D. Broadhurst et al. 2018; Dunn, Broadhurst, Begley, et al. 2011; Want et al. 2013). After data acquisition, it is recommended to evaluate instrumental performance and compare biological (between sample) and technical variances (repeat QCs) using unsupervised multivariate statistical methods, such as principal component analysis (PCA). Overall, QC samples ideally cluster closely together on a 2D scores plot when compared to the overall biological variance from the individual study samples **(Figure 1.10 (A))** (D. Broadhurst et al. 2018). Furthermore, depending on the type and total number of biological specimens analyzed, a coefficient of variance (CV) < 20%(Dunn, Broadhurst, Begley, et al. 2011; Sangster et al. 2006) or < 30%, (Lewis et al. 2016; Want et al. 2010) is considered an adequate threshold for precision for metabolites in discovery-based metabolomic studies (D. Broadhurst et al. 2018; Gika et al. 2008). Additionally, the use of control charts for depicting random changes in responses for metabolites analyzed from QCs is an excellent strategy for evaluating long-term system drift, as well as detecting potential batch effects especially for shared/multi-user instruments over weeks or months of continuous and especially intermittent operation (Wehrens et al. 2016). In order to minimize batch effects in metabolomics, several algorithms have been developed to perform batch correction including empirical Bayes approaches (W. E. Johnson et al. 2007) where

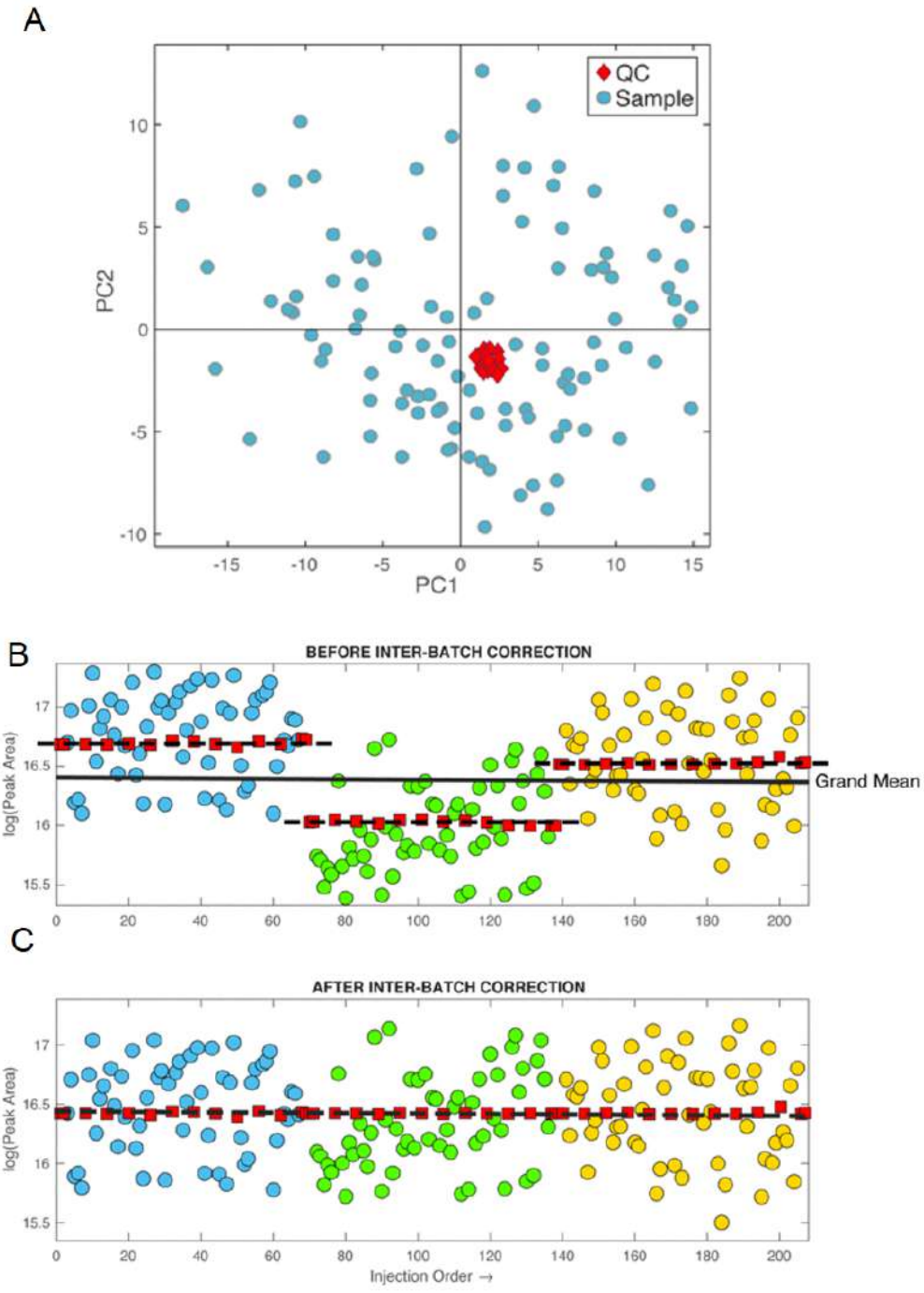

Figure 1.10: (A) Representative 2D PCA scores plot illustrating good technical variance through tight QC clustering (red) in comparison to the biological variance exhibited by the individual samples (blue). (B) Control chart depicting batch effects observed when individual study samples from multiple batches (blue = batch 1, green = batch 2, yellow = batch 3) are injected on the same instrumentation across several days. Using intermittent QCs (red) implemented in the workflow, batch correction can be performed (C) to correct for between-batch systematic error. Reproduced from Broadhurst *et al.* 2018 with permission (D. Broadhurst et al. 2018).

intermittent QCs injected during the experimental run are used to generate a smoothed model for specific feature intensities that can be used for correction as illustrated in **Figure 1.10 (B) and (C)** (Dunn, Broadhurst, Begley, et al. 2011). However, due to the a diverse range of instrumental platforms and data workflows adopted in metabolomics, a single unified QA/QC procedure will not fit all laboratories. Nonetheless specific guidelines outlined here are increasingly adopted to promote good analytical practice and transparency in reporting.

1.2.4 Data preprocessing and statistical analysis

Data preprocessing is a critical step in the nontargeted metabolomics for converting raw, complex data acquired through appropriate NMR or MS-based platforms to a clean data matrix suitable for statistical analysis and metabolite identification (Hendriks et al. 2011; van den Berg et al. 2006). This encompasses several steps including data filtering, peak detection and spectral deconvolution, time alignment and normalization and/or scaling (Castillo et al. 2011; Yi et al. 2016). In MS-based workflows, noise filtering is a crucial process that aims to separate authentic molecular features from background signal, chemical noise (*i.e.,* from buffers and solvents) and/or random noise from instrumental interference. ESI is a soft ionization technique readily used in hyphenated-MS metabolomics platforms, including direct infusion/flow injection analysis, as well as LC and CE separation platforms. Often, each metabolite can generate several in-source fragments, isotope signals and adduct ions (*e.g.*, $[M + Na]^+$)that should be removed to eliminate redundant information in the data matrix and avoid false positives (Dunn et al. 2013). Thereafter, through peak detection and spectral deconvolution, an authentic molecular feature reflecting a unique metabolite is annotated based on two orthogonal parameters, such as accurate mass and retention time (*m/z*:RT), which reduces data overfitting in cases when thousands of molecular features are detected among a much smaller number of samples. Currently, there are several open source programs (*e.g.*, XCMS (Benton et al. 2008; Smith et al. 2006), MAVEN (Clasquin

et al. 2012; Melamud et al. 2010), apLCMS (Yu et al. 2009)) that integrate both filtering and peak detection algorithms into a single function (Castillo et al. 2011; Yi et al. 2016). For almost all types of metabolomics data, peak alignment is imperative in order to correct for instrumental drifts or interferences during data acquisition, such as retention and/or migration time shifts in separation-based MS platforms especially when using HILIC and CE without adequate column re-equilibration or temperature regulation. A number of time alignment procedures/algorithms have been developed and employed in metabolomics studies including correlation optimized warping (COW) (Nielsen et al. 1998), dynamic time warping (DTW) (Pravdova et al. 2002) and recursive alignment by fast Fourier transform (RAFFT) (Wong et al. 2005). Time alignment allows molecular features to be compared and grouped accordingly between samples prior to statistical analysis (Castillo et al. 2011; Liland 2011). Additionally, missing values often emerge in metabolomics datasets due to heterogeneity of the study cohort (*i.e.,* biological variance) and/or limitations in sensitivity of the platform employed when metabolite concentrations are below the method detection limit. Metabolites that are inconsistently detected above a user-defined threshold (*e.g.*, < 75%) among individual samples are removed to avoid skewing the data. For representative metabolites that are frequently detected in the majority of samples, a suitable missing value estimation method can then be applied. Employing an inappropriate estimation method can potentially introduce further bias and consequently, affect statistical outcomes and interpretation. Common methods for handling missing features and/or non-detects in metabolomics include replacement with a small, predefined value (*i.e.,* half the detection limit or the metabolite response measured in the dataset), mean/median replacement, or estimating missing data using various imputation algorithms such as the k-nearest neighbor (KNN) method or Bayesian PCA missing value estimation (Hrydziuszko and Viant 2012).

Thereafter, normalization and scaling methods can be applied to remove variations in the raw data due to analytical noise, sampling pretreatments or experimental bias while retaining the inherent biological variation (Hendriks et al. 2011; Yi et al. 2016). A common strategy in MS-based workflows is to normalize feature responses to internal standards, based on the assumption that systematic error exclusively contributes to the variance observed in the internal standards. For tissue metabolomics studies, feature responses are also often normalized to the (wet or dry) weight of tissue specimen analyzed, to account for variations in tissue weights. Prior to statistical analysis, mathematical transformations (*i.e., log* transformation, power transformation) are employed to correct for heteroscedasticity and skewed distribution in the datasets (van den Berg et al. 2006; Yi et al. 2016). Scaling methods (*i.e.,* autoscaling, pareto scaling, range scaling) are used to correct for variances in feature abundances, where variables with high abundance are scaled down to reduce their influence on statistical analysis compared with metabolites of lower abundance (Liland 2011; van den Berg et al. 2006). According to Broadhurst and Kell, it is imperative to choose appropriate univariate and multivariate statistical analyses to avoid false discoveries in metabolomics studies (D. I. Broadhurst and Kell 2006). In order to perform parametric, univariate tests such as the student's t-test or analysis of variance (ANOVA), the data must have a normal, Gaussian distribution. Thus, normality testing is a crucial step prior to statistical analysis as most metabolomics data are often skewed and not normally distributed. Graphical methods (*i.e.,* histograms) as well as univariate normality tests such as the Kolmogorov-Smirnov (K-S) or Shapiro-Wilk (S-W) tests should be used to assess normality. Furthermore, mathematical transformations such as *log* transformation may be used to attempt to transform skewed distributions to a Gaussian distribution. However, if the data remains skewed, even after applying transformations, non-parametric tests must be used (*i.e.,* Mann-Whitney U test) (D. I. Broadhurst and Kell 2006).

For large, complex metabolomics datasets, univariate significance testing is performed for tens to hundreds of metabolites simultaneously. Therefore, multiple hypothesis testing correction is essential in order to minimize false positives (*i.e.,* Type I errors) (Saccenti et al. 2014; Vinaixa et al. 2012). The Bonferroni correction represents a conservative multiple hypothesis testing approach that adjusts the statistical *p*-value threshold (*i.e.,* $\alpha = 0.05$) in proportion to the number of variables (*i.e.,* metabolites, *n*) in the dataset (*i.e.,* α/n) (D. I. Broadhurst and Kell 2006). While this approach minimizes false positives by controlling the family wise error (FWER), applying a stringent threshold increases the potential for false negatives (*i.e.,* Type II errors) (Vinaixa et al. 2012). Other multiple testing correction methods such as the False Discovery Rate (FDR) provide less rigorous approaches for controlling false positives while also controlling for false negatives. For instance, the Benjamini-Hochberg procedure consists of adjusting the statistical *p*-values to a unique, *q*-value (or *p*-corrected value) for each metabolic feature, based on statistical significance ranking of all features (Storey and Tibshirani 2003; Vinaixa et al. 2012). Regardless of the ultimate method chosen, it is crucial to correct for multiple testing when performing multiple univariate statistical tests in order to incorrectly reject a null hypothesis due to random chance and control Type I and II errors.

Metabolomics datasets are characterized as highly dimensional/multivariate due to hundreds of metabolites being measured concurrently from numerous samples. Multivariate statistical analysis methods can therefore be used to evaluate the relationship (*i.e.,* correlations, covariances) amongst all the metabolites simultaneously (Saccenti et al. 2014). Unsupervised methods are exploratory methods used to assess the overall data structure of the dataset while observing trends and groupings due to inherent variation amongst the data without *a priori* information on the data structure (Hendriks et al. 2011; Yi et al. 2016). PCA is a frequently used method for dimensionality reduction, that aims to decompose the

multivariate data to fewer principal components, where a majority of the inherent variation in the dataset is captured within the first few components (Hendriks et al. 2011; Liland 2011). Hierarchical Clustering Analysis (HCA) is also a widely used, exploratory method in metabolomics to reveal natural groupings among samples or variables (*i.e.,* metabolites) based on similarities in the form of distances or correlations (Liland 2011). Other unsupervised methods such as Self Organization Mapping (SOM) and Parallel Factor Analysis (PARAFAC) can also be utilized in metabolomics for dimensionality to reveal informative parts of the data from noise (Hendriks et al. 2011).

In contrast, supervised methods have *a priori* information regarding the data structure and thus, are often used to generate predictive models for classification (Yi et al. 2016). Partial Least Squares Discriminant Analysis (PLS-DA) is a widely used supervised method in metabolomics that maximizes covariances between independent variables (*e.g.,* external stimuli) and the dependent variables (*i.e.,* metabolite responses) in the form of components of lower dimensionality (Saccenti et al. 2014). Furthermore, PLS-DA can also reveal informative metabolites that discriminate amongst the groups in the form of variable ranking (*i.e.,* variable importance in projection). Modifications to the PLS-DA method have also been utilized in metabolomics for classification modelling including orthogonal (O)–PLS-DA (Trygg and Wold 2002) and multilevel PLS-D (Westerhuis et al. 2010). Furthermore, other supervised methods can also be encompassed in metabolomics as pattern recognition strategies such as SVM and random forests (RF) (Yi et al. 2016). However, it is imperative to validate these predictive models using supervised methods to decrease the risk of data overfitting and avoiding false discoveries (D. I. Broadhurst and Kell 2006; Liland 2011). Cross-validation and test-set validation are readily used validation methods in metabolomics (Liland 2011). In cross-validation, the dataset is split into mutually exclusive *n* subgroups of equal size; the model is trained *n* times where one of the subgroups are held out

as an internal validation set. Thereafter, the reproducibility (R2) and predictive ability (Q2) of the model are unraveled. Ideally, test set validation methods should be used to assess the accuracy of the model and is often underutilized in metabolomics studies. In test set validation, the data set is split into a training set and validation set (2:1). The training set is used to optimize the predictive model, while the validation set assesses the model accuracy that was previously optimized by the training set. Lastly, a test set (15-20% training set) is comprised of independent samples randomly selected from the training and validation test sets, which is used to better assess model accuracy (D. I. Broadhurst and Kell 2006). Other methods such as bootstrapping, permutation testing and rotation tests can also be used for method validation in metabolomics studies.

1.2.5 Unknown metabolite identification using high resolution MS/MS

Due to the chemical diversity of the human metabolome that is composed of a complex array of environmental exposures and by-products of host metabolism, the majority of detectable molecular features in MS based metabolomics remains largely unknown (Dunn et al. 2013). Indeed, a major fraction of the human metabolome is derived from exogenous metabolites, such as dietary and lifestyle influences, pharmaceuticals and the microbiome (Bujak et al. 2014; Dunn et al. 2013; Wikoff et al. 2009). As a result, few publicly available databases (*i.e.,* HMDB (Wishart et al. 2018), KEGG (Ogata et al. 1999), METLIN (Smith et al. 2005)) provide incomplete metabolite information on *all* metabolites present in human biospecimens, so reliance on structural elucidation for chemical identification of unknown metabolites is imperative prior to biological interpretation (Bujak et al. 2014). This remains a significant bottleneck in nontargeted MS-based metabolomics studies (Dunn 2008; Wishart 2011). According to the Chemical Analysis Working Group of the Metabolomics Standard Initiative, four levels of metabolite identification are described in **Table 1.3** as reporting standards in metabolomics studies.

Table 1.3: Four levels of metabolite identification confidence defined by the Metabolomics Standard Initiative. Adapted by Dunn, *et al.* (Dunn et al. 2013)

Level	Confidence of ID	Support
1	Confidently identified compounds	Comparison of at least two or more properties with an authentic chemical standard under identical analytical conditions
2	Putatively annotated compounds	Comparison of physiochemical properties and/or spectra with publically available databases without reference to authentic chemical standards
3	Putatively annotated compound classes	Comparison of physiochemical properties and/or spectral similarity of known class of compounds
4	Unknown compounds	Unidentified and unclassified metabolites but can still be differentiated and quantified based on spectral data

It is noteworthy that while the probability of *level 1* identification is high for most compounds, stereoisomers that appear similar or identical in terms of both RT/MT as well as mass spectral characteristics must be considered. In order to elucidate accurate, unambiguous identifications of isomers, a suitable chromatographic method for chiral separations or NMR can be used to determine structural configurations of the stereoisomers (Dunn et al. 2013). This is especially important when the different configurations plays biologically important roles, such as *cis/trans* unsaturated fatty acids.

In order to facilitate metabolite identification in non-targeted metabolomic workflows, accurate mass measurement is required to successfully match the molecular features to a small number of putative or most likely molecular formulas. This can be achieved using high resolution MS instruments after appropriate mass calibration (Scheltema et al. 2008). Furthermore, recent advances in commercial software from MS vendors have allowed automated generation of putative molecular formulas based on mass spectral features, such as the accurate mass of the molecular ion, as well as its isotopic pattern and charge state ($[M+H]^+$). Another

strategy to reduce the number of putative molecular formulas is to apply the seven golden rules proposed by Kind and Fiehn (Kind and Fiehn 2007; Lommen 2014). The rules consist of restricting the number of elements during formula generation, applying LEWIS and SENIOR rules, applying isotopic pattern filters, checking for hydrogen/carbon ratios, checking for elemental ratios of heteroatoms (*i.e*., nitrogen, oxygen, phosphate and sulfur *vs.* carbon) and checking element ratio probabilities (Kind and Fiehn 2007). Developed methods in stable ^{13}C isotope labelling can also be applied to aid in structural identification and quantification through differentiating between biologically derived metabolite ions from background (Giavalisco et al. 2008, 2009).

As aforementioned, in order to achieve *level 1* identification for a metabolite of interest, two or more orthogonal properties must be compared (*e.g., m/z*, RT or MT, fragmentation mass spectrum) to an authentic standard under identical acquisition conditions. Tandem mass spectrometry (MS/MS) has gained widespread use as a tool for unambiguous metabolite identification in metabolomics studies. It is often performed using a targeted approach following data acquisition in order to (1) differentiate molecular features with the same molecular formula but similar chemical structure and/or (2) compare fragmentation spectra to public databases, mass spectral libraries and authentic standards for compound identification (Dunn et al. 2013). For instance, **Figure 1.11** illustrates previous work by DiBattista *et al*. comparing MS/MS spectra of a putatively identified metabolite, ophthalmic acid (OPA, *m/z* 290.1349) in a representative dried blood spot (DBS) extract to the authentic, chemical standard under identical optimal collisional induced energies (CID 10V) in the form of a mirror plot. Unambiguous identification (*level 1*) was confirmed based on excellent spectral matching for three distinct product ions, *m/z* 58.0644, *m/z* 161.0917 and *m/z* 215.1022, and their relative intensities as well as low mass error (DiBattista et al. 2019).

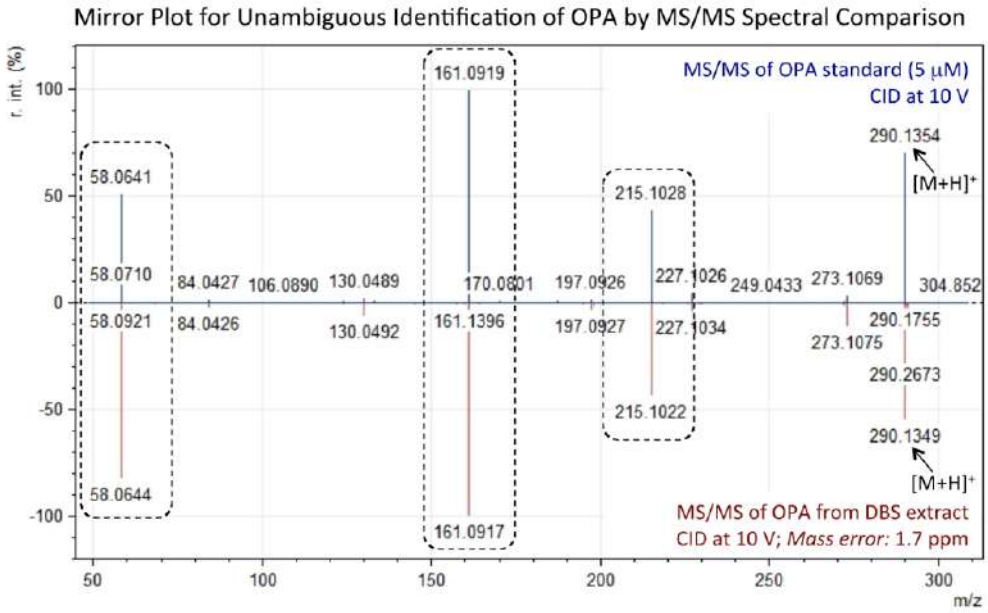

Figure 1.11: Mirror plot comparing MS/MS spectra of ophthalmic acid (OPA *m/z* 290.1349; red trace) in a pooled DBS extract to an authentic standard (blue trace). High matching score was achieved based on three characteristic product ions (*m/z* 58.0644, *m/z* 161.0917, *m/z* 215.1022) CID experiments performed at 10V. Reproduced by DiBattista *et al.* 2018 with permission (DiBattista et al. 2019).

Recently, there have been rapid developments in computational MS/MS software that can further assist in metabolite identification, particularly when authentic standards are not available (Hufsky et al. 2014). These approaches include MS/MS spectrum prediction that aims to directly predict mass spectra (*e.g.,* MyCompoundID (Huan et al. 2015)), *in silico* fragmentation, which generates *in silico* derived mass spectra to match experimental MS/MS spectrum (*e.g.,* MetFrag (Wolf et al. 2010), FiD (Heinonen et al. 2008), FingerID (Heinonen et al. 2012)) and *de novo* fragmentation to elucidate the structure of a precursor ion based on the observed fragments of the experimental spectrum (*e.g..,* fragmentation trees (Böcker and Rasche 2008; Rasche et al. 2011)).

Other approaches such as applying prior biological (*e.g.,* enzymatic transformations) and chemical (*e.g.,* physiochemical properties based on RT/MT

behaviour, ionization behaviour) knowledge can assist in metabolite identification (Draper et al. 2009; Dunn et al. 2013; Yi et al. 2016). Furthermore, correlation analysis (*i.e.,* Pearson*,* Spearman rank) can be used to reveal associations between metabolites ($p < 0.05$) resulting from commonly derived metabolic pathways and/or enzymatic reactions (Macedo et al. 2017). **Figure 1.12** highlights *in silico* approaches used by DiBattista *et al.* to identify an unknown, modified glutathione analogue (*m/*z 388.1094) in DBS extracts. After confirming a tentative molecular formula based on its accurate mass, charge state and isotope patterning, a thiol-specific chemical reactivity test was performed where excess dithiothreitol (DTT) was added as a reducing agent to a representative DBS extract. This resulted in attenuation of the signal and formation of a new reduced thiol (*m/z* 470.1438) as well as reduced glutathione (GSH, *m/z* 308.091) confirming the unknown metabolite was a mixed oxidized glutathione disulfide. The distinct fragmentation patterning generated through CID experiments of the precursor ion and chemical reactivity tests confirmed that the unknown ion was identified as an N-glycated glycine mixed oxidized glutathione (Glc-GSSG) (DiBattista et al. 2019)

1.3 Current trends and challenges in tissue metabolomics in clinical research

Tissue-based metabolomics studies have increased significantly within the last decade, especially in the context of human health and chronic diseases. Since tissues are the origins of metabolic changes due to external stressors such as viral infections or carcinogen exposure, they are deemed a suitable specimen to analyze to further elucidate mechanisms underlying disease pathogenesis. However, recent metabolomics studies performed in human samples have shifted towards using tissue specimen with complimentary minimally invasive biological specimen (*e.g.,* serum, urine, feces) as a more holistic approach in determining perturbations in both intracellular and circulatory/systemic metabolites as a result of disease progression and thus, find a mechanistic link among both specimens by offering a more convenient sample type for screening or testing in the population.

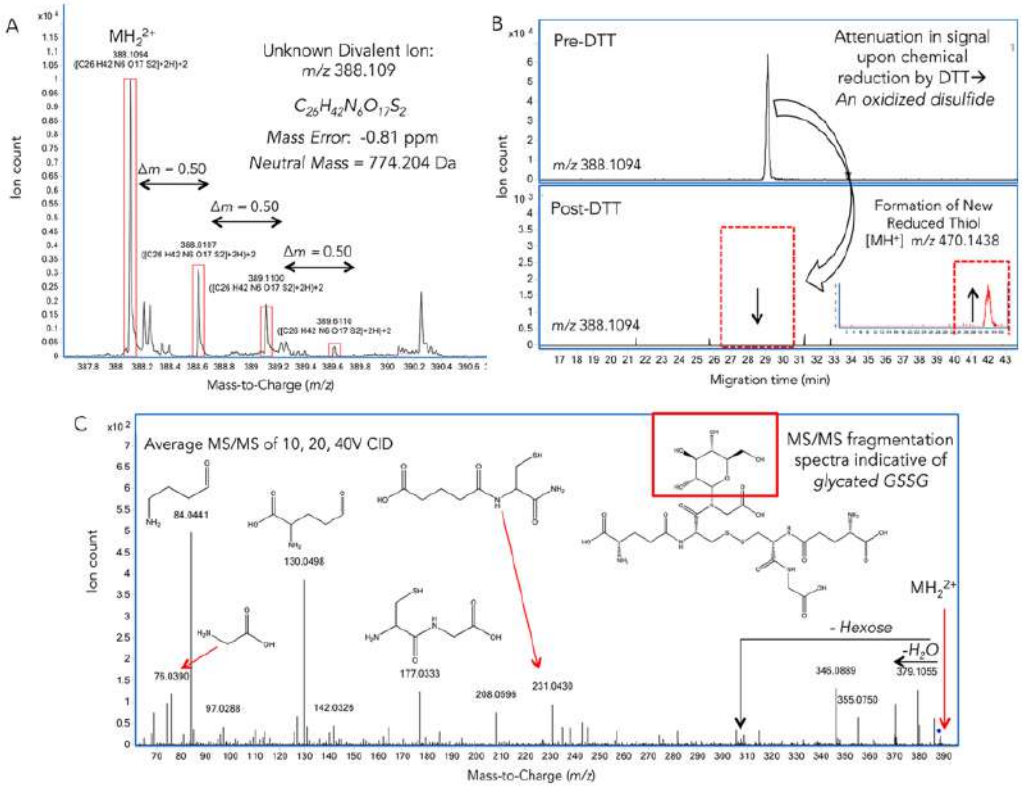

Figure 1.12: (A) Full scan TOF-MS spectra of unknown metabolite highlighting its most likely molecular formula as a divalent protonated species [MH_2^{2+}] based on its accurate mass, charge state and isotopic patterning. (B) Thiol-specific chemical reactivity test performed by addition of DTT to a pooled DBS resulting in the attenuation of the signal and formation of a new reduced thiol (*m/z* 470.144) suggesting the unknown metabolite as a mixed oxidized disulfide. (C) MS/MS fragmentation spectra consistent with a mixed oxidized glutathione disulfide with a modified N-glycated glycine residue. Reproduced by DiBattista *et al.* 2018 with permission (DiBattista et al. 2019).

If metabolites are identified in *both* specimen to be differentially expressed between cancerous *vs.* adjacent noncancerous tissue and/or diseased *vs.* control samples, the metabolite can be used as a potential, tissue-derived biomarker for assessing disease diagnosis, predicting progression or disease subtypes or monitoring treatment responses to therapy without reliance on invasive tissue biopsy procedures. **Table 1.4** summarizes key tissue metabolomics studies recently published with applications in clinical medicine including biomarker discovery for disease diagnosis and monitoring progression. Perhaps one of the most well-known tissue metabolomics studies to date was the discovery of sarcosine as a marker for prostate

cancer published in *Nature* by Sreekumar *et al*. in 2009 (Sreekumar et al. 2009). Elevations in sarcosine were observed in metastatic and clinically localized prostate cancer tissues compared to benign tissues (n = 42); these changes were associated with cancer progression and notably, observed in patient matched serum (n = 110) and urine (n = 110) samples. This link between sarcosine and prostate cancer progression led the authors to conclude that sarcosine could be a promising, potential biomarker for prostate cancer. However, since its publication, there have been conflicting studies reporting poor associations between sarcosine levels and prostate cancer progression in both urine (Jentzmik et al. 2010) and serum (Ankerst et al. 2015), suggesting its limited utility for prostate cancer screening. These discordant findings may be due to a number of inconsistencies in the study design and sample collection procedures of these validation studies. For instance, in a study published by de Vogel *et al.*, it was revealed that high serum sarcosine levels were associated with reduced prostate cancer risk, contrary to the first findings by Sreekumar *et al*. (De Vogel et al. 2014). However, it was reported that a large time window between serum sarcosine measurement and biopsy was reported which may have explained the disparity in results among both studies. In fact, an editorial published by Jack A. Schalken in the journal, *European Urology*, emphasizes the need for standardization of biomarker validation studies, substrate collection procedures and parameters in order to make biomarker studies more comparable (Schalken 2010). While the role of sarcosine in the diagnosis of prostate cancer currently remains unclear, the preliminary findings published Sreekumar *et al*. provided a basis for determining less invasive biomarkers derived from the direct site of disease origin (*i.e.* tissue) for diagnosis and disease progression, while also revealing unknown underlying molecular mechanisms of the disease. Care must be taken when validating these biomarkers in biospecimens within larger cohorts in future studies in order to make appropriate conclusions regarding their diagnostic utility in the population.

Other tissue metabolomics studies have used similar approaches for biomarker discovery for disease diagnosis and prognosis. Huang *et al*. performed nontargeted metabolite profiling to determine markers for differentiating tumour tissues from adjacent and distal noncancerous tissues in HCC patients (n = 50). Metabolic correlation networks revealed upregulations in fatty acids, glycolytic metabolites, and amino acids, while downregulations in bile acids, TCA cycle intermediates, phospolipids and short chain acylcarnitines were also observed. Of these metabolites differentially expressed in HCC tumour tissue and noncancerous tissue, a combination of betaine and propionylcarnitine were shown to be significantly different in serum of HCC patients (n = 139) from patients with non-malignant liver diseases including cirrhosis (n = 81) and hepatitis (n = 81), demonstrating the diagnostic potential of this metabolite panel in the clinical diagnosis of HCC (Q. Huang et al. 2013). More and colleagues used a similar approach to determine potential biomarkers in serum of invasive ductal carcinoma (IDC) patients (n = 76), benign patients (n = 33) and healthy controls (n = 33) that were highly correlated to IDC cancer progression seen in tissues (n = 24 IDC, n = 24 benign, n = control). Three amino acid metabolites (tyrosine, tryptophan and creatine) were shown in both the serum and tissue to be differentially expressed as a result of IDC progression, suggesting a bi-directional interaction between both specimens and potential biomarkers that could be used in monitoring IDC progression and severity for future studies (More et al. 2017). Recently, Wang *et al.* performed nontargeted metabolomics on paired colon tissues and plasma samples from CRC patients (n = 34) undergoing colorectal surgery to discover metabolite correlations among both specimen that could provide deeper insight to CRC pathogenesis (Z. Wang et al. 2019) . As a result, over 240 metabolites (143 unregulated, 70 downregulated) were consistently detected and dysregulated in both tumour derived tissue and plasma of CRC patients. The authors then sought out to select a panel of tissue-derived metabolites for CRC diagnosis and prognosis using additional plasma samples obtained from CRC patients (n = 73) and sex-

Table 1.4: Metabolomics studies recently published that encompass paired tissue and less invasive biofluids for applications in biomarker discovery, disease diagnosis and progression in clinical research.

Disease	Specimen	Analytical Platform(s)	Key Findings	Ref
Prostate Cancer (PCA)	Prostate (*n* = 50) Urine (*n* = 110) Plasma (*n* =110)	LC-MS, GC-MS	- Increased sarcosine observed in metastatic and clinically localized tissue, urine and serum due to cancer progression compared to negative controls	(Sreekumar et al. 2009)
Hepatocellular carcinoma (HCC)	Liver (*n* = 50) Serum (*n* = 298)	LC-MS	- Increased amino acids, SFAs, MUFAs, glycolytic metabolites; decreased bile acids, PUFAs, short chain acylcarnitines in tumour tissues -Betaine and propionylcarnitine in serum differentially expressed in HCC patients compared to cirrhosis and chronic hepatitis patients	(C.-C. Huang et al. 2009)
Invasive Ductal Carcinoma (IDC)	Breast (*n* = 72) Serum (*n* = 142)	LC-MS, GC-MS	- Tyrosine, tryptophan and creatine showed differences in both tissue and serum due to IDC progression compared to healthy controls	(More et al. 2017)
Colorectal cancer (CRC)	Colon (*n* = 50) Fecal (*n* = 70)	^{1}H NMR	-Decreased butyrate; increased succinate, alanine, lactate and glutamine differentially expressed in tumour tissues and feces compared to healthy controls	(Y. Lin et al. 2019)
Colorectal cancer (CRC)	Colon (*n* = 68) Plasma (*n* = 282)	LC-MS	-8 metabolite panel (creatinine, dihydrothymine, tryptophan, xanthine, tyrosine, gluconic-γ-lactone, his-gly and chenodeoxycholic acid) significantly differed in tumour tissue and plasma compared to adjacent, normal tissue and controls respectively.	(Z. Wang et al. 2019)

Abbreviations: SFA = Short chain fatty acids,, MUFA = monounsaturated fatty acids, PUFA = polyunsaturated fatty acids

matched polyp controls (n = 73). Eight metabolites including amino acids (tryptophan, tyrosine, creatinine), bile acids (chenodeoxycholic acid), dipeptides (histidinyl-glycine), purine metabolites (dihydrothymine, xanthine) and gluconolactones (gluconic-γ-lactone) were selected as potential biomarkers for monitoring CRC progression (Z. Wang et al. 2019). Additionally, Lin *et al*. used NMR-based metabolomics to determine metabolite signatures of CRC in paired tumour tissues (n = 50) and fecal samples (n = 70). The authors observed consistent changes in butyrate, lactate, alanine, glutamate and succinate in colonic tissues and feces of CRC patients, compared to healthy controls, suggesting the potential utility of fecal samples as a novel, less invasive specimen for early detection of CRC (Y. Lin et al. 2019).

Despite the utility of using tissues for nontargeted metabolomics studies, persistent challenges still remain including limitation in tissue quantities and lack in standardization of tissue extraction procedures. As a result, recent efforts have been made by metabolomics researchers to address these issues. Since 2007, several studies have been performed to standardize tissue extraction procedures for NMR and MS-based platforms (C. Y. Lin et al. 2007; Wu et al. 2008). Earlier studies focused on developing rapid yet simple metabolite extraction methods that result in high metabolite recoveries. However, these methods were optimized on only one to two tissue specimens (*i.e*., liver, skeletal muscle) and thus, may not be applicable to other tissue types that differ in composition. In 2012, Römisch-Margl and colleagues sought out to develop a simple, high throughput metabolite extraction method amenable for several tissue types (*i.e.,* liver, kidney, skeletal muscle, adipose and brain) in two different species (*i.e.,* bovine, mouse) using a targeted metabolomics approach (Römisch-Margl et al. 2011). Various extraction solvents were tested including: methanol, ethanol, phosphate buffer as well as combinations of different solvent systems (*e.g*., ethanol and dichloromethane). While some

extraction procedures performed better in some tissue types compared to others, overall methanol extractions were preferred for most tissue types and amenable for both NMR and hyphenated-MS techniques (Römisch-Margl et al. 2011). Most recently, Zukunft *et al*., developed a high throughput extraction method for a wide range of murine tissues, given the high incidence of mouse models being utilized in tissue metabolomics studies in the last 5 years (Zukunft et al. 2018). Optimization of extraction protocols were performed on over 10 different tissue types (*i.e.,* liver, kidney, skeletal muscle, adipose, brain, pituitary gland, lung, bone, adrenal glands, testes, ovaries) using three solvent systems (*i.e.,* methanol, phosphate buffer, and ethanol with phosphate buffer). In general, methanol and a mixture of ethanol with phosphate buffer provided high metabolite yields, for both hydrophilic (*e.g.,* amino acids, acylcarnitines) and lipid (*e.g.,* glycerophospholipids) metabolites, with good reproducibility (CV<15%) and ionization efficiency for most murine tissues (Zukunft et al. 2018).

Due to the invasive nature of tissue biopsies in humans, limited sample quantities are typically obtained (~60 – 120 mg wet weight) (Alves et al. 2015) and often need to be utilized for other "omics"-based platforms (*e.g.,* transcriptomics, proteomics) or clinical tests (*e.g.* histopathology, cytology). Therefore, nontargeted tissue metabolomics studies often face the challenge of achieving broad metabolite coverage with minimal tissue samples. Recent studies have developed standardized workflows to overcome this challenge by maximizing the amount of metabolite information from the same tissue. Vorkas *et al*., developed a pipeline for untargeted analysis using a simple extraction protocol to extract hydrophilic and lipid metabolites from the same arterial tissue to improve metabolome coverage while employing UPLC-MS as a single platform. The proposed workflow implements extensive QA/QC practices (*e.g.,* intermittent injections of pooled QCs and blank samples) while also employing unbiased LC-MS/MS acquisition during data acquisition to aid in unknown identification to permit simultaneous collection of

structural information while reducing analysis time. This work demonstrates recent developments in methodology that addresses gaps in tissue metabolomics studies (*i.e.,* need for multiple analytical platforms, limitations in sample quantities) that can be applied in future studies to achieve high data quality, broad metabolite coverage while minimizing false discoveries (Vorkas et al. 2015).

1.4 Thesis motivations and objectives: new innovations in biomarker discovery and tissue metabolomics

Metabolomics provides a unique approach for biomarker discover for early detection of treatable diseases of unknown etiology while also providing insights to the underlying mechanisms regarding disease pathophysiology. Biomarker discoveries in metabolomics have relied on surrogate biofluids (*e.g.,* plasma or serum) as a more convenient sample type for screening or testing in populations. Despite its less invasive sample collection, biofluids are non-organ specific reflecting numerous biochemical processes within organs throughout the body, which may complicate biological interpretations. Thus, metabolomics studies on tissue specimens are necessary in order to gain direct insights to the intracellular metabolic changes occurring at the direct site of the disease. In this context, the work in this thesis contributes to new innovations in biomarker discovery and tissue metabolomics using multiplexed separations with unique data workflows and stringent QC. The first part of this thesis focuses on the discovery of novel, putative blood-based biomarkers for population-based screening of high risk adults to NASH progression (*Chapter II*) as well as early detection of sarcopenia related muscle loss and function in high risk older adults (*Chapter III*). The second part of this thesis describes two unique tissue metabolomics studies. The first study involves characterizing the human skeletal muscle metabolome and matching fasting plasma specimens from a cohort of recreationally active males participating in standardized exercise trials following bicarbonate pre-treatment (*Chapter IV*). The second study involves the comprehensive characterization of murine placental

tissue from maternal dams fed a controlled diet during gestation to determine the role of biological sex on adaptive metabolic responses on placental function, fetal growth and development (*Chapter V*).

1.4.1 Multiplexed separations for serum γ-glutamyl-dipeptides in NASH patients

Nonalcoholic Fatty Acid Liver Disease (NAFLD) is a spectrum of liver diseases that has drastically increased in prevalence in Western populations due to the rise in the metabolic syndrome and insulin resistance (Benedict and Zhang 2017). While a majority of NAFLD patients exhibit mild forms of liver diseases, up to 30% often progress to severe forms of diseases such as non-alcoholic steatohepatitis (NASH), fibrosis and cirrhosis where irreversible liver damage can result (Angulo 2002). The pathogenesis is complex and multifactorial, contributed by genetic, epigenetic and environmental factors; however it remains largely unknown including its progression to NASH (Dowman et al. 2010). Thus, there is an urgent need to advance our understanding of NAFLD disease progression while elucidating its pathogenesis in order to identify disease severity in patients that are at higher risk for liver-associated morbidity and/or mortality (Rowe 2018). *Chapter II* presents a targeted, high throughput screening platform developed through an industrial collaboration with Human Metabolome Technologies (HMT) Inc. in Tsuruoka, Japan, for rapid screening of serum γ-glutamyl-dipeptides in NASH patients (n = 116, Age: 52 ± 15 years). Through rigorous method optimization and validation, this work demonstrates the utility of this multiplexed, metabolomics workflow in large scale metabolomics studies that incorporates extensive QA/QC practices to reduce bias and false discoveries while increasing sample throughput. Unsupervised pattern recognition methods (*i.e.*, HCA) revealed significant distinct NASH subgroups based on circulating the γ-glutamyl dipeptide levels, which were inversely correlated with serum γ-glutamyl glutamyltransferase (GGT) activity. Collectively, these findings suggested the key role of the γ-glutamyl dipeptide cycle

in the pathogenesis and progression of NASH that may provide better risk assessment of NASH patients who suffer from co-morbidities, while complementing current liver enzyme screens and histopathology.

1.4.2 Plasma metabolic phenotyping for assessing the impact of short-term step reduction in older adults

Sarcopenia is characterized as the involuntary loss of skeletal muscle mass, strength and function that occurs concurrently with aging around the fifth decade of life, at an annual rate of 1-2% (Janssen et al. 2002; Walston 2012; Ziaaldini et al. 2017). The onset and progression of sarcopenia is caused by multiple factors (*e.g.,* chronic inflammation, hormonal changes, malnutrition, prolonged physical inactivity) (Landi et al. 2015; Marty et al. 2017; Walston 2012), that elicit physiological and morphological changes in skeletal muscle structure and function (Shafiee et al. 2017; Ziaaldini et al. 2017). The progressive decline in muscle quality results in numerous adverse effects such as physical impairments (*e.g.*, disability and mobility disorders) and increases chronic disease risks (*e.g.,* type 2 diabetes), leading to an overall decline in the quality of life among the elderly (Shafiee et al. 2017; Ziaaldini et al. 2017), while placing a burden on medical resources. Evidently, there is an urgent need to implement public policies to develop preventatives strategies for sarcopenia progression, especially among increasing geriatric populations. However, the underlying molecular mechanisms associated with sarcopenia remain unclear. In *Chapter III*, nontargeted metabolite profiling was performed using multisegment injection-capillary electrophoresis-mass spectrometry (MSI-CE-MS) in a cohort of healthy older adults (n = 17, Age: 69±4 years) participating in a two week step reduction intervention (<1000 steps/day), followed by two weeks of recovery, returning to normal habitual activity. Repeated fasting plasma specimens were collected at baseline, after step reduction and following recovery. Short-term step reduction elicited increases in plasma metabolites associated with muscle energy metabolism (glutamine,

creatine, carnitine and deoxycarnitine) as a result of deceased myofibrillar protein synthesis, compared to baseline. Decreases in uremic toxins (indoxyl sulfate, andhippuric acid) and changes in glutathione precursors (oxoproline and methionine) were also observed with step reduction. Interestingly, these metabolites did not fully return to baseline levels following recovery. To the best of our knowledge, this is the first metabolomics study to report the impacts of acute physical inactivity in overweight/pre-diabetic older adults to elicit metabolic dysregulation to stimulate muscle disuse in a community setting less severe than prolonged bed rest or hospitalization. Our findings revealed important underlying metabolic pathways that advance our understanding of the pathophysiology of sarcopenia while providing putative markers for routine monitoring of sarcopenia progression in older adults.

1.4.3 Muscle metabolome characterization for assessing the impact of interval exercise and bicarbonate ingestion

Bicarbonate is an alkalinizing agent that has long been touted as a supplement to attenuate muscle fatigue and improve exercise performance and/or recovery (Carr et al. 2011; McNaughton et al. 2016; Shelton and Kumar 2010). Despite over 80 years of research efforts in assessing the effects of bicarbonate on strenuous exercise in human interventions, the precise mechanisms of action beyond blood pH and muscle bioenergetics remain to be fully elucidated (Carr et al. 2011). In *Chapter IV,* we employed two orthogonal analytical platforms for nontargeted metabolite profiling using MSI-CE-MS and targeted analysis of electrolytes (*e.g.,* potassium, sodium, magnesium, calcium) using CE with indirect UV detection to characterize mass-limited muscle tissue biopsies (≈ 2 mg fried mass) and paired plasma specimens from a cohort of healthy, active men (n =7, Age = 22 ± 2 years) participating in standardized interval exercise trials with and without oral bicarbonate pretreatment (0.4 g/kg body mass). In this double-blinded, placebo-controlled, cross-over study design, muscle tissue biopsies and matching plasma

specimens were collected at rest, post-exercise and recovery. A quantitative, tissue extraction protocol was first developed for mass-limited, lyophilized tissue (< 5 mg) in order to maximize metabolite recovery without deleterious oxidation or hydrolysis effects. Thereafter, characterization of the human skeletal muscle metabolome was achieved resulting in the identification and quantification of more than 80 polar/ionic metabolites (CV < 30%) were consistently detected in a majority (> 75%) of the samples. Complementary statistical methods revealed specific biomarkers associated with interval exercise and/or bicarbonate treatment responses. Our findings showed that bicarbonate ingestion prior to interval exercise elicited a modest treatment effect on metabolic pathways associated with ionic homeostasis (potassium), purine degradation (uric acid), glutathione metabolism (oxidized mixed disulfides) and histidine-containing dipeptide (anserine), that has previously been unreported within human skeletal muscle. This work is crucial in order to advance our basic understanding of acute alkalosis and its impact on the preservation of contracting muscle function during exercise-induced stress and metabolic acidosis. Moreover, this study emphasized the importance paired tissue and plasma specimens for gaining more holistic, deeper insights on skeletal muscle health.

1.4.4 Placental metabolome characterization for elucidating *in utero* sex specific adaptations

The placenta is a key metabolically, active organ that plays functional roles in nutrient delivery, gas exchange and fetal waste removal while providing insights to maternal and fetal interactions during gestation (Gabory et al. 2013). There is growing evidence suggesting that the biological sex associated with the placenta influences fetal responses to external stimuli *in utero* during pregnancy; many of which are mediated by placental genes, proteins and steroid pathways (Clifton 2010). However, the precise biochemical mechanisms associated with sex-specific adaptations to pregnancy and its link to placental function and fetal development

have yet to be elucidated. Herein, multisegment injection-capillary electrophoresis-mass spectrometry (MSI-CE-MS) was used as a multiplexed metabolomics platform to characterize maternal murine placental tissue (≈ 1-2 mg dried weight) in mice fed a controlled diet prior to and during gestation. Characterization of the placental metabolome resulted in more than 130 unique, polar/ionic and lipid metabolites that spanned a wide dynamic range. Overall, our findings revealed subtle differences in metabolic profiles between male (n = 14) and female (n = 14) placentae derived from the same control-fed maternal mice. Interestingly, metabolites involved in beta-oxidation (short-chain acylcarnitines) as well as purine degradation (uric acid) were increased in females compared to males. These findings will advance our understanding of how males and females elicit different metabolic adaptations in the placenta that may contribute to differences in placental function, fetal growth and development.

1.5 References

Aeffner, F., Wilson, K., Martin, N. T., Black, J. C., Hendriks, C. L. L., Bolon, B., et al. (2017). The gold standard paradox in digital image analysis: Manual versus automated scoring as ground truth. *Archives of Pathology and Laboratory Medicine*. *141*(9): 1267-1275. doi:10.5858/arpa.2016-0386-RA

Alonso, A., Marsal, S., & Julià, A. (2015). Analytical Methods in Untargeted Metabolomics: State of the Art in 2015 *Frontiers in Bioengineering and Biotechnology. 3*, 23. doi: 10.3389/fbioe.2015.00023

Alturkistani, H. A., Tashkandi, F. M., & Mohammedsaleh, Z. M. (2015). Histological Stains: A Literature Review and Case Study. *Global Journal of Health Science*. *8*(3): 72-79. doi:10.5539/gjhs.v8n3p72

Alves, R. D. A. M. A. M., Dane, A. D., Harms, A., Strassburg, K., Seifar, R. M., Verdijk, L. B., et al. (2015). Global profiling of the muscle metabolome: method optimization, validation and application to determine exercise-induced metabolic effects. *Metabolomics*, *11*(2), 271–285. doi:10.1007/s11306-014-0701-7

Angulo, P. (2002). Nonalcoholic Fatty Liver Disease. *New England Journal of Medicine*, *346*(16), 1221–1231. doi:10.1056/NEJMra011775

Ankerst, D. P., Liss, M., Zapata, D., Hoefler, J., Thompson, I. M., & Leach, R. J. (2015). A case control study of sarcosine as an early prostate cancer detection biomarker Urological oncology. *BMC Urology*. *15*, 99

doi:10.1186/s12894-015-0095-5

Balog, J., Sasi-Szabó, L., Kinross, J., Lewis, M. R., Muirhead, L. J., Veselkov, K., et al. (2013). Intraoperative tissue identification using rapid evaporative ionization mass spectrometry. *Science Translational Medicine*. 5(194), 194ra93. doi:10.1126/scitranslmed.3005623

Bathen, T. F., Geurts, B., Sitter, B., Fjøsne, H. E., Lundgren, S., Buydens, L. M., et al. (2013). Feasibility of MR Metabolomics for Immediate Analysis of Resection Margins during Breast Cancer Surgery. *PLoS ONE*. *8*(4), e61578. doi:10.1371/journal.pone.0061578

Beltran, A., Suarez, M., Rodríguez, M. A., Vinaixa, M., Samino, S., Arola, L., et al. (2012). Assessment of compatibility between extraction methods for NMR- and LC/MS-based metabolomics. *Analytical Chemistry*, *84*(14), 5838–5844. doi:10.1021/ac3005567

Ben-Yehuda, D., Polliack, A., Okon, E., Sherman, Y., Fields, S., Lebenshart, P., et al. (1996). Image-guided core-needle biopsy in malignant lymphoma: Experience with 100 patients that suggests the technique is reliable. *Journal of Clinical Oncology*. *14*(9), 2431-2434. doi:10.1200/JCO.1996.14.9.2431

Benedict, M., & Zhang, X. (2017). Non-alcoholic fatty liver disease: An expanded review. *World Journal of Hepatology*. *9*(16), 715-732. doi:10.4254/wjh.v9.i16.715

Benton, H. P., Wong, D. M., Trauger, S. A., & Siuzdak, G. (2008). XCMS2: Processing tandem mass spectrometry data for metabolite identification and structural characterization. *Analytical Chemistry*. *80*(16)*, 6382-6389.* doi:10.1021/ac800795f

Bichat, X. (1977). *Recherches physiologiques sur la vie et la mort. Recherches physiologiques sur la vie et la mort.* New York: Arno Press. doi:10.5962/bhl.title.33811

Bijkerk, R., Aleksinskaya, M. A., Duijs, J. M. G. J., Veth, J., Husen, B., Reiche, D., et al. (2019). Neutral endopeptidase inhibitors blunt kidney fibrosis by reducing myofibroblast formation. *Clinical Science*. *133*(2), 239-252. doi:10.1042/cs20180882

Böcker, S., & Rasche, F. (2008). Towards de novo identification of metabolites by analyzing tandem mass spectra. *Bioinformatics*. *24*(16)*, i49-i55.* doi:10.1093/bioinformatics/btn270

Bothwell, J. H. F., & Griffin, J. L. (2011). An introduction to biological nuclear magnetic resonance spectroscopy. *Biological Reviews*. *86*(2): 493-510. doi:10.1111/j.1469-185X.2010.00157.x

Broadhurst, D., Goodacre, R., Reinke, S. N., Kuligowski, J., Wilson, I. D., Lewis, M. R., & Dunn, W. B. (2018). Guidelines and considerations for the use of system suitability and quality control samples in mass spectrometry assays applied in untargeted clinical metabolomic studies. *Metabolomics*. *14*, 72 doi:10.1007/s11306-018-1367-3

Broadhurst, D. I., & Kell, D. B. (2006). Statistical strategies for avoiding false discoveries in metabolomics and related experiments. *Metabolomics*. *2*(4),

171-196. doi:10.1007/s11306-006-0037-z

Bujak, R., Struck-Lewicka, W., Markuszewski, M. J., & Kaliszan, R. (2014). Metabolomics for laboratory diagnostics. *Journal of Pharmaceutical and Biomedical Analysis*. *113*, 108-120. doi:10.1016/j.jpba.2014.12.017

Burns, M. A., He, W., Wu, C. L., & Cheng, L. L. (2004). Quantitative pathology in tissue MR spectroscopy based human prostate metabolomics. *Technology in Cancer Research and Treatment*. *3*(6), 591-598. doi:10.1177/153303460400300609

Carr, A. J., Hopkins, W. G., Gore, C. J., & Carr, A.J., Hopkins, W.G., Gore, C. J. (2011). Effects of acute alkalosis and acidosis on performance: a meta-analysis. *Sports Med.*, *41*(10), 801–814. doi:10.2165/11591440-000000000-00000

Castillo, S., Gopalacharyulu, P., Yetukuri, L., & Orešič, M. (2011). Algorithms and tools for the preprocessing of LC-MS metabolomics data. *Chemometrics and Intelligent Laboratory Systems*. *108*(1), 23-32. doi:10.1016/j.chemolab.2011.03.010

Chen, W., Lu, S., Wang, G., Chen, F., & Bai, C. (2017). Staging research of human lung cancer tissues by high-resolution magic angle spinning proton nuclear magnetic resonance spectroscopy (HRMAS 1 H NMR) and multivariate data analysis. *Asia-Pacific Journal of Clinical Oncology*. *13*(5), e232-e238. doi:10.1111/ajco.12598

Cheng, L. L., Lean, C. L., Bogdanova, A., Wright, S. C., Ackerman, J. L., Brady, T. J., & Garrido, L. (1996). Enhanced resolution of proton NMR spectra of malignant lymph nodes using magic-angle spinning. *Magnetic Resonance in Medicine*. *36*(5), 653-658. doi:10.1002/mrm.1910360502

Clasquin, M. F., Melamud, E., & Rabinowitz, J. D. (2012). LC-MS data processing with MAVEN: A metabolomic analysis and visualization engine. *Current Protocols in Bioinformatics*. *37*(1). doi:10.1002/0471250953.bi1411s37

Clendinen, C. S., Monge, M. E., & Fernández, F. M. (2017). Ambient mass spectrometry in metabolomics. *Analyst*. *142*(17), 3101-3117. doi:10.1039/c7an00700k

Clifton, V. L. (2010). Review: Sex and the Human Placenta: Mediating Differential Strategies of Fetal Growth and Survival. *Placenta*, *31*(SUPPL.), S33-S39. doi:10.1016/j.placenta.2009.11.010

Comanescu, M., Annaratone, L., D'Armento, G., Cardos, G., Sapino, A., & Bussolati, G. (2012). Critical steps in tissue processing in histopathology. *Recent patents on DNA & gene sequences*. *6*(1), 22-32.

De Vogel, S., Ulvik, A., Meyer, K., Ueland, P. M., Nygård, O., Vollset, S. E., et al. (2014). Sarcosine and other metabolites along the choline oxidation pathway in relation to prostate cancer - A large nested case-control study within the JANUS cohort in Norway. *International Journal of Cancer*. *134*(1), 197-206. doi:10.1002/ijc.28347

Diamandis, E. P. (2012). The failure of protein cancer biomarkers to reach the

clinic: why, and what can be done to address the problem? *BMC Medicine*. *10*, 87. doi:10.1186/1741-7015-10-87

DiBattista, A., McIntosh, N., Lamoureux, M., Al-Dirbashi, O. Y., Chakraborty, P., & Britz-Mckibbin, P. (2019). Metabolic Signatures of Cystic Fibrosis Identified in Dried Blood Spots for Newborn Screening Without Carrier Identification. *Journal of Proteome Research*, *18*(3), 841–854. doi:10.1021/acs.jproteome.8b00351

Dinges, S. S., Vandergrift, L. A., Wu, S., Berker, Y., Habbel, P., Taupitz, M., et al. (2019). Metabolomic prostate cancer fields in HRMAS MRS-profiled histologically benign tissue vary with cancer status and distance from cancer. *NMR in Biomedicine*. e4038. doi:10.1002/nbm.4038

Dowman, J. K., Tomlinson, J. W., & Newsome, P. N. (2010). Pathogenesis of non-alcoholic fatty liver disease. *Q J Med*, *103*(2), 71–83. doi:10.1093/qjmed/hcp158

Draper, J., Enot, D. P., Parker, D., Beckmann, M., Snowdon, S., Lin, W., & Zubair, H. (2009). Metabolite signal identification in accurate mass metabolomics data with MZedDB, an interactive m/z annotation tool utilising predicted ionisation behaviour "rules." *BMC Bioinformatics*. *10*, 27. doi:10.1186/1471-2105-10-227

Dudzik, D., Barbas-Bernardos, C., García, A., & Barbas, C. (2018). Quality assurance procedures for mass spectrometry untargeted metabolomics. a review. *Journal of Pharmaceutical and Biomedical Analysis*. *147*, 149-173. doi:10.1016/j.jpba.2017.07.044

Dunn, W. B. (2008). Current trends and future requirements for the mass spectrometric investigation of microbial, mammalian and plant metabolomes. *Physical Biology*. *5*(1), 011001.doi:10.1088/1478-3975/5/1/011001

Dunn, W. B., Broadhurst, D., Begley, P., Zelena, E., Francis-Mcintyre, S., Anderson, N., et al. (2011). Procedures for large-scale metabolic profiling of serum and plasma using gas chromatography and liquid chromatography coupled to mass spectrometry. *Nature Protocols*. *6*(7), 1060-1083. doi:10.1038/nprot.2011.335

Dunn, W. B., Broadhurst, D. I., Atherton, H. J., Goodacre, R., & Griffin, J. L. (2011). Systems level studies of mammalian metabolomes: the roles of mass spectrometry and nuclear magnetic resonance spectroscopy. *Chemical Society reviews*. *40*(1), 387-426. doi:10.1039/b906712b

Dunn, W. B., & Ellis, D. I. (2005). Metabolomics: Current analytical platforms and methodologies. *TrAC - Trends in Analytical Chemistry*. *24*(4), 285-294. doi:10.1016/j.trac.2004.11.021

Dunn, W. B., Erban, A., Weber, R. J. M., Creek, D. J., Brown, M., Breitling, R., et al. (2013). Mass appeal: Metabolite identification in mass spectrometry-focused untargeted metabolomics. *Metabolomics*, *9*(SUPPL.1), 44–66. doi:10.1007/s11306-012-0434-4

Dunn, W. B., Wilson, I. D., Nicholls, A. W., & Broadhurst, D. (2012). The importance of experimental design and QC samples in large-scale and MS-

driven untargeted metabolomic studies of humans. *Bioanalysis*. *4*(18), 2249-2264. doi:10.4155/bio.12.204

Eberlin, L. S., Norton, I., Orringer, D., Dunn, I. F., Liu, X., Ide, J. L., et al. (2013). Ambient Mass Spectrometry for the Intraoperative Molecular Diagnosis of Human Brain Tumors. *Proceedings of the National Academy of Sciences*, *110*(5), 1611–6. doi:10.1227/01.neu.0000428422.82081.62

Fuhrer, T., & Zamboni, N. (2015). High-throughput discovery metabolomics. *Current Opinion in Biotechnology*. *31*, 73-78. doi:10.1016/j.copbio.2014.08.006

Gabory, A., Ferry, L., Fajardy, I., Jouneau, L., Gothié, J. D., Vigé, A., et al. (2012). Maternal Diets Trigger Sex-Specific Divergent Trajectories of Gene Expression and Epigenetic Systems in Mouse Placenta. *PLoS ONE*, *7*(11), e47986. doi:10.1371/journal.pone.0047986

Gabory, A., Roseboom, T. J., Moore, T., Moore, L. G., & Junien, C. (2013). Placental contribution to the origins of sexual dimorphism in health and diseases: Sex chromosomes and epigenetics. *Biology of Sex Differences*. *4*(1), 5. doi:10.1186/2042-6410-4-5

Garvey, S. M., Dugle, J. E., Kennedy, A. D., McDunn, J. E., Kline, W., Guo, L., et al. (2014). Metabolomic profiling reveals severe skeletal muscle group-specific perturbations of metabolism in aged FBN rats. *Biogerontology*. *15*(3), 217-232. doi:10.1007/s10522-014-9492-5

Geier, F. M., Want, E. J., Leroi, A. M., & Bundy, J. G. (2011). Cross-platform comparison of caenorhabditis elegans tissue extraction strategies for comprehensive metabolome coverage. *Analytical Chemistry*. *83*(10), 3730-3736. doi:10.1021/ac2001109

German, J. B., Pan, H., Reifsnyder, P. R., Leiter, E. H., & Watkins, S. M. (2002). Lipid metabolome-wide effects of the PPARγ agonist rosiglitazone. *Journal of Lipid Research*. *43*(11), 1809-1817. doi:10.1194/jlr.m200169-jlr200

Gharib, H., Goellner, J. R., & Johnson, D. A. (1993). Fine-needle aspiration cytology of the thyroid. A 12-year experience with 11,000 biopsies. *Clinics in laboratory medicine*. *13*(3), 699-709.

Giavalisco, P., Hummel, J., Lisec, J., Inostroza, A. C., Catchpole, G., & Willmitzer, L. (2008). High-resolution direct infusion-based mass spectrometry in combination with whole13C metabolome isotope labeling allows unambiguous assignment of chemical sum formulas. *Analytical Chemistry*. *80*(24), 9417-9425. doi:10.1021/ac8014627

Giavalisco, P., Köhl, K., Hummel, J., Seiwert, B., & Willmitzer, L. (2009). 13C isotope-labeled metabolomes allowing for improved compound annotation and relative quantification in liquid chromatography-mass spectrometry-based metabolomic research. *Analytical Chemistry*. *81*(15), 6546-6551. doi:10.1021/ac900979e

Gika, H. G., Macpherson, E., Theodoridis, G. A., & Wilson, I. D. (2008). Evaluation of the repeatability of ultra-performance liquid chromatography-TOF-MS for global metabolic profiling of human urine samples. *Journal of*

Chromatography B: Analytical Technologies in the Biomedical and Life Sciences. *871*(2), 299-305. doi:10.1016/j.jchromb.2008.05.048

Gonzalez-Riano, C., Garcia, A., & Barbas, C. (2016). Metabolomics studies in brain tissue: A review. *Journal of Pharmaceutical and Biomedical Analysis*, *130*, 141–168. doi:10.1016/j.jpba.2016.07.008

Gonzalez-Riano, C., Tapia-González, S., García, A., Muñoz, A., DeFelipe, J., & Barbas, C. (2017). Metabolomics and neuroanatomical evaluation of post-mortem changes in the hippocampus. *Brain Structure and Function*. *222*(6), 2831-2853. doi:10.1007/s00429-017-1375-5

Goodacre, R. (2005). Metabolomics - The way forward. *Metabolomics*, *1*(1), 1–2. doi:10.1007/s11306-005-1111-7

Gress, F., Gottlieb, K., Sherman, S., & Lehman, G. (2001). Endoscopic ultrasonography-guided fine-needle aspiration biopsy of suspected pancreatic cancer. *Annals of Internal Medicine*. *134*(5), 459-464. doi:10.7326/0003-4819-134-6-200103200-00010

Guenther, S., Muirhead, L. J., Speller, A. V. M., Golf, O., Strittmatter, N., Ramakrishnan, R., et al. (2015). Spatially resolved metabolic phenotyping of breast cancer by desorption electrospray ionization mass spectrometry. *Cancer Research*.*75*(9), 1828-1837. doi:10.1158/0008-5472.CAN-14-2258

Haigh, E. (1984). *Xavier Bichat and the Medical Theory of the Eighteenth Century*. London: Wellcome Institute for the History of Medicine.

Hatazawa, Y., Senoo, N., Tadaishi, M., Ogawa, Y., Ezaki, O., Kamei, Y., & Miura, S. (2015). Metabolomic analysis of the skeletal muscle mice overexpressing PGC-1α. *PLoS ONE*. *10*(6), e0129084. :10.1371/journal.pone.0129084

Haukaas, T. H., Euceda, L. R., Giskeødegård, G. F., Lamichhane, S., Krohn, M., Jernström, S., et al. (2016). Metabolic clusters of breast cancer in relation to gene- and protein expression subtypes. *Cancer and Metabolism*. 4,12 doi:10.1186/s40170-016-0152-x

Heinonen, M., Rantanen, A., Mielikäinen, T., Kokkonen, J., Kiuru, J., Ketola, R. A., & Rousu, J. (2008). FiD: A software for ab initio structural identification of product ions from tandem mass spectrometric data. *Rapid Communications in Mass Spectrometry*. *22*(19), 3043-3052. doi:10.1002/rcm.3701

Heinonen, M., Shen, H., Zamboni, N., & Rousu, J. (2012). Metabolite identification and molecular fingerprint prediction through machine learning. *Bioinformatic*s. *28*(18), 2333-2341. doi:10.1093/bioinformatics/bts437

Hendriks, M. M. W. B. W. B., Eeuwijk, F. A. va. Van, Jellema, R. H., Westerhuis, J. a., Reijmers, T. H., Hoefsloot, H. C. J. J., & Smilde, A. K. (2011). Data-processing strategies for metabolomics studies. *TrAC - Trends in Analytical Chemistry*, *30*(10), 1685–1698. doi:10.1016/j.trac.2011.04.019

Hiraoka, K., Nishidate, K., Mori, K., Asakawa, D., & Suzuki, S. (2007). Development of probe electrospray using a solid needle. *Rapid Communications in Mass Spectrometry*. *21*(18), 3139-3144.

doi:10.1002/rcm.3201
Holmes, E., Wijeyesekera, A., Taylor-Robinson, S. D., & Nicholson, J. K. (2015). The promise of metabolic phenotyping in gastroenterology and hepatology. *Nature Reviews Gastroenterology and Hepatology*. *12*(8), 458-471. doi:10.1038/nrgastro.2015.114
Hrydziuszko, O., & Viant, M. R. (2012). Missing values in mass spectrometry based metabolomics: An undervalued step in the data processing pipeline. *Metabolomics. 8*(1), 161-174. doi:10.1007/s11306-011-0366-4
Huan, T., Tang, C., Li, R., Shi, Y., Lin, G., & Li, L. (2015). MyCompoundID MS/MS Search: Metabolite Identification Using a Library of Predicted Fragment-Ion-Spectra of 383,830 Possible Human Metabolites. *Analytical Chemistry. 87*(20), 10619-10626. doi:10.1021/acs.analchem.5b03126
Huang, C.-C., Lin, W.-T., Hsu, F.-L., Tsai, P.-W., & Hou, C.-C. (2009). Metabolomics investigation of exercise-modulated changes in metabolism in rat liver after exhaustive and endurance exercises. *European Journal of Applied Physiology*, *108*(3), 557–566. doi:10.1007/s00421-009-1247-7
Huang, Q., Tan, Y., Yin, P., Ye, G., Gao, P., Lu, X., et al. (2013). Metabolic characterization of hepatocellular carcinoma using nontargeted tissue metabolomics. *Cancer Research*. *73*(16), 4992-5002. doi:10.1158/0008-5472.CAN-13-0308
Hufsky, F., Scheubert, K., & Böcker, S. (2014). Computational mass spectrometry for small-molecule fragmentation. *TrAC - Trends in Analytical Chemistry*. 53, 41-48. doi:10.1016/j.trac.2013.09.008
Ioannidis, J. P. A. (2007). Why most published research findings are false: Author's reply to Goodman and Greenland [7]. *PLoS Medicine*. *2(*8), e124. doi:10.1371/journal.pmed.0040215
Jankevics, A., Merlo, M. E., de Vries, M., Vonk, R. J., Takano, E., & Breitling, R. (2012). Separating the wheat from the chaff: A prioritisation pipeline for the analysis of metabolomics datasets. *Metabolomics*. *8*(Suppl1), 29-36. doi:10.1007/s11306-011-0341-0
Janssen, I., Heymsfield, S. B., & Ross, R. (2002). Low relative skeletal muscle mass (sarcopenia) in older persons is associated with functional impairment and physical disability. *Journal of the American Geriatrics Society*. *50*(5), 889-896.
Jentzmik, F., Stephan, C., Miller, K., Schrader, M., Erbersdobler, A., Kristiansen, G., et al. (2010). Sarcosine in Urine after Digital Rectal Examination Fails as a Marker in Prostate Cancer Detection and Identification of Aggressive Tumours. *European Urology*. *59*(1), 12-18. doi:10.1016/j.eururo.2010.01.035
Johnson, C. H., Ivanisevic, J., & Siuzdak, G. (2016). Metabolomics: beyond biomarkers and towards mechanisms. *Nature reviews. Molecular cell biology*. *17*(7), 451-459. doi:10.1038/nrm.2016.25
Johnson, W. E., Li, C., & Rabinovic, A. (2007). Adjusting batch effects in microarray expression data using empirical Bayes methods. *Biostatistics*,

8(1), 118–127. doi:10.1093/biostatistics/kxj037

Jung, J. W., Lee, M. S., Choi, H.-J., Jung, S., Lee, Y.-J., Hwang, G.-S., & Kwon, T.-H. (2016). Mass spectrometric imaging of metabolites in kidney tissues from rats treated with furosemide. *American Journal of Physiology-Renal Physiology*. *310*(11), F1317-F1327. doi:10.1152/ajprenal.00524.2015

Kind, T., & Fiehn, O. (2007). Seven Golden Rules for heuristic filtering of molecular formulas obtained by accurate mass spectrometry. *BMC Bioinformatics*. *8*, 105. doi:10.1186/1471-2105-8-105

Kleiner, D. E., Brunt, E. M., Van Natta, M., Behling, C., Contos, M. J., Cummings, O. W., et al. (2005). Design and validation of a histological scoring system for nonalcoholic fatty liver disease. *Hepatology*, *41*(6), 1313–1321. doi:10.1002/hep.20701

Kuehnbaum, N. L., & Britz-McKibbin, P. (2013). New Advances in Separation Science for Metabolomics: Resolving Chemical Diversity in a Post-Genomic Era. *Chemical Reviews*. *113*(4), 2437-2468. doi:10.1021/cr300484s

Kun, M. (1847). A new instrument for the diagnosis of tumours. *Month J Med Sci*, *7*, 853–853.

Landi, F., Calvani, R., Cesari, M., Tosato, M., Martone, A. M., Bernabei, R., et al. (2015). Sarcopenia as the Biological Substrate of Physical Frailty. *Clinics in Geriatric Medicine*, *31*(3), 367–374. doi:10.1016/j.cger.2015.04.005

Lewis, M. R., Pearce, J. T. M., Spagou, K., Green, M., Dona, A. C., Yuen, A. H. Y., et al. (2016). Development and Application of Ultra-Performance Liquid Chromatography-TOF MS for Precision Large Scale Urinary Metabolic Phenotyping. *Analytical Chemistry*. *88*(18), 9004-9013. doi:10.1021/acs.analchem.6b01481

Lieblein-Boff, J. C., Johnson, E. J., Kennedy, A. D., Lai, C. S., & Kuchan, M. J. (2015). Exploratory metabolomic analyses reveal compounds correlated with lutein concentration in frontal cortex, hippocampus, and occipital cortex of human infant brain. *PLoS ONE*. *10*(8), e0136904. doi:10.1371/journal.pone.0136904

Liland, K. H. (2011). Multivariate methods in metabolomics - from pre-processing to dimension reduction and statistical analysis. *TrAC - Trends in Analytical Chemistry*. *30*(6), 827-841. doi:10.1016/j.trac.2011.02.007

Lin, C. Y., Wu, H., Tjeerdema, R. S., & Viant, M. R. (2007). Evaluation of metabolite extraction strategies from tissue samples using NMR metabolomics. *Metabolomics*, *3*(1), 55–67. doi:10.1007/s11306-006-0043-1

Lin, Y., Ma, C., Bezabeh, T., Wang, Z., Liang, J., Huang, Y., et al. (2019). 1 H NMR-based metabolomics reveal overlapping discriminatory metabolites and metabolic pathway disturbances between colorectal tumor tissues and fecal samples. *International Journal of Cancer*. doi:10.1002/ijc.32190

Lommen, A. (2014). Ultrafast PubChem searching combined with improved filtering rules for elemental composition analysis. *Analytical Chemistry*. *86*(11), 5463-5469. doi:10.1021/ac500667h

Łukasiewicz, E., Ziemiecka, A., Jakubowski, W., Vojinovic, J., Bogucevska, M.,

& Dobruch-Sobczak, K. (2017). Fine-needle versus core-needle biopsy – which one to choose in preoperative assessment of focal lesions in the breasts? Literature review. *Journal of Ultrasonography. 17*(71), 267-274. doi:10.15557/JoU.2017.0039

Ly, A., Ono, J. C., Hughes, K. S., Pitman, M. B., & Balassanian, R. (2016). Fine-needle aspiration biopsy of palpable breast masses: Patterns of clinical use and patient experience. *Journal of the National Comprehensive Cancer Network. 14*(5), 527-536. doi:10.6004/jnccn.2016.0061

Macedo, A. N., Mathiaparanam, S., Brick, L., Keenan, K., Gonska, T., Pedder, L., et al. (2017). The Sweat Metabolome of Screen-Positive Cystic Fibrosis Infants: Revealing Mechanisms beyond Impaired Chloride Transport. *ACS Central Science*, *3*(8), 904–913. doi:10.1021/acscentsci.7b00299

Martin, H. E., & Ellis, E. B. (1930). Biopsy by Needle Puncture and Aspiration. *Ann Surg*, *92*, 169–81. doi:10.3322/canjclin.36.2.71

Marty, E., Liu, Y., Samuel, A., Or, O., & Lane, J. (2017). A review of sarcopenia: Enhancing awareness of an increasingly prevalent disease. *Bone*. *105,* 276-286. doi:10.1016/j.bone.2017.09.008

Masson, P., Alves, A. C., Ebbels, T. M. D. D., Nicholson, J. K., & Want, E. J. (2010). Optimization and evaluation of metabolite extraction protocols for untargeted metabolic profiling of liver samples by UPLC-MS. *Analytical chemistry*, *82*(18), 7779–86. doi:10.1021/ac101722e

Masson, P., Spagou, K., Nicholson, J. K., & Want, E. J. (2011). Technical and biological variation in UPLC-MS-based untargeted metabolic profiling of liver extracts: Application in an experimental toxicity study on galactosamine. *Analytical Chemistry. 83*(3), 1116-1123. doi:10.1021/ac103011b

McNaughton, L. R., Gough, L., Deb, S., Bentley, D., & Sparks, S. A. (2016). Recent Developments in the Use of Sodium Bicarbonate as an Ergogenic Aid. *Current Sports Medicine Reports*, *15*(4), 233–244. doi:10.1249/JSR.0000000000000283

Melamud, E., Vastag, L., & Rabinowitz, J. D. (2010). Metabolomic analysis and visualization engine for LC - MS data. *Analytical Chemistry. 82*(23), 9818-9826. doi:10.1021/ac1021166

Meller, S., Meyer, H.-A., Bethan, B., Dietrich, D., Maldonado, S. G., Lein, M., et al. (2015). Integration of tissue metabolomics, transcriptomics and immunohistochemistry reveals *ERG*- and gleason score-specific metabolomic alterations in prostate cancer. *Oncotarget*. *7*(2), 1421-1438. doi:10.18632/oncotarget.6370

Meyer, J. E., Smith, D. N., Lester, S. C., Kaelin, C., DiPiro, P. J., Denison, C. M., et al. (1999). Large-core needle biopsy of nonpalpable breast lesions. *Journal of the American Medical Association*. *281*(17), 1638-1641. doi:10.1001/jama.281.17.1638

More, T. H., RoyChoudhury, S., Christie, J., Taunk, K., Mane, A., Santra, M. K., et al. (2017). Metabolomic alterations in invasive ductal carcinoma of breast:

A comprehensive metabolomic study using tissue and serum samples. *Oncotarget*. *9(*2), 2678-2696. doi:10.18632/oncotarget.23626

Nassar, A. (2011). Core needle biopsy versus fine needle aspiration biopsy in breast-A historical perspective and opportunities in the modern era. *Diagnostic Cytopathology*. *39*(5), 380-388. doi:10.1002/dc.21433

Nemes, P., & Vertes, A. (2007). Laser ablation electrospray ionization for atmospheric pressure, in vivo, and imaging mass spectrometry. *Analytical Chemistry*. *79*(21), 8098-8106. doi:10.1021/ac071181r

Nielsen, N. P. V., Carstensen, J. M., & Smedsgaard, J. (1998). Aligning of single and multiple wavelength chromatographic profiles for chemometric data analysis using correlation optimised warping. *Journal of Chromatography A*. doi:10.1016/S0021-9673(98)00021-1

Ogata, H., Goto, S., Sato, K., Fujibuchi, W., Bono, H., & Kanehisa, M. (1999). KEGG: Kyoto encyclopedia of genes and genomes. *Nucleic Acids Research*. *805*(1-2), 17-35. doi:10.1093/nar/27.1.29

Padia, S. A., Baker, M. E., Schaeffer, C. J., Remer, E. M., Obuchowski, N. A., Winans, C., & Herts, B. R. (2009). Safety and efficacy of sonographic-guided random real-time core needle biopsy of the liver. *37(*3), 138-143. *Journal of Clinical Ultrasound*. doi:10.1002/jcu.20553

Paine, M. R. L., Kim, J., Bennett, R. V., Parry, R. M., Gaul, D. A., Wang, M. D., et al. (2016). Whole reproductive system non-negative matrix factorization mass spectrometry imaging of an early-stage ovarian cancer mouse model. *PLoS ONE*. *11*(5), e0154837. doi:10.1371/journal.pone.0154837

Patti, G. J., Yanes, O., & Siuzdak, G. (2012). Innovation: Metabolomics: the apogee of the omics trilogy. *Nature reviews. Molecular cell biology*, *13*(4), 263–9. doi:10.1038/nrm3314

Pravdova, V., Walczak, B., & Massart, D. L. (2002). A comparison of two algorithms for warping of analytical signals. *Analytica Chimica Acta*. *456*(1), 77-92. doi:10.1016/S0003-2670(02)00008-9

Rasche, F., Svatoš, A., Maddula, R. K., Böttcher, C., & Böcker, S. (2011). Computing fragmentation trees from tandem mass spectrometry data. *Analytical Chemistry*. *83*(4), 1243-1251. doi:10.1021/ac101825k

Römisch-Margl, W., Prehn, C., Bogumil, R., Röhring, C., Suhre, K., & Adamski, J. (2011). Procedure for tissue sample preparation and metabolite extraction for high-throughput targeted metabolomics. *Metabolomics*, *8*(1), 133–142. doi:10.1007/s11306-011-0293-4

Rosa, M. (2008). Fine-needle aspiration biopsy: A historical overview. *Diagnostic Cytopathology*, *36*(11), 773–775. doi:10.1002/dc.20915

Rowe, I. A. (2018). Too much medicine: overdiagnosis and overtreatment of non-alcoholic fatty liver disease. *The Lancet Gastroenterology and Hepatology*. *3*(1), 66-72. doi:10.1016/S2468-1253(17)30142-5

Saccenti, E., Hoefsloot, H. C. J., Smilde, A. K., Westerhuis, J. a., & Hendriks, M. M. W. B. (2014). Reflections on univariate and multivariate analysis of metabolomics data. *Metabolomics*, *10*(3), 361–374. doi:10.1007/s11306-013-

0598-6
Sangster, T., Major, H., Plumb, R., Wilson, A. J., & Wilson, I. D. (2006). A pragmatic and readily implemented quality control strategy for HPLC-MS and GC-MS-based metabonomic analysis. *Analyst*. *131*(10), 1075-1078. doi:10.1039/b604498k
Satoh, K., Yachida, S., Sugimoto, M., Oshima, M., Nakagawa, T., Akamoto, S., et al. (2017). Global metabolic reprogramming of colorectal cancer occurs at adenoma stage and is induced by MYC. *Proceedings of the National Academy of Sciences*. *114*(37), E7697-E7706. doi:10.1073/pnas.1710366114
Schalken, J. A. (2010). Is Urinary Sarcosine Useful to Identify Patients With Significant Prostate Cancer? The Trials and Tribulations of Biomarker Development. *European Urology*. *58*(1), 19-20. doi:10.1016/j.eururo.2010.02.025
Scheltema, R. A., Kamleh, A., Wildridge, D., Ebikeme, C., Watson, D. G., Barrett, M. P., et al. (2008). Increasing the mass accuracy of high-resolution LC-MS data using background ions - A case study on the LTQ-Orbitrap. *Proteomics*. *8*(22), 4647-4656. doi:10.1002/pmic.200800314
Shafiee, G., Keshtkar, A., Soltani, A., Ahadi, Z., Larijani, B., & Heshmat, R. (2017). Prevalence of sarcopenia in the world: A systematic review and meta- analysis of general population studies. *Journal of Diabetes and Metabolic Disorders*. 16, 21. doi:10.1186/s40200-017-0302-x
Shelton, J., & Kumar, G. V. P. (2010). Sodium Bicarbonate—A Potent Ergogenic Aid? *Food and Nutrition Sciences*, *1*(1), 1–4. doi:10.4236/fns.2010.11001
Shrestha, B., Nemes, P., Nazarian, J., Hathout, Y., Hoffman, E. P., & Vertes, A. (2010). Direct analysis of lipids and small metabolites in mouse brain tissue by AP IR-MALDI and reactive LAESI mass spectrometry. *Analyst*. *135*(4), 751-758. doi:10.1039/b922854c
Singhal, N. K., Huang, H., Li, S., Clements, R., Gadd, J., Daniels, A., et al. (2017). The neuronal metabolite NAA regulates histone H3 methylation in oligodendrocytes and myelin lipid composition. *Experimental Brain Research. 235*(1), 279-292. doi:10.1007/s00221-016-4789-z
Smith, C. A., O'Maille, G., Want, E. J., Qin, C., Trauger, S. A., Brandon, T. R., et al. (2005). METLIN: a metabolite mass spectral database. *Therapeutic drug monitoring*. *26*(6), 747-751.
Smith, C. A., Want, E. J., O'Maille, G., Abagyan, R., & Siuzdak, G. (2006). XCMS: Processing mass spectrometry data for metabolite profiling using nonlinear peak alignment, matching, and identification. *Analytical Chemistry*. *78*(3), 779-787. doi:10.1021/ac051437y
Sreekumar, A., Poisson, L. M., Rajendiran, T. M., Khan, A. P., Cao, Q., Yu, J., et al. (2009). Metabolomic profiles delineate potential role for sarcosine in prostate cancer progression. *Nature*. *457*(7231), 910-914. doi:10.1038/nature07762
Storey, J. D., & Tibshirani, R. (2003). Statistical significance for genomewide studies. *Proceedings of the National Academy of Sciences*. *100*(16), 9440-

9445. doi:10.1073/pnas.1530509100
Takáts, Z., Wiseman, J. M., Gologan, B., & Cooks, R. G. (2004). Mass spectrometry sampling under ambient conditions with desorption electrospray ionization. *Science*. *306*(5695), 471-473. doi:10.1126/science.1104404
Tang, L., Zeng, J., Geng, P., Fang, C., Wang, Y., Sun, M., et al. (2018). Global metabolic profiling identifies a pivotal role of proline and hydroxyproline metabolism in supporting hypoxic response in hepatocellular carcinoma. *Clinical Cancer Research*. *24*(2), 474-485. doi:10.1158/1078-0432.CCR-17-1707
Tarnopolsky, M. A., Pearce, E., Smith, K., & Lach, B. (2011). Suction-modified Bergstrom muscle biopsy technique: experience with 13, 500 procedures. *Muscle Nerve*, *43*(5), 717–725. doi:10.1002/mus.21945
Tate, A. R., Foxall, P. J. D., Holmes, E., Moka, D., Spraul, M., Nicholson, J. K., & Lindon, J. C. (2000). Distinction between normal and renal cell carcinoma kidney cortical biopsy samples using pattern recognition of 1H magic angle spinning (MAS) NMR spectra. *NMR in Biomedicine. 13*(2), 64-71.
Titford, M. (2014). Progress in the Development of Microscopical Techniques for Diagnostic Pathology. *Journal of Histotechnology*. *32(*1), 9-19. doi:10.1179/his.2009.32.1.9
Trygg, J., & Wold, S. (2002). Orthogonal projections to latent structures (O-PLS). *Journal of Chemometrics*. *16*(3) doi:10.1002/cem.695
Tsang, T. M., Griffin, J. L., Haselden, J., Fish, C., & Holmes, E. (2005). Metabolic characterization of distinct neuroanatomical regions in rats by magic angle spinning 1H nuclear magnetic resonance spectroscopy. *Magnetic Resonance in Medicine*. *53*(5), 1018-1024. doi:10.1002/mrm.20447
van den Berg, R. A., Hoefsloot, H. C. J., Westerhuis, J. A., Smilde, A. K., & van der Werf, M. J. (2006). Centering, scaling, and transformations: improving the biological information content of metabolomics data. *BMC genomics*, *7*, 142. doi:10.1186/1471-2164-7-142
Vandergrift, L. A., Decelle, E. A., Kurth, J., Wu, S., Fuss, T. L., Defeo, E. M., et al. (2018). Metabolomic Prediction of Human Prostate Cancer Aggressiveness: Magnetic Resonance Spectroscopy of Histologically Benign Tissue. *Scientific Reports*. *8*(1), 4997. doi:10.1038/s41598-018-23177-w
Veenstra, T. D., & Zhou, M. (2009). Tissue Proteomics and Metabolomics: An Excellent Start and a Promising Future. *Journal of Proteome Research*, *8*(4), 1617–1617. doi:10.1021/pr900157d
Vinaixa, M., Samino, S., Saez, I., Duran, J., Guinovart, J. J., & Yanes, O. (2012). A guideline to univariate statistical analysis for LC/MS-based untargeted metabolomics-derived data. *Metabolites*. *2*(4), 775-795. doi:10.3390/metabo2040775
Vorkas, P. A., Isaac, G., Anwar, M. A., Davies, A. H., Want, E. J., Nicholson, J. K., & Holmes, E. (2015). Untargeted UPLC-MS profiling pipeline to expand

tissue metabolome coverage: Application to cardiovascular disease. *Analytical Chemistry*. *87*(8), 4184-4193. doi:10.1021/ac503775m

Walston, J. D. (2012). Sarcopenia in older adults. *Current Opinion in Rheumatology*. *24*(6), 623-627. doi:10.1097/BOR.0b013e328358d59b

Wang, Y., Liu, S., Hu, Y., Li, P., & Wan, J. B. (2015). Current state of the art of mass spectrometry-based metabolomics studies - a review focusing on wide coverage, high throughput and easy identification. *RSC Advances*. *5*, 78728-78737. doi:10.1039/c5ra14058g

Wang, Z., Cui, B., Zhang, F., Yang, Y., Shen, X., Li, Z., et al. (2019). Development of a Correlative Strategy to Discover Colorectal Tumor Tissue Derived Metabolite Biomarkers in Plasma Using Untargeted Metabolomics. *Analytical Chemistry*. *91*(3), 2401-2408. doi:10.1021/acs.analchem.8b05177

Want, E. J., Masson, P., Michopoulos, F., Wilson, I. D., Theodoridis, G., Plumb, R. S., et al. (2013). Global metabolic profiling of animal and human tissues via UPLC-MS. *Nature Protocols*. *8*(1), 17-32. doi:10.1038/nprot.2012.135

Want, E. J., Wilson, I. D., Gika, H., Theodoridis, G., Plumb, R. S., Shockcor, J., et al. (2010). Global metabolic profiling procedures for urine using UPLC-MS. *Nature Protocols*. *5*(6), 1005-1018. doi:10.1038/nprot.2010.50

Webb, A. J. (2001). Early microscopy: History of fine needle aspiration (FNA) with particular reference to goitres. *Cytopathology*, *12*, 1–6. doi:10.1046/j.1365-2303.2001.00276.x

Wehrens, R., Hageman, J. A., van Eeuwijk, F., Kooke, R., Flood, P. J., Wijnker, E., et al. (2016). Improved batch correction in untargeted MS-based metabolomics. *Metabolomics*, *12*(5). doi:10.1007/s11306-016-1015-8

Westerhuis, J. A., van Velzen, E. J. J. J., Hoefsloot, H. C. J. J., & Smilde, A. K. (2010). Multivariate paired data analysis: Multilevel PLSDA versus OPLSDA. *Metabolomics*, *6*(1), 119–128. doi:10.1007/s11306-009-0185-z

Wikoff, W. R., Anfora, A. T., Liu, J., Schultz, P. G., Scott, L. A., Peters, E. C., & Siuzdak, G. (2009). Metabolomics analysis reveals large effects of gut microflora on mammalian blood metabolites. *Proceedings of the National Academy of Sciences*. *106*(1), 3698-3703. doi:10.1073/pnas.0812874106

Wishart, D. S. (2011). Advances in metabolite identification. *Bioanalysis*. *3*(15), 1769-1782. doi:10.4155/bio.11.155

Wishart, D. S. (2016). Emerging applications of metabolomics in drug discovery and precision medicine. *Nature Reviews Drug Discovery*. *15*(7), 473-484. doi:10.1038/nrd.2016.32

Wishart, D. S., Feunang, Y. D., Marcu, A., Guo, A. C., Liang, K., Vázquez-Fresno, R., et al. (2018). HMDB 4.0: The human metabolome database for 2018. *Nucleic Acids Research*. *46*(D1), D608-D617. doi:10.1093/nar/gkx1089

Wolf, S., Schmidt, S., Müller-Hannemann, M., & Neumann, S. (2010). In silico fragmentation for computer assisted identification of metabolite mass spectra. *BMC Bioinformatics*. *11*, 148. doi:10.1186/1471-2105-11-148

Wong, J. W. H., Durante, C., & Cartwright, H. M. (2005). Application of fast

fourier transform cross-correlation for the alignment of large chromatographic and spectral datasets. *Analytical Chemistry*. *77*(17), 5655-5661. doi:10.1021/ac050619p

Wu, H., Southam, A. D., Hines, A., & Viant, M. R. (2008). High-throughput tissue extraction protocol for NMR- and MS-based metabolomics. *Analytical biochemistry*, *372*(2), 204–12. doi:10.1016/j.ab.2007.10.002

Yi, L., Dong, N., Yun, Y., Deng, B., Ren, D., Liu, S., & Liang, Y. (2016). Chemometric methods in data processing of mass spectrometry-based metabolomics: A review. *Analytica Chimica Acta*. *914*, 17-34. doi:10.1016/j.aca.2016.02.001

Yoshimura, K., Chen, L. C., Mandal, M. K., Nakazawa, T., Yu, Z., Uchiyama, T., et al. (2012). Analysis of renal cell carcinoma as a first step for developing mass spectrometry-based diagnostics. *Journal of the American Society for Mass Spectrometry*. *23*(10), 1741-1749. doi:10.1007/s13361-012-0447-2

Yu, T., Park, Y., Johnson, J. M., & Jones, D. P. (2009). apLCMS-adaptive processing of high-resolution LC/MS data. *Bioinformatics*. *25*(15), 1930-1936. doi:10.1093/bioinformatics/btp291

Zelena, E., Dunn, W. B., Broadhurst, D., Francis-McIntyre, S., Carroll, K. M., Begley, P., et al. (2009). Development of a robust and repeatable UPLC - MS method for the long-term metabolomic study of human serum. *Analytical Chemistry*. *81(*4), 1357-1364. doi:10.1021/ac8019366

Zhang, A., Sun, H., Wang, P., Han, Y., & Wang, X. (2012). Modern analytical techniques in metabolomics analysis. *Analyst*. *137*(2), 293-300. doi:10.1039/c1an15605e

Zhao, C., Xie, P., Yong, T., Wang, H., Chung, A. C. K., & Cai, Z. (2018). MALDI-MS Imaging Reveals Asymmetric Spatial Distribution of Lipid Metabolites from Bisphenol S-Induced Nephrotoxicity. *Analytical Chemistry*. *90*(5), 3196-3204. doi:10.1021/acs.analchem.7b04540

Ziaaldini, M. M., Marzetti, E., Picca, A., & Murlasits, Z. (2017). Biochemical Pathways of Sarcopenia and Their Modulation by Physical Exercise: A Narrative Review. *Frontiers in Medicine*. *4,* 167. doi:10.3389/fmed.2017.00167

Zukunft, S., Prehn, C., Röhring, C., Möller, G., Hrabě de Angelis, M., Adamski, J., & Tokarz, J. (2018). High-throughput extraction and quantification method for targeted metabolomics in murine tissues. *Metabolomics*, *14*(1). doi:10.1007/s11306-017-1312-x

Chapter II
Rapid Screening of Serum γ-Glutamyl Dipeptides for Risk Assessment of Patients with Nonalcoholic Steatohepatitis and Impaired Glutathione Salvage Pathway

Michelle Saoi, Kazunori Sasaki, Hitoshi Sagawa, Kaori Abe, Tomimo Kogiso,
Katsutoshi Tokushige, Etsuko Hashimoto, Yoshiaki Ohashi,
and Philip Britz-McKibbin

J. Proteome Res, **2019** (Under Review)

M.S. performed all the experiments including sample preparation, data acquisition using MSI-CE-MS/MS, data processing, interpretation, statistical analysis and wrote the initial draft for publication. K.S. and K.A. assisted with sample preparation and data acquisition using MSI-CE-MS/MS. H.S designed the capillary tubing sleeve used in the MSI-CE-MS/MS experiments. T.K., K.T. and E.H. obtained ethics approval, provided serum specimens, patient clinical information and provided valuable feedback and revised the manuscript. Y.O. assisted with interpretation, provided valuable feedback and revised the manuscript. P.B.M wrote and provided feedback on the manuscript draft.

Chapter II: Rapid Screening of Serum γ-Glutamyl Dipeptides for Risk Assessment of Patients with Nonalcoholic Steatohepatitis and Impaired Glutathione Salvage Pathway

2.1 Abstract

Non-alcoholic fatty liver disease (NAFLD) is the most common preventable chronic liver disorder in developed countries whose prevalence is increasing worldwide due to its association with obesity, metabolic syndrome and type 2 diabetes. However, the exact mechanisms of NAFLD pathophysiology remain poorly understood including its progression to the more severe non-alcoholic steatohepatitis (NASH). New advances for early detection and monitoring of NASH progression are limited due to the lack of specific blood biomarkers requiring invasive liver biopsies for histopathology. Herein, multisegment injection-capillary electrophoresis-tandem mass spectrometry (MSI-CE-MS/MS) is validated as a high throughput, robust and quantitative platform for targeted analysis of a panel of sixteen serum γ-glutamyl dipeptides from a cohort of NASH adult patients from Japan (median age=50 years, median BMI=27 kg/m^2, *n*=116). Multiplexed electrophoretic separations based on MSI-CE-MS/MS enable the design of customized serial sample injection formats and unique data workflow for accurate determination of γ-glutamyl dipeptides with quality control, whereas use of a liquid coolant device to the capillary outlet improved long-term migration time stability. Unsupervised pattern recognition methods revealed two distinctive NASH sub-groups despite having similar clinical phenotypes and NASH activity scores (median NAS ≈ 6.0) based on their circulating γ-glutamyl dipeptide status. There was an inverse correlation between serum γ-glutamyl dipeptide concentrations and γ-glutamyltransferease (GGT) enzyme activity (r = -0.46; p = 2.5 E-7) inferring a low-risk (*n*=64) as compared to a high-risk (*n*=52) patient sub-group with defective glutathione salvage pathway and likely poor clinical prognosis. Our findings highlight the key role of defects in the γ-glutamyl cycle for differentiation of NASH

patients that may enable better risk assessment of long-term survivorship as a complement to standard liver enzyme screens and histopathology.

2.2 Introduction

Nonalcoholic fatty liver disease (NAFLD) is one of the leading causes of chronic liver diseases in developed countries with an overall prevalence of 20-30%, which is characterized by the accumulation of fat in hepatocytes not caused by excessive alcohol consumption, steatogenic medication, viral infection or inherited genetic disease.[1,2] The alarming rise in NAFLD prevalence coincides with a global epidemic of obesity, metabolic syndrome and insulin resistance elicited by a poor diet and/or an increasingly sedentary lifestyle.[2] NAFLD encompasses a complex disease spectrum ranging from steatosis to more severe forms of liver disease, including nonalcoholic steatohepatitis (NASH), fibrosis and cirrhosis, where progressive inflammation and liver damage is evident.[3] Over 70% of NAFLD patients exhibit simple steatosis and are largely asymptomatic, however those that suffer from more severe forms, such as NASH are at risk for lower life expectancies with poor prognosis due to liver failure.[4] As a result, liver transplantation remains the only viable treatment option in more advanced stages of NASH-associated cirrhosis,[5] whereas lifestyle modifications are efficacious for the treatment of early stages of NAFLD with a loss > 10% of body weight reported to improve necroinflammation.[6] As a result, there is an urgent need for prevention of liver disease progression in NAFLD on a population level, including risk assessment tools for identifying patients who are at higher risk for liver-associated morbidity and/or mortality.[7]

There remains a lack of an international consensus on methods optimal for routine screening of NAFLD with recommendations for increased vigilance among adults having metabolic comorbidities, including obesity, type 2 diabetes and dyslipidemia.[8] Conventional liver enzyme blood tests, including elevations in

alanine aminotransferase (ALT), aspartate aminotransferase (AST) and/or γ-glutamyltransferase (GGT) may be indicative of liver function abnormalities and inflammation, however a normal test result may not exclude NAFLD due to its poor sensitivity.[7] Formal diagnosis of suspected patients is typically achieved by abdominal ultrasound imaging followed by confirmation with histopathology; Nonalcoholic fatty liver (NAFL) is defined as the presence of ≥ 5% hepatic steatosis without evidence of hepatocellular injury, whereas NASH is defined as ≥ 5% hepatic steatosis together with inflammation and hepatocyte injury (*i.e.,* ballooning) with or without any fibrosis.[9] As a result, liver biopsies remain the gold standard for distinguishing NAFL from NASH based on standardized histological grading/scoring systems, such as the NAFLD Activity Score (NAS)[10,11] However, liver biopsies are highly invasive, prone to complications and costly to perform in routine clinical settings while being prone to intra- and inter-pathologist variability.[12] Alternatively, there is growing interest in developing less invasive blood biomarkers notably for predicting liver inflammation and advanced fibrosis without biopsies, but these have been far less validated for NASH as compared to other chronic liver diseases.[13,14] Recently, Soga *et al.*[15] identified a series of γ-glutamyl dipeptides from nontargeted metabolomic studies as potential serum biomarkers for characterizing liver disease progression among nine different forms of liver disease, including differentiating NASH from simple steatosis. However, the clinical utility of serum γ-glutamyl dipeptides have not yet been investigated for routine screening or prognostic testing in large NASH patient populations as compared to standard biochemical tests and histopathology from liver biopsies.

Herein, we introduce a high throughput platform for quantitative determination of sixteen serum γ-glutamyl dipeptides from a cohort of adult Japanese NASH patients (n=116) using multisegment injection-capillary electrophoresis-tandem mass spectrometry (MSI-CE-MS/MS).[16-19] MSI-CE-MS/MS offers a multiplexed platform for simultaneous analysis of seven or more

samples within a single run using customized serial injection configurations as compared to conventional separation methods,[20] which allows for stringent quality control and batch correction optimal for large-scale epidemiological studies.[21,22] Additionally, the use of a liquid coolant tubing sleeve for better thermal regulation of the capillary section outlet prior to the ion source is demonstrated to improve overall long-term migration time stability in conjunction with excellent technical precision and accuracy for reliable serum γ-glutamyl dipeptide quantification. Noteworthy, unsupervised multivariate pattern recognition identified two distinctive sub-groups of NASH patients with contrasting circulating γ-glutamyl dipeptide status despite having similar liver histopathology test results that was inversely correlated with serum GGT activity. We hypothesize that lower circulating γ-glutamyl dipeptides may reflect an impaired glutathione salvage pathway among high-risk NASH patients susceptible to increased oxidative stress/inflammation and likely poor clinical prognosis.

2.3 Materials and Methods

2.3.1 Study Cohort

Fasting serum samples were collected from a cohort of adult Japanese patients (*n*=116) from Tokyo Women's Medical University who were diagnosed with probable (NAS = 3-4, 14%) or definitive NASH (NAS ≥ 5.0, 86%) with a median NAS of 6.0 (ranging from 3.0 to 7.5) following standardized histopathology grading and exclusion of excessive alcohol intake and/or other chronic liver diseases. Written informed consent was acquired from all the patients and the study design followed the ethical guidelines of the 1975 Declaration of Helsinki. Standard liver enzyme and blood protein tests were performed at the Tokyo Women's Medical University using serum aliquots stored at -20 °C, which were also used for determination of serum γ-glutamyl dipeptides in this study. **Table 2.1** summarizes all the patient characteristics and clinical information of the NASH cohort, as well

Table 2.1: Summary of the characteristics of a cohort of Japanese NAFLD patients who were classified in two sub-groups based on their distinctive serum γ-glutamyl dipeptide status

Clinical Parameter*	Full Cohort (*n*=116)	Subgroup A[d] (*n*=52)	Subgroup B[d] (*n*=64)	*p*-value[d]
Age (years)	53 (21)	50 (22)	54 (22)	0.15
Sex M	56 (48%)	28 (54%)	28 (44%)	--
F	60 (52%)	24 (46%)	36 (56%)	
Albumin (g/dL)	4.4 (0.50)	4.5 (0.63)	4.3 (0.50)	0.23
Platelet count (x 10^9/L)	21 (10)	23 (11)	21 (9)	0.62
AST (μmmol/min)	43 (35)	50 (42)	40 (30)	0.24
ALP (μmmol/min)	249 (131)	267 (127)	234 (116)	0.11
ALT (μmmol/min)	67 (67)	77 (101)	58 (68)	0.090
GGT (μmmol/min)	64 (97)	122 (116)	52 (53)	1.04E-04
Total cholesterol (mg/dL)	205 (51)	210 (63)	190 (46)	0.61
Triglycerides (mg/dL)	138 (109)	143 (128)	132 (95)	0.23
BMI (kg/m^2)	27 (6.1)	27 (7.8)	27 (5.7)	0.25
HbA1c (%)	5.9 (1.3)	6.1 (1.4)	5.8 (1.2)	0.46
Diabetes[a]	57 (49%)	26 (50%)	31 (48%)	--
Hyperlipidemia[a]	77 (66%)	34 (65%)	43 (67%)	--
Hypertension[a]	59 (51%)	25 (48%)	34 (63%)	--
NASH Activity Score (NAS)[b]	6.0 (2.0)	6.0 (1.2)	6.0 (2.0)	--
Fibrosis Score[c]	3.0 (1.0)	3.0 (2.0)	3.0 (3.0)	--

** All clinical data expressed as median (interquartile range); p-values obtained from Mann-Whitney U test, where abbreviations refer to AST: Aspartate aminotransferase; ALT: Alanine aminotransferase; GGT: γ-Glutamyltransferase; ALP: Alkaline phosphatase.*

[a] NASH patients with one condition (10/88); two conditions: hyperlipidemia and hypertension (13/88), diabetes and hyperlipidemia (8/88) or diabetes and hypertension (7/88), and with all three conditions (25/88).

[b] NAS determined from sum of steatosis, inflammation and ballooning scores, where NAS ≥ 5.0 is defined as NASH, whereas < 3.0 is non-NASH and NAS = 3-4 is considered a probable NASH diagnosis (n=106).

[c] Fibrosis score determined from histopathology based on increasing scale of liver scarring from 0-1, 2, 3 to 4.

[d] Differentiation of NASH patients into two distinct sub-groups was derived from HCA algorithm based on their serum γ-glutamyl dipeptide status, where statistical significance ($p < 0.05$) was based on a Mann-Whitney U test.

as the histopathology grading based on the NASH clinical research's network (NASH CRN) scoring system for NAFLD.[23]

2.3.2 Instrumentation

Targeted profiling of serum γ-glutamyl dipeptides from NASH patients was performed on an Agilent G7100 CE system coupled to an Agilent 6460 triple quadrupole mass spectrometer equipped with an Agilent Dual ESI Source (Agilent Technologies Inc. Tokyo, Japan). Separations were performed on a 110 cm long uncoated fused silica capillary with a 50 μm inner diameter under a 30 kV voltage at 25 °C under normal polarity. The background electrolyte (BGE) consisted of 1 M formic acid with 15% *vol* acetonitrile (pH 1.80). The serial injection configuration consisted of 7 discrete hydrodynamic sample plugs for 5 s interspaced with BGE spacers for 40 s at 100 mbar.[16] The sheath liquid composition consisted of 60% *vol* methanol with 0.5% *vol* formic acid delivered at a flow rate of 9 μL/min, whereas the ion source conditions for electrospray ionization consisted of a capillary voltage at 4 kV, nebulizer at 7 psi, and dry gas at 300 °C at 7 L/min. Multiple reaction monitoring (MRM) under positive ion mode detection was used to increase sensitivity and selectivity for determination of 16 serum γ-glutamyl dipeptides similar to settings reported by Hirayama *et al.*[20]

2.3.3 Serum Extract Preparation and Method Calibration/Validation

A modified Bligh-Dyer extraction was performed on the thawed serum samples as described elsewhere.[20] Briefly, 450 μL of methanol, 500 μL of chloroform and 200 μL of deionized water were added as pre-chilled solvents to a 50 μL aliquot of human serum. After vortexing and centrifugation at 4 °C, the upper aqueous layer containing polar/ionic metabolites, including γ-glutamyl dipeptides were isolated. Thereafter, the aqueous serum extract was filtered using a 5 kDa MWCO ultrafiltration tube with centrifugation at 9,100 *g* for 2 h to filter out protein. The aqueous serum filtrates were subsequently dried under a flow of N_2 and

reconstituted in 25 μL of 200 mM ammonium acetate (pH 5.0) containing the internal standard, thiomorpholinoacetic acid-1,1'-dioxide (TAD) with a final concentration of 50 μM, which was used for data normalization in MSI-CE-MS/MS. Seven-point calibration curves were prepared using commercial standards (HiPep Laboratories, Kyoto, Japan) over a wide linear dynamic range from 0.010 to 50 μM depending on specific γ-glutamyl dipeptide. All calibrant solutions were prepared in deionized water with 50 μM of TAD as the internal standard, which was used for data normalization to correct for changes in electroosmotic flow and on-capillary injection volume between samples, which was used for determination of relative migration times (RMT) and relative peak areas (RPA) for serum γ-glutamyl dipeptides, respectively. For assessment of method accuracy when using MSI-CE-MS/MS, 2.5 μL of each γ-glutamyl dipeptides were spiked into 2.5 μL of a pooled serum extract at four different concentration levels (ranging from 0.01 to 25 μM) depending on the average baseline concentration of each dipeptide from NASH patients. Also, technical precision was evaluated based on repeated analysis of a pooled serum extract (n=20) that served as a QC, which was introduced in randomized sample injection positions for every run over the entire workflow when using MSI-CE-MS/MS. Further validation studies were also performed involving a comparison of long-term migration time stability of serum γ-glutamyl dipeptides with/without temperature control of the capillary from all NASH patients (n=116), as well as a direct comparison of separation performance using a conventional single injection in CE-MS/MS relative to multiplexed injections by MSI-CE-MS/MS on a sub-set of serum samples from NASH patients (n=15).

2.3.4 Data Processing and Statistical Analysis

Data analysis for this study was performed using Agilent MassHunter Qualitative Analysis (B 07.00) and Microsoft Excel. All γ-glutamyl dipeptide ion responses were normalized to a single non-deuterated internal standard, TAD. Prior to multivariate and univariate statistical analysis, normality testing was performed on

SPSS (IBM Corp. Released 2011. IBM SPSS Statistics for Windows, Version 20.0. Armonk, NY: IBM Corp.) using the Shapiro-Wilk's test for normality ($p < 0.05$). Multivariate statistical analysis methods, including principal component analysis (PCA), correlation matrices, as well as a hierarchal clustering analysis (HCA) using a Euclidean distance measure and Ward clustering algorithm were performed on Metaboanalyst 4.0 using generalized *log*-transformed and autoscaled data unless otherwise stated.[24] Univariate, non-parametric statistical tests including Mann Whitney-U test was performed on all patient clinical data on SPSS. Analysis of Covariance (ANCOVA) was applied to *log*-transformed data where *p*–values were adjusted using sex as a covariate. To correct for multiple hypothesis testing, a false discovery rate (FDR) correction using the Benjamini-Hochberg procedure was applied in this work.

2.4 Results

2.4.1 Multiplexed separations of γ-glutamyl dipeptides from NASH patients by MSI-CE-MS/MS

In order to increase sample throughput and quality control for rapid analysis of serum γ-glutamyl dipeptides, we have introduced an integrated data workflow that takes advantage of customized serial injection configurations involving 7 discrete samples analyzed within a single run when using MSI-CE-MS/MS. In this case, serum extracts were prepared from a cohort of overweight adult Japanese NASH patients (n=116) with a median age of 53 years and a BMI of 27 kg/m^2 having severe liver inflammation and fibrosis as reflected by a median NAS of 6.0, and a more sensitive NAS including fibrosis (NAS+Fibrosis) of 9.0 as two diagnostic scores of NASH.[25] Standard histopathology from liver tissue biopsies of these patients demonstrated high grades of fibrosis, as well as inflammation, ballooning and steatosis with the majority of NAFLD cases with a definitive NASH diagnosis (NAS ≥ 5.0, 86%) as listed in **Table S2.1 of the Supporting Information**. This largely sex-balanced cohort comprised a heterogeneous group of NASH patients

who were also co-morbid with hyperlipidemia, hypertension and/or type 2 diabetes with about 28% having all three adverse cardiometabolic health conditions as summarized in **Table 2.1**. Multiple reaction monitoring (MRM) transitions for sixteen serum γ-glutamyl dipeptides and an internal standard were acquired when using MSI-CE-MS/MS under positive ion mode conditions as listed in **Table S2.2 of the Supporting Information**. MSI-CE-MS enables the design of customized data workflows that has several merits for large-scale targeted metabolomics studies as highlighted in **Figure 2.1**, including more than a 3-fold improvement in sample throughput as compared to a conventional single injection format in CE-MS/MS decreasing acquisition times from about 59 h to under 19.3 h for analysis of serum extracts from the NASH cohort (*n*=116). Moreover, each run also includes a pooled serum extract that serves as a quality control (QC) allowing for assessment of technical precision and continuous monitoring of signal drift in ESI-MS in every run, including more robust batch-correction adjustments as compared to conventional intermittent QC runs.[21,22] Absolute quantification for γ-glutamyl dipeptides is achieved by performing a seven-point calibration curve (run#1), as well as spike/recovery studies at four different concentration levels for reliable γ-glutamyl dipeptide quantification (run#23). Additionally, QC runs are performed intermittently throughout the entire data workflow (runs#2, 13 and 24) to check for long-term migration time and current stability for serum γ-glutamyl dipeptides notably when using newly conditioned (unmodified) fused-silica capillaries, which also includes blank extracts. A series of four representative extracted ion electropherograms are also depicted in **Figure 2.1** for serum γ-Glu-Val (*m/z* 247.1 →72.1), including a calibration curve showing a linear increase (R^2 = 0.999) in ion response ratio over a 100-fold concentration range, a QC run of repeated pooled serum extracts with excellent precision (CV = 4.0%, *n*=6) when normalized to an IS without evidence of sample carry-over effects between injections for the blank extract. Also, a randomized serial injection of six different serum extracts from

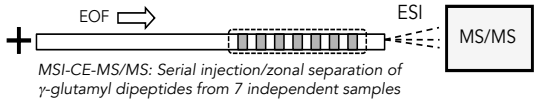

Experiment	Vial Position 1	2	3	4	5	6	7
1	Calibrant 1	Calibrant 2	Calibrant 3	Calibrant 4	Calibrant 5	Calibrant 6	Calibrant 7
2	QC	QC	QC	Blank	QC	QC	QC
3	21	76	69	QC	71	68	112
4	7	QC	29	56	14	116	52
5	31	66	5	83	23	QC	44
6	98	15	35	59	28	2	QC
7	42	25	105	101	QC	77	38
8	4	95	QC	100	107	79	17
9	19	8	9	74	33	QC	85
10	QC	26	84	37	111	87	113
11	12	91	61	65	QC	92	3
12	QC	106	43	78	109	22	6
13	QC	QC	QC	Blank	QC	QC	QC
14	40	99	39	QC	54	20	93
15	36	104	96	18	75	QC	72
16	62	QC	50	16	110	53	13
17	30	34	81	86	49	58	QC
18	10	80	QC	46	89	102	51
19	90	QC	108	88	24	27	94
20	57	11	67	1	41	QC	47
21	45	63	82	115	114	48	QC
22	97	QC	103	64	70	55	60
23	QC	73	32	Spike/Recovery Low	Spike/Recovery Mid 1	Spike/Recovery Mid 2	Spike/ Recovery High
24	QC	QC	QC	Blank	QC	QC	QC

(A) External calibration curves

(B) Intermittent system stability & carry-over check

(C) A QC placed in random positions in each run to assess instrument stability

(D) Spike & recovery to assess accuracy

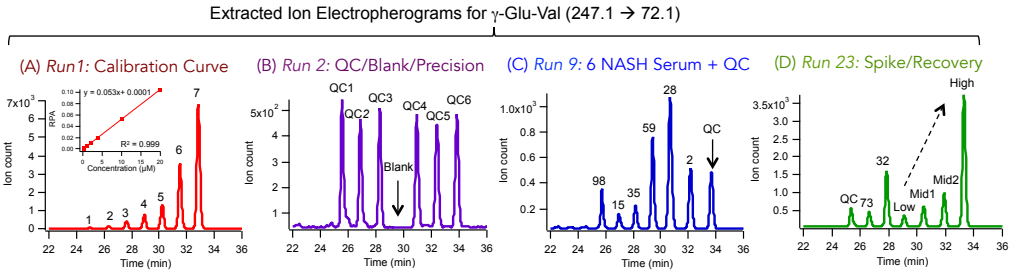

Figure 2.1: Representative extracted ion electropherograms (EIEs) of different serial injection configurations when using MSI-CE-MS/MS as a high throughput method for targeted analysis of serum γ-glutamyl dipeptides. Multiplexed separations enables the design of customized injection configurations that reflect an experimental design as depicted in the analytical workflow to analyze 116 serum extracts from a cohort of adult NASH patients (n=116) within a single day, including stringent measures to assure precision, accuracy and quality control (QC). Representative experiments are highlighted for γ-Glu-Val that involve various serial injection configurations involving 7 independent samples analyzed within a single run by MSI-CE-MS/MS, including (a) 7-point calibration curve using authentic standards for reliable quantification of γ-glutamyl dipeptides over a wide dynamic range, (b) replicate injections of pooled serum as QC sample with blank extract to assess technical precision and lack of sample carry-over, (c) randomized analysis of six serum extract samples from individual NASH patients together with a QC highlighting the biological variance of γ-Glu-Val concentrations between subjects as compared to the grand mean from the pooled serum sample, and (d) a spike/recovery study in pooled serum at four different concentration levels to demonstrate accurate determination of γ-glutamyl dipeptides in human serum.

different NASH patients highlights significant biological variance between-patients as compared to the QC, as well as spike/recovery studies that shows a proportional increase in ion response for γ-Glu-Val at four different concentration levels added to pooled serum samples. As a result, MSI-CE-MS offers a versatile multiplexed separation platform for rapid data acquisition with stringent QC, where rigorous calibration and validation studies can be readily programmed automatically within a fully integrative data workflow.

2.4.2 Stabilization of Migration Time with Liquid Coolant in MSI-CE-MS/MS

A major source of migration time stability in CE are associated with variations in electroosmotic flow (EOF) that has long hindered large-scale clinical applications of CE-MS within an accredited laboratory setting.[26] Depending of the specific CE-MS instrumental configuration/vendor, temperature control is often limited to a section of the capillary held within a cassette using convection (air) or a liquid coolant, whereas sections of the capillary outlet coupled to the ion source are often exposed to fluctuating ambient temperatures. In this work, we compared the performance of a customized capillary tubing sleeve that was designed to provide better temperature control over the entire capillary using a circulating liquid coolant at a temperature similar to cassette (at 25 °C), whereas the sample tray was set at 4 °C to minimize sample evaporation when analyzing large-batches of samples by MSI-CE-MS/MS. In this case, all serum samples from NASH patients (n=116) using a standardized data workflow (**Figure 2.1**) were analyzed twice independently without (August 2015) and with (January 2016) the use of an insulated capillary tubing as shown in **Figure 2.2(A).** Overall, temperature control of the outer capillary significantly improved the long-term migration time stability for serum γ-glutamyl dipeptides measured in QC samples (n=20) with an average RMT of CV = 1.2% as compared to CV= 1.8% (without temperature control) as highlighted in a 2D scores plot from a principal component analysis (PCA) in

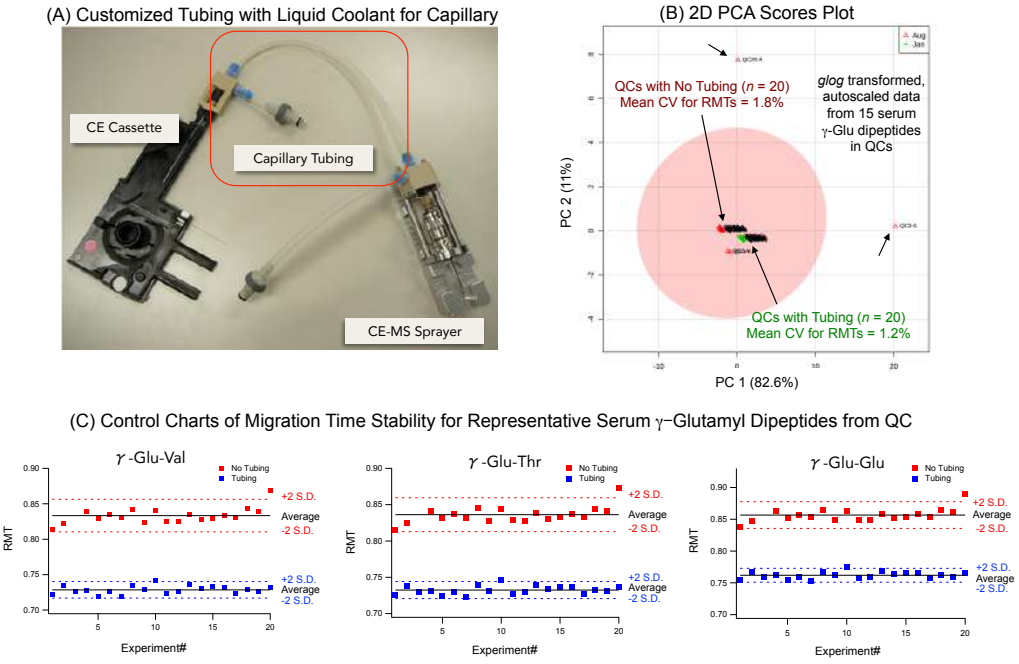

Figure 2.2: (a) An insulated tubing prototype with liquid coolant used to minimize migration time variability due to an exposed section of capillary (from cassette to CE-MS interface) when using MSI-CE-MS/MS for analysis of large batches of serum samples from NASH patients (n=116). (b) A 2D scores plot using PCA for comparing the overall migration time variance (i.e., RMT) for 15 serum γ-glutamyl dipeptides consistently measured in QC samples (CV < 30%, n=20) from NASH patients, which highlights the larger variability with two outlier runs (arrows) when performing analyses without tubing (mean CV = 1.8%) as compared to with tubing (mean CV = 1.2%) and liquid coolant for more stable CE separations. (c) Representative control charts of γ-glutamyl dipeptides from repeat analysis of pooled serum extracts as QCs included with each experimental run when analyzing the entire cohort of serum samples using MSI-CE-MS/MS originally without tubing (August 2015, red) and then independently with tubing (January 2016, blue).

Figure 2.2(B). Additionally, there were fewer outliers caused by major shifts in EOF as shown in extracted ion electropherograms for the internal standard at three different runs acquired over the entire workflow (**Figure S2.1 of the Supporting Information**). Better thermal management of repeated electrophoretic separations with a liquid coolant was achieved despite similar average current readings (≈ 22 μA) resulting in longer apparent migration times and lower RMTs as compared to runs performed without temperature control of the capillary outlet (*i.e.,* no tubing). This also coincided with better resolution achieved for certain γ-glutamyl dipeptides from isobaric interferences in serum extracts from NASH patients, such as γ-Glu-Gln that was resolved from γ-Glu-Lys and an unknown isobar from serum

extracts (**Figure S2.2 of the Supporting Information**). Control charts depicted in **Figure 2.2C** demonstrates that improved long-term migration time stability was achieved in MSI-CE-MS runs for three representative serum γ-glutamyl dipeptides measured in repeat QC samples (*n*=20). Additionally, a direct comparison of ten consistently measured serum γ-glutamyl dipeptide concentrations (*n*=150) was measured using a conventional low throughput, single injection CE-MS method[20] and then compared to serial sample injections using MSI-CE-MS/MS on a sub-set of fifteen serum samples from NASH patients. In this case, good mutual agreement was achieved between both methods as reflected by a mean bias of 9.2% with few outliers outside agreement limits together with a slope close to unity (**Figure S2.3 Supporting Information**). For these reasons, experimental data from MSI-CE-MS/MS with improved thermal management of the capillary was used in subsequent work as it provided greater sample throughput with better data fidelity when analyzing large numbers and different batches of samples collected over time.

2.4.3 Method Validation for Reliable Quantification of Serum γ-Glutamyl Dipeptides

A summary of several major figures of merit from MSI-CE-MS/MS is summarized in **Table 2.2** where γ-glutamyl dipeptides are listed based on their characteristic migration behavior in CE from fast migration cationic dipeptides (*e.g.,* γ-Glu-Orn) to slowly migrating bulky/aromatic (*e.g.,* γ-Glu-Trp) amino acid substituents. Overall, the overall precision of RMT (*n*=20) was under 1% for most γ-glutamyl dipeptides from serum extracts migrating close to the internal standard with the exception of the three fast migrating cationic dipeptides (CV ≈ 3%). Similarly, the median technical precision for quantification of γ-glutamyl dipeptides from pooled QC serum extracts based on their integrated ion response ratio to an internal standard was acceptable (CV ≈ 13%, *n*=20) with certain dipeptides prone to greater variation (CV = 20-28%) due to their lower abundance in serum (γ-Glu-Trp, *S/N* ≈ 5) or detection of minor/partially overlapping isobaric interferences (γ-Glu-Gly and

Table 2.2: Summary of the figures of merit of MSI-CE-MS/MS for reliable γ-glutamyl dipeptide determination using pooled serum samples from NASH patients

γ-Glutamyl Dipeptide	Mean RMT	LOD (μM)	LOQ (μM)	Linearity (R^2)	Linear Range (μM)	RMT Precision (%CV)[a]	RPA Precision (%CV)[a]	Mean Recovery (%)[b]
γ-Glu-Orn	0.458	0.02	0.05	1.0000	0.1-10	2.9	17	106
γ-Glu-Arg	0.469	0.18	0.55	0.9992	0.1-10	3.0	18	130
γ-Glu-His	0.471	0.06	0.19	0.9996	0.05-5.0	2.8	4.0	111
γ-Glu-Gly	0.685	0.08	0.24	1.000	0.2-20	1.1	20	--
γ-Glu-Ala	0.703	0.08	0.23	0.9999	0.1-10	1.0	26	--
γ-Glu-Ser	0.725	0.10	0.31	0.9997	0.1-10	0.9	28	108
γ-Glu-Val	0.729	0.17	0.50	0.9998	0.2-20	0.8	4.0	102
γ-Glu-Thr	0.733	0.10	0.29	0.9998	0.1-10	0.8	6.0	97
γ-Glu-Asn	0.736	0.05	0.16	0.9997	0.05-5.0	0.9	22	106
γ-Glu-Met	0.746	0.02	0.06	0.9998	0.02-2.0	0.8	7.0	106
γ-Glu-Gln	0.754	0.55	1.67	0.9997	0.5-50	1.4	13	112
γ-Glu-Phe	0.751	0.03	0.08	0.9995	0.02-2.0	0.7	6.0	104
γ-Glu-Glu	0.762	0.34	104	0.9999	0.5-50	0.7	5.0	104
γ-Glu-Trp	0.763	0.02	0.05	0.9993	0.01-1.0	0.7	22	113
γ-Glu-Cit	0.771	0.06	0.18	0.9996	0.05-5.0	0.7	13	115
γ-Glu-Tyr	0.773	0.02	0.05	0.9998	0.02-2.0	0.7	9.0	106

[a] *Technical precision for relative peak area (RPA) and relative migration time (RMT) for serum γ-glutamyl dipeptides based on normalization to an internal standard, which was measured in pooled serum extracts as QCs (n = 20) throughout the analysis of all NASH patient samples (n=116) by MSI-CE-MS/MS.*

[b] *Average recovery for accurate quantification of γ-glutamyl dipeptides in pooled serum from NASH patients at four different concentration levels (low, mid level 1, mid level 2, and high level).*

γ-Glu-Ala). In all cases, excellent calibration linearity (R^2 > 0.999) was achieved over a 100-fold with concentration detection limits (LOD, S/N = 3) of about 50-100 nM depending on the specific γ-glutamyl dipeptide. Also, method accuracy was evaluated based on spike-recovery studies performed at four different levels above baseline concentrations of γ-glutamyl dipeptides in pooled serum samples, which was acceptable with a mean recovery of 108%; however, poor recoveries were measured at the lowest concentration level spiked since in some cases the added amount of calibrant did not significantly change the measured ion response notably

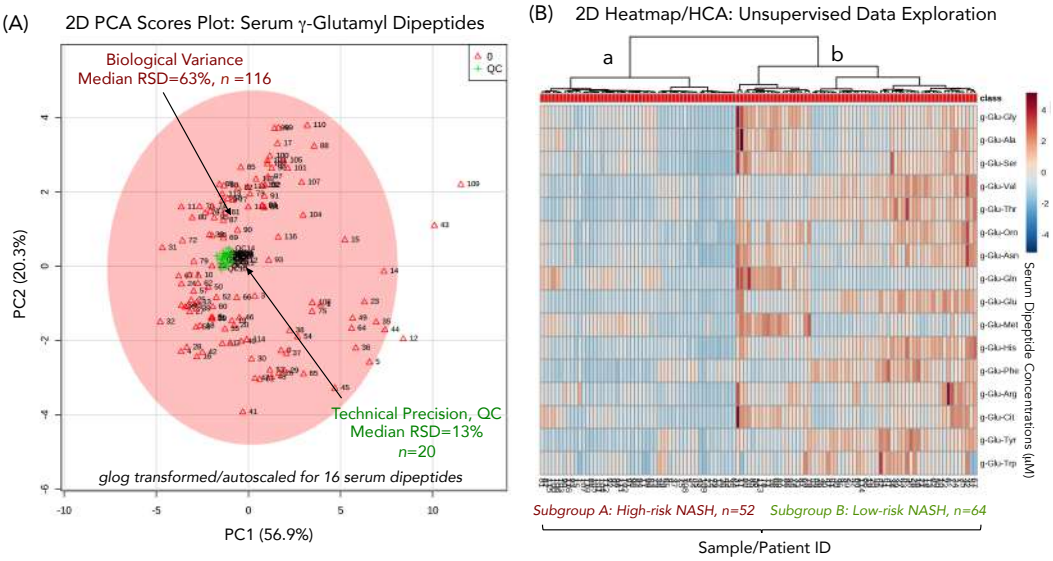

Figure 2.3: (a) Data structure overview based on a 2D scores plot using PCA that compares the considerable between-subject biological variance (median CV = 63%) of sixteen γ-glutamyl dipeptide concentrations measured from a cohort of adult NASH patients (*n*=116) as compared to the technical precision (median CV = 13%) of the method based on repeated analysis of a pooled serum sample as QC (*n*=20) analyzed in every MSI-CE-MS run. (b) Unsupervised pattern recognition using HCA revealed two distinctive patient sub-groups within cohort based on contrasting γ-glutamyl dipeptide status measured in serum, which were subsequently designated as a high-risk NASH and a low-risk NASH phenotype reflecting low and high circulating serum γ-glutamyl dipeptide concentrations, respectively.

for higher abundance γ-glutamyl dipeptide in serum as summarized in **Table S2.3 of the Supporting Information**. A 2D PCA scores plot is also depicted in **Figure 2.3**, which provides an overview of the biological variance of sixteen serum γ-glutamyl dipeptide concentrations (median CV = 63%, *n* = 116) between individual NASH patients as compared to the technical variance of the method (median CV = 13%, *n*=20) from sample extraction and data analysis. **Figure 2.3(B)** also shows a 2D heat map together with a hierarchical clustering analysis (HCA), which unexpectedly identified two distinctive sub-groups of NASH patients with either low (*i.e.,* sub-group A or high-risk NASH patients, *n*=52) or high (*i.e.,* sub-group B or high-risk NASH patients, *n*=64) circulating concentrations of γ-glutamyl dipeptides. **Table S2.4 of the Supporting Information** summarizes the average serum concentrations measured for sixteen different γ-glutamyl dipeptides which

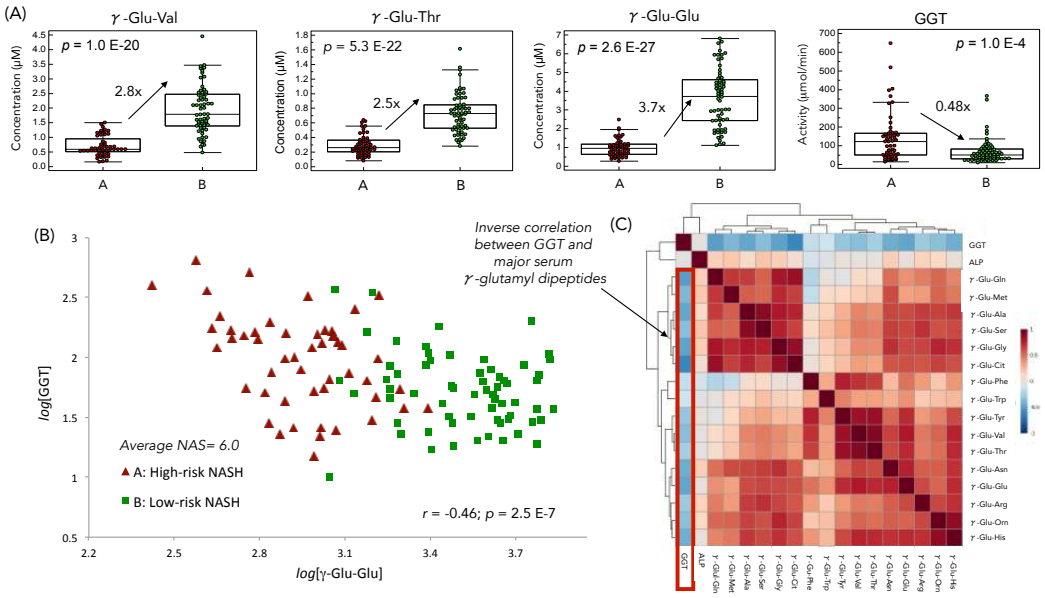

Figure 2.4: (a) Metabolic phenotyping a sub-set of NASH patients (n=116, average NAS = 6.0) identified based on their contrasting γ-glutamyl dipeptide status in serum as shown for three top-ranked compounds (γ-Glu-Glu, γ-Glu-Thr, γ-Glu-Val), which were inversely correlated with GGT activity, whereas (b) shows a *log-log* plot demonstrating a linear correlation between serum γ-Glu-Glu concentrations and GGT activity (r = -0.46, p = 2.5 E-7), and (c) a correlation matrix confirming strong co-linearity among all serum γ-glutamyl dipeptides as compared to GGT activity. Low-risk NASH patients were indicated by high circulating concentrations of γ-glutamyl dipeptide and low serum GGT activity, whereas high-risk NASH patients were consistent with low circulating concentrations of γ-glutamyl dipeptide and a corresponding high serum GGT activity with likely poor clinical outcomes.

were ranked ordered based on their significance using ANCOVA (after adjustment to sex) to discriminate between two main sub-groups of NASH patients classified based on HCA. For instance, serum γ-Glu-Glu, γ-Glu-Thr and γ-Glu-Val were among the top-ranked of γ-glutamyl dipeptides for sub-typing NASH patients with large effect sizes (> 0.50), as well as F-value, p-value (or q-value, FDR) and mean fold-change (FC) ratio. Interestingly, the two distinctive sub-groups of NASH patients identified by their contrasting γ-glutamyl dipeptide status reflective of underlying differences in glutathione recycling capacity otherwise did not have any significant difference in other clinical parameters listed in **Table 2.1**, including, age, BMI, standard blood biochemical tests, or disease co-morbidity prevalence with the exception of serum GGT activity (p = 1.04 E-4). Importantly, there was no

significant association of γ-glutamyl dipeptide concentrations with histopathology grading among NASH patients in terms of severity of steatosis, NAS, and fibrosis (**Table S2.5-S2.7** and **Figure S2.4 of the Supporting Information**). Indeed, **Figure 2.4** demonstrates metabolic phenotyping the NASH cohort into two major sub-groups based on their contrasting γ-glutamyl dipeptide status, where circulating γ-Glu-Glu concentrations show an inverse correlation with serum GGT activity (r =-0.46, p = 2.5 E-7) that were measured independently by two different analytical platforms. Additionally, **Figure S2.5 of the Supporting Information** comparing receiver operating characteristic (ROC) curves based on serum γ-Glu-Glu concentration (AUC = 0.958, p < 1.0 E-5) and GGT activity (AUC = 0.694, p = 2.0 E-4) show good to excellent performance to discriminate NASH sub-groups who differ primarily in their liver glutathione recycling capacity as mediated by the γ-glutamyl cycle[27] despite having similar histopathology results and fibrosis grading (median NAS 6.0 and NAS+Fibrosis ≈ 9.0).

2.5 Discussion

Liver biopsies remain the gold standard for confirmatory diagnosis of NASH from a majority of asymptomatic NAFLD cases, where standardized histological scoring systems are used to determine liver disease severity.[8] However, liver biopsies are invasive, costly to perform, prone to complications, and are susceptible to bias and sampling variability that may delay timely diagnoses in the absence of high quality ultrasound imaging data or abnormal blood liver enzymes test results. A pilot study by Soga *et al.*[15] previously reported that patients with mild steatosis (n=9) had higher concentrations of six γ-glutamyl dipeptides as compared to severe NASH patients (n=11) and thus, proposed that these dipeptides may serve as less invasive biomarkers for routine screening of liver disease severity among NAFLD patients without biopsies. However, this study did not extensively validate the specificity nor the clinical utility of γ-glutamyl dipeptides for screening diverse NASH patient populations who often suffer from several extra-hepatic health conditions

complicating their disease prognosis, including obesity, hypertension, hyperlipidemia and/or type 2 diabetes (**Table 2.1**). In this work, we first developed and extensively validated a rapid method for quantification of sixteen serum γ-glutamyl dipeptides from a heterogeneous cohort of NASH patients when using a multiplexed separation platform based on MSI-CE-MS/MS (**Figure 2.1**).[16-19] Hirayama *et al.*[20] recently demonstrated that CE-MS/MS requires smaller sample volumes while allowing for faster total analysis times that is less prone to sample matrix effects as compared to reversed-phase LC-MS/MS. However, sample throughput, migration time stability and long-term robustness remain major obstacles that hinder large-scale clinical applications of CE-MS/MS technology. In our case, customized serial injection configurations in MSI-CE-MS/MS enable analysis of seven discrete samples within a single run that improves throughput by over three-fold with better data fidelity as compared to conventional single injection separation formats. Additionally, various experimental designs can be integrated within an automated data workflow, including rapid acquisition of calibration curves, spike-recovery studies, as well as QC and/or blank samples to monitor and correct for long-term signal drift and sample carry-over effects, respectively.[21,22] The installation of a capillary tubing with circulating liquid coolant also allowed for better thermal control of electrophoretic separations significantly reducing RMT variance by about 34% (**Figure 2.2)** with improved long-term stability (**Figure S2.1**) and peak capacity for resolving γ-glutamyl dipeptides from isobaric interferences in human serum (**Figure S2.2**). Overall, there was excellent mutual agreement between γ-serum glutamyl dipeptide concentrations measured via single injection CE-MS/MS as compared to MSI-CE-MS/MS (**Table 2.2; Figure S2.3**), which demonstrated acceptable technical precision (mean CV ≈ 13%), accuracy (mean recovery ≈ 108%) and linearity (R^2 > 0.999) for reliable quantification over a 100-fold linear dynamic range with nanomolar detection limits (LOD ≈ 100 nM). However, certain low abundance γ-glutamyl dipeptides were prone to partial overlap with other isobaric interferences in serum extracts resulting in higher

variance and potential bias, such as γ-Glu-Gly, γ-Glu-Ala and γ-Glu-Phe. In this case, the introduction of electrokinetic spacers between hydrodynamic sample plugs used in MSI-CE-MS may further improve peak capacity for resolving γ-glutamyl dipeptides from several unknown isobaric interferences in serum by retaining the effective capillary length used for separation.[28]

A major finding in this study was the identification of two sub-groups of NASH patients with contrasting serum γ-glutamyl dipeptides concentration profiles (**Table S2.4**) when using HCA as an unsupervised multivariate analysis method for pattern recognition (**Figure 2.3**); indeed, there was considerable biological variance in circulating γ-glutamyl dipeptides measured between-patients (median CV ≈ 63%, *n*=116) as compared to technical precision based on the repeated analysis of pooled serum extracts as QC samples (*n*=20). Further analysis revealed that these two distinctive NASH sub-types classified based on their circulating γ-glutamyl dipeptide status had otherwise similar clinical disease phenotypes, as well as standard blood biochemical tests and disease co-morbidities with the exception of differences in serum GGT activity (**Table 2.1**). For instance, we confirmed that serum γ-glutamyl dipeptides were not able to stratify patients based on steatosis (S1-S3), inflammation (I0/1 to I3), and fibrosis severity (F0/1 to F4) in our patient cohort (**Table S2.1**; **Table S2.5-2.7**), including NAS (**Figure S2.4**) and NAS+Fibrosis. Consequently, our results indicate that serum γ-glutamyl dipeptides are not suitable biomarkers for differentiating fibrosis severity among NASH patients, such as new predictive models and blood-based tests for non-invasive assessment of inflammation or fibrosis in NAFLD.[29] These results may be contingent on the specific patient population examined in this work since a majority were diagnosed with NASH as compared to a small sub-set with borderline or probable diagnosis (14%), whereas no early stage NAFLD cases with mild steatosis and NAS < 3.0 were included. However, the inverse correlation between serum γ-glutamyl dipeptide concentrations and GGT activity (**Figure 2.4**) inferred that a

sub-set of high-risk NASH patients may be susceptible to glutathione insufficiency due to impairments in the γ-glutamyl cycle with poor clinical prognosis. For instance, a longitudinal study with thirteen year follow-up reported that out-patients with GGT activity > 10-14 μmol/min as part of a routine screening panel were at greater risk for all causes cancer, hepatobillary and vascular related mortalities with unfavorable prognosis for long-term survival after adjustment for age and sex.[30] This upper threshold range for serum GGT activity was exceeded in NASH patients evaluated in this study notably among the higher risk sub-group A (**Table 2.1**; **Figure S2.5**). Although elevated GGT is often associated with hepatobillary diseases and excessive alcohol consumption,[31,32] it also has been shown to be associated with diverse pathological processes, including incident metabolic syndrome, type 2 diabetes and cardiovascular disease outcomes,[33-35] which are prevalent among NASH patients but are not predicted by standard histopathological parameters.[36] Similarly, a NASH diagnosis itself did not increase liver-specific or overall mortality as opposed to the rate of severe liver disease progression according to fibrosis stage.[37] As illustrated in **Figure 2.5**, the primary role of GGT, a membrane-bound glycoprotein with an active site directed towards the outer cell surface, is to metabolize extracellular reduced glutathione (GSH) allowing for recycling of precursor amino acids, namely Cys-Gly that is transported within liver to support intracellular glutathione biosynthesis since it is rate-limited by the availability of Cys.[38] Indeed, recent clinical trials have demonstrated the promising therapeutic efficacy of oral treatment with glutathione (300 mg/day over 4 mo) in patients with NAFLD with better responses reported for younger patients without diabetes.[39] Further studies are needed to more clearly delineate the prognostic value of serum γ-glutamyl dipeptide status and optimal cut-off concentrations (**Figure S2.5**) in predicting clinical outcomes in NASH patients as compared to serum GGT activity that is prone to enzyme denaturation and false negatives due to sample handling and delays to storage.

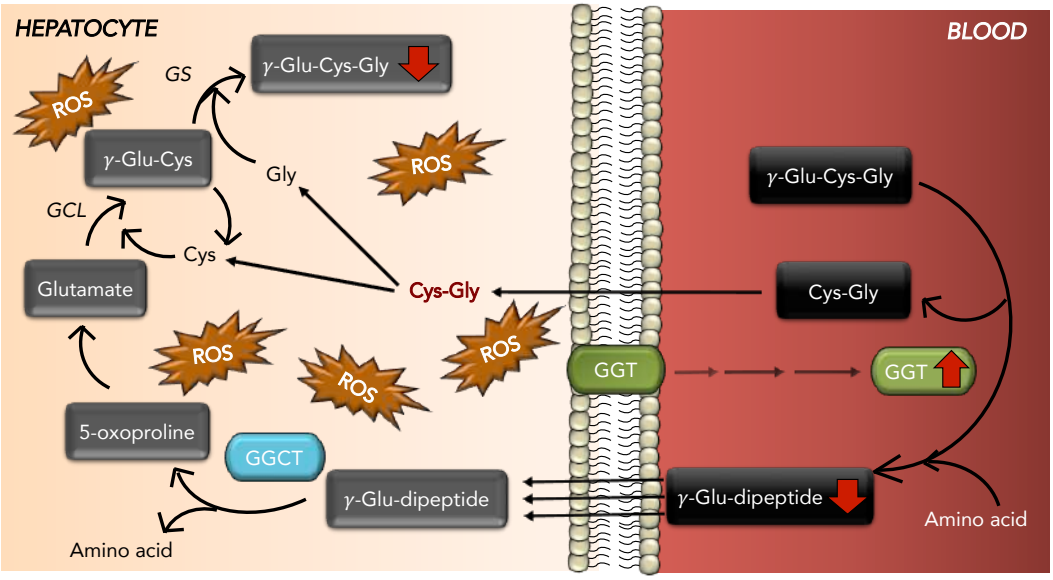

Figure 2.5: Schematic overview of the role of the γ-glutamyl cycle for risk assessment of NASH prognosis among patients with similar liver histopathology and metabolic disease co-morbidities, where high-risk NASH patients are indicative of lower circulating γ-glutamyl dipeptide concentrations and higher serum GGT activity In this case, impairments to the γ-glutamyl cycle reduce the salvage pathway for glutathione biosynthesis within hepatocytes with deleterious oxidative stress due to elevated ROS production. Abbreviations include: GGT = γ-glutamyl transferase; GGCT = γ-glutamyl cyclotransferase; GCL = glutamate cysteine ligase; GS = glutathione synthase

2.6 Conclusion

This work is the first to validate a multiplexed separation platform and integrated data workflow based on MSI-CE-MS/MS for reliable analysis of a panel of serum γ-glutamyl dipeptides from a large cohort of overweight Japanese NASH patients who also suffer from several other cardiometabolic co-morbidities. Also, the introduction of an insulating tubing with liquid coolant provided greater long-term migration time stability when analyzing large batches of serum samples by MSI-CE-MS/MS offering greatly improved sample throughput and quality control as compared to conventional single injection separation formats. Overall, good reproducibility, accuracy, linearity and robustness were demonstrated for quantification of serum γ-glutamyl dipeptide concentrations with few isobaric interferences. In contrast to earlier pilot studies, it was shown that serum γ-glutamyl-dipeptides were not associated with standardized histopathology

parameters based on liver biopsies from NASH patients. Instead, it was discovered that two distinctive NASH sub-groups in this cohort could be classified based on their contrasting serum γ-glutamyl dipeptide concentration profiles, which were inversely correlated with serum GGT activity. Our findings inferred the important role of the γ-glutamyl cycle in maintaining redox homeostasis and intracellular glutathione reserves during oxidative stress, which is relevant in the pathophysiology of advanced stages of NAFLD with severe liver inflammation and fibrosis. Importantly, we hypothesize that serum γ-glutamyl dipeptides may serve as useful prognostic indicators of long-term survivorship and all causes mortality, where high-risk NASH patients are defined by low circulating concentrations of γ-glutamyl dipeptides that coincided with higher serum GGT activity. Ultimately, this work may potentially pave way for better risk assessment tools for predicting liver-associated complications among NAFLD patients that are not feasible by conventional liver blood tests and histopathology. Also, this approach may enable better treatment monitoring of NASH patients when validating novel diet and/or lifestyle interventions designed to support glutathione biosynthesis and prevent liver disease progression.

2.7 References

(1) Dowman, J. K.; Tomlinson, J. W.; Newsome, P. N. Pathogenesis of Non-Alcoholic Fatty Liver Disease. *Q J. Med.* **2010**, *103*, 71–83.

(2) Benedict, M.; Zhang, X. Non-Alcoholic Fatty Liver Disease: An Expanded Review. *World J. Hepatol.*, **2017**, *9*, 715–732.

(3) Angulo, P. Nonalcoholic Fatty Liver Disease. *N. Engl. J. Med.* **2002**, *346*, 1221–1231.

(4) Hui, J.M.; Kench, J.G.; Chitturi, S.; Sud, A.; Farrell, G.C.; Byth, K.; Hall, P.; Khan, M.; George, J. Long-term Outcomes of Cirrhosis in Nonalcoholic Steatohepatitis Compared with Hepatitis C. *Hepatology* **2003**, *38*, 420–427.

(5) Leoni, S.; Tovoli, F.; Napoli, L.; Serio, I.; Ferri, S.; Bolondi, L. Current Guidelines for the Management of Non-alcoholic Fatty Liver Disease: A

Systematic Review with Comparative Analysis. *World J. Gastroenterol.* **2018**, *24*, 3361–3373.

(6) Zelber-Sagi, S.; Godos, J.; Salomone, F. Lifestyle Changes for the Treatment of Nonalcoholic Fatty Liver Disease: A Review of Observational Studies and Intervention Trials *Therap. Adv. Gastroenterol.* **2016**, *9*, 392–407.

(7) Nasr, P.; Kechagias, S. Natural History of NAFLD/NASH. *Curr. Hepatol. Rep.* **2017**, *16*, 391–397.

(8) Chalasani, N.; Younossi, Z.; Lavine, J.E.; Charlton, M.; Cusi, K.; Rinella, M.; Harrison, S.A.; Brunt, E.M.; Sanyal, AJ. The Diagnosis and Management of Nonalcoholic Fatty Liver Disease: Practice Guidance from the American Association for the Study of Liver Diseases. *Hepatology* **2018**, *67*, 328-357.

(9) Rowe, I. A. Too Much Medicine: Overdiagnosis and Overtreatment of Non-Alcoholic Fatty Liver Disease. *Lancet Gastroenterol. Hepatol.*, **2018**, *3*, 66–72.

(10) Dyson, J. K.; Anstee, Q. M.; McPherson, S. Non-Alcoholic Fatty Liver Disease: A Practical Approach to Diagnosis and Staging. *Frontline Gastroenterol.* **2014**, *5*, 211–218;

(11) Kleiner, D. E.; Brunt, E. M.; Van Natta, M.; Behling, C.; Contos, M. J.; Cummings, O. W.; Ferrell, L. D.; Liu, Y. C.; Torbenson, M. S.; Unalp-Arida, A.; Yeh, M.; McCullough, A. J.; Sanyal, A. J. Design and Validation of a Histological Scoring System for Nonalcoholic Fatty Liver Disease. *Hepatology* **2005**, *41*, 1313–1321.

(12) Ratziu, V.; Charlotte, F.; Heurtier, A.; Gombert, S.; Giral, P.; Bruckert, E.; Grimaldi, A.; Capron, F.; Poynard, T. Sampling Variability of Liver Biopsy in Nonalcoholic Fatty Liver Disease. *Gastroenterology* **2005**, *128*, 1898–1906.

(13) Ratziu, V.; Massard, J.; Charlotte, F.; Messous, D.; Imbert-Bismut, F.; Bonyhay, L.; Tahiri, M.; Munteanu, M.; Thabut, D.; Cadranel, J. F.; Le Bail, B.; de Ledinghen, V.; Poynard, T. Diagnostic Value of Biochemical Markers (FibroTest-FibroSURE) for the Prediction of Liver Fibrosis in Patients with Non-Alcoholic Fatty Liver Disease. *BMC Gastroenterol.* 2006, *6*, 6.

(14) Munteanu, M.; Tiniakos, D.; Anstee, Q.; Charlotte F.; Marchesini, G.;

Bugianesi, E.; Trauner, M.; Romero Gomez, M.; Oliveira, C.; Day, C.; Dufour, J.F.; Bellentani, S.; Ngo, Y.; Traussnig, S.; Perazzo, H.; Deckmyn, O.; Bedossa, P.; Ratziu, V.; Poynard, T.; FLIP Consortium and the FibroFrance Group. Diagnostic Performance of FibroTest, SteatoTest and ActiTest in Patients with NAFLD using the SAF Score as Histological Reference. *Aliment Pharmacol Ther.* **2016**, *44*, 877–889.

(15) Soga, T.; Sugimoto, M.; Honma, M.; Mori, M.; Igarashi, K.; Kashikura, K.; Ikeda, S.; Hirayama, A.; Yamamoto, T.; Yoshida, H.; Otsuka, M.; Tsuji, S.; Yatomi, Y.; Sakuragawa, T.; Watanabe, H.; Nihei, K.; Saito, T.; Kawata, S.; Suzuki, H.; Tomita, M.; Suematsu, M. Serum Metabolomics Reveals γ-Glutamyl Dipeptides as Biomarkers for Discrimination Among Different Forms of Liver Disease. *J. Hepatol.* **2011**, *55*, 896–905.

(16) Kuehnbaum, N.L.; Kormendi, A.; Britz-McKibbin, P. Multisegment Injection-Capillary Electrophoresis-Mass Spectrometry: A High-throughput Platform for Metabolomics with High Data Fidelity. *Anal Chem.* **2013**, *85*, 10664–10669.

(17) DiBattista, A.; McIntosh, N.; Lamoureux, M.; Al-Dirbashi, O. Y.; Chakraborty, P.; Britz-McKibbin, P. Temporal Signal Pattern Recognition in Mass Spectrometry: A Method for Rapid Identification and Accurate Quantification of Biomarkers for Inborn Errors of Metabolism with Quality Assurance. *Anal. Chem.* **2017**, *89*, 8112–8121.

(18) Macedo, A. N.; Mathiaparanam, S.; Brick, L.; Keenan, K.; Gonska, T.; Pedder, L.; Hill, S.; Britz-McKibbin, P. The Sweat Metabolome of Screen-Positive Cystic Fibrosis Infants: Revealing Mechanisms beyond Impaired Chloride Transport. *ACS Cent. Sci.* **2017**, *3*, 904–913.

(19) Saoi M.; Percival, M.; Nemr, C.; Li ,A.; Gibala, M.; Britz-McKibbin, P. Characterization of the Human Skeletal Muscle Metabolome for Elucidating the Mechanisms of Bicarbonate Ingestion on Strenuous Interval Exercise. *Anal Chem.* **2019**, *91*, 4709–4718.

(20) Hirayama, A.; Igarashi, K.; Tomita, M.; Soga, T. Development of Quantitative Method for Determination of γ -Glutamyl Peptides by Capillary Electrophoresis Tandem Mass Spectrometry: An Efficient Approach Avoiding Matrix Effect. *J. Chromatogr. A* **2014**, *1369*, 161–169.

(21) Azab, S.; Ly, R.; Britz-McKibbin, P. Robust Method for High-Throughput Screening of Fatty Acids by Multisegment Injection-Nonaqueous Capillary Electrophoresis-Mass Spectrometry with Stringent Quality Control. *Anal Chem.* **2019**, *91*, 2329–2336.

(22) DiBattista, A.; McIntosh, N.; Lamoureux, M.; Al-Dirbashi, O.Y.; Chakraborty, P.; Britz-McKibbin, P. Metabolic Signatures of Cystic Fibrosis Identified in Dried Blood Spots For Newborn Screening Without Carrier Identification. *J. Proteome Res.* **2019**, *18*, 841–854.

(23) Cummings, O. W.; Tonascia, J.; Chalasani, N. Generalizability of the NASH CRN Histological Scoring System for Nonalcoholic Fatty Liver Disease. *J Clin. Gastroenterol.* **2011**, *45*, 55–58.

(24) Chong, J.; Soufan, O.; Li, C.; Caraus, I.; Li, S.; Bourque, G.; Wishart, D. S.; Xia, J. MetaboAnalyst 4.0: Towards More Transparent and Integrative Metabolomics Analysis. *Nucleic Acids Res.* **2018**, *46*, W486–W494.

(25) Santiago-Rolón, A.; Purcell, D.; Rosado, K.; Toro, D. H. A Comparison of Brunt's Criteria, the Non-Alcoholic Fatty Liver Disease Activity Score (NAS), and a Proposed NAS Scoring that Includes Fibrosis in Non-Alcoholic Fatty Liver Disease Staging. *P R Health Sci. J.* **2015**, *34*, 189–194.

(26) Boizard, F.; Brunchault, V.; Moulos, P.; Breuil, B.; Klein, J.; Lounis, N.; Caubet, C.; Tellier, S.; Bascands, J. L.; Decramer, S.; Schanstra, J. P.; Buffin-Meyer, B. A Capillary Electrophoresis Coupled to Mass Spectrometry Pipeline for Long Term Comparable Assessment of the Urinary Metabolome. *Sci. Rep.* **2016**, *6*, 34453.

(27) Griffith, O. W.; Bridges, R. J.; Meister, A. Evidence that the Gamma-Glutamyl Cycle Functions in Vivo Using Intracellular Glutathione: Effects of Amino Acids and Selective Inhibition of Enzymes. *PNAS* **1978**, *75*, 5405–5408.

(28) Saoi, M.; Li, A.; McGlory, C.; Stokes, T. von Allmen, M. T.; Phillips, S. M.; Britz-McKibbin, P. Metabolic Perturbations from Step Reduction in Overweight and Prediabetic Older Persons: Plasma Biomarkers of Abrupt Changes in Physical Activity. *Metabolites* **2019** (*under review*).

(29) Vilar-Gomez, E.; Chalasani, N. Non-invasive Assessment of Non-alcoholic Fatty Liver Disease: Clinical Prediction Rules and Blood-based Biomarkers. *J. Hepatol.* **2018**, *68*, 305–315.

(30) Kazemi-Shirazi, L.; Endler, G.; Winkler, S.; Schickbauer, T.; Wagner, O.; Marsik, C. Gamma Glutamyltransferase and Long-term Survival: Is it Just the Liver? *Clin. Chem.* **2007**, *53*, 940–946.

(31) Whitfield, J. B. Gamma Glutamyl Transferase. *Crit. Rev. Clin. Lab. Sci.*

2001, *38*, 263–355.

(32) Lee, D. H.; Blomhoff, R.; Jacobs, D. R. Is Serum Gamma Glutamyltransferase a Marker of Oxidative Stress? *Free Radic Res*, **2004,** *38*, 535–539.

(33) Ruttmann, E.; Brant, L. J.; Concin, H.; Diem, G.; Rapp, K.; Ulmer, H.; Vorarlberg Health Monitoring and Promotion Program Study Group. Gamma-Glutamyltransferase as a Risk Factor for Cardiovascular Disease Mortality: An Epidemiological Investigation in a Cohort of 163,944 Austrian Adults. *Circulation,* **2005**,112, 2130–2137.

(34) André, P.; Balkau, B.; Vol, S.; Charles, M. A.; Eschwège, E.; DESIR Study Group. Gamma-Glutamyltransferase Activity and Development of the Metabolic Syndrome (International Diabetes Federation Definition) in Middle-aged Men and Women: Data from the Epidemiological Study on the Insulin Resistance Syndrome (DESIR) Cohort. *Diabetes Care* **2007**, *30*, 2355–2361.

(35) Liu, C. F.; Zhou, W. N.; Fang, N. Y. Gamma-Glutamyltransferase Levels and Risk of Metabolic Syndrome: A Meta-analysis of Prospective Cohort Studies. *Int. J. Clin. Pract.* **2012**, *66*, 692–698.

(36) Hagström, H.; Nasr, P.; Ekstedt, M.; Hammar ,U.; Stål, P.; Askling, J.; Hultcrantz, R.; Kechagias, S. Cardiovascular Risk Factors in Non-alcoholic Fatty Liver Disease. *Liver Int.* **2019**, 39, 197–204.

(37) Hagström, H.; Nasr, P.; Ekstedt, M.; Hammar, U.; Stål, P.; Hultcrantz, R.; Kechagias, S. Fibrosis Stage But Not NASH Predicts Mortality and Time to Development of Severe Liver Disease in Biopsy-proven NAFLD. *J. Hepatol.* **2017**, 67, 1265-1273.

(38) Honda, Y.; Kessoku, T.; Sumida, Y.; Kobayashi, T.; Kato, T.; Ogawa, Y.; Tomeno, W.; Imajo, K.; Fujita, K.; Yoneda, M.; Kataoka, K.; Taguri, M.; Yamanaka, T.; Seko, Y.; Tanaka, S.; Saito, S.; Ono, M.; Oeda, S.; Eguchi, Y.; Aoi, W.; Sato, K.; Itoh, Y.; Nakajima, A. Efficacy of Glutathione for the Treatment of Nonalcoholic Fatty Liver Disease: An Open-label, Single-arm, Multicenter, Pilot Study. *BMC Gastroenterol.* **2017**, *17*, 96.

(39) Pizzorno, J. Glutathione! *Integr. Med. (Encinitas)* **2014**, *13*, 8–12.

2.8 Supporting Information

Table S2.1: Distribution of standardized histopathology grading score of Japanese NASH patients, including sub-groups of patients identified from unsupervised pattern recognition using HCA

Histopathology Characteristic	Grade	Full Cohort (*n*=111)	Subgroup A (*n*=52)	Subgroup B (*n*=64)
Fibrosis Grade (F-Score)	0-1	13	5	8
	2	25	13	12
	3	47	17	30
	4	26	14	12
Inflammation (I-Score)	0-1	5	2	3
	2	53	24	29
	3	53	23	30
Ballooning	0-1	68	28	39
	2	40	20	20
Steatosis Grade (S-Score)	1	11	4	7
	2	35	21	14
	3	66	25	41

Table S2.2: MRM parameters employed for targeted analysis of sixteen serum γ-glutamyl dipeptides using MSI-CE-MS/MS as adapted from Hirayama *et al.* (2014).[20]

Compound	Q1 (*m/z*)	Q3 (*m/z*)	Fragmentor voltage (V)	Collision energy (V)
TAD (IS)	194.1	148.1	100	13
γ-Glu-Gly	205.1	84.1	80	25
γ-Glu-Ala	219.1	84.1	70	21
γ-Glu-Ser	235.1	84.1	85	25
γ-Glu-Val	247.1	72.1	100	17
γ-Glu-Thr	249.1	84.1	90	29
γ-Glu-Orn	262.1	70.1	85	29
γ-Glu-Asn	262.1	133.1	100	9
γ-Glu-Gln	276.1	84.1	70	29
γ-Glu-Glu	277.1	84.1	65	29
γ-Glu-Met	279.1	150	95	9
γ-Glu-His	285.1	156	90	9
γ-Glu-Phe	295.1	120.1	80	25
γ-Glu-Arg	304.2	175.1	90	12
γ-Glu-Cit	305.2	70.1	95	37
γ-Glu-Tyr	311.1	182.1	70	13
γ-Glu-Trp	334.1	188.1	70	21

Table S2.3: Spike and recovery studies performed on 14 γ-glutamyl dipeptide standards spiked at four different concentrations levels in pooled serum QC samples from NASH patients

	% Recovery			
Compound	**Level 1**	**Level 2**	**Level 3**	**Level 4**
γ-Glu-Ser	192	107	114	104
γ-Glu-Val	89	103	103	101
γ-Glu-Thr	80	92	96	104
γ-Glu-Orn	51	167	97	105
γ-Glu-Asn	133	114	101	104
γ-Glu-Gln	162	118	113	104
γ-Glu-Glu	126	103	105	104
γ-Glu-Met	227	104	112	102
γ-Glu-His	104	136	96	102
γ-Glu-Phe	45	99	103	109
γ-Glu-Arg	124	115	137	140
γ-Glu-Cit	168	121	110	114
γ-Glu-Tyr	150	116	103	99
γ-Glu-Trp	178	131	95	114
Overall Recovery (%)	131±53	116±19	106±11	108±10

Table S2.4: Serum γ-glutamyl dipeptide concentrations and liver enzyme activities for two sub-groups of NASH patients classified by their γ-glutamyl dipeptide status using ANCOVA.

γ-Glutamyl Dipeptide	A-High Risk (*n*=52)[a]	B-Low Risk (*n*=64)[a]	*F*-value	*p*-value[b]	*q*-value[b]	Effect Size[c]	FC[d]
γ-Glu-Glu	0.98±0.46	3.63±1.56	208	2.55E-27	4.59E-26	0.65	3.70
γ-Glu-Thr	0.30±0.14	0.73±0.27	145	5.29E-22	4.76E-21	0.56	2.46
γ-Glu-Val	0.70±0.34	1.95±0.82	132	1.03E-20	6.17E-20	0.54	2.77
γ-Glu-Tyr	0.15±0.07	0.32±0.11	102	1.58E-17	7.10E-17	0.48	2.06
γ-Glu-His	0.34±0.16	0.91±0.32	90	4.56E-16	1.64E-15	0.44	2.71
γ-Glu-Orn	0.59±0.31	1.46±0.60	85	2.12E-15	6.37E-15	0.43	2.48
γ-Glu-Asn	0.19±0.08	0.37±0.14	77	2.61E-14	5.88E-14	0.41	1.99
γ-Glu-Gln	2.79±1.69	3.10±2.97	77	2.61E-14	5.88E-14	0.41	1.11
γ-Glu-Phe	0.17±0.09	0.35±0.14	71	1.36E-13	2.71E-13	0.39	2.09
γ-Glu-Ser	0.78±0.45	1.66±0.73	53	6.18E-11	1.11E-10	0.34	2.12
γ-Glu-Arg	0.56±0.38	1.26±0.71	50	1.62E-10	2.66E-10	0.32	2.23
γ-Glu-Trp	0.03±0.01	0.05±0.02	46	8.02E-10	1.14E-09	0.30	1.67
γ-Glu-Gly	1.29±1.00	3.11±1.81	45	8.23E-10	1.14E-09	0.28	2.41
γ-Glu-Ala	0.57±0.41	1.22±0.84	26	1.68E-06	2.16E-06	0.20	2.12
γ-Glu-Cit	0.11±0.07	0.20±0.13	14	3.42E-04	3.85E-04	0.14	1.87
γ-Glu-Met	0.15±0.08	0.21±0.16	1	0.472	0.472	0.01	1.38
GGT	144±133	69±65	16	1.04E-04	1.25E-04	0.13	0.48

[a] *Average γ-glutamyl dipeptide serum concentrations and their standard deviation measured by MSI-CE-MS/MS*

[b] *p-values adjusted for sex, whereas q-values are based on False Discovery Rate using a Benjamini-Hochberg procedure for multiple hypothesis correction.*

[c] *Effect size using Partial Eta Square where small effects > 0.01, medium effects > 0.06 and large effects > 0.14*

[d] *Average fold-change (FC) based on ratio of γ-glutamyl dipeptide concentrations in sub-groups of patients (B/A).*

Table S2.5: Summary of serum γ-glutamyl dipeptides concentrations in adult Japanese NASH patients (*n*=111) based on steatosis severity (S1-S3) from histopathology

Compound	Mean serum concentration (μM) with ± 1s			*p*-value*
	S1 (*n*=11)	S2 (*n*=35)	S3 (*n*=66)	
γ-Glu-Gly	3.22±2.66	2.20±1.66	2.20±1.65	0.545
γ-Glu-Ala	1.36±1.14	0.92±0.91	0.93±0.61	0.489
γ-Glu-Ser	1.67±1.08	1.20±0.70	1.30±0.74	0.395
γ-Glu-Val	1.57±1.22	1.12±0.77	1.49±0.87	0.104
γ-Glu-Thr	0.64±0.37	0.43±0.26	0.58±0.31	0.051
γ-Glu-Orn	1.40±0.96	1.04±0.60	1.02±0.62	0.524
γ-Glu-Asn	0.37±0.24	0.29±0.13	0.28±0.13	0.612
γ-Glu-Gln	3.51±3.14	3.33±2.88	2.67±2.22	0.540
γ-Glu-Glu	3.50±2.53	2.09±1.82	2.44±1.58	0.114
γ-Glu-Met	0.20±0.13	0.17±0.13	0.19±0.15	0.711
γ-Glu-His	0.77±0.45	0.61±0.40	0.65±0.37	0.447
γ-Glu-Phe	0.28±0.17	0.21±0.13	0.29±0.15	0.019
γ-Glu-Arg	1.27±0.92	0.75±0.46	1.02±0.72	0.090
γ-Glu-Cit	0.26±0.19	0.16±0.10	0.15±0.11	0.134
γ-Glu-Tyr	0.25±0.13	0.21±0.13	0.26±0.11	0.065
γ-Glu-Trp	0.04±0.02	0.04±0.02	0.04±0.02	0.633

**p-value obtained from Kruskal-Wallis Test*

Table S2.6: Summary of serum γ-glutamyl dipeptide concentrations in the NASH study cohort (*n*=106) based on NASH Activity Score (NAS) for borderline/probable and definitive diagnosis

Dipeptide	Mean serum concentration (μM) with ± 1s		*p*-value*
	Borderline NASH (*n*=19) NAS < 5	NASH (*n*=87) NAS ≥ 5	
γ-Glu-Gly	2.20±1.61	2.34±1.64	0.713
γ-Glu-Ala	1.07±0.78	0.96±0.73	0.605
γ-Glu-Ser	1.27±0.81	1.33±0.70	0.719
γ-Glu-Val	1.39±1.03	1.41±0.87	0.781
γ-Glu-Thr	0.52±0.30	0.55±0.31	0.683
γ-Glu-Orn	1.17±0.88	1.07±0.59	0.905
γ-Glu-Asn	0.33±0.20	0.29±0.13	0.612
γ-Glu-Gln	3.45±3.12	2.78±2.31	0.462
γ-Glu-Glu	2.43±2.18	2.46±1.67	0.415
γ-Glu-Met	0.15±0.14	0.19±0.14	0.250
γ-Glu-His	0.69±0.43	0.66±0.38	0.806
γ-Glu-Phe	0.24±0.13	0.27±0.15	0.617
γ-Glu-Arg	0.89±0.65	0.98±0.66	0.471
γ-Glu-Cit	0.21±0.11	0.15±0.10	0.119
γ-Glu-Tyr	0.22±0.11	0.25±0.12	0.368
γ-Glu-Trp	0.04±0.02	0.04±0.02	0.889

**p-value obtained from Mann-Whitney U Test*

Table S2.7: Summary of the relationship of serum γ-glutamyl dipeptides concentrations in adult Japanese NASH patients (*n*=111) based on fibrosis score from histopathology

Dipeptide	Mean serum concentration (µM) with ± 1s				*p*-value*
	F1 (*n*= 13)	F2 (*n*= 25)	F3 (*n*= 47)	F4 (*n*= 26)	
γ-Glu-Gly	2.09±1.46	2.02±1.91	2.50±1.54	2.31±2.24	0.417
γ-Glu-Ala	0.95±0.68	0.82±0.66	1.03±0.66	0.99±1.14	0.433
γ-Glu-Ser	1.19±0.68	1.30±0.92	1.27±0.71	1.48±0.86	0.729
γ-Glu-Val	1.53±0.96	1.31±1.01	1.52±0.87	1.15±0.76	0.244
γ-Glu-Thr	0.63±0.33	0.47±0.29	0.56±0.31	0.53±0.30	0.386
γ-Glu-Orn	1.09±0.70	0.94±0.73	1.15±0.59	1.04±0.70	0.407
γ-Glu-Asn	0.29±0.17	0.29±0.20	0.31±0.12	0.26±0.15	0.195
γ-Glu-Gln	2.74±2.31	3.85±3.20	2.91±2.27	2.67±2.85	0.579
γ-Glu-Glu	2.98±2.09	2.23±1.94	2.47±1.48	2.35±2.08	0.470
γ-Glu-Met	0.20±0.17	0.15±0.14	0.18±0.13	0.22±0.15	0.414
γ-Glu-His	0.76±0.48	0.59±0.42	0.67±0.34	0.62±0.41	0.493
γ-Glu-Phe	0.29±0.13	0.25±0.13	0.27±0.15	0.26±0.17	0.700
γ-Glu-Arg	1.10±1.06	0.98±0.67	0.98±0.62	0.85±0.62	0.796
γ-Glu-Cit	0.18±0.09	0.17±0.12	0.16±0.11	0.16±0.16	0.783
γ-Glu-Tyr	0.27±0.11	0.21±0.12	0.24±0.11	0.27±0.15	0.493
γ-Glu-Trp	0.04±0.02	0.04±0.02	0.04±0.02	0.04±0.02	0.252

**p-value obtained from Kruskal-Wallis Test*

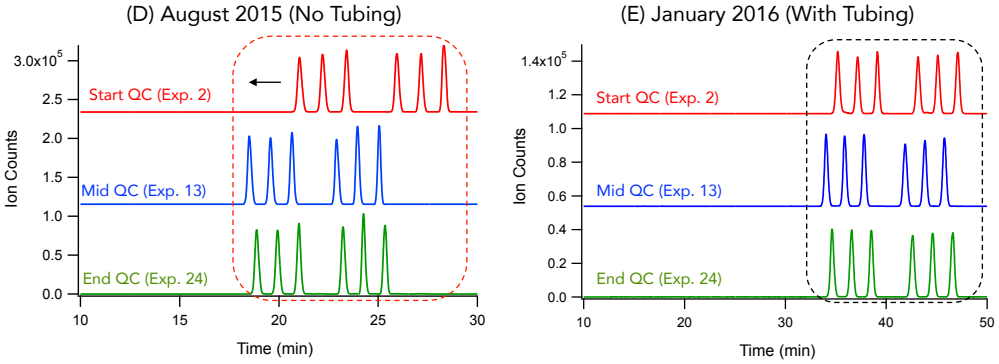

Figure S2.1: Representative extracted ion electropherograms (EIEs) for the internal standard (TAD) added to pooled serum extracts from NASH patients as QC samples (together with a blank extract) analyzed at the start (run#2), middle (run#13) and end (run#24) of data workflow when using MSI-CE-MS/MS. These runs were performed independently either without (August 2015) and with (January 2016) temperature control of the capillary outlet with a tubing sleeve and circulating liquid coolant. Note changes in apparent migration times due to differences in solution viscosity and greater migration time stability of runs performed with thermal control of the capillary outlet.

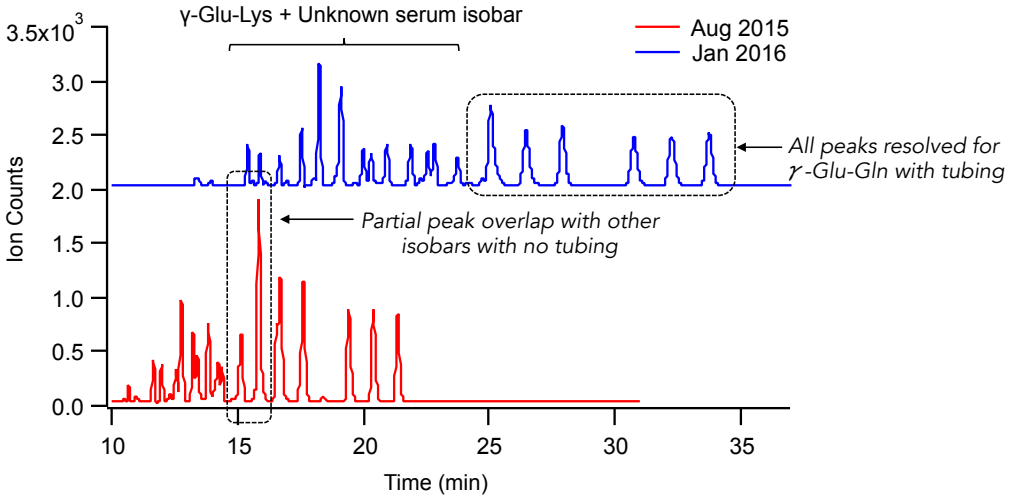

Figure S2.2: An overlay to two ion electropherograms for the mid-QC run (run#13) in the standardized data workflow performed independently without (August 2015) and with (January 2016) temperature control of the capillary outlet highlighting the longer migration times and greater peak capacity improves the resolution of γ-Glu-Glu from its isobar γ-Glu-Lys as well unknown minor serum isobaric interference.

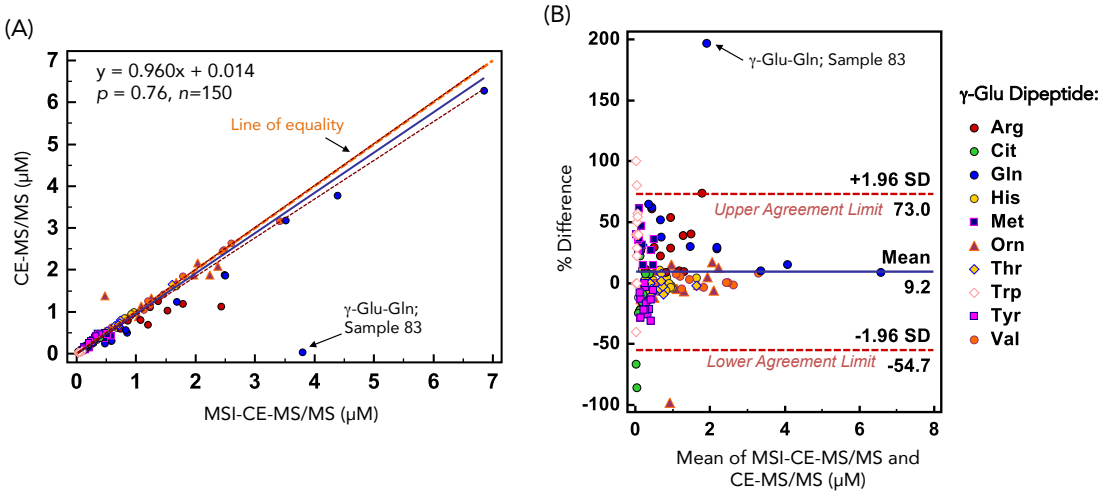

Figure S2.3: (a) A Passing-Bablok regression analysis and (b) % difference Bland-Altman plot comparing the quantification of 10 serum γ-glutamyl dipeptides consistently measured from fifteen NASH patients (n=150) using a conventional single injection CE-MS/MS method as compared to the multiplexed separation method based on MSI-CE-MS/MS. Overall, good mutual agreement was achieved for measured γ-glutamyl dipeptide concentrations in serum extracts with a slope of 0.960 within line of equity, as well as a mean bias of 9.2% with few outlier data outside agreement limits ($p < 0.05$; ± 2 s).

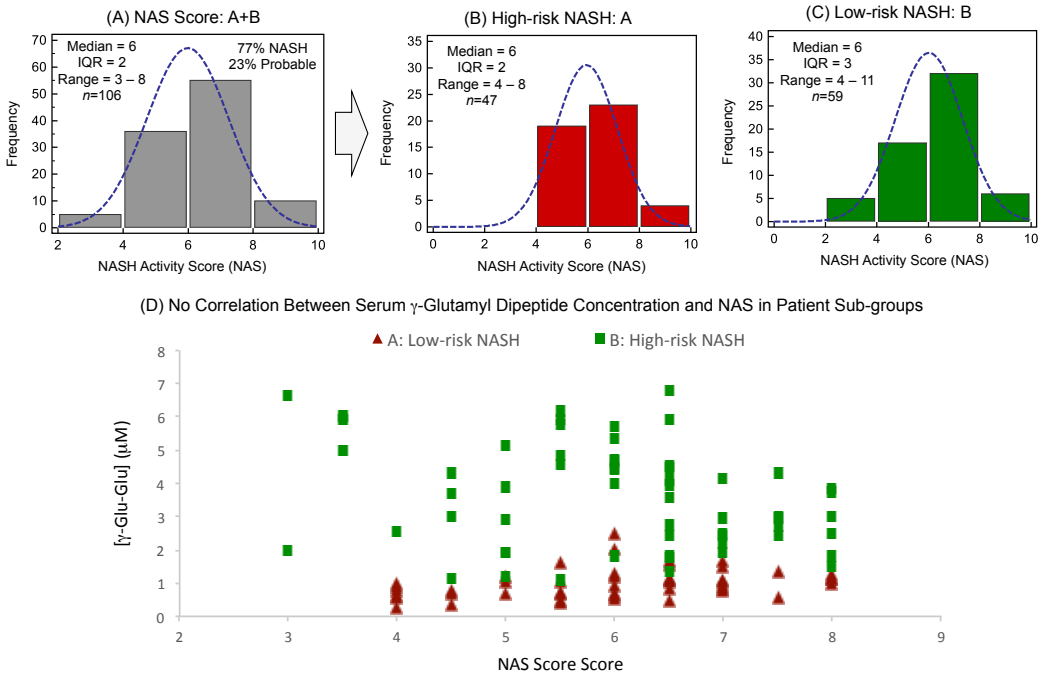

Figure S2.4: A summary of the distribution of NAS data (median NAC = 6.0) from a cohort of probable and mostly definitively diagnosed NASH patients (*n*=111) after standardized histopathology, which highlights that both sub-sets of NASH patients with differential serum γ-glutamyl dipeptide status have equivalent severity of liver steatosis, ballooning and/or inflammation. Similar results were also noted for fibrosis grade scoring, as well as NAS+Fibrosis distributions among NASH patients confirming that there was no direct association between measured serum γ-glutamyl dipeptide concentrations and histopathology diagnostic scoring.

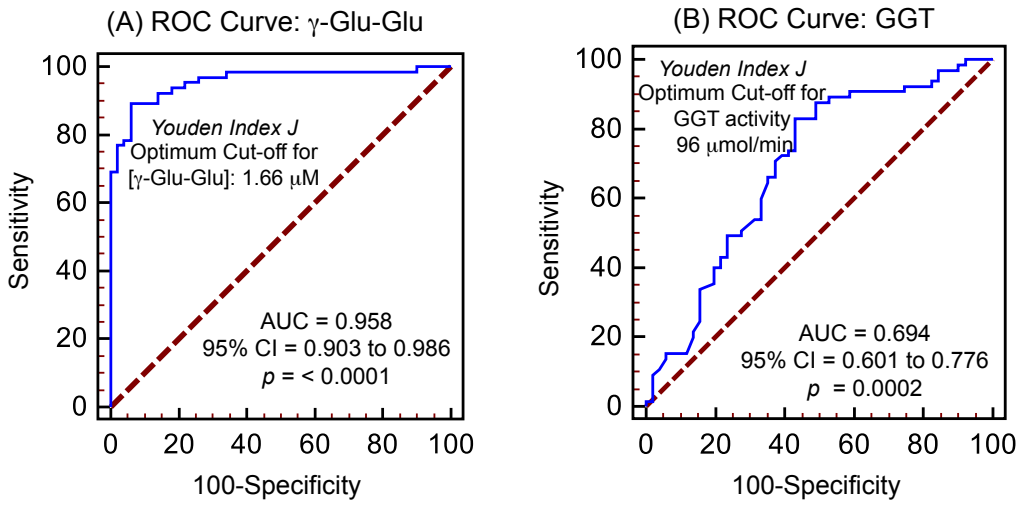

Figure S2.5: A comparison of receiver operating characteristic (ROC) curves from (a) the top-ranked serum γ-glutamyl dipeptide (γ-Glu-Glu concentration) as compared to (b) GGT activity that were measured in a cohort of adult Japanese NASH patients (n=116) who were largely comorbid with other metabolic conditions, including hypertension, dyslipidemia and type 2 diabetes. Overall, there was a negative correlation between γ-Glu-Glu and GGT activity (r = 0.46, p = 2.5 E-7), however γ-Glu-Glu was able to better discriminate (AUC = 0.958) between a sub-set of low-risk (n=64) and high-risk (n=52) NASH patients as compared to GGT activity (AUC = 0.694). Optimum cut-off concentrations for γ-Glu-Glu in serum are 1.66 μM as compared to 96 μmol/min for GGT activity for differentiation between two sub-groups of NASH patients based on their γ-glutamyl dipeptide status.

Chapter III
Metabolic Perturbations from Step Reduction in Overweight and Prediabetic Older Persons: Plasma Biomarkers of Abrupt Physical Inactivity

Michelle Saoi, Alice Li, Chris McGlory, Tanner Stokes, Mark T. von Allmen, Stuart M. Phillips and Philip Britz-McKibbin

Metabolites, **2019** (Under Review)

M.S. performed all the experiments including sample preparation, data acquisition using MSI-CE-MS, data processing, interpretation, statistical analysis and wrote the initial draft for publication. A.L. assisted with sample preparation and interpretation. C.M., T.S., M.v.A and S.M.P obtained ethics approval for study, designed the study, provided plasma specimens, assisted with interpretation, provided valuable feedback and revised the initial manuscript. P.B.M provided feedback on the manuscript draft.

Chapter III: Metabolic Perturbations from Step Reduction in Overweight and Prediabetic Older Persons: Plasma Biomarkers of Abrupt Physical Inactivity

3.1 Abstract

Sarcopenia is the age-related loss of skeletal muscle mass, strength and function, which may be accelerated during periods of physical inactivity. Declines in skeletal muscle and functionality not only impacts mobility, but also increases chronic disease risk, such as type 2 diabetes. The aim of this study was to measure adaptive metabolic responses to acute changes in habitual activity in a cohort of overweight, pre-diabetic older adults (age = 69 ± 4 years; BMI = 27 ± 4 kg/m^2, n=17) when using nontargeted metabolite profiling by multisegment injection-capillary electrophoresis-mass spectrometry. Participants completed two weeks of step reduction (< 1000 steps/day) followed by a two week recovery period, where fasting plasma samples were collected at three time intervals at baseline, after step reduction and following recovery. Two weeks of step reduction elicited increases in circulatory metabolites associated with a decline in muscle energy metabolism and increased protein degradation, including glutamine, carnitine and creatine (q < 0.05; effect size > 0.30), as well as methionine and deoxycarnitine (p < 0.05; effect size ≈ 0.20) as compared to baseline. Similarly, decreases in uremic toxins in plasma that promote muscle inflammation, indoxyl sulfate and hippuric acid, as well as oxoproline, a by-product of glutathione metabolism were also associated with inactivity (p < 0.05; effect size > 0.20). Our results indicate that older persons are susceptible to metabolic changes to short-term step reduction that were not fully reversible with resumption of normal ambulatory activity over the same time period. These plasma biomarkers may enable early detection of inactivity-induced metabolic dysregulation in older persons at risk for sarcopenia that is not readily measured by imaging methods, which is also applicable towards the design of effective therapeutic interventions to counter these deleterious changes in support of healthy ageing.

3.2 Introduction

Sarcopenia is the progressive, degenerative decline in skeletal muscle mass, function and strength and is measurable after the fifth decade of life [1–3] affecting 5-13% of 60-70 year olds and up to 50% in those 80 years and older [4]. Multiple factors contribute to sarcopenia, including age-related biological changes (*e.g.*, chronic inflammation, oxidative stress, hormonal alterations), malnutrition (*e.g.*, decreased protein and total caloric intake), as well as physical inactivity [1,4,5]. All these stressors contribute to profound physiological and morphological changes in skeletal muscle structure and function, leading to a loss in functionality and independence [2,6] with greater physical frailty [7]. Increasing rates of obesity have also been implicated in the higher incidence of sarcopenia, with older adults faced with the combined metabolic burdens of excess adiposity and reduced muscle mass referred to as sarcopenic obesity [8]. Nevertheless, a consensus on an exact definition of sarcopenia remains elusive due to comorbidity with other diseases, as well as inconsistent thresholds, reference standards and instrumental methods used for measuring lean body mass despite its recent recognition as an independent condition in 2016 [9].

The current gold-standard for diagnosis of sarcopenia relies on imaging techniques based on dual-energy X-ray absorptiometry (DXA) that provides an index of skeletal muscle mass [10]; however inaccuracies have been reported when comparing data from different manufacturers/instruments [11], and sensitivity is limited when detecting small changes in muscle mass for early detection of sarcopenia. For these reasons, qualitative measures of muscle strength and function are also assessed using standardized performance tests such as the handgrip strength test [12], gait speed [13], and short physical performance battery (*i.e.,* balance, walking speed and strength) [14]. Thus, both functional and quantitative measures of skeletal muscle health are needed to better distinguish sarcopenia from other muscle-related ageing processes prevalent in older adults since gains in muscle

mass do not necessarily prevent age-related loss in muscle strength [15]. The progressive loss in muscle quality, strength and metabolic decline contributes to a profound decline in quality of life in affected seniors with deleterious health outcomes, including physical impairments, chronic disease risk (*e.g.,* type 2 diabetes), as well as cognitive impairments and depression [2,6]. For these reasons, sarcopenia places an increasingly severe burden on public healthcare resources due to loss of mobility, with greater risk for falls or fractures resulting in new or prolonged hospitalization and institutionalization [16,17]. Direct and indirect healthcare expenditures associated with sarcopenia are projected to expand dramatically due to an ageing demographic in most developed countries [5].

As a result, there is an urgent need to implement public policies that promote healthy ageing to prevent sarcopenia on a population level; however, a fundamental understanding of the molecular mechanisms associated with sarcopenia is lacking, including reliable screening tools for identifying high risk individuals. Herein, we performed nontargeted metabolite profiling using multisegment injection-capillary electrophoresis-mass spectrometry (MSI-CE-MS) on plasma samples collected from a cohort of older adults who completed two weeks of reduced daily stepping, followed by two weeks of recovery upon return to habitual ambulatory activity [18]. We aimed to elucidate adaptive metabolic responses to abrupt changes in physical activity (via step reduction), an increasingly common scenario in aging, based on dynamic changes in the plasma metabolome at three time intervals during the intervention. Our work identified a panel of circulating biomarkers that reflect inactivity-induced metabolic dysregulation corresponding to early stages of protein degradation within muscle tissue. To the best of our knowledge, this is the first metabolomics study to examine the systemic effects from physical inactivity on overweight/pre-diabetic older persons at risk for sarcopenia, which was used as a model system of muscle disuse less severe than prolonged bed-rest or hospitalization cases.

3.3 Results

3.3.1 High throughput metabolomic studies of plasma filtrates using MSI-CE-MS

Multiplexed separations based on MSI-CE-MS offer a high throughput platform for biomarker discovery in metabolomics that is optimal for analysis of mass or volume-restricted biological specimens ranging from dried blood spot punches, infant sweat specimens to skeletal muscle tissue biopsies [19–22]. Major improvements in sample throughput are achieved without added infrastructure costs or complicated column switching programs, which allows for stringent quality control (QC) and batch correction [23]. To date, previous studies have employed a serial hydrodynamic injection of discrete sample plugs (*i.e.,* typically seven) between alternating segments of background electrolyte (BGE) within a single experimental run [24]. In this work, we implemented a modified serial injection format in MSI-CE-MS comprising of 13 plasma filtrate samples when using electrokinetic BGE spacers in order to further boost sample throughput (< 3 min/sample), separation resolution and peak capacity as compared to conventional single injection separations. This process initiates zonal electrophoretic separation of ions and their isomers/isobars immediately after each sample injection and thus, takes advantage of the total effective capillary length as shown in **Figure 3.1A**. Novel experimental workflows can be designed in MSI-CE-MS via customized, serial injection configurations that is effective for metabolite authentication when performing nontargeted profiling in order to reject a plethora of background or redundant signals (*e.g*., in-source fragments, isotope signals, adduct ions) generated in ESI-MS [20,25]. For example, a randomized injection of plasma filtrate samples from each participant was analyzed in duplicate with a distinct dilution pattern (1:1, 1:2, 2:1) to encode sample position information reflecting the study design of the experiment (**Figure 3.1B**). Each run in MSI-CE-MS also includes a pooled QC and/or blank filtrate to assess technical precision and confirm the lack of sample carry-over between injections. Each ion was annotated based on its characteristic

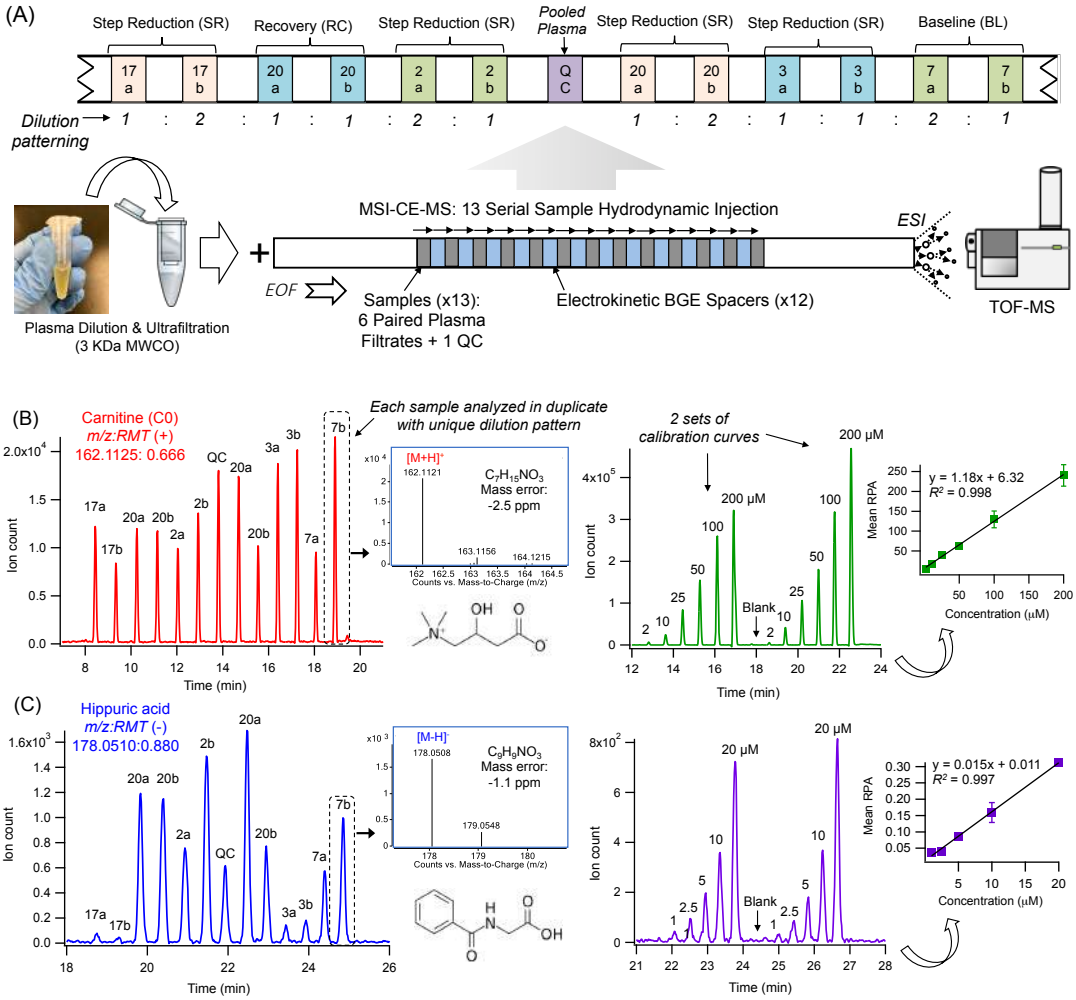

Figure 3.1: Multiplexed separations by MSI-CE-MS for rapid metabolite profiling of 13 samples within a single run, including their reliable identification and quantification in plasma. (A) Plasma filtrate samples were prepared after ultrafiltration and then randomly analyzed as paired duplicates using a temporal dilution pattern (1:2, 1:1, 2:1) at three time points in this repeated measures step reduction intervention. Also, a pooled plasma QC and/or blank filtrate sample was injected within each in run in order to assess technical precision and potential sample carry-over effects, respectively. (B) Representative extracted ion electropherograms for a cationic plasma metabolite, carnitine as denoted by its *m/z*:RMT (162.112:0.666, $[M+H]^+$) and most likely molecular formula with low mass error. Two different serial injection configurations in MSI-CE-MS are depicted here, including a randomized analysis of six pairs of plasma samples from each participant at a specific time point from this study, and a duplicate six-point calibration curve for metabolite quantification. (C) Two analogous extracted ion electropherograms are shown for a major anionic plasma metabolite detected under negative ion mode, hippuric acid as denoted by its *m/z*:RMT (178.0510:0.880, $[M-H]^-$) and most likely molecular formula with low mass error. Note the much larger between-subject biological variance of plasma hippuric acid relative to circulating levels of carnitine, which is also evident based on comparison to the mean average from the peak intensity of each QC.

accurate mass and relative migration time (*m/z*:RMT) under positive (+) or negative (-) ion mode detection with putative identification (*level 2*) based on its most likely molecular formula using high resolution MS as shown in extracted ion electropherograms for representative cationic (**Figure 3.1B**) and anionic (**Figure 3.1C**) plasma metabolites, such as carnitine (162.112:0.666 as $[M+H]^+$) and hippuric acid (178.051:0.880 as $[M-H]^-$). Unambiguous identification of plasma metabolites (*level 1*) was then achieved based on their co-migration and MS/MS spectra match when compared to an authentic standard based on recommended guidelines from the Metabolomics Standards Initiative [26,27]. Once identified, a different injection format in MSI-CE-MS was used to acquire calibration curves for metabolite quantification in plasma samples as shown for a series of calibrant solutions for carnitine and hippuric acid under positive and negative ion modes, respectively (**Figure 3.1B, C**).

3.3.2 Plasma metabolic phenotyping of healthy seniors in a step reduction study

This work involved nontargeted metabolite profiling of plasma samples collected from a cohort of overweight, pre-diabetic older men and women participating in a step reduction trial (ClinicalTrials.gov #NCT03039556) [18]. In order to minimize confounding effects, all participants were provided standardized meals for 3 days prior to clinical visits to collect fasting plasma in the morning while maintaining normal habitual diet/activity with exception of the two-week step reduction period (< 1000 steps/day). Only participants (n=17 of 22) who had complete fasting plasma samples collected at three time intervals were included in this study [18], which included slightly more males (58%) with a mean age of 69 years who were largely overweight Caucasians with a mean BMI of 27 kg/m^2 recruited from the local community as summarized in **Table 3.1**. Overall, all participants underwent about an eight-fold reduction (p = 2.70 E-6) in habitual physical activity via step reduction as compared to baseline and recovery periods as confirmed by a

Table 3.1: Summary of physical and clinical characteristics and daily activity of study cohort

	Baseline (BL)	**Step Reduction (SR)**	**Recovery (RC)**	***p*-value***
Sex	10 male, 7 female	-	-	
Age (years)	69 ± 4	-	-	
Body Mass (kg)	75 ± 14	76 ± 15	76 ± 15	0.26
BMI ($kg \cdot m^2$)	27 ± 4	27 ± 4	27 ± 4	0.16
Daily Energy Expenditure (kJ)	9890 ± 2680	8118 ± 1350	9498 ± 2310	2.99 E-04
Myofibrillar Protein Synthesis (% per day)	1.50 ± 0.06	1.33 ± 0.05	1.32 ± 0.14	0.040
Pedometer Steps (per day)	7550 ± 3320	980 ± 84	7345 ± 3850	2.70 E-06
Armband steps (per day)	6375 ± 3560	1248 ± 850	5612 ± 3740	1.33 E-04
Fasting glucose (mM)	5.24 ± 0.61	5.31 ± 0.92	5.47 ± 0.73	0.26
(mg/dL)	94 ± 11	96 ± 17	99 ± 13	0.26
2h Post-OGTT glucose (mM)	7.6 ± 1.5	9.0 ± 2.4	8.2 ± 2.9	0.070
(mg/dL)	137 ± 26	163 ± 43	147 ± 53	0.070

** p-values determined using a one-way repeated measures ANOVA*

pedometer assigned to each participant, as well as independent armband measurements [18]. As expected, this drastic change in habitual activity resulted in a corresponding decrease in total energy expenditure (p = 2.99 E-4), and a modest reduction in myofibrillar protein biosynthesis (p = 0.040) following step reduction [18]. All participants were generally healthy and moderately active upon recruitment for this study; however, standardized oral glucose tolerance tests (OGTT) during clinical visits revealed that a majority (53%) of participants were at risk for prediabetes at baseline due to impaired fasting glucose (6.1-6.9 mM) and/or impaired glucose tolerance (2hPG = 7.8 – 11 mM) based on diagnostic criteria defined by Diabetes Canada [28]. After completing step reduction and recovery periods, three additional subjects had 2hPG levels that satisfied criteria for prediabetes. Therefore, after the intervention about 88% of the study cohort were defined as prediabetic who are at risk for cardiovascular disease [29], with three (23%) subjects at highest risk since they both had impaired fasting glucose and

impaired glucose tolerance results. **Supplemental Figure S3.1** depicts individual changes in glucose metabolism for all participants in this study, which also highlights that one participant with borderline impaired fasting glucose at baseline later developed diabetes after step reduction. Indeed, step reduction resulted in a modest overall decrease in glucose tolerance (p = 0.070) in this cohort of largely pre-diabetic, overweight older persons.

Figure 3.2(A) depicts the overall study design which included repeat fasting plasma samples collected at three time intervals for each participant at baseline, after 2 weeks of step reduction and after recovery when resuming normal ambulatory activity for 2 weeks. Stringent selection criteria were applied when performing nontargeted metabolite profiling of plasma in order to reduce bias and false discoveries as described elsewhere [20,21]. Briefly, after initial metabolite authentication and identification when using a dilution trend filter on a pooled plasma sample, only frequently detected plasma metabolites measured in the majority of samples in this cohort (> 75%), with acceptable technical precision based on repeated analysis of QCs (average CV < 30%, n=25), were included in the final data matrix. Overall, a total of 47 polar/ionic metabolites from plasma filtrate samples satisfied these selection criteria with most metabolites identified with authentic standards (*level 1*), including circulating amino acids, acylcarnitines, biogenic amines, organic acids and various secondary metabolites as their glucuronide, glycine, or sulfate conjugates (**Table S3.1 of Supporting Information**). As expected, the overall biological variance in the plasma metabolome was considerably larger (median CV = 33%, n=51) as compared to the technical precision for QCs (median CV = 15%, n=25) as shown in the 2D scores plots from a principal component analysis (PCA) in **Figure 3.2B.** A 2D heat map with hierarchical cluster analysis (HCA) summarizes the overall data structure involving 47 plasma metabolites denoted by their *m/z*:RMT consistently measured in the majority of participants at three time points in this study. In all cases, average

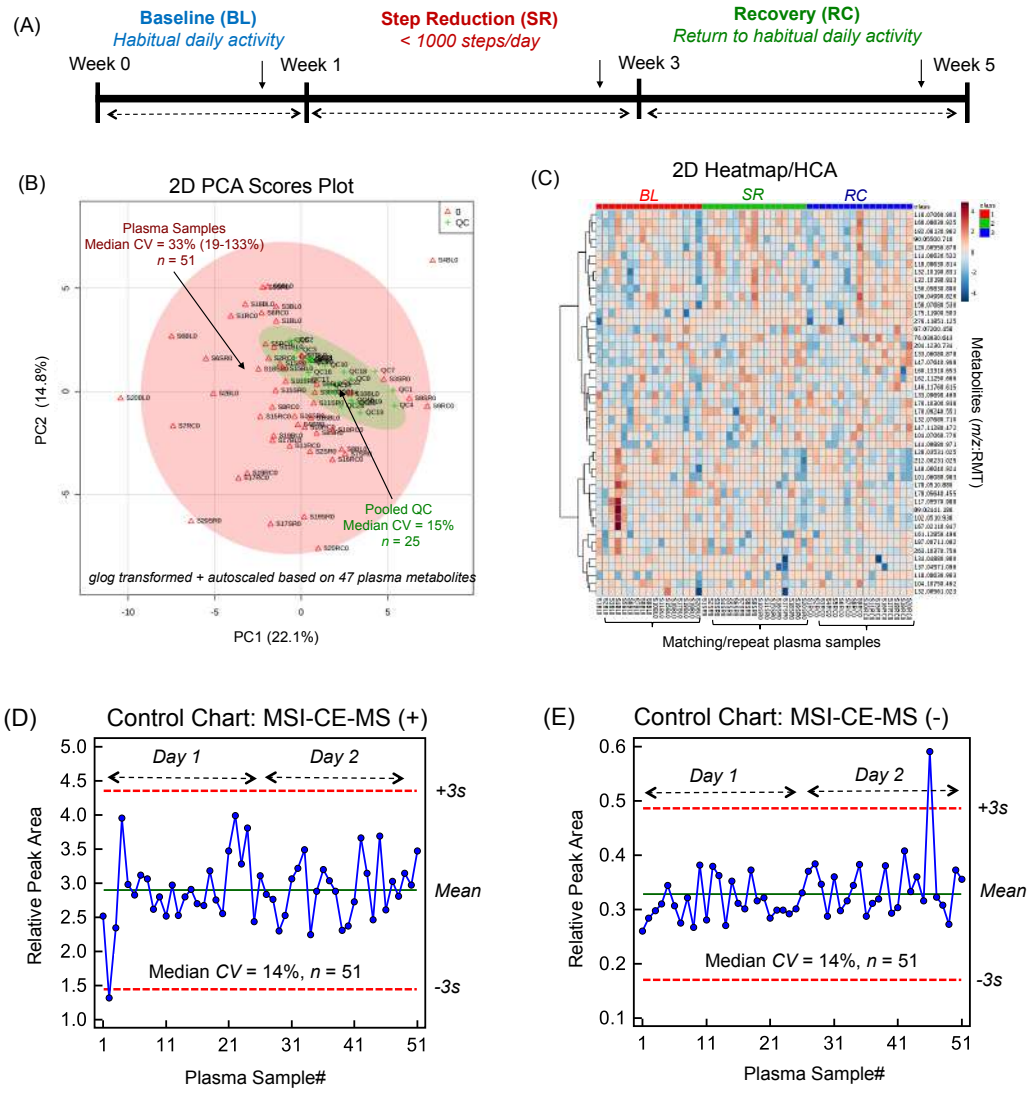

Figure 3.2: An overview of the study design and data structure from metabolome analyses using MSI-CE-MS for matching fasting plasma samples collected at three time intervals for all participants. (A) Study design of this repeat measures step reduction intervention trial with fasting plasma samples collected at three time intervals, including baseline (BL), after 2 weeks of step reduction (SR) and following 2 weeks of recovery to habitual physical activity (RC). Two unsupervised multivariate data analysis methods for summarizing *glog*-transformed and autoscaled plasma metabolome data, including a (B) PCA with a 2D scores plot used to compare overall biological variance of fasting plasma samples to the technical precision from repeat analysis of pooled QC, and (C) 2D heat map with HCA for depicting overall data structure in this study. Also, control charts for recovery standard (F-Phe) measured under (D) positive ion and (E) negative ion modes for all plasma samples highlights acceptable intermediate precision (CV = 14%) with few outliers (2 out of 102) exceeding warning limits (± 3s).

ion responses for metabolites in MSI-CE-MS were normalized to an internal standard from the same injection position in order to correct for random variations in injection volume on-capillary [22]. Furthermore, control charts for the recovery standard (10 μM 4-fluorophenylalanine, F-Phe) added to all thawed plasma samples prior to ultrafiltration confirm acceptable intermediate precision (median CV = 14%, n=51) based on its normalized ion response measured in (D) positive ion mode using 3-chlorotyrosine (Cl-Tyr), and (E) negative ion mode using naphthalene monosulfonic acid (NMS) as internal standards with few outliers exceeding warning limits. As there was no evidence of long-term signal drift or systematic error, application of a QC-based batch correction algorithm was not deemed necessary unlike long-term/intermittent studies performed on shared instrumentation following service repairs and/or relocation [30]. As a result, MSI-CE-MS offers a rapid metabolomics platform for reliable metabolite quantification when relying on customized serial injections that encode mass spectral information temporally in the separation with stringent quality control.

3.3.3 Evaluating the effects short-term/acute physical inactivity in older pre-diabetic adults

The major goal of this work was to identify dynamic plasma metabolite signatures modulated by acute step reduction and subsequent recovery to normal habitual physical activity. Overall, eight plasma metabolites were found to undergo significant changes in circulation throughout the intervention period ($p < 0.05$; effect sizes > 0.20) when using a repeat measures 1-way ANOVA as summarized in **Table 3.2**. Plasma glutamine and carnitine increased after step reduction without returning back to baseline after the recovery period that satisfied a False Discovery Rate (FDR) adjustment for multiple hypothesis testing ($q < 0.05$). Additionally, plasma creatine, methionine and deoxycarnitine were also found to undergo analogous metabolic trajectories over time ($p < 0.05$). In contrast, three other plasma metabolites displayed an opposite trend with a significant decrease in

Table 3.2: Top plasma metabolites and ratiometric markers significantly perturbed due to short-term step reduction as compared to baseline and recovery periods in older adults (n = 17)

m/z:RMT:mode	Compound	*p*-value	*q*-value[a]	Effect size[b]	Pairwise comparison	BL-SR[c]	SR-RC[c]	BL-RC[c]
147.0764:0.908:p	Glutamine	5.80E-6	3.02E-4	0.53	BL-SR, BL-RC	1.30	1.01	1.31
	Creatine/ Oxoproline*	1.43E-4	1.49E-2	0.45	BL-SR, BL-RC, SR-RC	2.40	0.87	2.10
	Glutamine/ Indoxyl Sulfate	3.01E-4	0.015	0.40	BL-SR, BL-RC	2.65	0.90	2.39
	Carnitine/ Oxoproline	1.00E-3	0.010	0.35	BL-SR, BL-RC	1.87	0.88	1.65
	Creatine/ Indoxyl Sulfate*	1.42E-3	0.015	0.42	BL-SR, BL-RC	2.70	0.82	2.21
	Carnitine/ Indoxyl Sulfate	2.34E-3	0.015	0.32	BL-SR, BL-RC	2.13	0.86	1.82
162.1125:0.666:p	Carnitine (C0)	2.53E-3	0.019	0.31	BL-SR, SR-RC	1.21	0.87	1.05
132.0768:0.710:p	Creatine*	0.010	0.019	0.34	BL-SR, SR-RC	1.57	0.80	1.26
212.0023:1.025:n	Indoxyl sulfate	0.021	0.12	0.21	BL-SR, BL-RC	0.67	1.04	0.69
128.0353:1.025:n	Oxoproline	0.025	0.13	0.20	BL-SR	0.67	1.09	0.73
150.0583:0.890:p	Methionine*	0.028	0.13	0.21	BL-SR	1.20	0.93	1.11
178.051:0.880:n	Hippuric acid	0.033	0.14	0.19	BL-RC	0.71	0.96	0.68
146.1176:0.615:p	Deoxycarnitine*	0.044	0.17	0.19	BL-SR	1.16	0.96	1.12

*mode: p = positive mode, n = negative mode; *adjusted for sex; [a] p-adjusted value (q-value) based on False Discovery Rate (FDR) using Benjamini-Hochberg procedure; [b] Effect size measured using Partial Eta Square; [c] Mean fold-change ratio when comparing relative ion response ratio for metabolite between two time points.*

circulation after step reduction ($p < 0.05$) as compared to baseline or recovery time intervals, including indoxylsulfate, hippuric acid and oxoproline. Additionally, several ratiometric markers among the top-ranked plasma metabolites were found to increase the effect size (> 0.30) and statistical significance ($q < 0.05$, FDR) for most single plasma metabolites with the exception of glutamine as depicted in **Supplemental Figure S3.2**. As shown in the box-whisker plots in **Figure 3.3**, plasma glutamine, carnitine, creatine, methionine and deoxycarnitine showed similar trends with increasing circulating concentrations following step reduction yet remained persistently elevated after recovery when resuming normal ambulatory activity for two weeks. In contrast, plasma indoxyl sulfate, hippuric acid and oxoproline showed distinct decreases in circulation following step reduction relative to baseline. Nevertheless, there were large between-subject

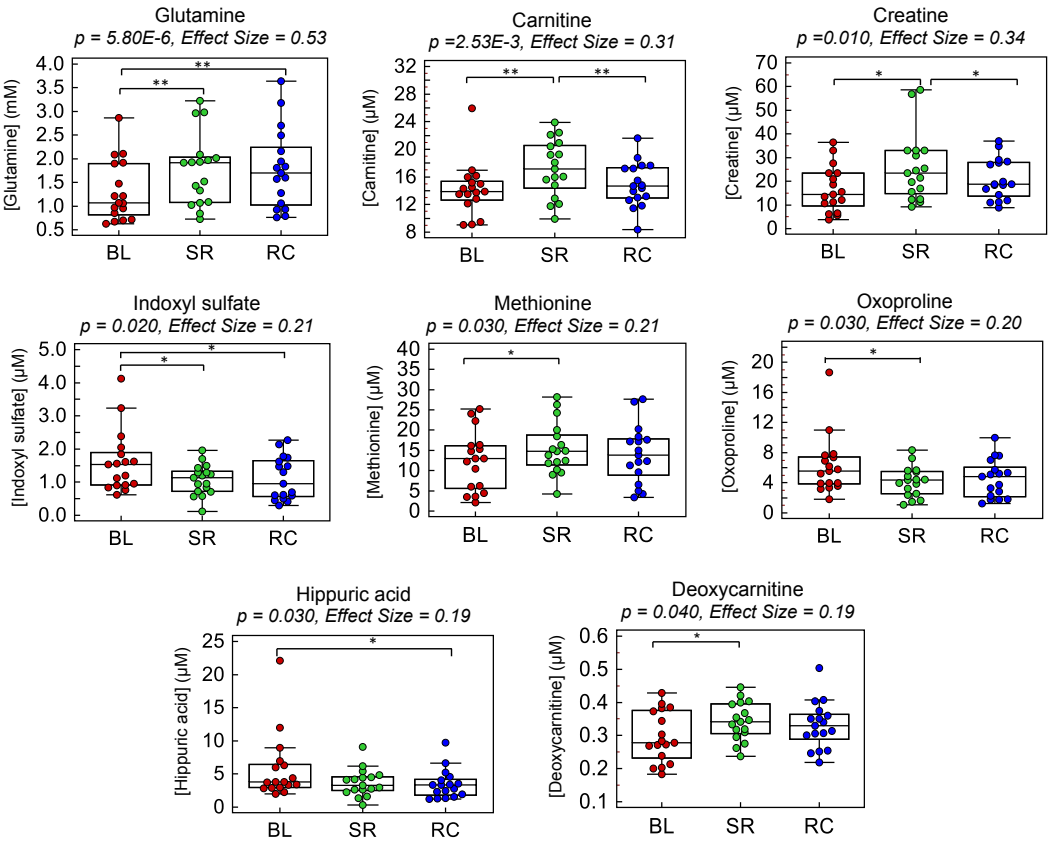

Figure 3.3: Box-whisker plots illustrating dynamic changes among eight top-ranked plasma metabolites modulated after two weeks of step reduction (SR) with a subsequent two week recovery (RC) period to normal physical activity as compared to baseline (BL) in a cohort of older pre-diabetic adults (*n* = 17). A one way repeated measures ANOVA test was performed to identify significant changes in circulating metabolite concentrations as summarized in Table 3.2, where a bracket represents a significant pairwise comparison (* $p < 0.05$; ** $q < 0.05$). Overall, these plasma metabolites reflect adaptive metabolic responses to physical inactivity/muscle disuse with step reduction that did not fully recover after resuming normal habitual physical activity.

variations in plasma metabolite concentrations at baseline, and variable responses to the step reduction trial when plotting individual metabolic trajectories among participants as shown in **Figure S3.3 of the Supporting Information**. For instance, while most subjects showed a general trend of increasing plasma carnitine following 2 weeks of step reduction, subject#8 (*i.e.,* a pre-diabetic/overweight male) showed an opposing trend with a decreasing carnitine trajectory over time with elevated baseline concentrations. Similarly, subject#4 (*i.e.,* a pre-diabetic/lean male) had unusually elevated baseline plasma concentrations of indoxylsulfate,

hippuric acid and oxoproline as compared to all other participants. This extent of biological variance exists even though participants were supplied with standardized meals for 3 days prior to clinical visits for blood collection while fasting. All plasma metabolites were adjusted for sex, however the extent of step reduction was not different between subjects as a potential confounder. Additionally, a correlation matrix among the eight top-ranked plasma metabolites associated with abrupt changes in physical activity from step reduction is shown in **Supplemental Figure S3.4**, which reveals strong co-linearity between circulating levels of indoxylsulfate and oxoproline (r = 0.881; p < 1.0 E-15), hippuric acid and oxoproline (r = 0.622; p < 1.1 E-6), hippuric acid and indoxylsulfate (r = 0.507; p < 1.4 E-4), as well as inverse correlations between glutamine and oxoproline (r = -0.502; p < 1.8 E-4), and glutamine and indoxylsulfate (r = -0.500; p < 1.8 E-4).

3.4 Discussion

Nontargeted metabolite profiling was performed on repeat plasma samples from a cohort of overweight, prediabetic older adults who completed two weeks of step reduction (< 1000 steps/day) followed by a two week recovery period resuming their normal habitual activity. Although all participants were generally healthy and moderately active, most were pre-diabetic (88%) following step reduction and therefore susceptible in developing type 2 diabetes; however only one participant (subject#19) with borderline aberrant glucose homeostasis at baseline transitioned to diabetes as shown in **Supplemental Figure S3.1**. Overall, all participants significantly reduced their ambulatory activity and energy expenditure over a 2 week period (**Table 3.1**). To the best of our knowledge, this is the first metabolomics study exploring adaptive metabolic responses to an abrupt change in physical activity involving older adults. Previous results from this cohort reported lower rates of myofibrillar protein biosynthesis using a deuterated water ingestion method, as well as a worsening of glycemic control with a modest elevation in circulatory inflammatory markers (*e.g.,* C-reactive protein, IL-6, TNF-α) following

step reduction [18]; however, there was no detectable reduction in DXA-measured fat free mass, BMI or muscle strength indicative of early stages of muscle protein degradation without measurable evidence (pre-clinical) of sarcopenia. Earlier bed-rest studies have reported substantial muscle atrophy and whole-body insulin resistance likely due to a more pronounced reduction in daily physical activity [31,32] as compared to this study. In contrast, a single day of bed rest was not reported to induce any changes in skeletal muscle deconditioning or gene expression associated with the regulation of muscle mass and insulin sensitivity [33], whereas changes in insulin sensitivity were elicited in young men following 2 weeks of step reduction in conjunction with overfeeding [34]. In our case, participants were requested to maintain habitual dietary patterns during the intervention with the exception of standardized meals consumed for 3 days prior to clinical visits.

Similar to previous targeted metabolomics studies which have focused on sarcopenic patients exhibiting poor muscle quality [35–37], several circulating metabolites closely associated with skeletal muscle metabolism were modulated by step reduction in this work. MSI-CE-MS was used as a high throughput platform in metabolomics that takes advantage of customized serial injection configurations for analysis of 13 samples within a single run, including pairs of plasma filtrates together with a pooled sample as a QC and/or blank (**Figure 3.1**). Overall, forty-seven plasma metabolites (**Supplemental Table S3.1**) were consistently detected in the majority of plasma samples with acceptable technical precision from a cohort of older adults participating in a repeated measures intervention trial (**Figure 3.2**). However, only eight plasma metabolites were found to undergo significant changes ($p < 0.05$) following physical inactivity via step reduction. These results are similar to independent data from measurements of myofibrillar protein and genes encoding several mitochondrial protein within muscle tissue [18]. In this work, plasma glutamine was by far the most significant biomarker associated with physical inactivity that increased 1.3-fold following step reduction (q = 3.02 E-4; effect size

= 0.53), which was independent of sex and extent of step reduction as potential confounders. In fact, plasma glutamine concentrations remained persistently elevated and did not fully return back to baseline after a 2 week recovery period to normal activity. These findings coincide with a recent report demonstrating that increases in plasma glutamine were associated with clinically diagnosed sarcopenic and community-dwelling and institutionalized elderly [37]. Glutamine is the most abundant amino acid in circulation [22] that is conditionally essential during periods of acute metabolic stress and it is largely derived from *de novo* synthesis in the skeletal muscle from glutamic acid and ammonia via glutamine synthetase [38,39]. While glutamine is involved in a myriad of metabolic pathways in the body (*i.e.,* nitrogen transport, signal transduction, energy metabolism etc.) [38], it plays a crucial role in regulating protein synthesis and breakdown within skeletal muscle, where glutamine is used for transporting nitrogen to the liver [40]. Indeed, decreasing concentrations of intramuscular glutamine accelerate protein catabolism resulting in a decline in skeletal muscle mass which is a hallmark of sarcopenia [38,41]. Therefore, the apparent increase in plasma glutamine from step reduction could be indicative of increased efflux of glutamine from skeletal muscle stores into circulation reflecting a catabolic physiological state among older adults as reflected by a decline in myofibrillar protein synthesis.

Adaptive changes in muscle energy metabolism from acute physical inactivity also play a major role in 1.21-fold increase by in plasma carnitine concentrations following step reduction (q = 0.020; effect size = 0.31). While carnitine may be derived from diet and/or endogenously synthesized in the liver, kidney and brain from trimethyllysine [42], plasma carnitine is a major source for skeletal muscle carnitine and subsequent synthesis of intracellular acylcarnitines for fatty acid β-oxidation. Thus, in the absence of changes in habitual diet during the intervention, our findings support that increased plasma carnitine concentrations with step reduction may be caused by its decreased uptake within skeletal muscle due to

fewer demands for muscle contractions with prolonged inactivity that triggers an increase in protein catabolism and a decline in mitochondrial biogenesis. Similarly, deoxycarnitine (or γ-butyrobetaine) showed a modest 1.16-fold increase in plasma concentrations as a result of step reduction (p = 0.044; effect size = 0.19). Deoxycarnitine is a known precursor of carnitine that undergoes hydroxylation via γ-butyrobetaine hydrolase (BBOX) in the liver and/or kidneys to form carnitine [43]. Thereafter, deoxycarnitine is released in circulation in order to be uptaken by skeletal muscle for storage. However, our results confirmed an accumulation in circulatory deoxycarnitine following step reduction, which was likely caused by a reduced uptake capacity within muscle tissue.

Similar to the trends identified in metabolite trajectories for glutamine, as well as carnitine and deoxycarnitine in plasma, two weeks of step reduction also resulted in a 1.6-fold increase in plasma creatine concentrations (p = 0.010; effect size = 0.34) as shown in **Figure 3.3**. Creatine is primarily synthesized in the kidneys and liver, subsequently excreted into circulation and further stored within skeletal muscle, where it plays important roles in energy metabolism and muscle function [44,45] as it is transformed into the high energy phosphate donor, phosphocreatine to regenerate ATP during active muscle contractions with strenuous exercise [22]. However, prolonged periods of physical inactivity have shown to severely decrease intramuscular creatine concentrations due to muscle atrophy and protein catabolism. For instance, MacDougall *et al.* [46] reported a 25% reduction in muscle phosphocreatine in healthy, recreationally active men after five weeks of experimentally-induced immobilization. Similar declines may be paralleled in older adults with sedentary lifestyles, including those that are hospital-bound and bed-ridden. As a result, increases in plasma creatine concentrations likely mirror a corresponding decrease in intramuscular creatine with greater muscle protein turn-over rates after two weeks of step reduction. A recent study by Garvey *et al.* [47] also reported increased plasma creatine levels and decreased muscle creatine in

aged rats, which was attributed to skeletal muscle "leak," promoting the excretion of creatine from skeletal muscle stores and preventing further uptake due to age-related declines in muscle mass.

Step reduction involving older adults also elicited a 1.2-fold increase in plasma methionine levels ($p = 0.028$; effect size = 0.21) as compared to baseline. Our findings coincided with a previous study by Moaddel *et al*. [36], concluding that increased circulating methionine levels were associated with low muscle quality in older persons. Methionine is an essential sulfur-containing amino acid that plays crucial roles in several metabolic processes (*e.g*., polyamine, creatine and phosphotidylcholine metabolism), as well as protein synthesis and redox homeostasis [48]. Methionine is also an immediate precursor of cysteine, a rate-limiting substrate for intracellular glutathione biosynthesis that is upregulated during oxidative stress, a hallmark of ageing and sarcopenic obesity who have higher circulatory levels of oxidized glutathione than non-sarcopenic controls [49]. Indeed, glutathione synthesis and intracellular glutathione concentrations both tend to decline with aging [50], which is exacerbated by low dietary protein and/or inadequate sulfur amino acid intake common among older persons [51]. Interestingly, our study also revealed several unexpected plasma biomarkers of physical inactivity as a result of step reduction, including indoxyl sulfate ($p = 0.021$) and hippuric acid ($p = 0.033$), as well as oxoproline ($p = 0.025$) with similar modest effect sizes (≈ 0.20). The former two plasma metabolites are uremic toxins that often accumulate in plasma due to chronic kidney disease (CKD) prevalent among patients with type 2 diabetes, which have been shown to contribute to deleterious health effects by stimulating muscle atrophy, protein catabolism and CKD-induced sarcopenia or uremic sarcopenia [52,53]. It is noteworthy that increased intramuscular indoxyl sulfate has recently been reported to induce metabolic alterations in skeletal muscle tissue that increase oxidative stress and triggers inflammatory cytokines (*e.g.,* TNF-α, IL-6) with higher expression of myostatin

and atrogin-1, leading to inhibition of muscle growth and development and thus muscle atrophy [53]. We hypothesize that the decline in plasma indoxyl sulfate following prolonged physical inactivity may be a result of its increased uptake within skeletal muscle that promotes muscle wasting in susceptible older adults. The exact biochemical role of hippuric acid in step reduction/muscle disuse is not clear, but both indoxyl sulfate and hippuric acid are major protein-bound uremic toxins [54] that are modulated by dietary intake, host liver metabolism and gut microbiota activity as reflected by their moderate co-linearity in fasting plasma samples analyzed in this study ($r = 0.507$; $p < 1.4$ E-4, **Supplemental Figure S3.4**). Our study also revealed a corresponding 0.67-fold lowering of plasma oxo-proline (or pyroglutamic acid), a known precursor of intracellular glutathione, produced through the γ-glutamyl dipeptide cycle that is a key glutathione salvage pathway activated during oxidative stress [55,56]. The adaptive decrease in circulating oxoproline concentrations after step reduction suggests its higher intramuscular uptake to promote glutathione biosynthesis in order to combat increases in reactive oxygen species (ROS) from muscle disuse. Interestingly, plasma oxoproline was strongly correlated to both indoxyl sulfate ($r = 0.881$; $p < 1.0$ E-15) and hippuric acid ($r = 0.622$; $p < 1.1$ E-6) implying a direct coupling of intra-muscular oxidative stress/glutathione depletion and increased uremic toxin uptake within muscle tissue resulting in lower oxoproline released in circulation. Similar to most other biomarkers of muscle disuse from step reduction (**Table 3.2**), plasma oxoproline concentrations remained persistently lower as compared to baseline even 2 weeks following recovery with a return to normal ambulatory activity. As access to residual muscle tissue specimens was not available for analysis in this study, muscle metabolomic studies [22] were not feasible to better understand the relationship between changes in circulatory metabolism and skeletal muscle health in older adults.

Figure 3.4 depicts an illustrative scheme that provides an overview of the adaptive metabolic changes following step reduction that may provide new targets for therapeutic interventions in managing or preventing sarcopenia among high-risk older persons. Overall, top-ranked plasma biomarkers of muscle disuse were largely associated with changes in skeletal muscle energy metabolism (creatine, carnitine, deoxycarnitine) and/or protein catabolism (glutamine), as well as glutathione biosynthesis (methionine, oxoproline), and uremic toxins (indoxyl sulfate, hippuric acid) which are likely contributing factors to metabolic acidosis, muscle protein wasting and uremic sarcopenia. In order to ameliorate the effects of protein catabolism (*i.e.*, muscle atrophy) due to aging, nutritional supplementation has long been proposed to increase muscle protein synthesis and thus, increase muscle mass in geriatric populations. Interestingly, many metabolites identified in this study (*e.g.,* glutamine, creatine and carnitine) are widely used dietary supplements for enhancing overall muscle health, strength and performance [57]. In fact, previous studies have demonstrated that high dose creatine supplementation led to improvements in muscle strength and performance in daily activities, while preventing bone loss in the older adults [58,59]. In contrast, glutamine supplementation in aged rats without physical activity showed no improvements in protein synthesis and thus, was insufficient to increase skeletal muscle mass to combat age-related muscle atrophy [60]. Similarly, oral supplementation with carnitine has not shown beneficial effects on skeletal muscle mass and function in older women [61] despite its widespread use as a nutritional supplement to support muscle energy metabolism. Alternatively, there is growing evidence that resistance training can elicit a number of metabolic adaptations that can combat the adverse effects associated with age-related declines in muscle mass and function in older persons [62,63]. These improvements can be further enhanced when coupling protein supplementation with resistance training to improve muscle mass and combat age-related muscle atrophy [64]. Future studies will validate the impact of safe yet effective lifestyle modifications based on diet and/or exercise to attenuate

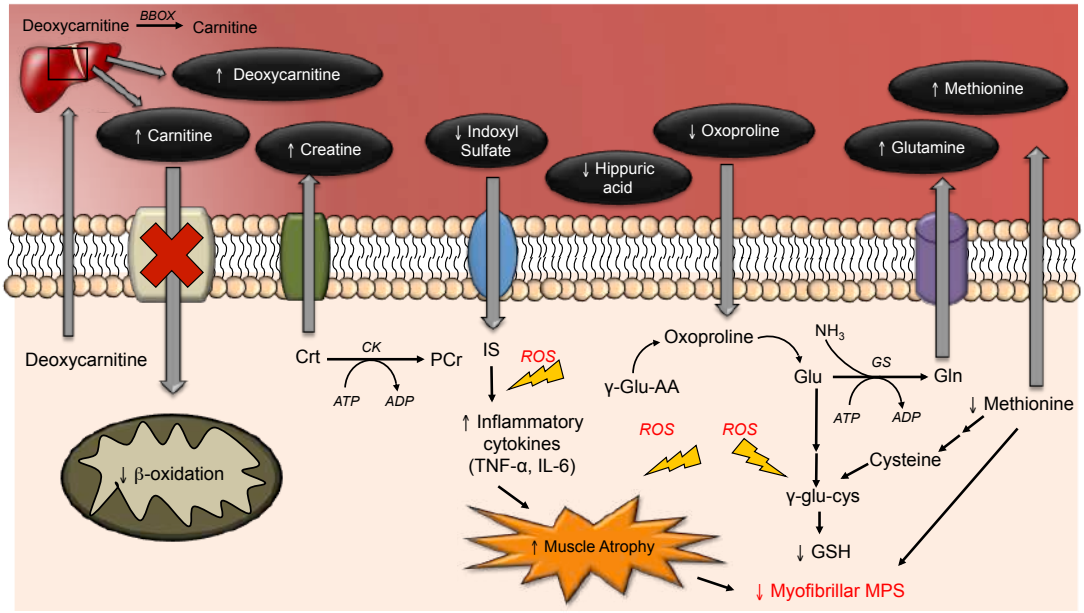

Figure 4: Schematic illustrating the metabolic effects on circulatory (systemic) metabolism and associated changes in skeletal muscle metabolism due to abrupt changes in physical activity from step reduction in older adults. Prolonged physical inactivity elicits several metabolic and physiological changes in skeletal muscle, including a lower rate of myofibrillar protein synthesis that may subsequently contribute to mitochondrial dysfunction and protein catabolism. This decline in muscle mass and quality likely results in the accumulation of plasma creatine and glutamine concentrations due to skeletal muscle export from major muscle stores. Additionally, plasma carnitine (and deoxycarnitine) concentrations increased likely due to reduced uptake capacity within skeletal muscle upon mitochondrial dysfunction leading to downregulation in lipid metabolism (i.e. β-oxidation) as well as other energy metabolism pathways. Step reduction also led to declines in circulating uremic toxins, indoxyl sulfate and hippuric acid. The reduction in indoxyl sulfate likely reflects greater intramuscular accumulation that contributes to an increase in oxidative stress products (ROS), and inflammatory cytokines (TNF-α, IL-6) thereby promoting muscle atrophy (wasting). Moreover, the increase in oxidative stress within skeletal muscle also depletes intracellular glutathione given limiting amounts of cysteine or methionine. Also, circulatory levels of oxoproline, a known intermediate involved in glutathione recycling, are transported within muscle for intracellular glutathione biosynthesis in response to oxidative stress due to short-term physical inactivity. BBOX: γ-Butyrobetaine hydrolase; Crt: Creatine; CK: Creatine kinase; Gln: Glutamine; Glu: Glutamic acid; GS: Glutamine synthetase; GSH: Glutathione; IL-6: Interleukin-6; IS: Indoxyl sulfate; MPS: Muscle protein synthesis; PCr: Phosphocreatine; ROS: Reactive oxidative species; TNF-α: Tumour necrosis factor alpha; γ-Glu-AA: γ-glutamyl-amino acids

the deleterious effects of physical inactivity on skeletal muscle health that promotes healthy ageing.

Although this work provided novel insights to the deleterious metabolic responses to physical inactivity in high-risk older adults, there were several study

limitations. Firstly, a larger and more diverse cohort of participants is needed to increase study power due to significant between-subject variance while further validating these findings in other community dwelling centres. Also, there were no measurable phenotypic changes in free fat mass, BMI or muscle strength in this study that likely require a longer intervention period of acute muscle disuse. Furthermore, access to muscle tissue biopsies is needed to better interpret adaptive metabolic changes in circulatory metabolism to those occurring strictly within skeletal muscle due to abrupt changes in habitual physical activity. While this study focused on the characterization of the polar/ionic metabolites in plasma, future studies should expand metabolome coverage to include circulating fatty acids and intact lipids when using multiplexed separations with nonaqueous-CE-MS [23] due to their essential roles in muscle energy metabolism and modulators of inflammation. A major finding of this study was that otherwise healthy and moderately active older persons were susceptible to metabolic stresses and catabolic processes that were not fully recoverable when resuming normal ambulatory activity, including a panel of plasma metabolites associated with muscle energy metabolism, protein breakdown and oxidative stress from glutathione depletion and inflammatory uremic toxin exposures. Additionally, these same metabolites may serve as useful biomarkers for monitoring sarcopenia progression and novel treatment interventions for its prevention. In this case, longer recovery times (> 2 weeks) can be explored to determine if these metabolic changes do indeed return to baseline, which may be accelerated with optimal resistance training and/or nutritional supplementation regimes suitable for older adults. The analysis of biomarkers identified in this work from non-invasive biological fluids, such as urine may enable effective screening of older adults for pre-symptomatic detection of sarcopenia that is not measurable by standard body imaging or muscle function tests.

3.5 Materials and Methods

3.5.1 Study Cohort and Intervention

This study was based on a previously published study where 22 older adults (12 men, 10 women) were recruited to undergo an acute step reduction intervention [18]. However, only 17 (10 men, 7 women) of the 22 participants were included in our study due to lack of plasma specimens available at each time point. Prior to the intervention, participants were screened to ensure they met the inclusion criteria (*i.e.*, non-smoking, free from chronic disease, moderately active, did not consume nonsteroidal anti-inflammatory drugs or medication for cholesterol management). The study protocol was approved by the Hamilton Integrated Research Board (REB #14-609). First, participants underwent 7 days of monitored normal physical activity (baseline; BL). Thereafter, participants underwent two weeks of step reduction (SR, < 1000 steps per day) followed by return to habitual physical activity for two weeks during recovery (RC). Daily step count was monitored using a hip-placed pedometer unit (Piezo SC-StepX Health System, StepsCount, Deep River, ON, Canada), which was internally validated with a SenseWear arm band accelerometer (BodyMedia, Pittsburg, PA, USA). During the last three days of each intervention period (BL, SR and RC), participants were provided with standardized meals (55% carbohydrate (CHO), 30% fat and 15% protein) in the form of flash frozen, prepackaged foods (Heart to Home, Hamilton, ON, Canada). Furthermore, at the end of each intervention period (BL, SR and RC), participants also performed an oral glucose tolerance test (OGTT) following a 10 h overnight fast where blood samples were obtained via an intravenous catheter inserted into an antecubital vein. After collection, blood samples were centrifuged at 4,000 *g* for 10 min at 4 ºC. Afterwards, all plasma samples were stored at -80 ºC prior to further preparation for metabolomics analysis.

3.5.2 Plasma Sample Preparation

Frozen raw plasma was slowly thawed on ice, vortexed for 30 s and aliquoted. An aliquot of 50 µL of plasma was diluted two-fold with ultra grade LC-MS water (Caledon Laboratories Ltd, Georgetown, ON, Canada) containing 40 µM of the recovery standards, 4-fluoro-L-phenylalanine (F-Phe) and 3-cyclohexylamino-1-propanesulfonic acid (CAPS), for both positive and negative mode ESI-MS. The diluted plasma was vortexed for 30 s and transferred to a pre-rinsed 3 kDa molecular weight cutoff (MWCO) ultrafiltration tube (Pall Life Sciences, Port Washington, NY, USA) and filtered at 14,000 *g* for 7.5 min to remove proteins with the plasma filtrate used for analysis. Ultrafiltration tubes were pre-rinsed with ultra grade LC-MS water, centrifuged for 5 min at 14,000 *g* and air dried for about 20 min prior to use. Thereafter, the plasma filtrates were obtained and aliquoted into two centrifuge tubes in order to prepare two aliquots with 1:2 ratio dilution for the temporal signal pattern recognition configuration for MSI-CE-MS analysis. For the 1-fold diluted samples, 20 µL of ultra grade LC-MS water containing 80 µM of the internal standards, 3-chloro-L-tyrosine (Cl-Tyr) and 2-napthalenesulfonic acid (NMS), and 16 mM of ^{13}C-glucose was added to 15 µL of plasma filtrate. For the 2-fold diluted samples, 30 µL of ultra grade LC-MS water containing the internal standards and ^{13}C-Glucose was added to 10 µL of plasma filtrate. The final concentrations of the recovery and internal standards were 10 µM and 2 mM for ^{13}C-Glucose in the diluted plasma filtrates for MSI-CE-MS analysis.

3.5.3 Nontargeted metabolite profiling of plasma filtrates by MSI-CE-MS

Nontargeted metabolite profiling using MSI-CE-MS was performed on an Agilent 7100 capillary electrophoresis (CE) instrument (Agilent Technologies Inc., Mississauga, ON, Canada) coupled to an Agilent 6230 Time-of-Flight Mass Spectrometer (TOF-MS) equipped with a coaxial sheath liquid (Dual EJS) Jetstream electrospray ion source with heated nitrogen gas. The CE separations were performed using uncoated fused-silica capillaries (Polymicro Technologies,

AZ, USA) with 50 μm inner diameter and 120 cm total length. The background electrolyte (BGE) consisted of 1 M formic acid with 15% *v/v* acetonitrile (pH 1.80) for positive ion mode, and 50 mM ammonium bicarbonate (pH 8.50) for negative ion mode, which were used for nontargeted profiling of cationic and anionic metabolites, respectively [20-22]. In order to minimize sample carryover between injections as well as polymer swelling/degradation upon contact with organic and/or ammonia-based solvents, the terminal ends of the capillary were burned using a MicrosolvCE Window Maker to remove 7 mm length of polyimide coating.

The serial sample injection sequence used in MSI-CE-MS consisted of 13 discrete samples injected hydrodynamically (5 s at 100 mbar) interspaced with BGE spacers injected electrokinetically at 30 kV for 75 s for the separation of cationic metabolites and 45 s for anionic metabolites. The separations were performed under normal polarity using a pressure gradient of 2 mbar/min from 0 to 40 min, with an applied voltage of 30 kV at 25°C. Between runs, the capillary was flushed for 15 min with BGE at 950 mbar. The sheath liquid compositions consisted of 60% methanol with 0.1% *v/v* formic acid for positive ion mode and 50% methanol for negative ion mode. Additionally, purine and hexakis(2,2,3,3-tetrafluoropropoxy)phosphazine (HP-921) (API-TOF Reference Mass Solution Kit, Agilent Technologies) were added to the sheath liquid as reference masses to provide real-time mass calibration during data acquisition. The sheath liquid was delivered at a rate of 10 μL/min using an Agilent 1260 Infinity series Isocractic Pump equipped with a 100:1 splitter. Data acquisition was performed in full-scan mode on the TOF-MS that spanned a mass range of 50-1700 *m/z* at an acquisition rate of 500 ms/spectrum. The ESI conditions were Vcap = 2000 V, nozzle voltage = 2000 V, nebulizer gas = 10 psi, sheath gas = 3.5 L/min at 195 °C, drying gas 8 L/min at 300 °C. whereas, the MS voltage settings were fragmentor = 120 V, skimmer = 65V and Oct1 RF= 750 V. During sample injection, the Vcap, nozzle voltage and nebulizer gas were turned off to minimize electrospray suctioning

effects. At the beginning of each day, the TOF-MS system was calibrated over 50-1700 *m/z* range before analysis using an Agilent tune mixture to ensure residual mass ranges did not exceed 0.30 ppm. Additionally, preventative maintenance was performed such as daily cleaning of the CE electrode and ion source with 50% *v/v* isopropanol using a lint-free cloth. Thereafter, a standard mixture and pooled QCs with blank were injected to equilibrate the CE-MS system and assess system stability prior to sample analysis. After sample analysis was completed each day, the capillary was flushed for 10 min with ultra grade LC-MS water and air dried for 10 min. The individual plasma samples were analyzed over four consecutive days in both positive and negative ESI-MS.

3.5.4 Data Processing and Statistical Analysis

All data processing and analysis were performed using Agilent MassHunter Qualitative Analysis B.06.00 and Microsoft Excel. All metabolite responses were normalized to the internal standard. Prior to univariate statistical analysis, normality testing was performed using the Shapiro-Wilk test ($p < 0.05$) on *log*-transformed data using SPSS (IBM SPSS Statistics for Windows, Version 20.0. NY, USA). A one way repeated measures analysis of variance (ANOVA; intervention (BL, SR, RC) as within-subjects factor) was also performed on SPSS. The Mauchly's sphericity test was initially used to determine if the data satisfied the sphericity assumption ($p > 0.05$); in cases where sphericity was violated, a Greenhouse-Geisser correction was applied accordingly. Furthermore, sex and baseline step count were tested as covariates for all metabolites and the *p*-values were adjusted accordingly when the effect of sex and/or baseline step count were significant. Pairwise comparisons using the Fischer's LSD was used for post-hoc analysis. To correct for multiple hypothesis testing, a false discovery rate (FDR) correction using the Benjamini-Hochberg procedure was applied. Prior to multivariate analysis, all data was generalized *log*-transformed and autoscaled. Multivariate

statistical analyses including principal component analysis (PCA) and hierarchical clustering analysis (HCA) were performed using Metaboanalyst 4.0 [65].

3.6 Conclusions

In this work, two weeks of acute physical inactivity induced adaptive metabolic changes in a cohort of overweight and prediabetic older adults who did not fully return to baseline after resuming normal ambulatory activity. Our study demonstrated increases in plasma concentrations of several metabolites associated with muscle energy metabolism (creatine, carnitine and deoxycarnitine) and protein degradation/ammonia transport (glutamine) following step reduction due to muscle disuse with decreased myofibrillar protein biosynthesis. Interestingly, a decrease in plasma uremic toxins (indoxyl sulfate and hippuric acid) as well as changes in essential precursors of glutathione biosynthesis (oxoproline, methionine) was indicative of deleterious oxidative stress within skeletal muscle following an abrupt change in physical activity among high-risk older persons due to increased intramuscular inflammation. Of these metabolites, glutamine showed the most pronounced changes and largest effect size, whereas ratiometric biomarkers were found to further increase study power for other plasma metabolites. This study revealed important metabolic pathways that advance our understanding of sarcopenia at early stages of development while providing putative biomarkers applicable to routine monitoring of progressive loss in muscle mass and function in older persons. With the world's geriatric population projected to increase worldwide by 2050, preventative strategies are needed to mitigate the many socioeconomic and healthcare impacts of sarcopenia and frailty in order to improve quality of life and independence while reducing the need for support services and long-term care.

3.7 Acknowledgements

P.B.-M. and S.M.P. acknowledge funding support from the Natural Sciences and Engineering Research Council of Canada. P.B.-M. also thanks financial support from Genome Canada. M.S. also acknowledges support in the form of an Ontario Graduate Scholarship, and C.M. thanks Diabetes Canada for a Research Fellowship.

3.8 References

1. Rosenberg I.H. Sarcopenia: origins and clinical relevance. *J. Nutr.* **1997,** *127*, 990s–991s
2. Ziaaldini, M.M.; Marzetti, E.; Picca, A.; Murlasits, Z. Biochemical pathways of sarcopenia and their modulation by physical exercise: A narrative eeview. *Front. Med.* **2017,** *4*, 167.
3. Janssen, I.; Heymsfield, S.B.; Ross, R. Low relative skeletal muscle mass (sarcopenia) in older persons is associated with functional impairment and physical disability. *J. Am. Geriatr. Soc.* **2002**, *50*, 889-896.
4. Landi, F.; Calvani, R.; Cesari, M.; Tosato, M.; Maria Martone, A.; Ortolani, E.; Savera, G.; Salini, S.; N Sisto, A.; Picca, A.; et al. Sarcopenia: an overview on current definitions, diagnosis and treatment. *Curr. Protein Pept. Sci.* **2017**, *19*, 633-638.
5. Marty, E.; Liu, Y.; Samuel, A.; Or, O.; Lane, J. A review of sarcopenia: Enhancing awareness of an increasingly prevalent disease. *Bone* **2017,** 105, 276-286.
6. Shafiee, G.; Keshtkar, A.; Soltani, A.; Ahadi, Z.; Larijani, B.; Heshmat, R. Prevalence of sarcopenia in the world: A systematic review and meta-analysis of general population studies. *J. Diabetes Metab. Disord.* **2017,** *16*, 21.
7. Landi, F.; Calvani, R.; Cesari, M.; Tosato, M.; Martone, A.M.; Bernabei, R.; Onder, G.; Marzetti, E. Sarcopenia as the biological substrate of physical frailty. *Clin. Geriatr. Med.* **2015**, *31*, 367–374.
8. Molino, S.; Dossena, M.; Buonocore, D.; Verri, M. Sarcopenic obesity: An appraisal of the current status of knowledge and management in elderly people. *J. Nutr. Heal. Aging* **2016**, *20*, 780–788.
9. Beaudart, C.; Zaaria, M.; Pasleau, F.; Reginster, J.Y.; Bruyère, O. Health outcomes of sarcopenia: A systematic review and meta-analysis. *PLoS One* **2017**, *12*, e0169548.
10. Calvani, R.; Marini, F.; Cesari, M.; Tosato, M.; Anker, S.D.; Von Haehling, S.; Miller, R.R.; Bernabei, R.; Landi, F.; Marzetti, E. Biomarkers for physical frailty and sarcopenia: State of the science and future developments. *J. Cachexia. Sarcopenia Muscle* **2015,** *6*, 278-286.

11. Cesari, M.; Fielding, R.A.; Pahor, M.; Goodpaster, B.; Hellerstein, M.; van Kan, G.A.; Anker, S.D.; Rutkove, S.; Vrijbloed, J.W.; Isaac, M.; et al. Biomarkers of sarcopenia in clinical trials-recommendations from the International Working Group on Sarcopenia. *J. Cachexia. Sarcopenia Muscle* **2012,** *3*, 181-190.
12. Rantanen, T.; Guralnik, J.M.; Foley, D.; Masaki, K.; Leveille, S.; Curb, J.D.; White, L. Midlife hand grip strength as a predictor of old age disability. *J. Am. Med. Assoc.* **1999,** *281*, 558-560.
13. Studenski, S.; Perera, S.; Patel, K.; Rosano, C.; Faulkner, K.; Inzitari, M.; Brach, J.; Chandler, J.; Cawthon, P.; Connor, E.B.; et al. Gait speed and survival in older adults. *JAMA - J. Am. Med. Assoc.* **2011,** *305*, 50-58.
14. Guralnik, J.M.; Simonsick, E.M.; Ferrucci, L.; Glynn, R.J.; Berkman, L.F.; Blazer, D.G.; Scherr, P.A.; Wallace, R.B. A short physical performance battery assessing lower extremity function: Association with self-reported disability and prediction of mortality and nursing home admission. *Journals Gerontol.* **1994,** *49,* M85-94
15. Manini, T.M.; Clark, B.C. Dynapenia and aging: An update. *Journals Gerontol. - Ser. A Biol. Sci. Med. Sci.* **2012**, *67*, 28–40.
16. Janssen, I.; Shepard, D.S.; Katzmarzyk, P.T.; Roubenoff, R. The healthcare costs of sarcopenia in the United States. *J. Am. Geriatr. Soc.* **2004**, *52*, 80-85.
17. Bruyere, O.; Beaudart, C.; Ethgen, O.; Reginster, J.Y.; Locquet, M. The health economics burden of sarcopenia: A systematic review. *Maturitas* **2019**, *119*, 61–69.
18. McGlory, C.; Von Allmen, M.T.; Stokes, T.; Morton, R.W.; Hector, A.J.; Lago, B.A.; Raphenya, A.R.; Smith, B.K.; McArthur, A.G.; Steinberg, G.R.; et al. Failed recovery of glycemic control and myofibrillar protein synthesis with 2 weeks of physical inactivity in overweight, prediabetic older adults. *Journals Gerontol. - Ser. A Biol. Sci. Med. Sci.* **2018,** *73*, 1070-1077.
19. Kuehnbaum, N.L.; Gillen, J.B.; Kormendi, A.; Lam, K.P.; Dibattista, A.; Gibala, M.J.; Britz-Mckibbin, P. Multiplexed separations for biomarker discovery in metabolomics: Elucidating adaptive responses to exercise training. *Electrophoresis* **2015**, *36*, 2226–2236.
20. DiBattista, A.; McIntosh, N.; Lamoureux, M.; Al-Dirbashi, O.Y.; Chakraborty, P.; Britz-McKibbin, P. Temporal signal pattern recognition in mass spectrometry: A method for rapid identification and accurate quantification of biomarkers for inborn errors of metabolism with quality assurance. *Anal. Chem.* **2017**, *89*, 8112–8121.
21. Nori de Macedo, A.; Mathiaparanam, S.; Brick, L.; Keenan, K.; Gonska, T.; Pedder, L.; Hill, S.; Britz-McKibbin, P. The sweat metabolome of screen-positive cystic fibrosis infants: Revealing mechanisms beyond impaired chloride transport. *ACS Cent. Sci.* **2017**, *3*, 904–913.
22. Saoi, M.; Percival, M.; Nemr, C.; Li, A.; Gibala, M.; Britz-Mckibbin, P.

Characterization of the human skeletal muscle metabolome for elucidating the mechanisms of bicarbonate ingestion on strenuous interval exercise. *Anal. Chem.* **2019,** *91*, 4709-4718.

23. Azab, S.; Ly, R.; Britz-Mckibbin, P. Robust Method for High throughput screening of fatty acids by multisegment injection-nonaqueous capillary electrophoresis-mass spectrometry with stringent quality control. *Anal. Chem.* **2019**, *91*, 2329–2336.
24. DiBattista, A.; Rampersaud, D.; Lee, H.; Kim, M.; Britz-McKibbin, P. High throughput screening method for systematic surveillance of drugs of abuse by multisegment injection-capillary electrophoresis-mass spectrometry. *Anal. Chem.* **2017,** *89*, 11853-11891.
25. Kuehnbaum, N.L.; Kormendi, A.; Britz-McKibbin, P. Multisegment injection-capillary electrophoresis-mass spectrometry: A high-throughput platform for metabolomics with high data fidelity. *Anal. Chem.* **2013**, *85*, 10664–10669.
26. Dunn, W.B.; Erban, A.; Weber, R.J.M.; Creek, D.J.; Brown, M.; Breitling, R.; Hankemeier, T.; Goodacre, R.; Neumann, S.; Kopka, J.; et al. Mass appeal: Metabolite identification in mass spectrometry-focused untargeted metabolomics. *Metabolomics* **2013**, *9*, 44–66.
27. Yamamoto, M.; Pinto-Sanchez, M.I.; Bercik, P.; Britz-Mckibbin, P. Metabolomics reveals elevated urinary excretion of collagen degradation and epithelial cell turnover products in irritable bowel syndrome patients. *Metabolomics* **2019**, *15*, 82.
28. Punthakee, Z.; Goldenberg, R.; Katz, P. Definition, Classification and diagnosis of diabetes, prediabetes and metabolic syndrome. *Can. J. Diabetes* **2018**, *42*, S88–S103.
29. Huang, Y.; Cai, X.; Mai, W.; Li, M.; Hu, Y. Association between prediabetes and risk of cardiovascular disease and all cause mortality: Systematic review and meta-analysis. *BMJ* **2016**, *355*, i5953.
30. DiBattista, A.; McIntosh, N.; Lamoureux, M.; Al-Dirbashi, O.Y.; Chakraborty, P.; Britz-Mckibbin, P. Metabolic signatures of cystic fibrosis identified in dried blood spots for newborn screening without carrier identification. *J. Proteome Res.* **2019**, *18*, 841–854.
31. Dirks, M.L.; Wall, B.T.; Van De Valk, B.; Holloway, T.M.; Holloway, G.P.; Chabowski, A.; Goossens, G.H.; Van Loon, L.J. One week of bed rest leads to substantial muscle atrophy and induces whole-body insulin resistance in the absence of skeletal muscle lipid accumulation. *Diabetes* **2016**, *65*, 2862–2875.
32. Kenny, H.C.; Rudwill, F.; Breen, L.; Salanova, M.; Blottner, D.; Heise, T.; Heer, M.; Blanc, S.; O'Gorman, D.J. Bed rest and resistive vibration exercise unveil novel links between skeletal muscle mitochondrial function and insulin resistance. *Diabetologia* **2017**, *60*, 1491–1501.
33. Dirks, M.L.; Stephens, F.B.; Jackman, S.R.; Galera Gordo, J.; Machin, D.J.; Pulsford, R.M.; van Loon, L.J.C.; Wall, B.T. A single day of bed rest,

irrespective of energy balance, does not affect skeletal muscle gene expression or insulin sensitivity. *Exp. Physiol.* **2018**, *103*, 860–875.
34. Knudsen, S.H.; Hansen, L.S.; Pedersen, M.; Dejgaard, T.; Hansen, J.; Hall, G. Van; Thomsen, C.; Solomon, T.P.J.; Pedersen, B.K.; Krogh-Madsen, R. Changes in insulin sensitivity precede changes in body composition during 14 days of step reduction combined with overfeeding in healthy young men. *J. Appl. Physiol.* **2012**, *113*, 7–15.
35. Lustgarten, M.S.; Price, L.L.; Chale, A.; Phillips, E.M.; Fielding, R.A. Branched-chain amino acids are associated with muscle mass in functionally limited older adults. *Journals Gerontol. - Ser. A Biol. Sci. Med. Sci.* **2014**, *69*, 717-724.
36. Moaddel, R.; Fabbri, E.; Khadeer, M.A.; Carlson, O.D.; Gonzalez-Freire, M.; Zhang, P.; Semba, R.D.; Ferrucci, L. Plasma biomarkers of poor muscle quality in older men and women from the Baltimore Longitudinal Study of Aging. *Journals Gerontol. - Ser. A Biol. Sci. Med. Sci.* **2016**, *71*, 1266-1272.
37. Toyoshima, K.; Nakamura, M.; Adachi, Y.; Imaizumi, A.; Hakamada, T.; Abe, Y.; Kaneko, E.; Takahashi, S.; Shimokado, K. Increased plasma proline concentrations are associated with sarcopenia in the elderly. *PLoS One* **2017,** *12*, e0185206.
38. Meynial-Denis, D. Glutamine metabolism in advanced age. *Nutr. Rev.* **2016**, *74*, 225-236.
39. Gleeson, M. Dosing and efficacy of glutamine supplementation in human exercise and sport training. *J. Nutr.* **2008**, *138*, 2045S-2049S.
40. Smith, R.J. Glutamine metabolism and its physiologic importance. *J. Parenter. Enter. Nutr.* **2009**.
41. Mosoni, L.; Patureau Mirand, P.; Houlier, M..; Arnal M Age-related changes in protein synthesis measured in vivo in rat liver and gastrocnemius muscle. *Mech Ageing Dev* **1993**, *68*, 209–20.
42. Flanagan, J.L.; Simmons, P.A.; Vehige, J.; Willcox, M.D.; Garrett, Q. Role of carnitine in disease. *Nutr. Metab.* **2010**, *7*, 30.
43. Siliprandi, N.; Ciman, M.; Sartorelli, L. Myocardial carnitine transport. *Basic Res Cardiol* **1987**, *82*, 53–62.
44. Souza, R.A.; Miranda, H.; Xavier, M.; Lazo-Osorio, R.A.; Gouvea, H.A.; Cogo, J.C.; Vieira, R.P.; Ribeiro, W. Effects of high-dose creatine supplementation on kidney and liver responses in sedentary and exercised rats. *J. Sport. Sci. Med.* **2009**, *8*, 672-681.
45. Rawson, E.S.; Venezia, A.C. Use of creatine in the elderly and evidence for effects on cognitive function in young and old. *Amino Acids* **2011**, *40*, 1349-1362.
46. MacDougall, J.D.; Ward, G.R.; Sale, D.G.; Sutton, J.R. Biochemical adaptation of human skeletal muscle to heavy resistance training and immobilization. *J. Appl. Physiol.* **1977**, *43*, 700-703.
47. Garvey, S.M.; Dugle, J.E.; Kennedy, A.D.; McDunn, J.E.; Kline, W.; Guo,

L.; Guttridge, D.C.; Pereira, S.L.; Edens, N.K. Metabolomic profiling reveals severe skeletal muscle group-specific perturbations of metabolism in aged FBN rats. Biogerontology **2014**, 15:217-232.
48. Martinez, Y.; Li, X.; Liu, G.; Bin, P.; Yan, W.; Mas, D.; Valdivie, M.; Hu, C.-A.A.; Ren, W.; Yin, Y. The role of methionine on metabolism, oxidative stress, and diseases. *Amino Acids* **2017**, *49*, 2091–2098.
49. Bellanti, F.; Romano, A.D.; Lo Buglio, A.; Castriotta, V.; Guglielmi, G.; Greco, A.; Serviddio, G.; Vendemiale, G. Oxidative stress is increased in sarcopenia and associated with cardiovascular disease risk in sarcopenic obesity. *Maturitas* **2018** *109*, 6-12.
50. Rebrin, I.; Sohal R.S. Pro-oxidant shift in glutathione redox state during aging. *Adv. Drug Deliv. Rev.* **2008**, *60*,1545-1552.
51. McCarty, M.F.; DiNicolantonio, J.J. An increased need for dietary cysteine in support of glutathione synthesis may underlie the increased risk for mortality associated with low protein intake in the elderly. *Age (Dord.)* **2015**, *37*, 96.
52. Souza, V.A. de; Oliveira, D. de; Mansur, H.N.; Fernandes, N.M. da S.; Bastos, M.G. Sarcopenia in chronic kidney disease. *J. Bras. Nefrol.* **2015**, *37*, 98-105.
53. Sato, E.; Mori, T.; Mishima, E.; Suzuki, A.; Sugawara, S.; Kurasawa, N.; Saigusa, D.; Miura, D.; Morikawa-Ichinose, T.; Saito, R.; et al. Metabolic alterations by indoxyl sulfate in skeletal muscle induce uremic sarcopenia in chronic kidney disease. *Sci. Rep.* **2016**, *6*, 36618.
54. Vanholder; R., Pletinck; A., Schepers, E.; Glorieux, G. Biochemical and clinical impact of organic uremic retention solutes: A comprehensive update. *Toxins* **2018**, *10*, E33.
55. Castellano, I.; Merlino, A. *Gamma-Glutamyl Transpeptidases*; VII.; SpringerBriefs in Biochemistry and Molecular Biology, **2013**; ISBN 978-3-0348-0681-7.
56. Griffith, O.W.; Bridges, R.J.; Meister, A. Transport of gamma-glutamyl amino acids: role of glutathione and gamma-glutamyl transpeptidase. *Proc. Natl. Acad. Sci.* **1979**, *76*, 6319–6322.
57. Gotshalk, L.A.; Volek, J.S.; Staron, R.S.; Denegar, C.R.; Hagerman, F.C.; Kraemer, W.J. Creatine supplementation improves muscular performance in older men. *Med. Sci. Sports Exerc.* **2002**, *34*, 537-543.
58. Stout, J.; Sue Graves, B.; Cramer, J. Effects of creatine supplementation on the onset of neuromuscular fatigue threshold and muscle strength in elderly men and women (64 - 86 years). *J. Nutr. Heal. Aging* **2007**, *11*, 459-464.
59. Gotshalk, L.A.; Kraemer, W.J.; Mendonca, M.A.G.; Vingren, J.L.; Kenny, A.M.; Spiering, B.A.; Hatfield, D.L.; Fragala, M.S.; Volek, J.S. Creatine supplementation improves muscular performance in older women. *Eur. J. Appl. Physiol.* **2008**, *102*, 223-231.
60. Mignon, M.; Beaufrère, A.M.; Combaret, L.; Meynial-Denis, D. Does long-term intermittent treatment with glutamine improve the well-being of

fed and fasted very old rats? *J. Parenter. Enter. Nutr.* **2007**, *31*, 456-462.
61. Sawicka, A.K.; Hartmane, D.; Lipinska, P.; Wojtowicz, E.; Lysiak-Szydlowska, W.; Olek, R.A. L-carnitine supplementation in older women. A pilot study on aging skeletal muscle mass and function. *Nutrients* **2018**, *10,* 255.
62. Hassan, B.H.; Hewitt, J.; Keogh, J.W.L.; Bermeo, S.; Duque, G.; Henwood, T.R. Impact of resistance training on sarcopenia in nursing care facilities: A pilot study. *Geriatr. Nurs.* **2016**, *37*, 116-121.
63. Law, T.D.; Clark, L.A.; Clark, B.C. Resistance exercise to prevent and manage sarcopenia and dynapenia. *Annu. Rev. Gerontol. Geriatr.* **2016**, *36*, 205-228
64. Tieland, M.; Dirks, M.L.; van der Zwaluw, N.; Verdijk, L.B.; van de Rest, O.; de Groot, L.C.P.G.M.; van Loon, L.J.C. Protein supplementation increases muscle mass gain during prolonged resistance-type exercise training in frail elderly people: A randomized, Double-blind, placebo-controlled trial. *J. Am. Med. Dir. Assoc.* **2012**, *13*, 713-719.
65. Chong, J.; Soufan, O.; Li, C.; Caraus, I.; Li, S.; Bourque, G.; Wishart, D.S.; Xia, J. MetaboAnalyst 4.0: Towards more transparent and integrative metabolomics analysis. *Nucleic Acids Res.* **2018**, *46*, W486–W494.

3.9 Supporting Information

Table S3.1: Summary of 47 plasma metabolites consistently detected in majority (> 75%) of samples with adequate precision (QCs with CV < 30%, *n*=25) in this step reduction intervention study by MSI-CE-MS.

m/z:RMT:mode	Formula	Compound ID	Mass error (ppm)	Classification	CV%
67.0720:0.458:p	--	Unknown $[M+H]^+$	16.4	--	15.4
76.0393:0.643:p	$C_2H_5NO_2$	Glycine	11.3	Amino acid	15.0
90.0550:0.716:p	$C_3H_7NO_2$	Alanine	5.3	Amino acid	16.7
104.0706:0.776:p	$C_4H_9NO_2$	3-Aminoisobutyric acid (BAIBA)	5.1	Amino acid	16.6
104.1075:0.462:p	$C_5H_{14}NO$	Choline	6.0	Quaternary ammonium salt	24.8
106.0499:0.826:p	$C_3H_7NO_3$	Serine	1.2	Amino acid	15.3
114.0662:0.522:p	$C_4H_7N_3O$	Creatinine	-0.8	Amino acid	20.2
116.0706:0.903:p	$C_5H_9NO_2$	Proline	-1.8	Amino acid	12.5
118.0863:0.814:p	$C_5H_{11}NO_2$	Valine	-1.6	Amino acid	18.9
118.0863:0.963:p	$C_5H_{11}NO_2$	Betaine	-0.7	Amino acid	30.5
120.0655:0.878:p	$C_4H_9NO_3$	Threonine	-4.3	Amino acid	12.4
132.0656:1.023:p	$C_5H_9NO_3$	Hydroxyproline	0.9	Amino acid derivative	16.9
132.0768:0.710:p	$C_4H_9N_3O_2$	Creatine	-2.2	Amino acid derivative	20.9
132.1019:0.831:p	$C_6H_{13}NO_2$	Isoleucine	-2.3	Amino acid	16.3
132.1019:0.843:p	$C_6H_{13}NO_2$	Leucine	-2.1	Amino acid	15.3
133.0608:0.878:p	$C_4H_8N_2O_3$	Asparagine	-17.3	Amino acid	12.5
133.0969:0.469:p	$C_5H_{12}N_2O_2$	Ornithine	0.1	Amino acid	19.2
134.0488:0.980:p	$C_4H_7NO_4$	Aspartic Acid	-13.8	Amino acid	14.8
137.0457:1.096:p	$C_5H_4N_4O$	Hypoxanthine	-1.6	Purine derivative	19.9
144.0988:0.971:p	$C_7H_{13}NO_2$	Proline betaine	-2.3	Amino acid derivative	20.5
146.1176:0.615:p	$C_7H_{16}NO_2$	Deoxycarnitine	9.9	Amino acid derivative	17.1
147.0764:0.908:p	$C_5H_{10}N_2O_3$	Glutamine	-2.8	Amino acid	12.4
147.1128:0.472:p	$C_6H_{14}N_2O_2$	Lysine	-2.7	Amino acid	25.0
148.0604:0.924:p	$C_5H_9NO_4$	Glutamic Acid	-2.9	Amino acid	20.2
150.0583:0.890:p	$C_5H_{11}NO_2S$	Methionine	1.6	Amino acid	21.1

156.0768:0.530:p	$C_6H_9N_3O_2$	Histidine	-4.4	Amino acid	25.8
160.1331:0.653:p	$C_8H_{17}NO_2$	Unknown $[M+H]^+$	16.2	--	15.9
161.1285:0.496:p	$C_7H_{16}N_2O_2$	Unknown $[M+H]^+$	0.6	--	20.5
162.1125:0.666:p	$C_7H_{15}NO_3$	Carnitine	-2.3	Amino acid derivative	15.1
166.0863:0.925:p	$C_9H_{11}NO_2$	Phenylalanine	16.1	Amino acid	19.1
170.0924:0.551:p	$C_7H_{11}N_3O_2$	3-Methylhistidine	-3.9	Amino acid derivative	15.9
175.1190:0.503:p	$C_6H_{14}N_4O_2$	Arginine	-1.6	Amino acid	23.5
176.1030:0.938:p	$C_6H_{13}N_3O_3$	Citrulline	-1.1	Amino acid derivative	13.0
182.0812:0.962:p	$C_9H_{11}NO_3$	Tyrosine	-2.0	Amino acid	13.4
204.1230:0.734:p	$C_9H_{17}NO_4$	Acetylcarnitine	1.3	Acylcarnitine	19.5
276.1185:1.125:p	$C_{10}H_{17}N_3O_6$	Unknown $[M+H]^+$	-2.4	*NA*	13.2
89.0244:1.186:n	$C_3H_6O_3$	Lactic acid	5.8	Organic acid	6.1
101.0608:0.983:n	$C_5H_{10}O_2$	Isovaleric acid	-3.3	Fatty acid derivative	10.9
102.0510:0.936:n	$C_4H_9NO_2$	Dimethylglycine	0.5	Amino acid derivative	12.1
117.0557:0.988:n	$C_5H_{10}O_3$	2-Hydroxyvaleric acid	-3.0	Fatty acid derivative	25.4
128.0353:1.025:n	$C_5H_7NO_3$	Oxoproline	-1.2	Amino acid derivative	8.2
167.0211:0.947:n	$C_5H_4N_4O_3$	Uric acid	-1.0	Purine derivative	7.0
178.0510:0.880:n	$C_9H_9NO_3$	Hippuric acid	2.6	Organic acid	12.3
179.0564:0.455:n	$C_6H_{12}O_6$	Glucose	2.9	Monosaccharide	7.1
187.0071:1.082:n	$C_7H_8O_4S$	p-Cresol sulfate	-3.8	Phenylsulfate	23.8
212.0023:1.025:n	$C_8H_7NO_4S$	Indoxyl sulfate	20.4	Phenylsulfate	31.1
263.1037:0.759:n	$C_{13}H_{16}N_2O_4$	Phenylacetylglutamine	-1.9	Amino acid derivative	15.9

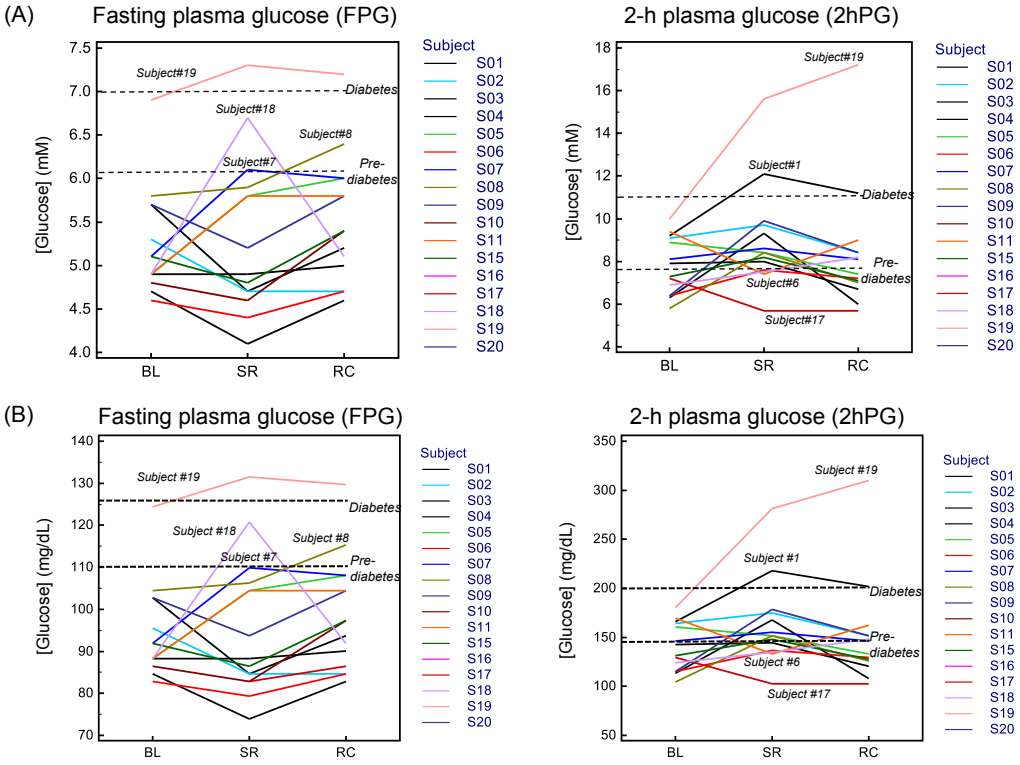

Figure S3.1: Summary of changes in fasting plasma glucose and oral glucose tolerance (2hPG) responses in terms of (A) mM and (B) mg/dL following step reduction and recovery in a cohort of overweight and largely pre-diabetic participants. Overall, 7 (of 15 or 47%) participants were defined as pre-diabetic with impaired glucose tolerance (7.8-11 mM or 140-199 mg/dL 2hPG) with one subject also having impaired fasting glucose at baseline (BL). However, following the step reduction (SR) and/or the recovery (RC) period, most participants in this cohort were defined as pre-diabetic (12 out of 15 or 80%) with one participant becoming diabetic with impaired fasting glucose (> 7.0 mM or 126 mg/dL) and grossly elevated 2hPG (> 11.1 mM or 200 mg/dL) based on diagnostic criteria defined by Diabetes Canada. Overall, there were only two participants in this cohort (among 15 with blood glucose measurements) who maintained normal glucose homeostasis and glucose tolerance throughout the intervention period.

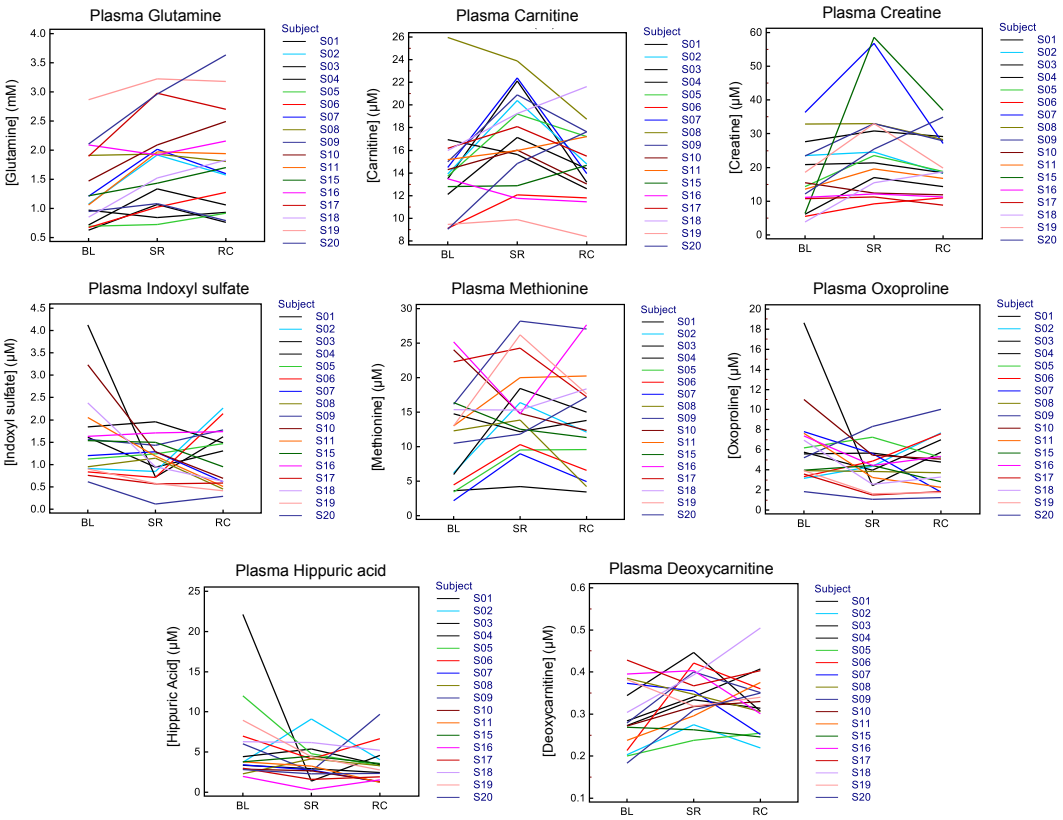

Figure S3.2: Individual metabolic trajectories for the top-ranked 8 plasma metabolites associated with physical inactivity from a cohort of overweight/pre-diabetic older adults at baseline (BL), following 2 weeks of step reduction (SR) and after resuming normal habitual activity upon recovery for two weeks (RC). Despite collection of blood specimens under standardized conditions with fasting/morning plasma samples collected after participants were provided 2 days of standardized meals, there was considerable between-subject variability in circulating plasma metabolite concentrations, including their dynamic responses to step reduction.

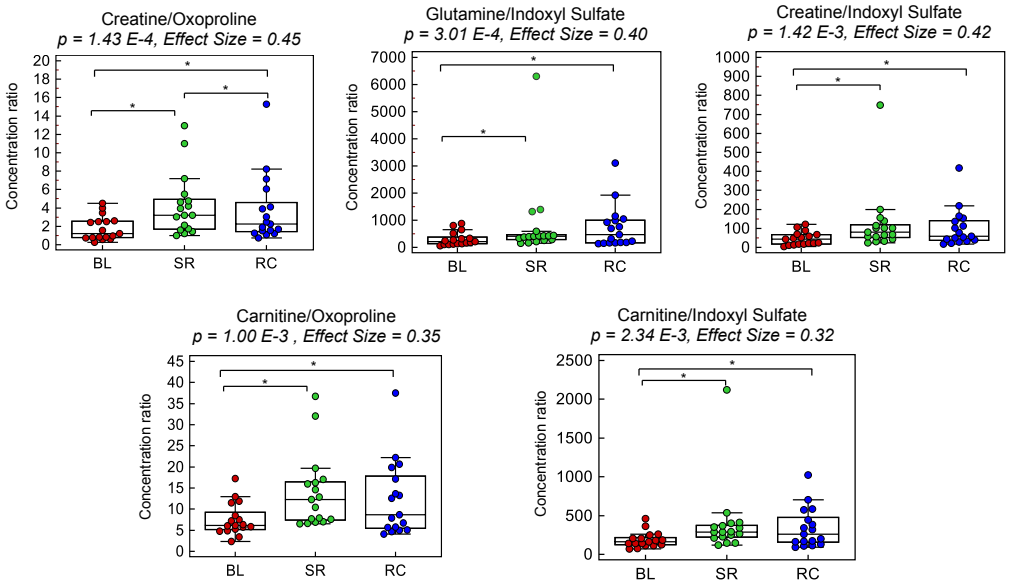

Figure S3.3: Ratiometric plasma markers associated with physical inactivity from a cohort of overweight/pre-diabetic older adults at baseline (BL), following 2 weeks of step reduction (SR) and after resuming normal habitual activity upon recovery for two weeks (RC). All ratiometric biomarker satisfied Benjamini-Hochberg adjustment ($q < 0.05$, FDR) for multiple hypothesis testing, which increased the effect size as compared to most single plasma metabolites (*e.g.,* creatine, oxo-proline, indoxylsulfate) with the exception of glutamine and carnitine. Overall, most ratiometric markers reflected significant changes in circulating metabolites associated with muscle tissue energy metabolism and oxidative stress upon step reduction with a persistent perturbation from baseline even after two weeks of recovery with normal habitual activity.

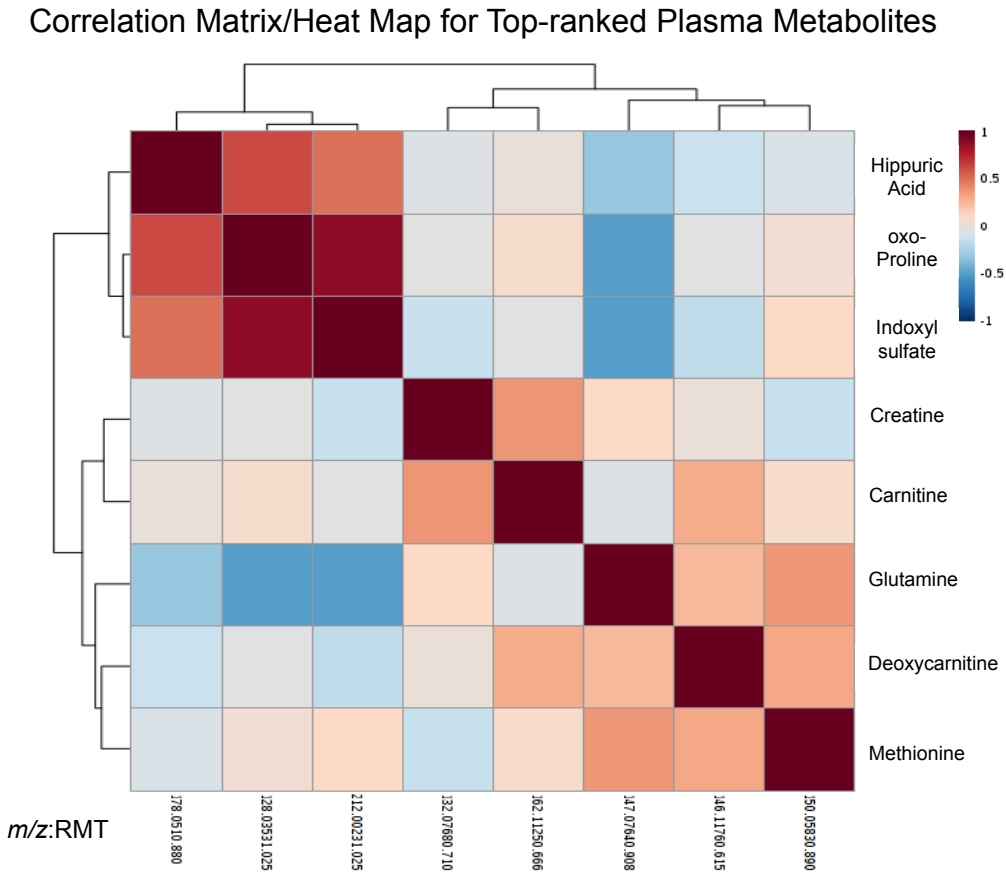

Figure S3.4: A correlation matrix/2D heat map among the top-ranked plasma metabolites (*glog*-transformed ion responses) identified in this step reduction intervention study, which highlights the strong co-linearity between circulating levels of indoxylsulfate and oxo-proline (r = 0.881; p < 1.0 E-15), hippuric acid and oxo-proline (r = 0.622; p < 1.1 E-6), as well as hippuric acid and indoxylsulfate (r = 0.507; p < 1.4 E-4). Additionally, there was an inverse correlation between glutamine and oxoproline (r = -0.502; p < 1.8 E-4), as well as glutamine and indoxylsulfate (r = -0.500; p < 1.8 E-4) suggesting common metabolic pathways involved in their regulation in circulation.

Chapter IV
Characterization of the Human Skeletal Muscle Metabolome for Elucidating the Mechanisms of Bicarbonate Ingestion on Strenuous Interval Exercise

Michelle Saoi, Michael Percival, Carine Nemr, Alice Li, Martin Gibala
and Philip Britz-McKibbin

Anal. Chem, **2019**, *91*, 4709-4718

M.S. performed all the experiments including optimization for sample preparation, data acquisition using MSI-CE-MS, data processing, interpretation, statistical analysis and wrote the initial draft for publication. C.N. developed and optimized method for electrolyte analysis using iCE-UV and acquired electrolyte data. A.L. assisted with sample preparation and data processing. M.P and M.G. obtained ethics approval for study, designed the study, provided muscle tissue and plasma specimens, assisted with interpretation, provided valuable feedback and revised the initial manuscript. P.B.M provided feedback on the manuscript draft.

Chapter IV: Characterization of the Human Skeletal Muscle Metabolome for Elucidating the Mechanisms of Bicarbonate Ingestion on Strenuous Interval Exercise

4.1 Abstract

Bicarbonate has long been touted as a putative ergogenic aid that improves exercise performance and blood buffering capacity during strenuous exercise. However, the underlying mechanisms of action of bicarbonate intake on skeletal muscle metabolism have yet to be fully elucidated. Herein, we apply two orthogonal analytical platforms for nontargeted profiling of metabolites and targeted analysis of electrolytes from mass-limited muscle tissue biopsies (≈ 2 mg dried mass) when using multisegment injection-capillary electrophoresis-mass spectrometry (MSI-CE-MS) and CE with indirect UV detection, respectively. Seven untrained men performed a standardized bout of high intensity interval exercise trial following either bicarbonate (0.40 g/kg) or placebo ingestion in a double-blinded, placebo-controlled, cross-over study design, where paired skeletal muscle tissue and plasma specimens were collected at three time intervals at rest, post-exercise and recovery. Optimization of a quantitative microextraction procedure was first developed for lyophilized tissue prior to characterization of the human muscle metabolome, which resulted in the identification and quantification of more than 80 polar/ionic metabolites reliably (CV < 30%) detected in a majority (> 75%) of samples with quality control. Complementary univariate and multivariate statistical methods were used to identify biomarkers associated with strenuous exercise and/or bicarbonate treatment responses, whereas structural elucidation of biologically significant intramuscular metabolites was performed using high resolution MS/MS. Importantly, bicarbonate ingestion prior to strenuous interval exercise was found to elicit a modest treatment effect ($p < 0.05$) as compared to placebo on metabolic pathways associated with ionic homeostasis (potassium), purine degradation (uric acid), and oxidative stress as regulated by glutathione metabolism (oxidized mixed glutathione disulfide) and histidine-containing dipeptides (anserine) within muscle tissue that was distinctive from dynamic metabolic changes measured in

circulation. This work provides deeper biochemical insights into the impact of acute alkalosis in preserving contracting muscle function during high-intensity exercise, which is also applicable to the study of muscle-related pathologies relevant to human health and ageing.

4.2 Introduction

High intensity interval-type exercise is characterized by intermittent periods of strenuous effort interspersed with brief recovery periods. Importantly, interval exercise elicits comparable, and in some cases, superior physiological and metabolic adaptations to traditional moderate-intensity endurance exercise that improves cardiometabolic health outcomes despite a five-fold lower exercise volume and time commitment.[1,2] However, this type of physical activity is also associated with significant metabolic disturbances within contracting skeletal muscle with the development of metabolic acidosis due to the high energetic demands for ATP regeneration beyond mitochondrial respiration capacity.[3] The acute decline in intracellular pH also contributes to altered muscle contractile function, perturbation of redox homeostasis and the development of fatigue.[4,5] As a result, efficacious yet safe dietary interventions (*i.e.,* ergogenic aids) that can attenuate metabolic acidosis while preserving muscle function during strenuous exercise have long been sought after to improve athletic performance and/or recovery in competitive sports.[6] Treatment interventions that support muscle function are also relevant for age-related muscle decline with ageing (*i.e.,* sarcopenia) that is exacerbated with extended hospitalization.[7]

The acute ingestion of alkalinizing agents, such as sodium bicarbonate, remain one of the most frequently investigated strategies to delay the onset of muscular fatigue following strenuous exercise.[8,9] Bicarbonate pretreatment at high dosages has been shown to effectively buffer blood pH during interval exercise and modulate selected markers of skeletal muscle substrate metabolism (*i.e.,* glycogen

breakdown).[10,11] However, other metabolic responses beyond muscle bioenergetics require further characterization given that muscle also secretes bioactive metabolites (*i.e.,* myobolites) into circulation with systemic effects on human physiology.[12] Herein, we report characterization of the human skeletal muscle metabolome derived from lyophilized muscle tissue biopsies (≈ 2 mg dried tissue) together with matching blood samples from a cohort of recreationally active males participating in standardized exercise trials following bicarbonate pretreatment in a double-blind, placebo-controlled cross-over study design. Due to the invasive nature of repeated tissue biopsies, there have been few metabolomics-based studies reported on skeletal muscle tissue from human trials involving exercise and/or dietary interventions.[13,14] Previous studies have performed targeted analysis of known metabolites when using several analytical platforms without absolute metabolite quantification nor the identification of novel muscle-derived metabolites. In our case, nontargeted metabolic profiling of the human skeletal metabolome was first performed using multisegment injection-capillary electrophoresis-mass spectrometry (MSI-CE-MS) as a multiplexed analytical platform for analysis of polar/ionic metabolites that is optimal for mass or volume-restricted biospecimens, such as dried blood spots.[15,16] A targeted assay based on CE with indirect UV detection was also applied for reliable determination of major electrolytes involved in ionic homeostasis. Rigorous method development to maximize metabolite recovery from human muscle tissue extracts is outlined in our work, including reference concentration ranges measured for a wide range of metabolites and electrolytes from matching muscle tissue and plasma/serum samples. Importantly, our work is the first to identify anserine within human skeletal muscle, a histidine-containing dipeptide derived from carnosine that was significantly modulated with bicarbonate pretreatment following strenuous exercise as compared to placebo. Overall, this work provides new mechanistic understanding of the modest treatment effects of bicarbonate ingestion on strenuous

interval exercise that extends well beyond its known role as a buffer to attenuate the lowering of blood pH.

4.3 Experimental Section

4.3.1 Study Cohort, Treatment Interventions and Interval Exercise Trials

The study was based on a previously published study that did not include comprehensive metabolite profiling,[17] where nine active young men were recruited to participate in a double-blinded, placebo-controlled crossover study design. The study protocol was approved by the Hamilton Integrated Research Ethics Board (#13-426). However, only seven of the nine participants had sufficient residual muscle tissue available in the present study ranging from 1.2 to 3.4 mg of dried mass with an average mass of 2.4 mg (n=42) collected for subjects at all time intervals. A summary of the physical characteristics and performance data of this cohort (n=7) is summarized in **Table S4.1.** Briefly, after 10 h of overnight fasting, each subject was fed a standardized breakfast the morning of each session. All participants ingested two doses of the placebo (2 x 0.14 $g \cdot kg^{-1}$ NaCl) or sodium bicarbonate (2 x 0.2 $g \cdot kg^{-1}$ $NaHCO_3$) at 90 and 30 min prior to exercise. The order of interventions was counterbalanced at least one week following the first session in a randomized fashion. The intense interval exercise regimen was completed on a LifeCycle 95 C1 cycle ergometer (Life Fitness, Schiller Park, IL) consisting of a 5 min warm up followed by 10 x 60 s high intensity cycling bouts at an intensity estimated to elicit approximately 90% of maximal heart rate (HR_{max}) for individual subjects interspaced with 60 s of low-intensity recovery at 50 W or rest. Blood samples were obtained at eight intervals during the protocol, however only three time points were analyzed in this work, namely pre-exercise (Pre), immediately post-exercise (Post) and after 3 h of recovery (Rec). All plasma (EDTA as anticoagulant) samples were promptly processed while serum samples were left at room temperature for 30 min and centrifuged at 1,400 *g* for 10 min at 4 ºC. Following centrifugation, serum/plasma samples were aliquoted and stored at -80

ºC until analysis. Skeletal muscle tissue biopsies were also collected at the same three time intervals as blood samples from the *vastus lateralis* under local anesthesia using a Bergström needle adapted with suction by a trained physician.[1] Muscle tissue biopsies were immediately frozen in liquid nitrogen and stored at -80 °C. Thereafter, muscle was dissected from any visible fat/connective tissue, lyophilized for 48 h using a benchtop freeze dryer system (Savant Instruments Inc., NY, USA) and then stored at -80 °C. All lyophilized muscle tissue samples were weighed using an electronic balance prior to extraction to allow for normalization of intramuscular metabolite responses/concentrations as described below.

4.3.2 Muscle Tissue Extraction Protocol

Freeze-dried muscle tissue samples (≈ 2 mg) were extracted using a modified Bligh Dyer extraction[18-20] to fractionate hydrophilic constituents. A two-step extraction procedure consisted of adding 64 µL ice cold methanol:chloroform (1:1) followed by 26 µL de-ionized water to induce phase separation. After vortexing for 10 min and centrifugation at 2,000 *g* at 4 °C for 20 min, the upper aqueous layer was aliquoted. Then, a second extraction on the residual muscle tissue was performed by adding a fresh aliquot of 32 µL of methanol:deionized (1:1) water. Following the same vortexing and centrifugation procedure, the second upper aqueous layer was combined to the first aliquot to maximize the recovery of metabolites from muscle tissue extracts. Prior to analysis, 5 µL of 3-chloro-*L*-tyrosine (Cl-Tyr) and 2-napthalenesulfonic acid (NMS) were added to 20 µL of muscle tissue extract with a final concentration of 25 µM, which served as internal standards for positive and negative mode detection, respectively. Further experimental details on the collection and sample workup of repeat plasma (for all metabolites and chloride) and serum (for all other electrolytes) specimens are described in the **Supporting Information**.

4.3.3 Nontargeted Metabolite Profiling by MSI-CE-MS

MSI-CE-MS experiments were performed on an Agilent G7100A CE (Agilent Technologies Inc., Mississauga, ON, Canada) equipped with a coaxial sheath liquid (Dual AJS) Jetstream electrospray ion source coupled to an Agilent 6230 TOF-MS system. Separations were performed using uncoated fused-silica capillaries (Polymicro Technologies, AZ, USA) with a total length of 120 cm and inner diameter of 50 μm when using an applied voltage of 30 kV at 25 °C. The background electrolyte (BGE) consisted of 1 M formic acid with 15% *vol* acetonitrile (pH 1.80) under positive ion mode, and 50 mM ammonium bicarbonate (pH 8.50) under negative ion mode for comprehensive analysis of cationic and anionic metabolites from matching muscle tissue extracts and plasma filtrates, respectively.[21] Terminal ends of the capillary had a 7 mm length of polyimide removed when using a burner in order to reduce sample carry-over effects, as well as potential deleterious swelling when in contact with organic solvent or ammonia based buffers that can lead to incidental capillary fractures.[22] Temporal signal pattern recognition using different serial sample injection configurations in MSI-CE-MS was applied for optimization of the tissue extraction protocol, nontargeted metabolite profiling of matching tissue extracts and plasma filtrates, and acquisition of calibration curves for absolute quantification of metabolites as described elsewhere.[15,23,24] Briefly, a seven sample serial injection format was used in MSI-CE-MS (with the exception of the tissue extraction optimization) and utilized alternating hydrodynamic injection sequences at 100 mbar for 5 s each sample that was followed by a 40 s BGE spacer. Thus, an MSI-CE-MS run consisted of a series of six alternating injections of each sample corresponding to matching placebo and bicarbonate treatment arms from the same subject which were randomized according to sample position, but paired according to the time point in the interventions (*i.e.,* Pre, Post and Rec). Also, a pooled quality control (QC) within each experimental run was also randomly inserted within each serial injection configuration when using MSI-CE-MS to assess technical variance while also

allowing for robust batch correction.[16] Between runs, the capillary was flushed for 15 min with BGE at 950 mbar. The sheath liquid was comprised of 60% *vol* MeOH with 0.1% *vol* formic acid for positive ion mode, and 50% *vol* MeOH for negative ion mode. The TOF-MS system was operated with full-scan data acquisition over a mass range of *m/z* 50-1700 and an acquisition rate of 500 ms/spectrum. The ESI conditions were Vcap = 2000 V, nozzle voltage = 2000 V, nebulizer gas =10 psi, sheath gas = 3.5 L/min at 195 °C, drying gas 8 L/min at 300 °C. whereas, the MS voltage settings were fragmentor = 120 V, skimmer = 65V and Oct1 RF = 750 V. Further details on unknown metabolite identification via collision-induced dissociation experiments using a QTOF-MS system, as well as data pre-processing, statistical analysis and batch-correction adjustments are described in the **Supporting Information**, including a supporting excel data file with original and batch-corrected muscle and plasma/serum metabolome data from this study.

4.3.4 Targeted Electrolyte Analysis by CE Indirect UV Detection

All CE with indirect UV experiments were performed on a P/ACE MDQ CE system (Beckman-Coulter, Fullerton, CA, USA) equipped with indirect UV detection at 214 nm at 25 ºC. Separations of inorganic cations was achieved using a BGE consisting of 5 mM formic acid, 12.5 mM creatinine, 3 mM 18-crown-6-ether at pH 4.0, which was adjusted using 1 M sulfuric acid.[25] Separations were performed under normal polarity using an uncoated fused-silica capillary with a total length of 60 cm and inner diameter of 50 µm using an applied voltage of 30 kV at 25 ºC. CE with indirect UV detection was also used for the analysis of plasma chloride using a BGE consisting of 0.4 M formic acid, 5 mM naphthalene disulfonate (NDS), 5 mM naphthalene trisulfonate (NTS) at pH 2.0.[26] Separations were performed on an uncoated fused-silica capillary with a total length of 60 cm and an inner diameter of 75 µm using an applied voltage of -18 kV (reversed polarity). A hydrodynamic injection for 10 s or 80 s (at 0.5 psi) was used for analysis of chloride and other major blood electrolytes, respectively. As plasma used a potassium salt of EDTA

as an anticoagulant, it was not used for analysis of cationic electrolytes, such as potassium. Further details on method validation and quality control (QC) performed for major serum electrolyte analysis by CE with indirect UV method are outlined in the **Supporting Information**.

4.4 Results and Discussion

4.4.1. Development of a Quantitative Tissue Extraction Protocol

A major constraint of tissue metabolomic studies is the invasive nature of acquiring percutaneous biopsies from human participants, notably repeat specimens from the same individual during exercise that are more heterogeneous than conventional biofluids (*e.g.,* plasma). As a result, standardized extraction protocols are needed for analysis of mass-limited muscle biopsies collected via the Bergström technique (≈100-200 mg of wet tissue)[27] when using multiple assays (*i.e.,* transcriptomics, enzymatic assays) and complementary metabolomics-based platforms.[13,15] Wu *et al.*[19] reported a high throughput extraction protocol for tissue (fish liver) metabolomics, however there have been few studies to date demonstrating quantitative recovery for a wide range of intra-cellular metabolites from human tissue specimens[28,29] to reduce false discoveries due to pre-analytical sources of bias.[30] Lyophilization of all muscle tissue was performed to allow for more efficient extraction of powdered/freeze-dried samples that can be accurately weighed out for normalization of ion responses or metabolite concentrations to total dried weight to reduce overall biological variance. We first performed four repeated rounds of extractions on muscle tissue (≈ 2 mg) in triplicate when using a modified Bligh-Dyer protocol.[18] To preserve the integrity of labile intra-cellular metabolites that are prone to oxidation (sulfhydryls) and hydrolysis (phosphagens), two recovery standards were added to the extraction solvent prior to sample processing. The extent of oxidation and hydrolysis was then evaluated based on the measured ratio of the oxidized/reduced forms of a synthetic reduced glutathione analog (*i.e.,* γ-Glu-Cys-Gly-OEt) and hydrolyzed/non-hydrolyzed forms of a stable isotope-labelled

nucleotide analog (*i.e.,* $^{13}C_{10}$-ATP) as shown in **Figure S4.1** of the **Supporting Information**. A five sample serial injection format in MSI-CE-MS comprising of four successive rounds of extracts performed on a pooled muscle tissue sample on ice (+4 °C) together with a blank extract (pre-chilled solvent alone) were analyzed within a single run as shown in **Figure 4.1(A)**. Overall, the first, second, third and fourth round of serial extracts resulted in an average recovery of (64 ± 6)%, (26 ± 4)%, (8 ± 2)% and (4 ± 2)% respectively, which was based on the analysis of 45 representative metabolites from three independent muscle tissue specimens as summarized in **Table S4.2**, including amino acids, acylcarnitines, organic acids, sugar phosphates and nucleotides. As a result, it was concluded that pooling together the first two upper layer aqueous fractions allowed for near exhaustive extraction (> 90% recovery) of polar/ionic metabolites from muscle tissue as shown for *O*-acetyl-*L*-carnitine (C2) and phosphocreatine (PCr) in **Figure 4.1(B)** while minimizing oxidation and hydrolysis artifacts (< 8%) during sample processing (**Figure S4.1**). Furthermore, our study also noted that repeat (*i.e.,* up to three) freeze-thaw cycles of muscle extracts generated lower recoveries for abundant yet labile intracellular phosphagens (*e.g.,* PCr, ATP) and reduced thiols (*e.g.,* reduced glutathione, GSH) with a concomitant increase in hydrolyzed/oxidized by-products, such as inorganic phosphate (PO_4^{3-}) and oxidized glutathione disulfide (GSSG). Thus, to minimize bias and accurately measure high energy phosphate donors/nucleotide pools and intracellular thiol redox status,[31] all muscle extracts were analyzed by pooling two aqueous fractions together after a single thaw on ice when stored at -80 °C.

4.4.2 Nontargeted Profiling of the Human Skeletal Muscle Metabolome

CE with indirect UV detection was used as a targeted approach for determination of major (involatile) electrolytes relevant to muscle contractile function, including potassium, sodium, calcium, magnesium and chloride. Key figures of merit are

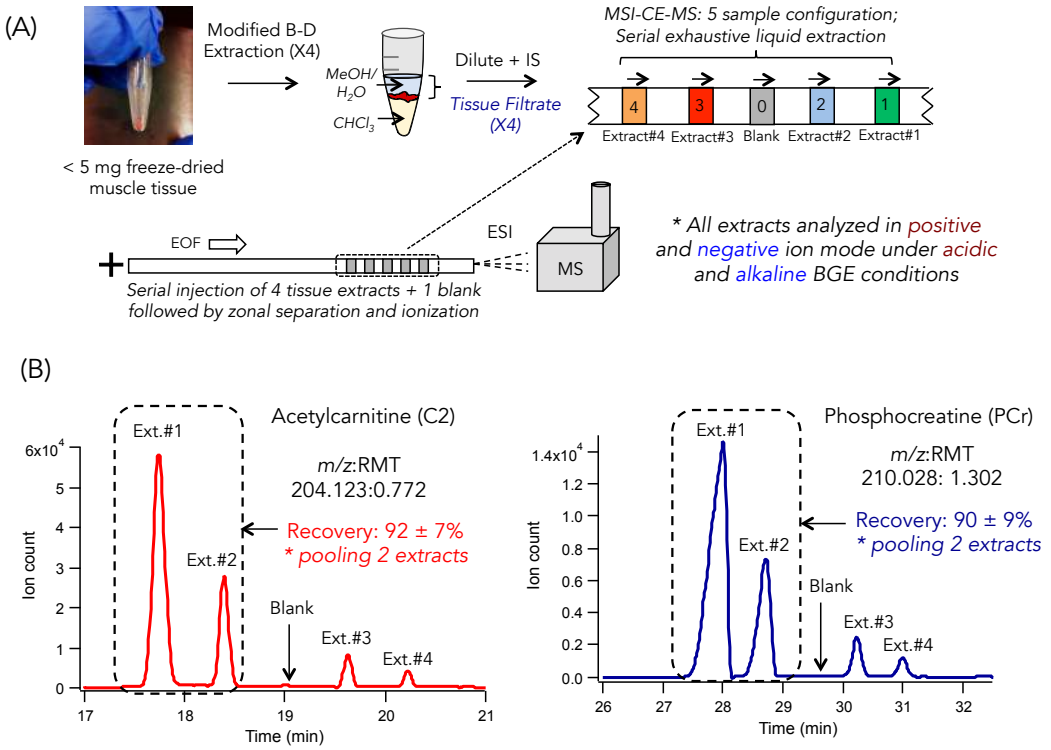

Figure 4.1: Sample workflow developed for optimization of a quantitative tissue extraction protocol for small amounts of lyophilized muscle tissue biopsies (≈ 2 mg dried weight). (A) MSI-CE-MS using a five sample serial injection configuration applied for evaluating metabolite recoveries after four repeated rounds of extractions based on a modified Bligh-Dyer procedure together with a blank (solvent) extraction. (B) Extracted ion electropherograms (EIE) for representative metabolites from muscle tissue extracts, acetylcarnitine (C2) and phosphocreatine (PCr) showing excellent recoveries (> 90%) when pooling together the first two extracts from the top aqueous layer without sample carry-over as reflected in blank extracts.

summarized in **Table S4.3** and **Figure S4.2**, which demonstrate good linearity (R^2 > 0.990) with acceptable detection limits (20-60 µM), mean recoveries (≈ 94%) and technical precision based on intermittent analysis of pooled serum extracts as QC samples (CV = 13%, n = 30) as shown in control charts. Also, MSI-CE-MS was used as a high throughput platform for nontargeted analysis of a wide array of polar/ionic metabolites that comprise of the human skeletal muscle metabolome. **Figure S4.3** depicts an overview of the data workflow used for selection of authentic metabolites from muscle tissue when using multiplexed separations with temporal signal pattern recognition,[15, 21] where each metabolite is annotated by their accurate mass and relative migration time (m/z:RMT) in positive (p) or negative (n)

ion mode. In this case, a dilution trend filter was used to effectively reject spurious, background and/or redundant ion signals (*i.e.,* isotope peaks, in-source fragments and/or adducts) that comprise the majority of molecular features generated in ESI-MS.[32] Overall, 84 muscle-derived metabolites (together with 5 electrolytes) satisfied several stringent selection criteria in this work, namely they were measured with adequate precision (CV < 30%, n=3, with 54 metabolites/electrolytes with CV < 15%) without a background signal measured in the blank while also undergoing a linear response change upon serial dilution. However, 76 metabolites/electrolytes were included within the final data matrix as they were detected in the majority (> 75%) of muscle tissue extracts (to avoid missing value inputs) while also still having adequate technical precision (CV < 30%, n=7) for pooled samples analyzed as QC. Most muscle metabolites were confidently identified based on co-migration after spiking pooled muscle extracts with an authentic standard (*level 1*), whereas 7 metabolites were tentatively identified based on their MS/MS spectra when compared to public databases (*level 2*), and 6 metabolites had unknown chemical structures and were denoted by their most likely molecular formulas (*level 3*). Additionally, this study included characterization of the plasma metabolome from the same subjects when using MSI-CE-MS (**Figure S4.4**) using analogous selection criteria outlined for muscle tissue, which comprised 60 polar/ionic metabolites and electrolytes reliably detected in the majority of samples. Furthermore, absolute quantification of a majority of identified muscle metabolites (mmol/kg) are also summarized in **Table S4.4** in comparison to their circulating concentrations from matching plasma/serum samples (mM) for a cohort of male subjects (placebo, n=7) at rest. Muscle metabolite concentrations spanned a wide dynamic range (0.04 to 316 mmol/kg) from low abundance compounds (*O*-propionylcarnitine) to major electrolytes (K^+) with several metabolites uniquely expressed within skeletal muscle as compared to plasma, including GSH, PCr, cAMP, ATP, glucose-1-phosphate, glycerol-3-phosphate, and carnosine. Interestingly, lidocaine (235.1805:0.844, MH^+) was also

detected in muscle tissue extracts since it was administered as a local anesthetic prior to acquiring tissue biopsies. Overall, similar metabolome coverage was achieved in MSI-CE-MS as compared to recent studies[12,13] which adopted a targeted strategy for analysis of more than 96 known muscle metabolites when using several different analytical platforms, including GC-MS (organic acids), UPLC-MS/MS (amino acids, acylcarnitines), ion pair-LC-MS/MS (nucleotides/coenzymes), LC-MS/MS (lipids), as well as specific enzyme assays (PCr, ATP, creatine). Major advantages of MSI-CE-MS include its higher throughput when relying on a single cost-effective platform for metabolomics with stringent QC, which allows for the discovery of novel metabolites from low amounts of residual muscle tissue specimens. It is important to note that although an average of 2 mg of dried muscle tissue was needed for accurate weighing and data normalization prior to extraction, only about 10 nL of a 20 μL extract (≈ 500 ng) is effectively injected on-column for muscle metabolomic analyses when using MSI-CE-MS.

4.4.3 Interval Exercise on Metabolome Dynamics in Muscle Tissue and Blood

An overview of this cross-over intervention study is shown in **Figure 4.2(A)**, where dynamic metabolic changes were measured from repeat muscle and blood specimens acquired from untrained males performing standardized ergometer cycling trials as a function of two factors, namely time of interval exercise (Pre, Post, Rec) and treatment (placebo, bicarbonate). **Figure 4.2(B)** depicts an extracted ion electropherogram for lactic acid, a classic biomarker of metabolic acidosis that has been shown to preserve muscle function during strenuous exercise,[33] which was measured in both muscle tissue extracts and plasma filtrates when using MSI-CE-MS. In this case, dynamic metabolic changes as a function of strenuous exercise time for each subject are evident within a single run based on elevations in lactic acid (> 4 to 7-fold-change, FC) immediately post-exercise (Post) as compared to baseline (Pre) and recovery (Rec) states. Additionally, the same run also captures

treatment responses to bicarbonate intervention on an individual level when comparing changes in lactic acid as a function of exercise time as compared to placebo together with a pooled sample that serves as a QC. **Figure 4.2(C)** shows quantitative lactic acid determination was achieved using a 7-point calibration curve, where ion responses were normalized to an internal standard (NMS) migrating from the same sample in MSI-CE-MS. **Figure S4.5** summarizes an inter-laboratory method comparison for plasma lactic acid determination (n=42) when using a commercial lactic acid analyzer[17] as compared to MSI-CE-MS, which showed good mutual agreement as reflected by a slope = 0.818 and a mean bias of 27% with few outliers based on a Passing-Bablok regression and Bland-Altman plot, respectively. This modest extent of negative bias is reasonable given that measurement of lactic acid by the colorimetric enzyme assay was performed shortly after blood collection, whereas it was completed after prolonged storage of samples over two years at -80 °C by MSI-CE-MS. Also, **Figure 4.2(D)** shows a 2D scores plot from a principal component analysis (PCA) that was used to demonstrate good overall technical precision for QCs (median CV = 10%) when measuring lactic acid and 75 other classes of polar/ionic metabolites and electrolytes comprising the muscle metabolome when compared to the overall biological variance (median CV = 40%) between samples after normalization to total dried weight. Similarly, **Figure 4.2(E)** highlights the paired data structure of the study design when using a 3D heat map with hierarchical cluster analysis (HCA), where each subject serves as their own control when completing exhaustive exercise trials with bicarbonate pretreatment relative to a placebo. The effects of interval exercise on dynamic metabolic changes for the placebo trial were first analyzed when using a one-way repeated measures ANOVA as summarized in **Table S4.5** and **Table S4.6**, respectively. Overall, 13 muscle metabolites and 23 plasma metabolites showed significant changes post-exercise ($p < 0.05$; effects sizes > 0.40) relative to baseline and recovery time points, which were related to metabolic pathways associated with muscle bioenergetics, including glycolysis (*e.g.,* malic acid), amino acid

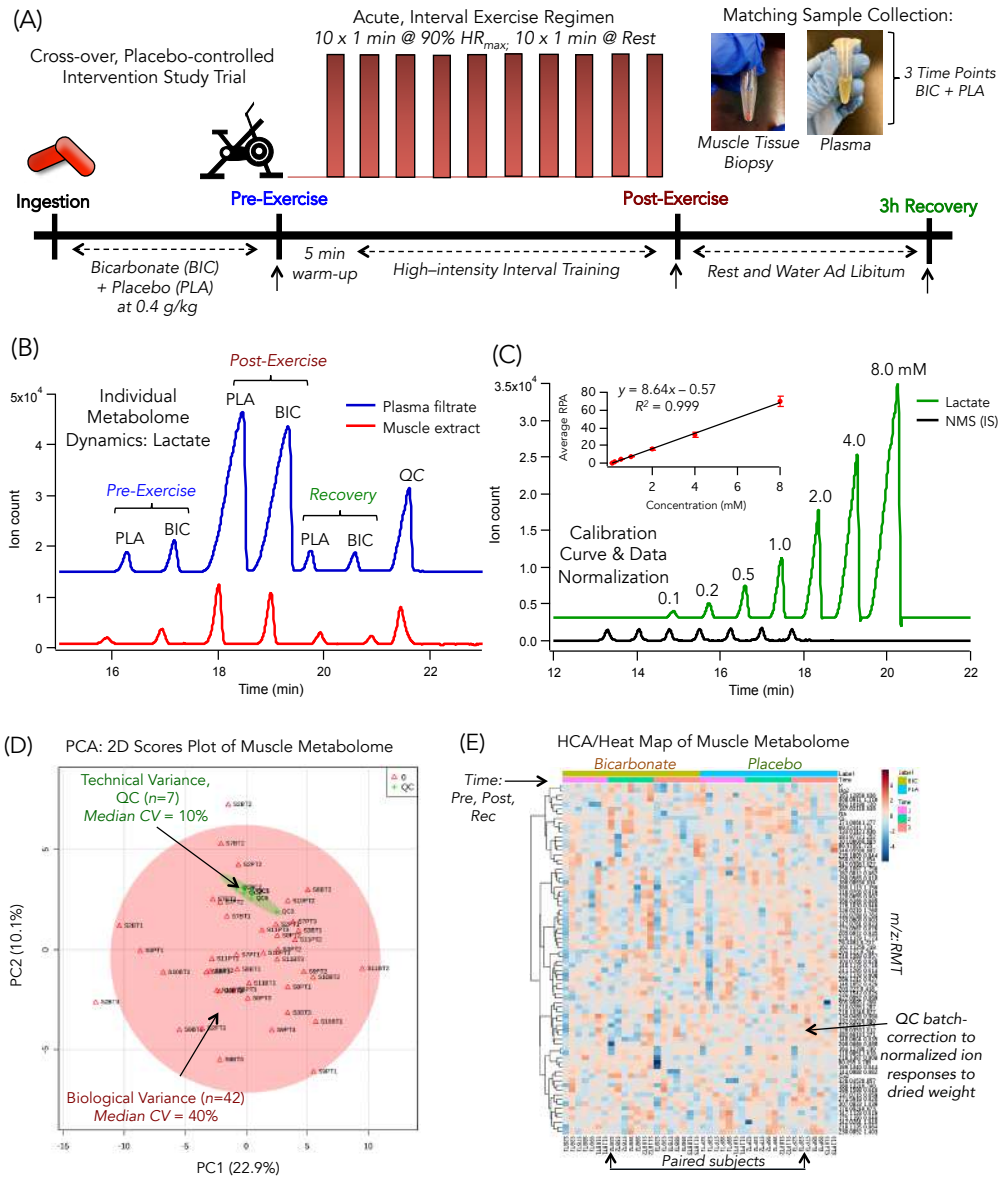

Figure 4.2: (A) Schematic of a placebo-controlled crossover study design involving a cohort of untrained males participating in strenuous interval exercise trials based on strenuous ergometer cycling. Matching muscle tissue biopsies and blood specimens were collected at three time intervals (Pre, Post, Rec at 3h) for the same subjects for the double-blinded placebo (PLA) and bicarbonate (BIC) treatment sessions. (B) Serial sample injection configuration used in MSI-CE-MS for revealing dynamic metabolomic changes (*e.g.,* lactic acid) as a function of exercise time and treatment based on paired plasma and muscle tissue samples analyzed for each subject together with a QC. (C) Calibration curve for quantification of lactic acid when using MSI-CE-MS, where ion responses are normalized to an internal standard (NMS) from the same sample position. Overview of data structure for the human skeletal muscle metabolome based on a (D) PCA 2D scores plot comparing technical (QC) and biological variance and a (E) 3D heatmap with hierarchical cluster analysis (HCA) for 76 ionic/polar metabolites and major electrolytes consistently measured (CV < 30%) in majority (> 75%) of muscle tissue specimens. Batch-corrected metabolite ion responses were normalized to dried weight (mg), *log*-transformed and autoscaled when using multivariate data analysis.

metabolism (*e.g.,* phenylalanine), ketone bodies (*e.g.,* 3-hydoxybutyric acid), purine degradation (*e.g.,* uric acid), nucleotide signalling (*e.g.,* GTP), and lipolysis (*e.g.,* glyercol-3-phosphate). **Figure 4.3** shows dynamic changes among four of the most significant metabolites quantified consistently in both muscle tissue (mmol/kg) and plasma (mM), including lactic acid, alanine, glutamic acid, and acetylcarnitine. As expected, both intramuscular and plasma lactic acid concentrations were elevated immediately post-exercise with a mean fold-change (FC) increase ranging from 4 (muscle) to 7 (plasma) relative to baseline or recovery states indicative of transient hyperlactatemia. These findings coincide with a decrease in muscle glycogen reported by Percival *et al.*[17] since it is used as primary carbohydrate source during prolonged strenuous exercise as accumulation of intramuscular lactic acid from glycolysis and oxidative phosphorylation pathways represents a physiological response to the high energetic demands for ATP within contracting muscle.[33] To preserve muscle function however, monocarboxylate transporters (MCTs) facilitate both H^+ and lactic acid efflux from the muscle into circulation, where lactic acid acts as a substrate for metabolism by other inactive tissue.[34] Interestingly, intramuscular lactic acid concentrations in this work were strongly correlated with both malic acid (r = 0.864; p = 4.56 E-7) and glycerol-3-phosphate (r = 0.848; p = 1.20E-6) highlighting the activation of central energy metabolism during strenuous exercise. Exercise-induced changes in amino acid metabolism were also widely measured in this study, most notably alanine and glutamic acid. In this case, alanine concentrations post-exercise were consistently elevated in both muscle tissue (p = 4.0E-4) and plasma (p = 8.70E-5), which subsequently decreased to levels slightly lower than baseline upon recovery. In contrast, intramuscular glutamic acid concentrations decreased immediately after exercise (p = 0.001) and reached levels slightly greater than baseline after recovery unlike the increase in plasma glutamic acid concentrations post-exercise (p = 0.005). These opposing temporal patterns are attributed to the activation of alanine aminotransferases with glycolytic pyruvate production at the onset of exercise,

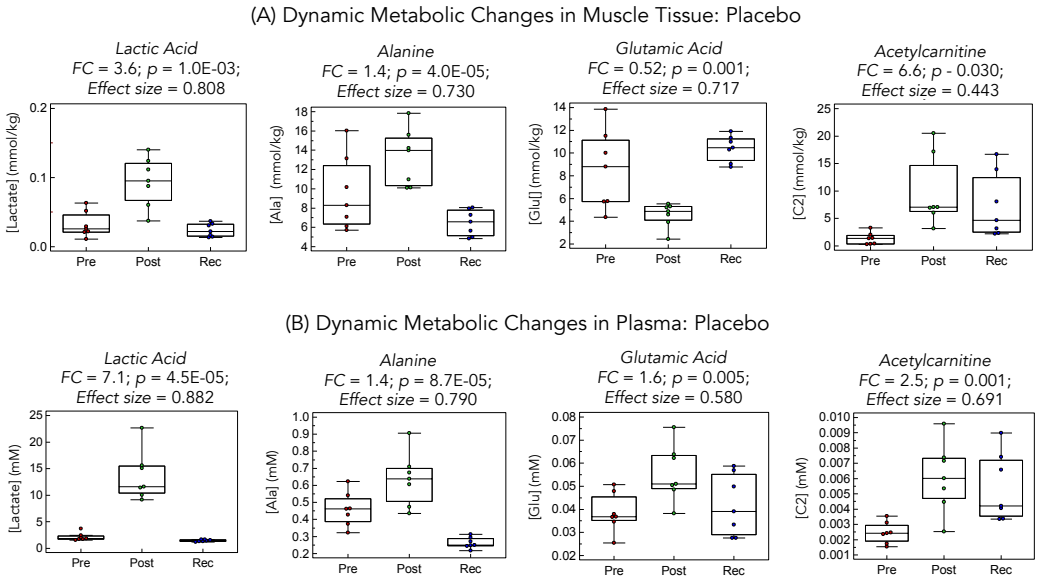

Figure 4.3: Dynamic metabolic changes following strenuous interval exercise using a one-way repeated measures ANOVA in (A) muscle tissue and matching (B) plasma samples from a cohort of untrained male subjects (n=7) at baseline (Pre), post-exercise (Post) and 3 h of recovery (Rec) after ingestion of (sodium chloride) placebo. These compounds were among the most significant metabolites consistently detected in both types of specimens with large effect sizes. Other muscle and/or plasma metabolites undergoing temporal changes upon strenuous exercise for the placebo are summarized in **Table S4.5** (muscle tissue) and **Table S4.6** (plasma) of the **Supporting Information**.

which catalyzes the conversion of glutamic acid into α-ketoglutarate, a key Krebs cycle intermediate. This process also results in formation of alanine and its export from contracting skeletal muscle into circulation with subsequent uptake into liver for gluconeogenesis that constitutes the "glucose-alanine" cycle.[35] Additionally, lipid metabolism via mitochondrial β-oxidation offers an alternative fuel source during high-intensity exercise as shown by time-dependent changes in acetylcarnitine measured within both muscle and plasma, which remained elevated post-exercise after a 3 h recovery period. Large yet persistent perturbations in short-chain acylcarnitines following strenuous exercise have been previously reported in both muscle tissue and plasma, which do not occur when performing bouts of low-intensity exercise.[36] Also, exercise training attenuates increases in plasma acetylcarnitine post-exercise due to adaptive improvements in muscle

mitochondrial oxidative capacity.[37] In fact, plasma 3-hydroxybutyric acid (**Table S4.6**) was notably elevated only after 3 h of recovery with a mean FC increase of 5.1 as compared to baseline ($p = 0.0008$; effect size = 0.719) reflecting a "delayed" post-exercise ketosis response.[38]

4.4.4 Exploring the treatment effects of bicarbonate ingestion following interval exercise

Since profound physiological and metabolic perturbations occur immediately after strenuous exercise, our study next focused on understanding the mechanisms of bicarbonate intake on intramuscular metabolism, which attenuates the lowering of blood pH post-exercise.[17] Due to the inherent paired data structure of this crossover study, a multilevel partial least squares-discriminant analysis (mPLS-DA)[39] was first used to differentiate metabolic phenotype changes due to high dose bicarbonate ingestion relative to placebo at the post-exercise time interval as shown in **Figure S4.6** (muscle tissue) and **Figure S4.7** (plasma/serum). Both mPLS-DA models showed good accuracy and robustness ($R^2 = 0.982$, $Q^2 = 0.853$; $R^2 = 0.955$, $Q^2 = 0.835$) and were validated by permutation testing ($p < 0.05$, $n = 1000$) as shown in their 2D scores plots. Additionally, top-ranked metabolites associated with bicarbonate intervention were selected based on their variable of importance in projection (VIP scores > 1.5) along the first component, such as uric acid and potassium within muscle tissue (12 compounds in total), as well as citric acid and chloride in plasma/serum (7 compounds in total). A two-way repeated measures ANOVA test was then used to confirm the statistical significance ($p < 0.05$; effect size > 0.50) of these candidate biomarkers of treatment responses to bicarbonate following strenuous exercise as summarized in **Table S4.7** (muscle tissue) and **Table S4.8** (plasma). **Figure 4.4(A)** depicts box-whisker plots for intramuscular concentrations of potassium, uric acid, glutathionylcysteine oxidized disulfide (GSH-Cys-SS), as well as an unknown ion (*m/z* 241.1295) that was subsequently identified as anserine (*level 1*) based on its co-migration and high resolution

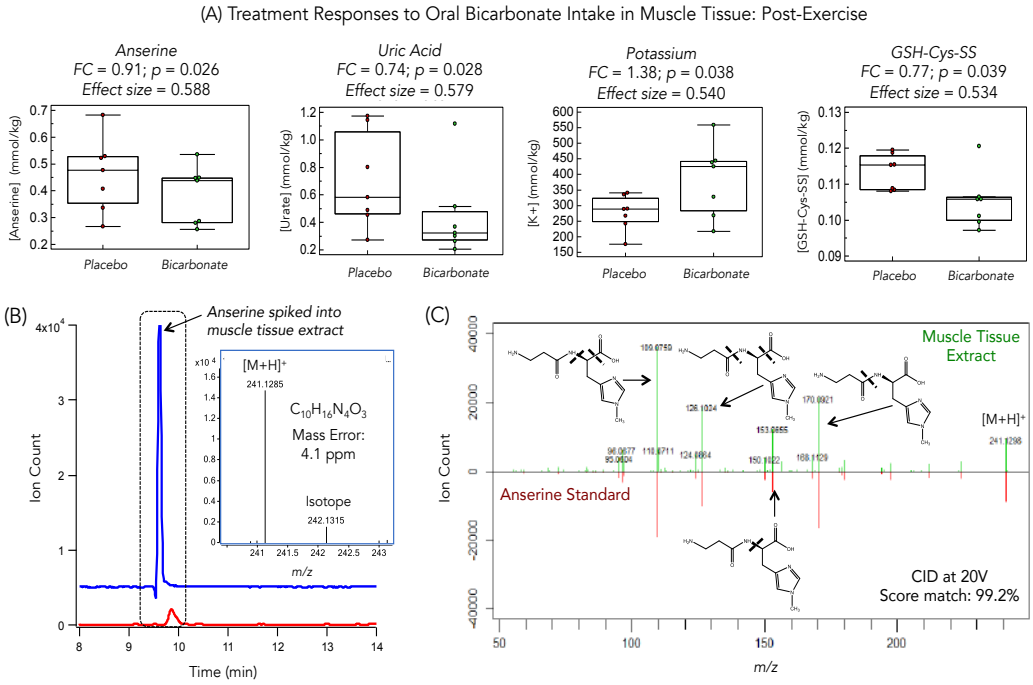

Figure 4.4: (A) Boxplots of four top-ranked intracellular metabolites/electrolytes ($p < 0.05$) associated with improved muscle function due to oral bicarbonate pretreatment following strenuous interval exercise in this placebo-controlled cross-over intervention study. A multi-level PLS-DA of metabolomic data (**Figure S4.7**) and then a two-way repeated measures ANOVA was performed for identification of metabolites/electrolytes from muscle tissue modulated by bicarbonate intervention immediately following exercise as compared to placebo. (B) Extracted ion electropherogram with full-scan mass spectrum of the unknown ion, subsequently identified unambiguously as anserine by comigration after spiking pooled muscle tissue with an authentic standard. (C) Also, a mirror plot comparing MS/MS spectra acquired for the unknown ion at 20 V as compared to anserine standard demonstrates a high matching score based on four characteristic product ions that is consistent with the β-alanyl-1-methylhistidine dipeptide.

MS/MS spectra with four characteristic products ions (at 20 V) that match well to an authentic standard as shown in **Figure 4.4(B, C)**. Intramuscular potassium concentrations increased 1.4-fold post-exercise with bicarbonate ingestion as compared to placebo ($p = 0.038$), whereas serum potassium concentrations were modestly attenuated by 0.87-fold post-exercise ($p = 0.047$). In this case, potassium efflux from muscle to the interstitium and venous blood occurs during strenuous exercise as a means to prevent K^+ induced decline in muscle force and contractibility at the onset of fatigue.[40] Interestingly, our findings indicate that

ingestion of bicarbonate induced a mild hypokalemic effect following strenuous exercise, which is consistent with previous studies where acute metabolic alkalosis has been shown to reduce K^+ efflux.[40, 41] An increase in intramuscular potassium post-exercise together with a lowering of its efflux into blood suggests bicarbonate-induced improvements in muscle contractibility that prevents cell membrane depolarization. Such changes may be governed by enhanced Na^+-K^+ pump activity that is typically suppressed with high-intensity exercise, but is restored by the alkalizing effects of bicarbonate.[41]

This study also revealed several unexpected outcomes with bicarbonate intervention, such as a 0.74-fold lowering of uric acid concentrations (p = 0.028) within skeletal muscle post-exercise as compared to placebo. Uric acid represents a terminal end-product of purine degradation due to irreversible ATP hydrolysis, which increases in serum following strenuous exercise activity.[42] In our case, uric acid concentrations were only significantly elevated post-exercise from baseline within muscle tissue (**Table S4.5**). Previous work has also demonstrated that plasma hypoxanthine, an intermediate of uric acid formation and biomarker of energetic stress, was significantly attenuated post-exercise after 6-weeks of interval training.[37] To date, there is little known regarding the effects of acute metabolic alkalosis on purine metabolism within skeletal muscle as most studies focus on changes in phosphagens and nucleotide pools (*i.e.,* ATP, PCr).[43] Additionally, modest bicarbonate treatment effects also affected intramuscular glutathione metabolism and redox homeostasis as reflected by a 0.77-fold lowering of GSH-Cys-SS concentrations (p = 0.039) post-exercise as compared to placebo. Importantly, this effect was not correlated with changes in either potassium or uric acid (p > 0.05). Strenuous exercise leads to increased oxidative stress within skeletal muscle due to the accumulation of reactive oxygen species (ROS) that may lead to oxidative damage of protein resulting in impaired contractility and muscle fatigue.[44] Intracellular antioxidants, such as glutathione (GSH) play crucial roles in

counteracting exercise-induced oxidative stress via reversible formation of oxidized disulfides, which can be enhanced with oral *N*-acetylcysteine ingestion to boost GSH recycling capacity during exhaustive exercise.[45] In this work, bicarbonate intake was found to attenuate GSH-Cys-SS concentrations within skeletal muscle post-exercise likely reflecting a decrease in intracellular oxidative stress and lower muscle protein oxidation. Additionally, anserine was identified for the first time within human skeletal muscle, which showed a modest decrease post-exercise following bicarbonate pretreatment (p = 0.026) as compared to placebo. Carnosine, a β-alanyl-histidine dipeptide is a major constituent within mammalian skeletal muscle that plays key roles in muscle contraction/excitation as an intracellular buffer and an antioxidant.[46] In our work, carnosine had mean baseline concentrations within skeletal muscle similar to GSH, glutamine and PCr (≈ 60 mmol/kg) at rest, which was only lower than intramuscular creatine (≈ 96 mmol/kg) and major electrolytes (> 200 mmol/kg for chloride, sodium and potassium) as summarized in **Table S4.4**. The biological activity of carnosine however is modulated via enzymatic transformations, including methylation (anserine), acetylation (*N*-acetylcarnosine), or decarboxylation (carcinine).[47] The former two histidine-containing dipeptides were identified and quantified within human muscle tissue, but had mean concentrations more than 120-fold lower than carnosine. As a result, the attenuation of anserine post-exercise with bicarbonate intake was indicative of lower carnosine methylation activity following strenuous exercise. While the exact function of specific carnosine metabolites within human skeletal muscle is not fully understood, animal studies have shown that methylation of carnosine to anserine enhances its antioxidant efficiency due to stronger interactions to neutralize superoxide (O_2^-) and hypochlorite (ClO^-) anion radicals.[48] Overall, this data supports that oral bicarbonate intervention had modest effects on lowering both oxidative stress (anserine, GSH-Cys-SS) and bioenergetic stress (uric acid) while maintaining ionic homeostasis (potassium) following strenuous exercise. Modest to strong treatment effects of bicarbonate (effect sizes = 0.53 to

0.71; $p < 0.05$) were also measured in circulation (plasma/serum) as shown in **Figure S4.8**, including a significant lowering of mean chloride and potassium concentrations post-exercise, as well as increases in three metabolites of central energy metabolism (*i.e.,* lactic acid, pyruvic acid, citric acid) and two branched-chain amino acid catabolites, namely α-ketoisovaleric acid and ketoleucine (α-ketoiscaproic acid). Interestingly, these two alpha-keto acids, and pyruvate were inversely correlated to serum potassium concentrations ($r > -0.67$; $p < 0.01$) suggesting common regulatory mechanisms in their transport into circulation.

An illustrative scheme that summarizes the pleiotropic effects of bicarbonate ingestion on strenuous exercise on key metabolic pathways within muscle tissue is depicted in **Figure S4.9**. Although new insights of the underlying mechanisms of bicarbonate action on skeletal muscle metabolism were achieved in this work, there were several study limitations. Firstly, a larger cohort is needed to increase study power due to between-subject variations in bicarbonate pharmacokinetics, enzyme activities, habitual diet and baseline cardiorespiratory fitness levels among participants despite including a standardized breakfast prior to exercise trials. However, the invasive nature of repeat muscle tissue biopsies during exercise trials placed practical limits on recruitment, which was comprised of young men. Also, bicarbonate interventions that link metabolic changes within skeletal muscle to improvements in exercise performance are recommended for future studies, such as reductions in self-perceived exertion or maximum heart rate, and increases of time to fatigue.[41] Although our study implemented a validated method for metabolomics with stringent quality control,[15] metabolome coverage was limited to polar/ionic metabolites and electrolytes. Recent advances in multiplexed CE-MS separations using non-aqueous buffer systems[49] now enable high throughput screening of fatty acids and intact lipids in order to expand metabolome coverage as required to fully understand the roles that alkalizing agents have on contracting skeletal muscle. Future metabolomic studies will also elucidate the mechanisms of

other nutraceuticals that counter fatigue during strenuous exercise, which may also offer therapeutic benefits for treatment of human diseases of unknown etiology as related to muscle dysfunction, such as chronic fatigue syndrome.[50]

4.5 Conclusions

This work represents the first study that uses a nontargeted and quantitative approach for characterization of the skeletal muscle metabolome from mass-restricted human tissue biopsies that applied a rigorous data workflow for metabolite authentication with quality control. A placebo-controlled, cross-over study design was used to evaluate treatment responses to bicarbonate ingestion following strenuous exercise with repeat muscle tissue and blood specimens collected from untrained participants. Extensive validation of an efficient extraction protocol for lyophilized muscle tissue achieved high recoveries for a wide range of polar/ionic metabolites and major electrolytes with good accuracy and technical precision without oxidation or hydrolysis artifacts. As expected, dynamic metabolomic studies for placebo exercise trials demonstrated large perturbations in metabolites primarily involved in muscle bioenergetics and ionic homeostasis in skeletal muscle and circulation. Noteworthy, our work revealed that bicarbonate pretreatment prevented potassium efflux from contracting muscle together with lower oxidative and energetic stress as reflected by modest reductions in anserine, GSH-Cys-SS, and uric acid concentrations post-exercise. While blood may act as a convenient and less invasive sample for biomarker discovery and routine analysis in human clinical trials as compared to skeletal muscle tissue, biochemical interpretations are often obscured since metabolites are derived from other organs and inactive tissues in the body. Thus, this study paves the way for routine metabolite profiling on mass-restricted tissue biopsies as required for deeper insights on skeletal muscle health and related myopathies, such as sarcopenia and frailty due to aging, sedentary inactivity and/or prolonged hospitalization.

4.6 Acknowledgements

P.B.M. and M.G. acknowledge funding support from the Natural Sciences and Engineering Research Council of Canada. P.B.M. also thanks financial support from Genome Canada. M.S. also acknowledges support in the form of an Ontario Graduate Scholarship, and M.P. was supported by a NSERC Canada Graduate Scholarship (Masters).

4.7 References

(1) Gibala, M. J.; McGee, S. L. *Am. Coll. Sport. Med.* **2008**, *36*, 58–63.

(2) Gibala, M. J.; Little, J. P.; Macdonald, M. J.; Hawley, J. A. *J. Physiol.* **2012**, *590*, 1077–1084.

(3) Robergs, R. A.; Ghiasvand, F.; Parker, D. *Am. J. Physiol. Regl. Integr. Comp. Physiol* **2004**, *287*, 502–516.

(4) Gladden, L. B. *J. Physiol.* **2004**, *558*, 5–30.

(5) Enoka, R. M.; Duchateau, J. *J. Physiol.* **2008**, *586*, 11–23.

(6) Porrini, M.; Del Bo', C. Ergogenic Aids and Supplements. *Front Horm. Res.* **2016**, *47*, 128–152.

(7) Welch, C.; Hassan-Smith, Z. K.; Greig, C. A.; Lord, J. M.; Jackson, T. A. *Aging Dis.* **2018**, *9*, 151–164.

(8) Shelton, J.; Kumar, G. V. P. *Food Nutr. Sci.* **2010**, *1*, 1–4.

(9) McNaughton, L. R.; Gough, L.; Deb, S.; Bentley, D.; Sparks, S. A. *Curr. Sports Med. Rep.* **2016**, *15*, 233–244.

(10) McNaughton, L. R.; Siegler, J.; Midgley, A. *Curr. Sports Med. Rep.* **2008**, *7*, 230–236.

(11) Edge, J., Bishop, D., Goodman, C. *J. Appl. Physiol.* **2006**, *101*, 918–925.

(12) Ibrahim, A.; Neinast, M.; Arany, Z.P. *Curr. Opin. Pharmacol.* **2017**, 34, 15–920.

(13) Alves, R. D. A. M.; Dane, A. D.; Harms, A.; Strassburg, K.; Seifar, R. M.; Verdijk, L. B.; Kersten, S.; Berger, R.; Hankemeier, T.; Vreeken, R. J. *Metabolomics* **2015**, *11*, 271–285.

(14) Fazelzadeh, P.; Hangelbroek, R. W. J.; Tieland, M.; de Groot, L. C. P. G. M.; Verdijk, L. B.; van Loon, L. J. C.; Smilde, A. K.; Alves, R. D. A. M.; Vervoort, J.; Muller, M.; van Duynhoven, J. P. M.; Boekschoten, M. V. *J. Proteome Res.* **2016**, *15*, 499–509.

(15) DiBattista, A.; McIntosh, N.; Lamoureux, M.; Al-Dirbashi, O. Y.; Chakraborty, P.; Britz-McKibbin, P. *Anal. Chem.* **2017**, *89*, 8112–8121.

(16) DiBattista, A.; McIntosh, N.; Lamoureux, M.; Al-Dirbashi, O. Y.; Chakraborty, P.; Britz-McKibbin, P. *J. Proteome. Res.* **2018**, *18*, 841-854
(17) Percival, M. E.; Martin, B. J.; Gillen, J. B.; Skelly, L. E.; MacInnis, M. J.; Green, A. E.; Tarnopolsky, M. A.; Gibala, M. J. *J. Appl. Physiol.* **2015**, *119*, 1303–1312.
(18) Bligh, E.; Dyer, W. *Can. J. Biochem. Physiol.* **1959**, *37*, 911–917.
(19) Wu, H.; Southam, A. D.; Hines, A.; Viant, M. R. *Anal. Biochem.* **2008**, *372*, 204–212.
(20) Lin, C. Y.; Wu, H.; Tjeerdema, R. S.; Viant, M. R. *Metabolomics* **2007**, *3*, 55–67.
(21) Macedo, A. N.; Mathiaparanam, S.; Brick, L.; Keenan, K.; Gonska, T.; Pedder, L.; Hill, S.; Britz-McKibbin, P. *ACS Cent. Sci.* **2017**, *3*, 904–913.
(22) Yamamoto, M.; Ly, R.; Gill, B.; Zhu, Y.; Moran-Mirabal, J.; Britz-McKibbin, P. *Anal. Chem.* **2016**, *88*, 10710–10719.
(23) Kuehnbaum, N. L.; Kormendi, A.; Britz-McKibbin, P. *Anal. Chem.* **2013**, *85*, 10664–10669.
(24) Kuehnbaum, N. L.; Gillen, J. B.; Gibala, M. J.; Britz-McKibbin, P. *Sci. Rep.* **2014**, *4*, 6166.
(25) Pacáková, V.; Coufal, P.; Štulík, K. *J. Chromatogr. A* **1999**, *834*, 257–275.
(26) Nori de Macedo, A.; Jiwa, M. I.; Macri, J.; Belostotsky, V.; Hill, S., Britz-McKibbin, P. *Anal. Chem.* **2013**, *85*, 11112–11120.
(27) Shanely, R. A.; Zwetsloot, K. A.; Triplett, N. T.; Meaney, M. P.; Farris, G. E.; Nieman, D. C. *J. Vis. Exp.* **2014**, *10*, 51812.
(28) Zukunft, S.; Prehn, C.; Röhring, C.; Möller, G.; Hrabě de Angelis M.; Adamski, J.; Tokarz, J. *Metabolomics* **2018***, 14*, 18.
(29) Misra, B.B., Upadhayay, R.P., Cox, L.A.; Olivier, M. *Metabolomics* **2018**, *14*, 75.
(30) Lim, M. D.; Dickherber, A.; Compton, C. C. *Anal. Chem.* **2011**, *83*, 8–13.
(31) D'Agostino, L.A.; Lam, K. P.; Lee, R.; Britz-McKibbin *J. Proteome Res.* **2011**, *10*, 592–603.
(32) Mahieu, N. G.; Patti, G. J. *Anal. Chem.* **2017**, *89*, 10397–10406.
(33) Robergs, R. A.; Ghiasvand, F.; Parker, D. *Am. J. Physiol. Regl. Integr. Comp. Physiol* **2004**, *287*, 502–516.
(34) Juel, C.; Halestrap, A. P. *J. Physiol.* **1999**, *517,* 633–642.
(35) Hatazawa, Y.; Qian, K.; Gong, D.-W.; Kamei, Y. *PLoS One* **2018**, *13*, e0190904.
(36) Hiatt, W. R.; Regensteiner, J. G.; Wolfel, E. E.; Ruff, L.; Brass, E. P. *J. Clin. Invest.* **1989**, *84*, 1167–1173.
(37) Kuehnbaum, N. L.; Gillen, J. B.; Kormendi, A.; Lam. K. P.; DiBattista, A.; Gibala, M. J., P. Britz-McKibbin *Electrophoresis* **2015**, *36*, 2226–2236.

(38) Pinckaers, P. J. M; Churchward-Venne, T. A.; Bailey, D.; van Loon, L. J. C. *Sports Med.* **2017**, *47*, 383–391.
(39) Westerhuis, J.A.; van Velzen, E. J. J.; Hoefsloot, H. C. J.; Smilde, A. K. *Metabolomic* **2010**, *6*, 119-128.
(40) Street, D.; Nielsen, J.-J.; Bangsbo, J.; Juel, C. *J. Physiol.* **2005**, *566*, 481–489.
(41) Sostaric, S. M.; Skinner, S. L.; Brown, M. J.; Sangkabutra, T.; Medved, I.; Medley, T.; Selig, S. E.; Fairweather, I.; Rutar, D.; McKenna, M. J. *J. Physiol.* **2006**, *570*, 185–205.
(42) Green, H. J.; Fraser, I. G. *Med. Sci. Sports Exerc.* **1988**, *20*, 55–59.
(43) Hollidge-Horvat, M. G. J.; Parolin, M. L.; Wong, D.; Jones, N. L.; Heigenhauser, G. J. *Am. J. Physiol. Endocrinol. Metab.* **2000**, *278*, 316–329.
(44) Steinbacher, P.; Eckl, P. *Biomolecules* **2015**, *5*, 356–377.
(45) Lee R., West D., Phillips S. M., Britz-McKibbin P. *Anal. Chem.* **2010**, 82, 2959–2968.
(46) Boldyrev, A. A.; Aldini, G.; Derave, W. *Physiol. Rev.* **2013**, *93*, 1803–1845.
(47) Boldyrev, A.; Abe, H. *Cell. Mol. Neurobiol.* **1999**, *19*, 163–175.
(48) Boldyrev, A. A. *Carnosine and Oxidative Stress in Cells and Tissues*; Nova Science Publishers, New York, **2007** (ISBN-13: 978-1600214110).
(49) Azab, S.; Lee, R.; Britz-McKibbin, P., *Anal. Chem.* **2019**, *91*, 2329-2336
(50) Tomas, C.; Newton, J., *Biochem. Soc. Trans.* **2018**, *46*, 547-553

4.8 Supporting Experimental

4.8.1 Blood Sample Preparation

Frozen raw plasma and serum aliquots were thawed slowly on ice, vortexed for 30 s and then ultrafiltrated using a 3 kDa molecular weight cut-off filter (Pall Life Sciences, Port Washington, NY) at 14,000 *g* for 20 min to sediment protein. The plasma ultrafiltrates were vortexed for 10 s and diluted 4-fold with deionized water with 25 μM of 3-chloro-*L*-tyrosine (Cl-Tyr) and 2-napthalenesulfonic acid (NMS) as internal standards for both positive and negative mode ESI-MS, respectively. Since K^+EDTA was used as an anticoagulant during plasma sample collection, serum specimens were used for CE with indirect UV detection to avoid interferences for potassium measurements as well as all other electrolytes with the exception of chloride. Otherwise, all other metabolites (and chloride) were measured using plasma samples. The serum/plasma ultrafiltrates were vortexed and diluted 10-fold with deionized water and 0.2 mM barium (for all cationic electrolytes) or perchlorate (for chloride), which were used as internal standards for electrolyte analysis by CE with indirect UV. All blood samples were analyzed at all three time points (Pre, Post, Rec) for both standardized high-intensity exercise trials (PLA, BIC) for all subjects with the exception of plasma chloride measurements (Pre, Post).

4.8.2 CE with Indirect UV: Method Validation with Quality Control

Although CE with indirect UV detection has been widely applied for inorganic electrolyte analysis, few methods have been extensively validated for clinical studies with rigorous quality control. Several figures of merit were assessed to determine the analytical performance of the assay to measure major electrolytes in complex biological samples. The CE assays showed excellent linearity ($R^2 > 0.997$) over a wide linear dynamic range, which spanned a 20- to 125-fold concentration range relevant to concentration levels typically found in blood and skeletal muscle. Furthermore, the method had adequate sensitivity for detecting major electrolytes

with a detection limit ranging from 20 to 60 μM. Precision was measured by analysis of pooled quality control (QC) samples over three days of analysis for each sample type. The assay was found to have good reproducibility with an average coefficient of variation (CV, n=30) of about 14% for RPAs and 0.8% for RMTs for electrolytes in serum filtrates. The accuracy of the method was evaluated via recovery studies, where standard solutions of electrolytes were spiked into pooled serum at three concentration levels except for sodium, which was spiked at one level due to its to high natural abundance. Overall, the method demonstrated good accuracy with an average bias of about 6%. Similar assay performance was also found in the analysis of muscle tissue extracts (data not shown). Furthermore, the robustness of the method was evaluated by intermittent analysis of three pooled QC serum samples over ten consecutive days of analysis as a way to evaluate long-term system stability as illustrated in control charts.

4.8.3 Tandem Mass Spectrometry for Unknown Identification

High resolution tandem mass spectrometry (MS/MS) was employed for structural elucidation of unknown muscle derived metabolites of biological significance in this study. Targeted MS/MS experiments were performed on an Agilent G7100A CE system (Agilent Technologies Inc., Mississauga, ON, Canada) with a coaxial sheath liquid (Dual AJS) Jetstream electrospray ion source connected to an Agilent 6500 iFunnel QTOF-MS. Pooled muscle tissue extracts (n = 7) were injected hydrodynamically using a conventional single sample injection plug at 50 mbar for 10 s followed by 5 s with BGE. Precursor ions were selected for collisional induced dissociation (CID) experiments at 10, 20 and 40 V. Mirror plots comparing MS/MS spectra of unknown metabolites from muscle tissue extracts were also compared to their respective authentic reference standard whenever available that were generating using the “InterpretMSSpectrum” R Package.

4.8.4 Data Pre-processing and Statistical Analysis

All MSI-CE-MS data were integrated and analyzed using Agilent MassHunter Qualitative Analysis B.07.00 and Microsoft Excel. Prior to statistical analysis, normality testing based on a Shapiro-Wilk test ($p < 0.05$) was performed using SPSS. A QC-based batch correction algorithm was also applied to all muscle extracts and plasma filtrate metabolomic data sets to adjust for long-term signal drift in ESI-MS.[1] Univariate statistical analysis and a repeated measures analysis of variance (ANOVA; two factors: time and treatment) were also performed on SPSS (IBM SPSS Statistics for Windows, Version 20.0. NY, USA). The Mauchly's sphericity test was initially used to determine if the data satisfied the sphericity assumption; in cases where sphericity was violated, a Greenhouse-Geisser correction was applied accordingly. All batch corrected data was pre-processed using *log*-transformation and autoscaling prior to multivariate statistical analysis. Furthermore, in the case of the data obtained from muscle extracts, metabolite responses were normalized to the total dried mass of each muscle specimen (mg). Multivariate statistical analyses, including principal component analysis (PCA), multilevel partial least-squares discriminant analysis (PLS-DA) and pathway analysis were performed using Metaboanalyst 4.0.[2] In evaluating the effects of bicarbonate supplementation on interval exercise, multilevel PLS-DA was employed in order to take advantage of the paired data structure in this double blind, placebo-controlled crossover study.[3] To validate each multilevel PLS-DA model, cross-validation and permutation testing ($n = 1000$) were also performed.

4.8.5 QC Based Batch-Correction: Minimizing Batch Variation and Signal Drift

Due the modest number of samples in this metabolomics study ($n = 49$), two different batches of individual muscle tissue extracts and plasma specimens were analyzed using MSI-CE-MS. An inherent feature of performing large metabolomics studies when using ESI-MS is significant batch variation due to long-term signal

drift, especially when performing analyses intermittently over long periods of time on a multi-user instrumental platform. As a result, a batch-correction using an adjustment algorithm based on empirical Bayesian frameworks[4] was employed in our study that takes advantage of the pooled QC samples included in each serial injection run when using MSI-CE-MS, as well as batch and injection sequence information. After batch correction, there was a significant improvement in overall technical variation ($p < 0.01$) with the median CV decreasing from 15% to 10% for all pooled muscle QCs ($n = 7$). Similarly, batch-corrected metabolomic data analyzed resulted in the median CV decreasing overall from 14% to 10% for all pooled plasma QCs ($n = 7$). Further details on the implementation of an optimal batch-correction algorithm when relying on multiplexed separation data workflows based on MSI-CE-MS are discussed elsewhere.[1]

4.9 Supporting References

(1) DiBattista, A.; McIntosh, N.; Lamoureux, M.; Al-Dirbashi, O. Y.; Chakraborty, P.; Britz-McKibbin, P. *J. Proteome. Res.* **2018**, *18*, 841-854
(2) Chong, J.; Soufan, O.; Li, C.; Caraus, I.; Li, S.; Bourque, G.; Wishart, D. S.; Xia, J. *Nucleic Acids Res.* **2018**, *46*, W486-W494.
(3) Westerhuis, J.A.; van Velzen, E. J. J.; Hoefsloot, H. C. J.; Smilde, A. K. *Metabolomics* **2010**, *6*, 119-128.
(4) Wehrens, R.; Hageman, J. A.; van Eeuwijk, F.; Kooke, R.; Flood, P. J.; Wijnker, E.; Keurentjes, J. J. B.; Lommen, A.; van Eekelen, H. D. L. M.; Hall, R. D.; Mumm, R.; de Vos, R. C. H. *Metabolomics* **2016**, *12*, 88.

Table S4.1: Physical characteristics and performance data of cohort (n =7)

Characteristic	Mean ± SD
Age (yr)	22 ± 1
Height (cm)	181 ± 7
Mass (kg)	77 ± 14
BMI (kg/m^2)	23 ± 3
Body Fat (%)	16 ± 5
VO_2 peak (mL/min/kg)	50 ± 8
Total $NaHCO_3$ (g)	31 ± 5
Total NaCl (g)	21 ± 4

Table S4.2: Summary of the extraction efficiency for 45 representative intra-cellular metabolites obtained after four rounds of modified Bligh Dyer extractions of pooled muscle tissue specimens (2 mg, $n = 3$)

		Percent Recovery (%)[a]			
***m/z*:RMT:mode**	**Metabolite**	**First Extraction**	**Second Extraction**	**Third Extraction**	**Fourth Extraction**
76.0393:0.725:p	Glycine	68±3	23±3	6.1±0.9	2.4±0.8
90.0550:0.775:p	Alanine	68±4	23±3	6.2±0.6	2.6±1.0
106.0499:0.858:p	Serine	64±3	25±2	7.4±0.8	3.6±1.6
114.0662: 0.646:p	Creatinine	65±1	26±1	5.9±0.7	2.7±0.8
116.0706:0.916:p	Proline	68±4	24±3	5.8±0.5	2.4±0.8
118.0863:0.850:p	Valine	70±4	23±3	6.6±0.5	<LOQ
118.0863:0.959:p	Betaine	63±2	27±3	7.4±0.8	3.2±1.0
120.0655:0.897:p	Threonine	68±3	23±2	5.9±0.7	2.9±1.3
123.0567:0.676:p	Unknown	59±9	33±0	9.7±0.6	<LOQ
132.0768:0.758:p	Creatine	66±4	25±4	6.2±0.5	2.4±0.9
132.1019:0.862:p	Isoleucine	62±6	25±2	8.6±1.9	4.6±2.2
132.1019:0.871:p	Leucine	72±5	19±2	5.7±1.0	3.1±1.3
134.0488:0.980:p	Aspartic acid	68±3	23±3	6.6±1.2	2.7±0.9
146.1176:0.704:p	Deoxycarnitine	68±4	24±3	6.2±1.4	2.7±1.0
147.0764:0.919:p	Glutamine	69±4	23±4	5.7±0.5	2.2±0.9
147.1128:0.605:p	Lysine	59±2	26±4	9.3±1.2	5.4±2.3
148.0604:0.931:p	Glutamic acid	70±4	23±4	5.4±0.2	2.0±0.7
150.0583:0.905:p	Methionine	56±5	37±3	6.3±0.3	<LOQ
156.0768:0.651:p	Histidine	66±4	25±3	6.9±0.7	2.9±0.8
160.1331:0.728:p	Unknown	60±4	32±4	5.7±0.8	2.2±0.8
162.1125:0.736:p	Carnitine (C0)	70±4	23±3	5.5±0.8	2.2±0.9
166.0863:0.931:p	Phenylalanine	60±3	28±3	7.4±0.4	4.4±2.3
175.1190:0.626:p	Arginine	56±1	26±3	10.7±1.0	6.8±2.3
176.1030:0.943:p	Citrulline	69±5	24±3	6.0±0.1	2.9±1.7
182.0812:0.960:p	Tyrosine	63±3	25±3	7.6±0.8	4.5±1.8
204.123:0.776:p	Acetylcarnitine (C2)	70±4	22±3	5.5±0.9	2.4±1.1
205.0972:0.931:p	Tryptophan	60±4	27±3	12.2±2.6	<LOQ
227.1139:0.606:p	Carnosine	65±4	26±4	6.9±0.4	2.6±0.5
230.0952:1.403:p	Unknown	67±3	23±2	6.8±0.9	4.2±1.8
248.1489:0.857:p	Hydroxybutrylcarnitine	68±5	27±5	7.9±1.3	<LOQ
269.1242:0.927:p	N-Acetylcarnosine	72±3	23±4	5.5±0.7	<LOQ
307.0833:1.039:p	Oxidized Glutathione (GSSG)	66±2	26±3	7.9±1.4	<LOQ

308.0911:1.118:p	Glutathione (GSH)	70±3	23±3	5.3±0.4	2.1±0.7
89.0244:1.149:n	Lactic acid	64±4	26±2	9.6±5.0	<LOQ
96.9700:1.720:n	Phosphoric acid	54±4	29±2	10.7±0.8	6.2±2.2
110.9851:1.619:n	Unknown	69±5	24±3	6.3±0.8	<LOQ
128.0353:1.016:n	Oxoproline	70±6	30±6	<LOQ	<LOQ
132.0302:0.990:n	Iminodiacetic acid	71±1	26±7	<LOQ	<LOQ
133.0142:1.943:n	Malic acid	68±6	27±4	7.4±0.1	<LOQ
167.0211:0.954:n	Uric acid	69±12	26±7	7.8±1.3	<LOQ
171.0064:1.277:n	Glycerol-3-phosphate	65±1	24±2	7.1±0.4	3.8±1.7
210.0285:1.287:n	Phosphocreatine	66±5	24±4	6.9±0.5	2.5±0.5
259.0224:1.054:n	Glucose-6-phosphate (G6P)	59±3	29±4	8.6±0.8	3.4±0.4
347.0398:1.027:n	IMP	64±10	33±10	<LOQ	<LOQ
505.9885:1.209:n	ATP	42±4	36±5	15.4±3.3	6.6±0.7
662.1019:0.720:n	NAD^+	66±6	25±3	7.4±2.1	2.8±1.5

[a] *Percent recovery expressed as average ± standard deviation (n=3)*

Table S4.3: Analytical figures of merit for quantitative analysis of major electrolytes in biological samples when using CE with indirect UV detection.

Electrolyte	**RMT**	**LOD (μM)**	**LOQ (μM)**	**Linear regression**	**Linearity (R^2)**	**Linear range (mM)**	**Recovery[a] (%)**	**Intermediate Precision[b] (*CV*, *n*=30)**
Ammonium	0.524 ± 0.011	60	200	y = 0.853 (±0.022)x + 0.011 (±0.050)	0.997	0.2-4.0	94 ± 7	--
Potassium	0.607 ± 0.012	60	200	y= 1.12 (±0.017)x - 0.034 (±0.038)	0.999	0.2-4.0	93 ± 4	13%
Sodium	0.782 ± 0.040	60	200	y= 1.62 (±0.014)x - 0.310 (±0.199)	1.000	0.2-25	86 ± 7	11%
Calcium	0.839 ± 0.010	30	100	y= 3.12 (±0.069)x - 0.005 (±0.078)	0.998	0.1-2.0	98 ± 7	17%
Magnesium	0.894 ± 0.009	20	60	y= 3.69 (±0.080)x - 0.028 (±0.054)	0.998	0.06-1.2	98 ± 4	12%

[a] *Spike/recovery studies performed at three concentration levels (except sodium) in pooled serum samples in triplicate for assessment of method accuracy.*
[b] *Intermediate precision assessed by intermittent analysis of three pooled serum filtrate samples over ten consecutive days (n=30) based on peak area integration of each electrolyte relative to the internal standard (Ba^{2+}).*

Table S4.4: Summary of 84 metabolites measured in matching muscle tissue biopsies and plasma/serum specimens collected from a cohort of placebo treated untrained males (n = 7) at baseline prior to interval exercise. Metabolites are classified according to their *m/z*:RMT, most likely molecular formula and mass error with most compounds confirmed by spiking with authentic standards (*level 1* identification). Absolute concentrations of intracellular (*i.e.,* skeletal muscle) and circulatory (*i.e.,* plasma/serum) metabolites were quantified using calibration curves from authentic standards for majority of compounds.

				Muscle	Blood
***m/z*:RMT:mode**	**Molecular Formula**	**Compound ID**	**Mass error (ppm)**	**Baseline Concentration (mmol/kg d.w.)**	**Baseline Concentration (mM)**
76.0393:0.725:p	$C_2H_5NO_2$	Glycine	11.8	5.0 ± 1.8	0.25 ± 0.02
90.0550:0.775:p	$C_3H_7NO_2$	Alanine	4.1	9.6 ± 3.9	0.47 ± 0.09
104.0706:0.828:p	$C_4H_9NO_2$	*N*-*N*-Dimethylglycine[a]	1.9	--	--
104.1075: 0.602: p	$C_5H_{14}NO$	Choline[a]	-2.9	--	0.02 ± 0.01
106.0499:0.858:p	$C_3H_7NO_3$	Serine	0.3	1.69 ± 0.52	0.11 ± 0.02
114.0662: 0.646: p	$C_4H_7N_3O$	Creatinine[a]	-2.0	--	0.06 ± 0.01
116.0706:0.916:p	$C_5H_9NO_2$	Proline	-0.3	3.32±1.61	0.21 ± 0.04
118.0863:0.850:p	$C_5H_{11}NO_2$	Valine[a]	-1.1	--	--
118.0863:0.959:p	$C_5H_{11}NO_2$	Betaine[a]	-1.4	--	--
120.0655:0.897:p	$C_4H_9NO_3$	Threonine	-0.3	2.03 ± 0.82	0.14 ± 0.01
123.0567:0.676:p	$C_6H_6N_2O$	Unknown $[M+H]^+$	6.0	--	--
126.0219:1.760:p	$C_2H_7NO_3S$	Taurine	-0.8	43 ± 11	--
132.0768:0.758:p	$C_4H_9N_3O_2$	Creatine	4.0	96 ± 28	0.02 ± 0.01
132.1019:0.862:p	$C_6H_{13}NO_2$	Isoleucine[a]	-12.1	--	0.06 ± 0.02
132.1019:0.871:p	$C_6H_{13}NO_2$	Leucine[a]	-3.8	--	--
133.0608:0.897:p	$C_4H_8N_2O_3$	Asparagine	3.0	0.98 ± 0.27	0.05 ± 0.01
134.0488:0.980:p	$C_4H_7NO_4$	Aspartic Acid	-37.8	0.54*	--
137.0715:0.659:p	$C_7H_8N_2O$	*N*-Methylnicotinamide[c]	-24.1	--	--
142.0264:1.640:p	$C_2H_8NO_4P$	*O*-Phosphoethanolamine[c]	-4.2	--	--
144.0988:0.974:p	$C_7H_{13}NO_2$	Proline betaine	19.9	0.04 ± 0.02	--
146.1176:0.704:p	$C_7H_{15}NO_2$	Deoxycarnitine	-0.2	0.37 ± 0.13	0.0013 ± 0.0002
146.1652:0.420:p	$C_7H_{19}N_3$	Spermidine[d]	-6.4	--	--
147.0764:0.919:p	$C_5H_{10}N_2O_3$	Glutamine	4.1	57 ± 16	20 ± 3
147.1128:0.605:p	$C_6H_{14}N_2O_2$	Lysine	-2.5	1.42 ± 0.61	0.14 ± 0.06
148.0604:0.931:p	$C_5H_9NO_4$	Glutamic acid	1.8	8.67 ± 3.74	0.04 ± 0.02
150.0583:0.905:p	$C_5H_{11}NO_2S$	Methionine	-1.3	0.30 ± 0.20	0.04 ± 0.01
156.0768:0.651:p	$C_6H_9N_3O_2$	Histidine[a]	-0.2	--	0.08 ± 0.01

160.1331:0.728:p	$C_8H_{17}NO_2$	Unknown $[M+H]^+$	1.0	--	--
161.1285:0.636:p	$C_7H_{16}N_2O_2$	Unknown $[M+H]^+$	5.6	--	--
162.1125:0.736:p	$C_7H_{15}NO_3$	Carnitine (C0)	4.3	14 ± 4	0.01*
164.1278:0.730:p	$C_7H_{17}NO_3$	Unknown $[M+H]^+$	1.2	--	--
166.0863:0.931:p	$C_9H_{11}NO_2$	Phenylalanine	-1.2	0.49 ± 0.30	0.07 ± 0.02
170.0924:0.659:p	$C_7H_{11}N_3O_2$	3-Methylhistidine	1.2	0.21 ± 0.18	0.02 ± 0.01
175.1190:0.626:p	$C_6H_{14}N_4O_2$	Arginine	-1.7	0.68 ± 0.27	0.08 ± 0.02
176.1030:0.943:p	$C_6H_{13}N_3O_3$	Citrulline	-2.1	0.69 ± 0.41	0.04 ± 0.02
182.0812:0.960:p	$C_9H_{11}NO_3$	Tyrosine	-3.7	2.37 ± 1.03	0.70 ± 0.08
189.1346:0.630:p	$C_7H_{16}N_4O_2$	Homoarginine[c]	16.2	--	--
189.1598:0.627:p	$C_9H_{20}N_2O_2$	Trimethyllysine[c]	-12.0	--	--
203.2230:0.418:p	$C_{10}H_{26}N_4$	Spermine[d]	-2.8	--	--
204.123:0.776:p	$C_9H_{17}NO_4$	Acetylcarnitine (C2)	0.2	1.31 ± 0.80	0.0003*
205.0972:0.931:p	$C_{11}H_{12}N_2O_2$	Tryptophan	-3.1	0.19 ± 0.13	1.65 ± 0.19
218.1135:0.864:p	$C_8H_{15}N_3O_4$	Alanyl-glutamine[c]	0.3	--	--
218.1387:0.808:p	$C_{10}H_{19}NO_4$	Propionylcarnitine (C3)	-2.1	0.04 ± 0.02	--
227.1139:0.606:p	$C_9H_{14}N_4O_3$	Carnosine	4.1	59 ± 24	--
230.0952:1.403:p	$C_{17}H_{11}N$	Unknown $[M+H]^+$	1.2	--	--
232.1543:0.825:p	$C_{11}H_{21}NO_4$	Butyrylcarnitine (C4)	1.5	0.011 ± 0.005	--
235.1805:0.844:p	$C_{14}H_{22}N_2O$	Lidocaine[c]	3.8	--	--
241.1295:0.614:p	$C_{10}H_{16}N_4O_3$	Anserine[c]	1.1	0.45 ± 0.29	--
248.1489:0.857:p	$C_{11}H_{21}NO_5$	Hydroxybutyrylcarnitine[c]	-1.5	--	--
258.1097:1.758:p	$C_8H_{20}NO_6P$	Glycerophosphoryl-choline[c]	0.4	--	--
269.1242:0.927:p	$C_{11}H_{16}N_4O_4$	*N*-Acetylcarnosine	1.7	0.27 ± 0.17	--
274.5918:0.920:p	$C_{27}H_{25}N_5O_8$	Unknown $[M+2H]^{2+}$	-0.6	--	--
298.0968:0.888:p	$C_{11}H_{15}N_5O_3S$	5'-Methylthioadenosine[c]	-2.0	--	--
307.0833:1.039:p	$C_{20}H_{32}N_6O_{12}S_2$	Oxidized glutathione (GSSG)	-2.3	0.79 ± 0.49	--
308.0911:1.118:p	$C_{10}H_{17}N_3O_6S$	Reduced glutathione (GSH)	-1.1	64 ± 22	--
380.1113:1.159:p	$C_{18}H_9N_{11}$	Unknown $[M+H]^+$	-1.0	--	--
427.0952:0.999:p	$C_{13}H_{22}N_4O_8S_2$	Cysteineglutathione (GSH-Cys-SS)	-3.5	--	--
89.0244:1.149:n	$C_3H_6O_3$	Lactic acid	-9.2	32 ± 23	2.13 ± 0.94
96.9700:1.720:n	H_3O_4P	Inorganic phosphate	-2.4	8.97 ± 2.03	0.29 ± 0.05
101.0608:0.988:n	$C_5H_{10}O_2$	Isovaleric acid	1.0	0.38 ±-0.01	0.0004*
117.0193:1.928:n	$C_4H_6O_4$	Succinic acid[b]	-5.7	--	0.005 ± 0.002

128.0353:1.016:n	$C_5H_7NO_3$	Pyroglutamic acid	0.4	0.34 ± 0.14	0.014 ± 0.004
132.0302:0.990:n	$C_4H_7NO_4$	Iminodiacetic acid	-1.3	--	--
133.0142:1.943:n	$C_4H_6O_5$	Malic acid	-1.9	0.16 ± 0.12	0.003 ± 0.002
167.0211:0.954:n	$C_5H_4N_4O_3$	Uric acid	-5.6	0.37 ± 0.12	0.23 ± 0.01
171.0064:1.277:n	$C_3H_9O_6P$	Glycerol 3-phosphate	-3.3	0.46*	--
191.0197:2.139:n	$C_6H_8O_7$	Citric acid	2.8	--	0.03 ± 0.02
210.0285:1.287:n	$C_4H_{10}N_3O_5P$	Phosphocreatine	-2.6	53 ± 11	--
218.1034:0.827:n	$C_9H_{17}NO_5$	Pantothenic acid	0.7	0.14 ± 0.04	--
259.0224:1.054:n	$C_6H_{13}O_9P$	Glucose-6-phosphate (G6P)[a]	-0.1	4.36 ± 2.66	--
328.0452:0.857:n	$C_{10}H_{12}N_5O_6P$	cAMP	-35.1	0.08 ± 0.03	--
338.9888:1.499:n	$C_6H_{14}O_{12}P_2$	Fructose-1,6-bisphosphate (F1,6P)	-0.8	0.57 ± 0.25	--
346.0558:0.987:n	$C_{10}H_{14}N_5O_7P$	AMP[a]	5.2	--	--
347.0398:1.027:n	$C_{10}H_{13}N_4O_8P$	IMP	-1.5	0.36 ± 0.46	--
481.9772:1.252:n	$C_9H_{16}N_3O_{14}P_3$	CTP	8.2	0.32 ± 0.19	--
482.9613:1.271:n	$C_9H_{15}N_2O_{15}P_3$	UTP	5.4	0.48 ± 0.21	--
505.9885:1.209:n	$C_{10}H_{16}N_5O_{13}P_3$	ATP	4.8	17 ± 5	--
521.9834:1.174:n	$C_{10}H_{16}N_5O_{14}P_3$	GTP	-0.03	0.58 ± 0.33	--
662.1019:0.720:n	$C_{21}H_{28}N_7O_{14}P_2$	NAD^+	9.5	1.08 ± 0.31	--
K^+:CE-iUV	--	Potassium	--	316 ± 59	4.4 ± 0.4
Na^+: CE-iUV	--	Sodium	--	309 ± 109	151 ± 7
Ca^{2+}: CE-iUV	--	Calcium	--	2.2 ± 0.80	1.3 ± 0.1
Mg^{2+}: CE-iUV	--	Magnesium	--	44 ± 11	0.6 ± 0.05
Cl^-: CE-iUV	--	Chloride	--	206 ± 61	126 ± 73

** Standard deviation < LOQ*

[a] Not included in final matrix due to poor isomeric/isobaric resolution

[b] Multiply charged organic acids with poor peak shapes due to poor ionization efficiency

[c] Putatively annotated compounds

[d] Compounds obtained in the salt front and prone to ion suppression

Table S4.5: Dynamic (temporal) metabolic signatures of strenuous interval exercise within skeletal muscle upon ingestion of placebo for a cohort of untrained male participants (n = 7).

***m/z*:RMT:mode**	**Metabolite**	***p*-value[a]**	**Pairwise comparison**	**Effect size[b]**	**FC[c]**
90.0550: 0.775:p	Alanine	4.0E-04	Pre-Post; Post-Rec	0.730	1.43, 0.51
89.0244:1.149:n	Lactic Acid	0.001	Pre-Post; Post-Rec	0.808	3.56, 0.22
148.0604: 0.931:p	Glutamic Acid	0.001	Pre-Post; Post-Rec	0.717	0.52, 2.42
133.0142:1.943:n	Malic Acid	0.009	Pre-Post; Post-Rec	0.685	2.14, 0.37
521.9834:1.174:n	GTP	0.003	Pre-Rec; Post-Rec	0.615	1.28, 1.61
166.0863:0.931:p	Phenylalanine	0.006	Post-Rec	0.575	0.68
147.1128: 0.605:p	Lysine	0.011	Pre-Rec; Post-Rec	0.530	0.67, 0.69
205.0972:0.931:p	Tryptophan	0.011	Post-Rec	0.528	0.61
167.0211:0.954:n	Uric Acid	0.011	Pre-Post	0.525	1.76
171.0064:1.277:n	Glycerol-3-phosphate	0.012	Pre-Post	0.521	1.96
150.0583: 0.905:p	Methionine	0.025	Post-Rec	0.460	0.70
204.1230:0.776:p	Acetylcarnitine	0.030	Pre-Post; Pre-Rec; Post-Rec	0.443	6.56, 4.88, 0.74
182.0812:0.960:p	Tyrosine	0.049	Post-Rec	0.394	0.70

** mode: p = positive mode, n = negative mode. [a] p-values obtained using one factor (time) repeated measures ANOVA using $p < 0.05$ as cut-off threshold. [b] Effect size measured using Partial Eta Square. [c] Average fold-change (FC) based on the measured ion response ratio indicated by pairwise comparison. Pairwise comparison indicates which of the time points contribute significantly to overall p-value obtained from ANOVA.*

Table S4.6: Dynamic (temporal) metabolic signatures of strenuous interval exercise in blood (plasma or serum) upon ingestion of placebo for a cohort of untrained male participants (n = 7).

***m/z*:RMT:mode**	**Metabolite**	***p*-value[a]**	**Effect size[b]**	**Pairwise comparison**	**FC[c]**
89.0244:1.149:n	Lactic acid	4.5E-05	0.882	Pre-Post; Pre-Rec; Post-Rec	7.13; 0.63; 11.32
116.0706:0.916:p	Proline	4.9E-05	0.809	Pre-Rec; Post-Rec	0.61; 1.65
182.0812:0.960:p	Tyrosine	7.2E-05	0.796	Pre-Rec; Post-Rec	0.63; 1.49
90.0550:0.775:p	Alanine	8.7E-05	0.790	Pre-Post; Pre-Rec; Post- Rec	1.37; 0.58; 2.36
150.0583:0.905:p	Methionine	1.4E-04	0.772	Pre-Rec; Post-Rec	0.59; 1.64
96.9700:1.720:n	Phosphoric acid	4.3E-04	0.725	Pre-Post; Post-Rec	1.34; 1.33
103.0401:1.024:n	3-Hydroxybutyric acid	8.0E-04	0.719	Pre-Post; Pre-Rec; Post- Rec	1.53; 5.07, 0.30
120.0655:0.897:p	Threonine	0.0010	0.709	Pre-Rec; Post-Rec	0.68; 1.47
204.1230:0.776:p	Acetylcarnitine	0.0010	0.691	Pre-Post; Pre-Rec	2.48; 2.21
133.0608:0.897:p	Asparagine	0.0010	0.684	Pre-Rec; Post-Rec	0.67; 1.43
166.0863:0.931:p	Phenylalanine	0.0010	0.678	Pre-Rec; Post-Rec	0.77; 1.37
103.0401:1.050:n	2-Hydroxybutyric acid	0.013	0.653	Pre-Rec; Post-Rec	2.02; 0.52
117.0193:1.928:n	Succinic acid	0.018	0.618	Pre-Post; Pre-Rec; Post- Rec	2.61; 0.74, 3.52
132.0656:1.022:p	Hydroxyproline	0.004	0.606	Post-Rec	1.37
175.1190:0.626:p	Arginine	0.020	0.605	Pre-Rec; Post-Rec	0.63; 1.60
276.1185:1.102:p	Unknown	0.004	0.603	Pre-Post; Post-Rec	0.73; 0.68
148.0604:0.931:p	Glutamic acid	0.005	0.580	Pre-Post	1.63
76.0393:0.725:p	Glycine	0.007	0.560	Post-Rec; Pre-Rec	1.42; 0.82
176.1030:0.943:p	Citrulline	0.010	0.537	Post-Rec	1.29
CE-iUV	Potassium	0.011	0.528	Pre-Post	1.18
205.0972:0.931:p	Tryptophan	0.036	0.425	Pre-Post; Pre-Rec	1.27; 1.26
106.0499:0.858:p	Serine	0.049	0.394	Post-Rec	1.25

** mode: p = positive mode, n = negative mode. [a] p-values obtained using one factor (time) repeated measures ANOVA using $p < 0.05$ as cut-off threshold. [b] Effect size measured using Partial Eta Square. [c] Average fold-change (FC) based on the measured ion response ratio indicated by pairwise comparison. Pairwise comparison indicates which of the time points contributes significantly to overall p-value obtained from ANOVA.*

Table S4.7: Muscle tissue metabolites significantly different after strenuous interval exercise with oral bicarbonate pretreatment (*n*=7) as compared to placebo.

***m/z*:RMT:mode**	**Metabolite**	**Main effect**	***p*-value[a]**	**Effect size[b]**	**FC[c]**
241.1295:0.614:p	Anserine	Treatment	0.026	0.588	0.91
167.0211:0.954:n	Uric Acid	Treatment	0.028	0.579	0.74
CE-iUV	Potassium	Treatment x Time	0.038	0.540	1.38
427.0952:0.999:p	GSH-Cys-SS	Treatment	0.039	0.534	0.77

**mode: p = positive mode, n = negative mode [a] p-values obtained using two factor (time and treatment) repeated measures ANOVA using p < 0.05 as cutoff threshold. [b] Effect size measured using Partial Eta Square. [c] Average fold-change (FC) based on the measured ion response ratio of post-exercise levels for bicarbonate relative to placebo treatment arms.*

Table S4.8: Blood metabolites significantly different after strenuous interval exercise with oral bicarbonate pretreatment (*n*=7) as compared to placebo.

***m/z*:RMT:mode**	**Metabolite**	**Main effect**	***p*-value[a]**	**Effect size[b]**	**FC[c]**
CE-iUV	Chloride	Treatment x Time	0.008	0.711	0.76
129.0557:1.025:n	Ketoleucine	Treatment	0.010	0.694	1.50
160.1331:0.728:p	Unknown, $C_8H_{17}NO_2$	Treatment x Time	0.023	0.606	0.81
89.0244:1.149:n	Lactic acid	Treatment	0.030	0.570	1.17
87.0088:1.359:n	Pyruvic acid	Treatment	0.036	0.547	1.21
191.0197:2.139:n	Citric acid	Treatment	0.038	0.541	1.29
115.0456:1.094:n	α-Ketoisovaleric acid	Treatment	0.041	0.528	1.43
CE-iUV	Potassium	Treatment x Time	0.047	0.510	0.87

**mode: p = positive mode, n = negative mode [a] p-values obtained using two factor (time and treatment) repeated measures ANOVA using p < 0.05 as cutoff threshold. [b] Effect size measured using Partial Eta Square. [c] Average fold-change (FC) based on the measured ion response ratio of post-exercise levels for bicarbonate relative to placebo treatment arms.*

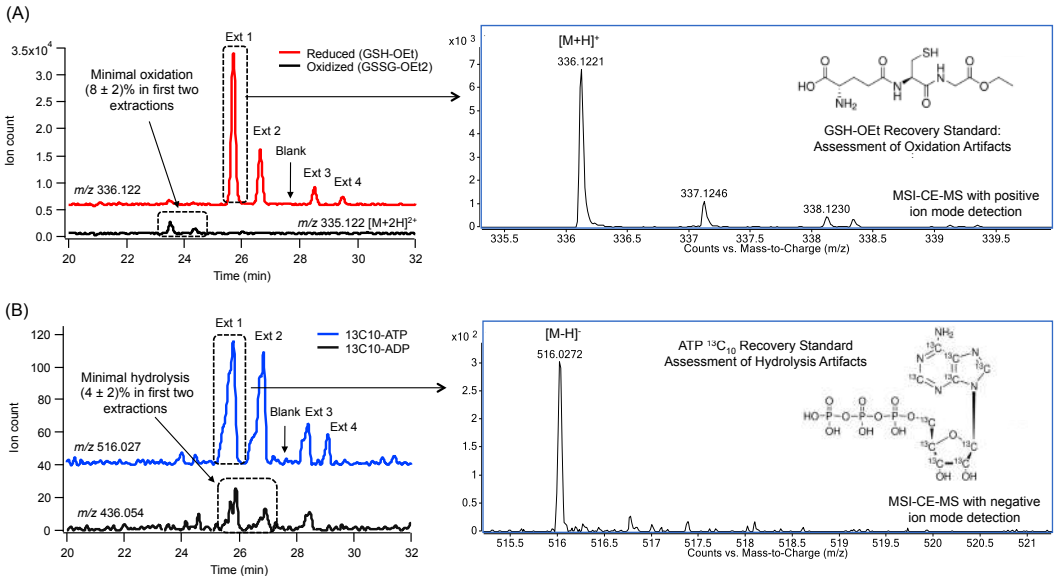

Figure S4.1: Recovery standards (25 µM) added to muscle tissue samples to evaluate extent of oxidation and hydrolysis artifacts incurred during extraction using four serial aliquots of fresh solvent, which were analyzed separately within the same run together with a blank extract when using MSI-CE-MS (A) A synthetic reduced glutathione analog (GSH-OEt) confirmed low residual levels of inadvertent oxidation when pooling together two serial extracts together while processing samples under ice at 4 °C with less than 8% oxidized disulphide detected. (B) Similarly, a stable-isotope labelled ATP highlighted low residual levels of hydrolysis when pooling together two serial extracts together with less than 4% of corresponding isotope-labelled ADP detected. Ionization efficiency was assumed similar for both precursor recovery standards and their by-products when calculating measured ratios since chemical standards were lacking in the latter case.

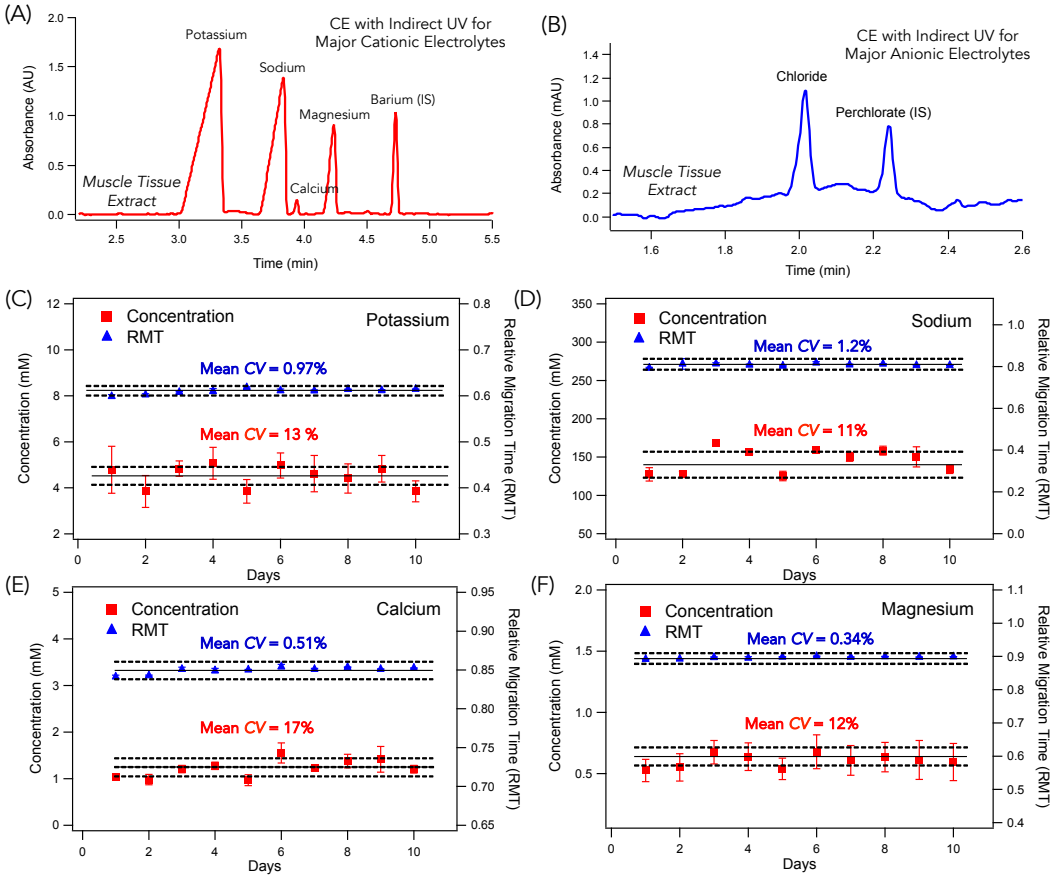

Figure S4.2: (A) Representative electropherogram for determination major electrolytes derived from a muscle tissue extract when using CE with indirect UV detection, where barium is used as an internal standard. (B) Representative electropherogram for determination of chloride derived from a muscle tissue extract when using CE with indirect UV detection, where perchlorate is used as an internal standard. Control charts for major electrolytes based on intermittent analysis of pooled blood samples as quality controls, including (C) potassium, (D) sodium, (E) calcium and (F) magnesium. Serum (potassium, sodium, magnesium, calcium) or plasma (chloride) samples were analyzed intermittently three times per day between batches of runs over 10 consecutive days (n = 30) in order to demonstrate method robustness with a mean CV of 0.76% and 14% in terms of relative migration time (RMT) and serum electrolyte concentrations from intermittent analysis of pooled serum filtrates as QC samples, respectively.

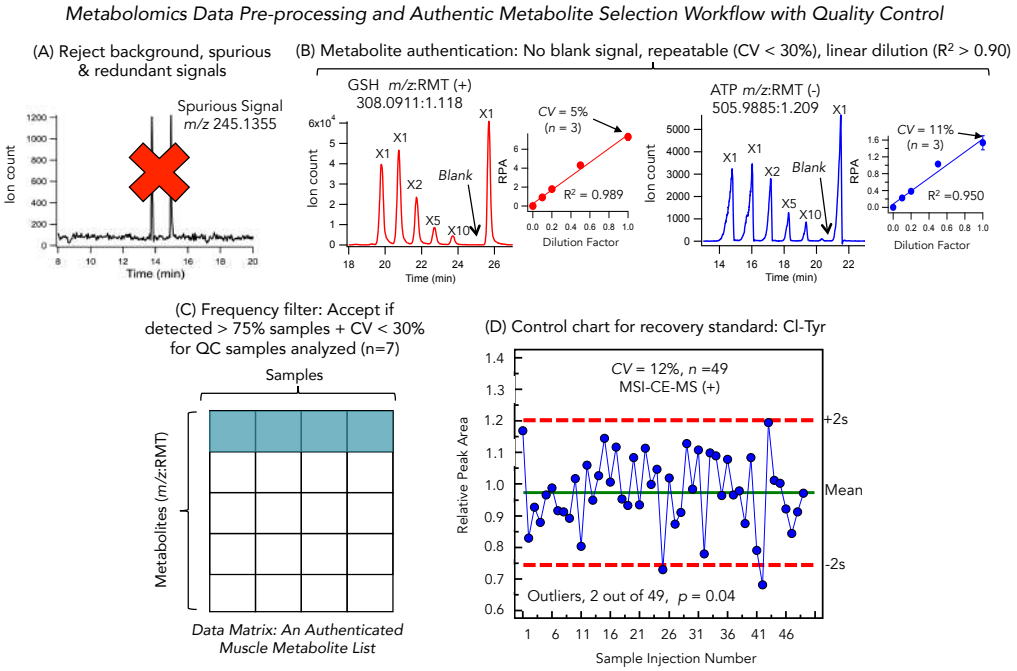

Figure S4.3: An overview of the data workflow for selection of authentic, reproducible yet representative metabolites from a pooled muscle tissue extract when using MSI-CE-MS. Untargeted metabolomics was first performed using a dilution trend filter that offers a rigorous screening approach to reject spurious signals, irreproducible peaks and/or background ions as required for authenticating muscle derived metabolites when using ESI-MS. (A) An extracted ion electropherogram (EIE) of a typical spurious signal (m/z 245.1355, ESI+) that does not fulfill selection criteria as an authentic metabolite from muscle extracts and is thus confidently rejected. In contrast, EIEs are also shown for reduced glutathione, GSH (m/z 308.0911, ESI+) and ATP (m/z 505.9885, ESI-), which both display characteristic temporal signal patterns, including a precisely measured signal at a given dilution (CV < 30%, *n*=3), the lack of a signal measured in the blank extract, and good linearity in signal based on expected dilution trend (R^2 > 0.90). This conservative approach to metabolite selection greatly reduces false discoveries and data overfitting when performing nontargeted metabolite profiling prior to multivariate statistical analysis since metabolites reliably detected in the majority (> 75%) of samples in the cohort are included in the final data matrix while also having CV < 30% (*n*=7) for pooled samples analyzed as quality control (QC). In this case, QC is ensured based on analysis of a randomly positioned pooled muscle tissue extract within every run when using MSI-CE-MS (**Figure 4.2**) that can also allow for robust batch correction due to long-term signal drift in ESI-MS. (D) A control chart also confirms good technical precision (CV = 12%) with few outliers when analyzing a batch of 49 muscle tissue extracts using MSI-CE-MS based on an recovery/internal standard (Cl-Tyr) that is added into all muscle tissue extracts.

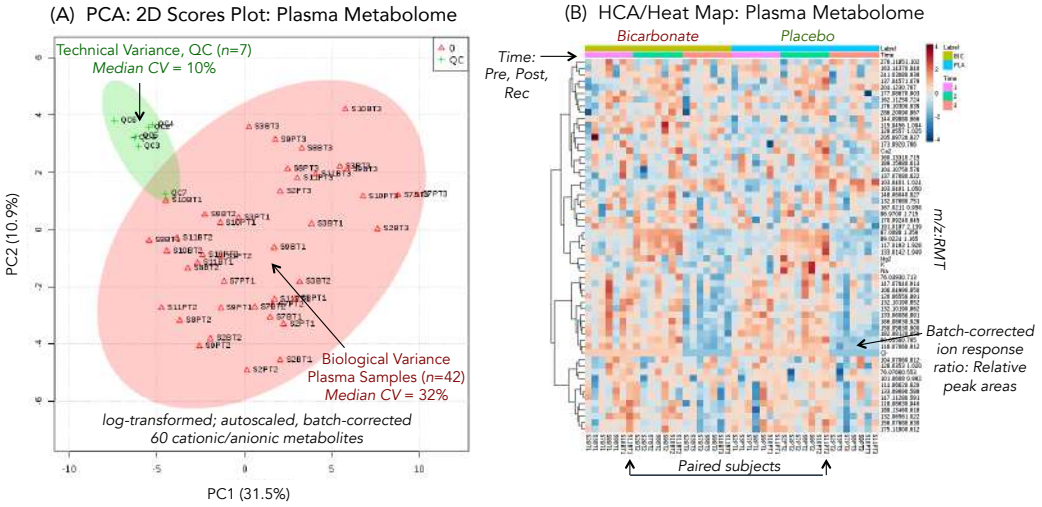

Figure S4.4: An overview of data obtained during the analysis of plasma filtrate samples collected from each subject (n=7) at three time points (Pre, Post, Rec) during strenuous interval exercise upon ingestion of both placebo and bicarbonate (n=42) and the pooled QC analyzed in each run (n=7) when using MSI-CE-MS. A total of 60 cationic/anionic metabolites were consistently measured (CV < 30%) in the majority (> 75%) of plasma samples analyzed in this work as annotated based on their characteristic accurate mass:relative migration time (m/z:RMT) in positive (p) or negative (n) ion mode. Unsupervised multivariate data analysis used for reviewing data structure while revealing overall trends or outliers, including (A) a principal component analysis (PCA) 2D scores plot that compares the magnitude of the biological variance of metabolites in plasma (median CV = 35%) relative to the technical variance of the method (median CV = 10%) and (B) a 3D heatmap with hierarchical cluster analysis (HCA) reflecting a double blinded placebo-controlled cross-over study design based on two variables, namely exercise time and treatment intervention. In all cases, metabolite responses were normalized to an internal standard (Cl-Tyr or NMS), *log*-transformed, autoscaled and batch-corrected. Major electrolytes in matching plasma or serum samples (Na^+, K^+, Ca^{2+}, Mg^{2+} and Cl^-) were also measured using two CE with indirect UV detection methods due their physiological relevance in muscle contractile function.

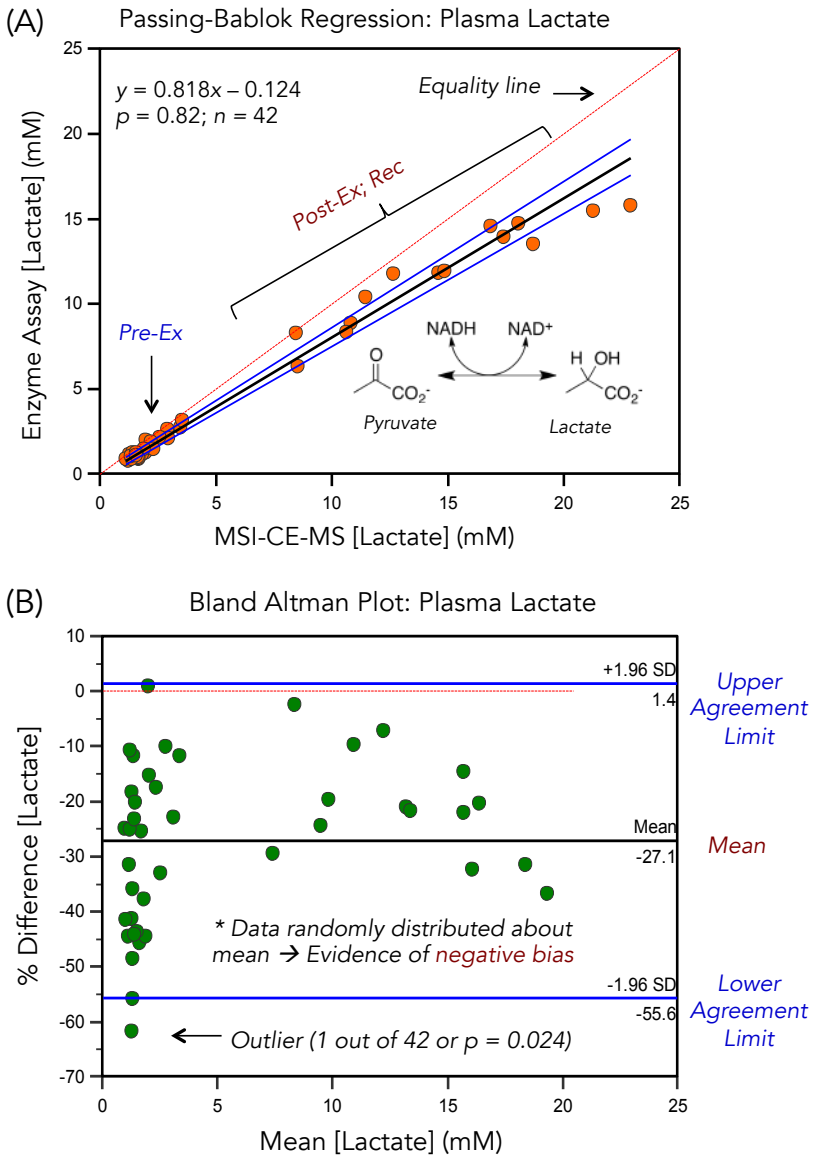

Figure S4.5: (A) A Passing Bablok regression scatter plot and (B) Bland Altman % difference plot used to evaluate the method performance between a commercial blood lactate analyzer (a colorimetric enzyme kinetic assay) as reported in Percival *et al.* (*J. Appl. Physiol.* **2015**, *119*, 1303) as compared to MSI-CE-MS for absolute quantification of plasma lactate concentrations. Overall, there was good mutual agreement between both analytical methods with few outliers beyond agreement limits with a modest extent of negative bias in reported lactate concentrations by MSI-CE-MS as compared to the lactate analyzer as reflected by a slope of 0.82 and average percent difference of 27%. The overall technical precision for plasma lactate based on repeated measurements of QC samples by MSI-CE-MS was about 14%. Plasma lactate was measured independently by MSI-CE-MS on frozen specimens after 2 years of storage at -80 °C as compared to blood lactate analyzer measurements.

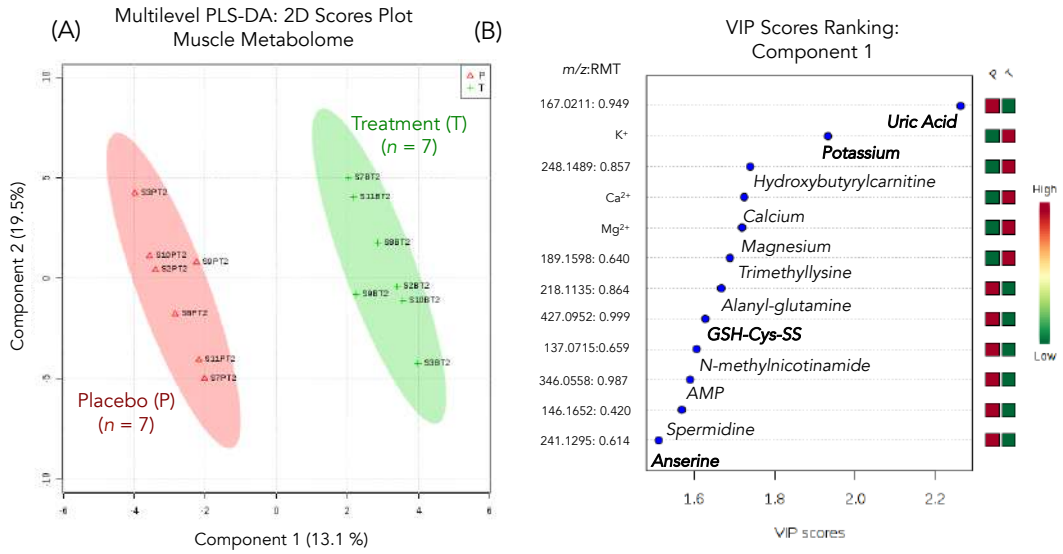

Figure S4.6: (A) Multilevel PLS-DA 2D scores plots of muscle tissue extracts illustrating differences in the metabolic phenotype of a cohort of untrained male subjects upon oral ingestion of placebo as compared to bicarbonate treatment immediately post-exercise (Post) that takes advantage of a paired/cross-over study design. Metabolite ion responses were normalized to internal standards, dry weight (mg), autoscaled and batch-corrected when using a perturbation test (R^2 = 0.982, Q^2 = 0.853, p = 0.04, n = 1000). (B) Variance in Projection (VIP) plot along component 1 for ranking the most significant intracellular muscle tissue metabolites (VIP > 1.5) discriminating between the placebo and bicarbonate treatments post-exercise.

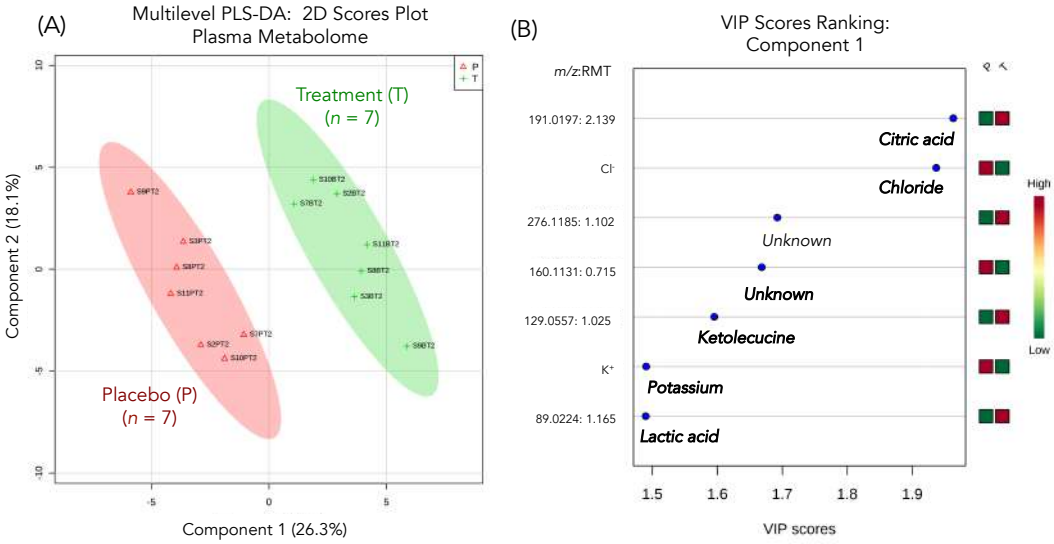

Figure S4.7: (A) Multilevel PLS-DA 2D scores plots of plasma filtrates illustrating differences in the metabolic phenotype of a cohort of untrained male subjects upon oral ingestion of placebo as compared to bicarbonate treatment immediately post-exercise (Post) that takes advantage of a paired/cross-over study design. Metabolite ion responses were normalized to internal standards, dry weight (mg), autoscaled and batch-corrected when using a perturbation test ($R^2 = 0.965$, $Q^2 = 0.863$, $p = 0.032$, $n = 1000$). (B) Variance in Projection (VIP) plot along component 1 for ranking the most significant circulating plasma metabolites (VIP > 1.5) discriminating between the placebo and bicarbonate treatments post-exercise.

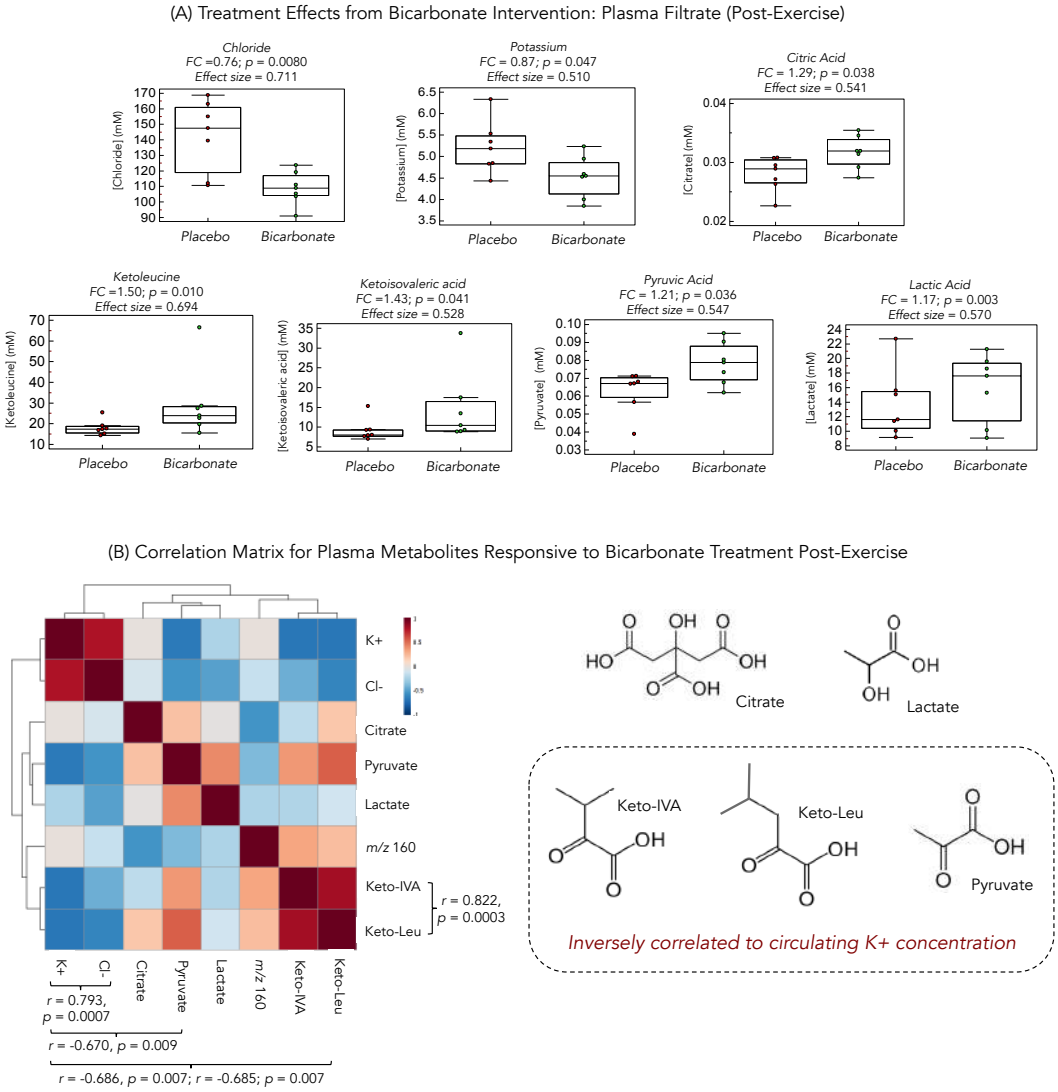

Figure S4.8: Correlation matrix/heat map (Pearson correlation; *log*-transformed data) for the top eight ranked plasma/serum metabolites significantly (**Table S4.7**) modulated by oral bicarbonate pretreatment immediately post-exercise as compared to placebo. As expected, strong positive correlations were found between circulating deaminated α-keto-acids from branched-chain amino acids, Keto-IVA, Keto-Leu ($r = 0.822$; $p = 0.0003$) and major electrolytes, potassium and chloride ($r = 0.793$; $p = 0.0007$). Additionally, circulating potassium concentrations were inversely correlated to three α-keto-acids, including Keto-IVA, Keto-Leu and pyruvate ($r > 0.670$; $p < 0.01$). The mild hypokalemic effect of bicarbonate intervention thus also impacts central energy metabolism and amino acid catabolism within contracting muscle tissue.

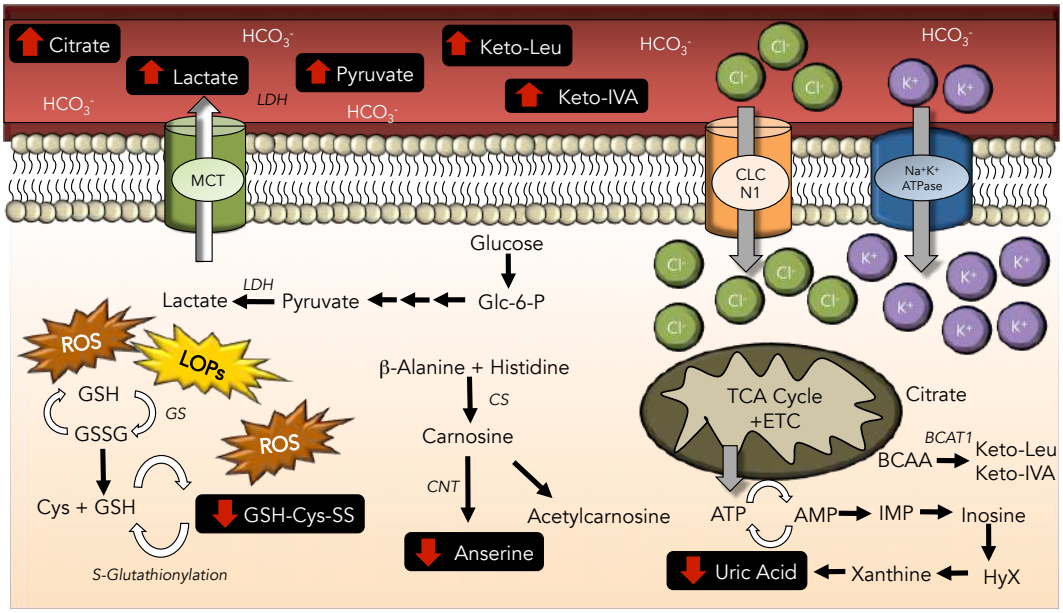

Figure S4.9: Overall summary of the pleiotropic effects of oral bicarbonate pretreatment on skeletal muscle and circulatory (systemic) metabolism following strenuous interval exercise on untrained participants. Metabolic alkalosis is attenuated by high dose bicarbonate ingestion resulting in reduced amounts of exercise-induced oxidative stress products (ROS, LOPs), which is reflected by lower concentrations of oxidized (mixed) disulfides (GSH-Cys-SS), antioxidants (anserine) and purine degradation products (uric acid) within skeletal muscle as compared to placebo immediately post-exercise. A mild hypokalemic effect was also observed, where bicarbonate intervention attenuated extracellular potassium leakage into blood, with a corresponding increase in potassium uptake into the skeletal muscle. Similarly, decreased extracellular chloride was also measured with bicarbonate pretreatment that was correlated positively to the mild hypokalemic effect, which together better preserve contracting muscle function post-exercise. Additionally, extracellular increases in glycolytic (lactate, pyruvate) and Krebs cycle (citric acid) metabolites were also measured in plasma due to oral bicarbonate intake, as well as increases in BCAA breakdown products (ketoisovaleric acid and ketoleucine). BCAA = Branched-chain amino acids; BCAT1 = Branched-chain amino acid transaminase; ClCN1 = Chloride channel protein; CNT = Carnosine-*N*-methyltransferase; CS: Carnosine synthase; GS: Glutathione synthase; Keto-Leu = ketoleucine; Keto-IVA= alpha-ketoisovaleric acid; LOPs: Lipid oxidation products; MCT= Monocarboxylate transporter; LDH = Lactate dehydrogenase; ROS: Reactive oxygen species.

Chapter V:
Placental Metabolomics for Functional Assessment of Sex-specific Adaptations in Fetal Development During Gestation

Michelle Saoi, Katherine M. Kennedy, Wajiha Gohir, Deborah M. Sloboda and Philip Britz-McKibbin

Metabolomics, **2019** (Under Review)

M.S. performed all the experiments including sample preparation, data acquisition using MSI-CE-MS, data processing, interpretation, statistical analysis and wrote the initial draft for publication. K.M.K, W.G. and D.M.S obtained ethics approval for study, designed the animal study, provided placenta specimens, assisted with interpretation, provided valuable feedback and revised the initial manuscript.
P.B.M provided feedback on the manuscript draft.

Chapter V: Placental Metabolomics for Functional Assessment of Sex-specific Adaptations in Fetal Development During Normal Gestation

5.1 Abstract

The placenta is a metabolically active interfacial organ that plays crucial roles in fetal nutrient delivery, gas exchange and waste removal reflecting dynamic maternal and fetal interactions during gestation. There is growing evidence that the sex of the placenta influences fetal responses to external stimuli *in utero*. However, the exact biochemical mechanisms associated with sex-specific metabolic adaptations to pregnancy and its link to placental function and fetal development remain poorly understood. Herein, multisegment injection-capillary electrophoresis-mass spectrometry (MSI-CE-MS) was used as a high throughput metabolomics platform to characterize lyophilized maternal placental tissue (~2 mg dried weight) from mice fed a standardized diet. Over 130 authentic metabolites were consistently measured from placental extracts when using a nontargeted metabolomics workflow with stringent quality control and batch correction. For the first time, our work revealed inherent differences in metabolic phenotypes that exist between male (n=14) and female (n=14) placentae derived from the same control-fed maternal mice. Intracellular metabolites associated with fatty acid oxidation and purine degradation were found to be significantly elevated in females as compared to male placentae ($p < 0.05$, effect size > 0.40), including uric acid, valerylcarnitine, hexanoylcarnitine, and 3-hydroxyhexanoylcarnitine. This work sheds new insights into sex-specific differences in placental mitochondrial function and protective mechanisms against deleterious oxidative stress that may impact fetal growth development and birth outcomes early in life as a result of environmental exposures or sub-optimal nutrition during pregnancy.

5.2 Introduction

The placenta is an interfacial organ that regulates complex maternal-fetal interactions during the course of pregnancy (Gabory et al. 2012). This metabolically active organ plays crucial roles in transferring nutrients and oxygen from maternal circulation to the fetus, as well as facilitating removal of waste products and synthesizing hormones, cytokines and growth factors to promote growth, cellular regulation and immune protection for the fetus (Gabory et al. 2013; Rossant and Cross 2001). Normal placental function is critical to ensure optimal birth outcomes for offspring while preventing placental-induced pregnancy complications, such as intrauterine growth restriction and preeclampsia (King et al. 2017). Since the placenta is often the first organ to develop during embryogenesis in mammals, it has been shown to be the origin of sexual dimorphism, thus it is considered a sexual organ (Gabory et al. 2013; Rossant and Cross 2001). There is growing evidence demonstrating the importance of sex-specific embryonic and fetal adaptations to adverse environments *in utero,* which are largely mediated by placental genes, proteins and steroid pathways (Clifton 2010). For instance, females more readily respond to abrupt changes to intrauterine environment, where developmental adaptations ultimately lead to functional changes in placental growth and development resulting in decreased fetal growth (Clifton 2010). In contrast, male feto-placental units have a more "minimalist approach" where they undergo very few placental changes and continue to grow normally under adverse *in utero* environment; however this places male fetuses at higher risk to exposures that may contribute to deleterious health impacts on later development as a result of environmental toxins and/or sub-optimal maternal diet (Dearden et al. 2018; Lorente-Pozo, 2018; Al-Qaraghouli & Fang, 2017).

Despite these known sex-specific mechanisms in fetal development, few studies have examined the impact of sexual dimorphism on placental growth, development and function in the absence of disease or adverse stimuli. Most reports

have focused primarily on measuring dynamic changes in transcriptome, genome and epigenome expression (Fattuoni et al. 2018; Rosenfeld 2015) with sparse work aimed at characterizing functional changes in the placental metabolome. Metabolomics offers a nontargeted approach for the detection and identification of low molecular weight metabolites (< 1 kDa) comprising a biofluid, cell, tissue or organism. Due to its sensitivity to changes in environmental and physiological stimuli, metabolomics provides a link between biochemical mechanisms and molecular phenotype that is closely associated with clinical outcomes (Patti et al. 2012). To date, adaptive metabolic changes within placentae during pregnancy have been largely analyzed in the context of adverse *in utero* environments, such as pregnancy complications (*e.g.,* preeclampsia, hypoxia, gestational diabetes) and maternal obesity (Dunn et al. 2012; Chi et al. 2014; Korkes et al. 2014; Austdal et al. 2015; Mumme et al. 2016; Fattuoni et al. 2018; Walejko et al. 2018). Herein, we investigated the impact of sex on the placental metabolome in normal uncomplicated murine pregnancies. For the first time, we examine the impact of sexual dimorphism on placental function based on comprehensive metabolic phenotyping of lyophilized placental tissue extracts when using multisegment injection-capillary electrophoresis-mass spectrometry (MSI-CE-MS). This method offers a high throughput platform for biomarker discovery in metabolomics with stringent quality control (QC) optimal for the analysis of mass-limited biospecimens (DiBattista et al. 2019; Macedo et al. 2017; Saoi et al. 2019). We sought to identify metabolite signatures distinguishing female from male placentae that underlie sex-dependent responses to environmental stressors early in life relevant to the developmental origins of health and disease (Dearden et al. 2018).

5.3 Experimental Section

5.3.1 Study Design and Cohort

We employed our validated model of high fat diet–induced obesity during a murine pregnancy (Gohir et al. 2019) to generate placental tissues. All animal experiments were performed at the McMaster Central Animal Facility and approved by the McMaster University Animal Research Ethics Board (Animal Utilization Protocol#12-10-38). Four week old female C57BL/6J mice (*n*=14) were randomized and fed a control diet with a macronutrient composition of 17% kcal fat, 29% kcal protein, and 54% kcal carbohydrate (HT8640 Teklad 22/5 Rodent Diet, Harlan, Indianapolis, IN, USA). The mice were fed the standardized control diet for six weeks prior to a five-day mating period with C57BL/6J control-fed male mice. After mating and confirmation of vaginal plug at embryonic day (E)18.5, pregnant mice were killed by cervical dislocation and whole placentas (~7-8 per dam) were dissected, collected, snap-frozen in liquid nitrogen and stored at -80 °C prior to subsequent lyophilization, liquid extraction and metabolite analysis. Two independent batches of placenta specimens from mice were collected and analyzed at different time periods in this study, including a first batch (*n*=9 female, *n*=9 male) of placental tissue in 2016, and a second batch (*n*=5 female, *n*=5 male) in 2018.

5.3.2 Sample Workup and Placental Extraction Procedure

Murine placental tissues were freeze-dried to form a fine powder to enable accurate weighing using an electronic balance. Lyophilization also enhances extraction efficiency and reproducibility as all ion responses for metabolites were normalized to total dried weight. For the analysis of polar/ionic metabolites, a modified two-step Bligh-Dyer extraction procedure was performed on freeze-dried placental tissue (~ 2 mg dried tissue) as recently developed for human muscle tissue biopsies (Saoi et al. 2019). Briefly, in the first extraction, 64 µL of ice cold methanol:chloroform (1:1) was added to the tissue, followed by 26 µL ice cold deionized water to induce phase separation. After vortexing for 10 min and

centrifugation at 2000 *g* at 4 ºC at 20 min, the upper aqueous layer was aliquoted. A second extraction on the residual placental tissue was performed through the addition of 32 µL of 50% *vol* methanol, followed by vortexing and centrifugation as described above. The second, upper aqueous layer was collected and combined with the first aliquot resulting in ~ 80 µL total volume of placental tissue extract. Prior to MSI-CE-MS analysis, 5 µL of the internal standards (25 µM), 3-chloro-*L*-tyrosine (Cl-Tyr) and 2-napthalenesulfonic acid (NMS), were added to an aliquot of 20 µL of placenta extract. For the analysis of total (hydrolyzed) fatty acids and bile acids in placental tissue (~ 1-2 mg dried tissue), a hydrolysis reaction combined with a modified methyl-*tert*-butyl ether (MTBE) extraction procedure was employed (Chen et al. 2013; Azab et al. 2019). First, hydrolysis of lipids was performed by the addition of 25 µL of butylated hydroxytoluene (BHT) in 0.1% *vol* toluene and 25 µL of 2.5 M of sulfuric acid to the freeze-dried placental tissue. After vortexing for 1 min, the samples were incubated in an oven at 80 °C for 1 h. Then, a MTBE extraction was performed by adding 500 µL of MTBE containing 50 µM of the stable-isotope labeled recovery standard, myristic acid-d_{27} to placental tissue. After vortexing for 30 min at room temperature, 250 µL of de-ionized water was added to induce phase separation, followed by 30 min of centrifugation at 4400 *g* at 4 °C. Then, ~ 250 µL of the upper ether layer was transferred and dried under nitrogen. Prior to MSI-NACE-MS analysis, dried samples were reconstituted in 25 µL of acetonitrile/isopropanol/water (70:20:10) with 10 mM of ammonium acetate and 50 µM of stearic acid-d_{35} as the stable-isotope labeled internal standard used for data normalization.

5.3.3 Nontargeted Metabolomics of Placental Extracts by MSI-CE-MS

All nontargeted metabolite profiling studies using aqueous and nonaqueous buffer systems were performed on an Agilent G7100 CE System (Agilent Technologies Inc., Mississauga, ON, Canada) coupled to a high resolution Agilent 6230 Time-of-Flight Mass Spectrometer (TOF-MS) equipped with a coaxial sheath liquid

(Dual AJS) Jetstream electrospray ion source. Separations for polar metabolites were achieved using uncoated fused-silica capillaries (Polymicro Technologies, AZ, USA) with 50 μm inner diameter and 120 cm total length, while 95 cm total length was used for lipid separations. A background electrolyte (BGE) composition of 1 M formic acid with 13% *vol* acetonitrile (pH 1.80) was used for the separation of cationic metabolites, while a BGE comprised of 50 mM ammonium bicarbonate (pH 8.5) was used for anionic metabolite separation. A nonaqueous BGE was used for separations of lipids based on MSI-nonaqueous capillary electrophoresis (NACE)-MS to fully solubilize ionic yet hydrophobic metabolites (*e.g.,* fatty acids, bile acids) from ether extracts using 35 mM ammonium acetate (pH 9.5) in 70% *vol* acetonitrile, 15% *vol* methanol, 5% *vol* isopropanol and 10% *vol* de-ionized water. A capillary window maker (MicroSolv, Leland, NC, USA) was used to remove 7 mm of polyimide from the terminal ends in order to minimize sample carryover and/or capillary swelling upon contact with organic and/or ammonia based buffers (Yamamoto et al. 2016; DiBattista, et al. 2017). The applied voltage was set to 30 kV at 25 °C to enable zonal separations to occur. Moreover, for lipid separations, the Vcap, nozzle voltage and nebulizer gas were turned off during serial sample injection to minimize electrospray suctioning effects. A seven sample serial injection format was used for nontargeted metabolite profiling with placenta tissue extracts injected hydrodynamically at 50 mbar for 5 s interspaced with seven BGE spacers for 40 s. Therefore, each MSI-CE-MS run consisted of six alternating injections of placental tissue extracts that were paired based on female and male placentae collected from the same dam. A pooled quality control (QC) was also included in each experimental run to assess system stability and performance, which was also used to correct for batch effects associated with long-term signal drift during data acquisition. An Agilent 1260 Infinity series Isocratic Pump equipped with a 100:1 splitter was used to deliver sheath liquid at a rate of 10 μL/min during separations. Sheath liquid compositions consisted of 60% *vol* methanol with 0.1% *vol* formic acid for positive and 50% *vol* methanol for negative

ion modes in MSI-CE-MS, whereas 80% *vol* methanol with 0.5% *vol* ammonium hydroxide was the sheath liquid for acidic lipids under negative ion mode when using MSI-NACE-MS. For real-time mass correction during data acquisition, 0.02% *vol* of purine and hexakis (2,2,3,3-tetrafluoropropoxy)phosphazine (HP-921) were added to the sheath liquid. Details on MSI-CE-MS workflow, ESI-MS conditions, and unknown metabolite identification using high resolution tandem mass spectrometry (MS/MS) are described in the **Supporting Information.**

5.3.4 Data Processing and Statistical Analysis

Data processing was performed using Agilent MassHunter Qualitative Analysis B.06.00 and Microsoft Excel. Prior to statistical analysis, all metabolite responses were normalized to the internal standards and the dry mass of each placenta sample (mg). Also, authenticated metabolites were reliably detected (QC for CV < 30%) in the majority (> 75%) of placental extracts analyzed in this study, whereas missing data inputs for a given metabolite was substituted with one half of its lowest measured response. Normality testing based on a Shapiro-Wilk test ($p < 0.05$) was performed using SPSS (IBM Corp. Released 2011. IBM SPSS Statistics for Windows, Version 20.0. Armonk, NY: IBM Corp.). A QC-based batch correction algorithm "BatchCorrMetabolomics" R package was used to correct for batch effects (Wehrens et al. 2016). Additional data preprocessing including generalized *log* transformation and autoscaling were performed prior to multivariate statistical analysis. Metaboanalyst 4.0 was used for multivariate statistical analysis including Principal Component Analysis (PCA), Partial Least-Square Discriminant Analysis (PLS-DA) and Hierarchal Clustering Analysis (HCA) (Chong et al. 2018). Univariate statistical analysis such as Mann Whitney *U* test was performed using *log* transformed data ($p < 0.05$) on SPSS for data that was not normally distributed. To correct for multiple hypothesis testing, a false discovery rate (FDR) using the Benjamini-Hochberg procedure was performed to obtain *q*-values (*i.e.,* adjusted *p*-values) for each top-ranked placental metabolite.

5.4 Results

5.4.1 Characterization of the Murine Placental Metabolome

Comprehensive metabolite profiling of murine placental extracts was performed using a multiplexed electrophoretic separation platform applicable to the analysis of a diverse range of polar/non-polar ionic metabolites using small amounts of lyophilized tissue specimens. **Figure 5.1** depicts an overview of the data workflow used for authenticating metabolites from unknown molecular features detected from placental tissue extracts; this process takes advantage of a serial injection format comprising of seven samples within a single run in conjunction with temporal signal pattern recognition when using MSI-CE-MS (DiBattista et al. 2017). Firstly, a dilution trend filter was used as a rigorous approach to reject background, spurious and redundant ion signals (*i.e.,* in-source fragments and/or adducts, isotope peaks) generated in ESI-MS (Mahieu & Patti 2017) that contribute to data over-fitting and false discoveries in metabolomics as shown in **Figure 5.1(a)**. Stringent selection criteria were also applied to confirm that metabolites measured from a pooled placental extract have adequate precision ($CV < 30\%$, $n = 3$) and linearity ($R^2 > 0.900$ upon serial dilution of a placental extract) without a signal detected in a blank extract as control. **Figure 5.1(b)** illustrates an extracted ion electropherogram for choline, a highly abundant intracellular metabolite detected from murine placental extracts satisfying all three selection criteria outlined above. Also, high resolution MS spectra were acquired for all metabolites that provides information on their accurate mass, charge state, and isotope pattern for determination of their most likely molecular formulae with low mass error (< 10 ppm). Overall, 135 authentic and reliably measured placental metabolites (79 cations, 27 anions, 29 acidic lipids) were confirmed from over 700 molecular features initially detected. A comprehensive list of placental metabolites are listed in **Table S5.1** and **Table S5.2**, where each metabolite is annotated based on their characteristic accurate mass and relative migration time (*m/z*:RMT) under positive (p) or negative (n) ion mode detection. However, only 122 metabolites were

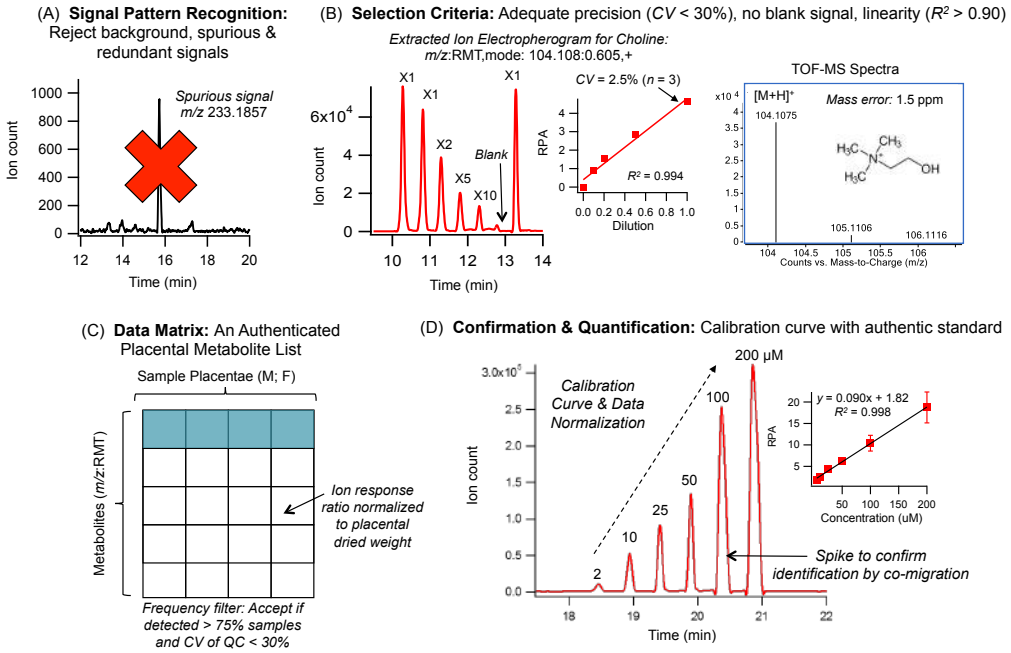

Figure 5.1: Overview of the metabolomics data workflow to authenticate placenta-derived metabolites when using multiplexed separations based on MSI-CE-MS. **a** A dilution trend filter was initially used to filter out background, spurious and redundant signals generated in ESI-MS to avoid false discoveries. A representative extracted ion electropherogram of a spurious peak (*m/z* 233.1857,+) is depicted that does not fulfill selection criteria and thus removed from a list of molecular features detected from a pooled placental extract. **b** Choline (*m/z*:RMT 104.108:0.605,+) is an authentic metabolite from placenta that can be measured with good precision (*CV* = 2.5%, *n*=3), lacks a signal in the blank extract and shows good linearity upon dilution (R^2 >0.90) forming a distinctive temporal signal pattern reflecting serial sample injection. **c** Using these selection criteria, a final data matrix of authentic placental metabolites was curated reliably detected in a majority of samples in the cohort (> 75%) with adequate precision (*CV* < 30%) based on pooled placental extracts used as QCs (*n*=12) in the study. **d** Absolute quantification for a majority of placental metabolites was performed using MSI-CE-MS where a 6-point calibration curve was performed in one experimental run; all signals were normalized to an internal standard and placental dried weight, and metabolite identification was confirmed by co-migration after spiking standard into a pooled sample.

included in the final metabolomics data matrix as these were consistently detected in a majority (> 75%) of individual murine placental samples analyzed in this study (*n*=28). Overall, representative and reliably measured placental metabolites comprised a wide array of compound classes associated with amino acid metabolism, redox homeostasis, central energy metabolism and fatty acid metabolism. Most placental metabolites were confidently identified (*level 1*) based on mass spectral matching and co-migration when spiked with an authentic standard, whereas 12 metabolites (~ 10%) were putatively identified (*level 2*) based

on comparing their MS/MS spectra to public databases. Additionally, 11 unknown features (~ 10%) were detected and annotated based on their most probable molecular formula (*level 3*) in accordance with recommendations from the Metabolomics Standards Initiative (Dunn et al. 2013). Absolute quantification for a majority of placental metabolites was achieved using a six-point calibration curve using authentic standards over a 100-fold linear dynamic range as depicted in **Figure 5.1(c)**, where ion responses were normalized to a non-deuterated internal standard (Cl-Tyr or NMS). Indeed, **Table S5.1** and **Table S5.2** also summarize the average intracellular concentrations for placental metabolites measured in this study that were normalized to total dried weight (μmol/mg).

5.4.2 High throughput Metabolite Profiling of Placenta Tissue

After characterizing the murine placental metabolome using stringent selection criteria to authenticate metabolites, MSI-CE-MS was then used to analyze individual sex-paired placental extracts (*i.e.,* female and male) from dams fed a standardized diet as shown in **Figure 5.2(a)**. In this case, between-sex differences in metabolite expression within placenta were measured by comparing their normalized ion responses by MSI-CE-MS while analyzing a QC for assessing technical precision and long-term signal drift. **Figure 5.2(b)** shows an extracted ion electropherogram for placenta-derived acetylcarnitine (C2), an important mediator of fatty acid metabolism in the mitochondria, which was recently demonstrated to decrease within placental tissues in both sexes when mice were fed a high fat diet during gestation (Gohir et al. 2019). Similarly, representative intracellular anionic metabolites from placental extracts were also measured in this work under negative ion mode conditions, including intracellular polar metabolites, such as uric acid (167.0211:0.960:n) and non-polar lipids, including long-chain polyunsaturated fatty acids, such as docosahexaenoic acid or DHA (327.2330:0.988:n).

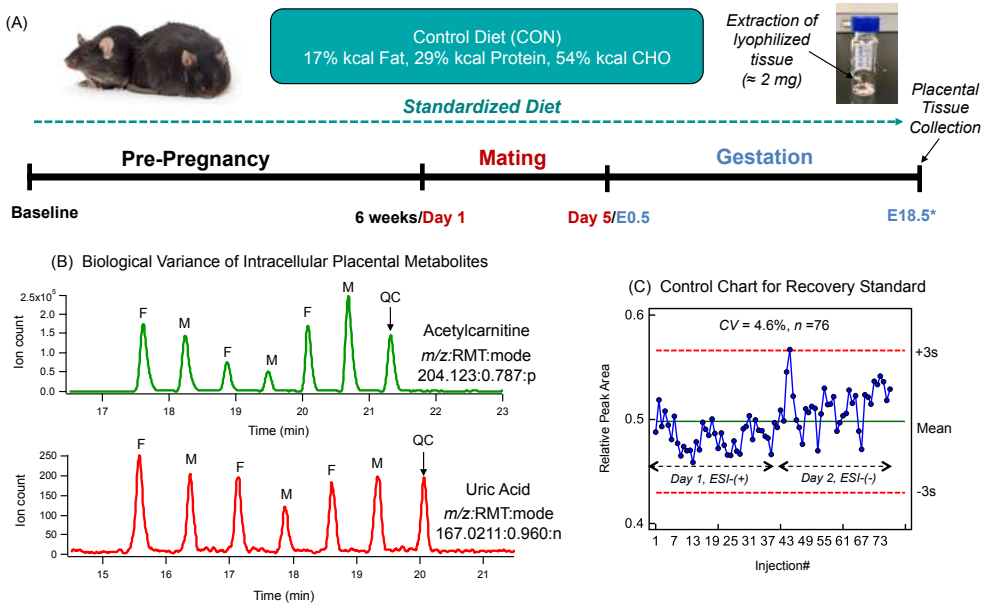

Figure 5.2: **a** Schematic overview of the study design where maternal mice were fed a standardized diet for six weeks prior to mating with a control-fed male with gestation for 17 days (0.5-18.5), and at the embryonic day, (E)18.5 murine placentae tissue were collected. **b** Representative extracted ion electropherograms for acetylcarnitine and uric acid that depict a seven sample plug serial injection configuration used for nontargeted metabolite profiling of placental extracts using MSI-CE-MS. Within one experimental run, three sex-paired placental tissue extracts were simultaneously analyzed from maternal dams fed a standardized diet together with a pooled sample as QC to assess and correct for long-term signal drift in ESI-MS. **c** Control charts for the recovery standard, F-Phe which was added in every tissue extract to confirm good long-term technical precision (*CV* = 4.6%, *n*=76) over two days when using MSI-CE-MS under positive and negative ion mode detection.

After data acquisition, instrumental performance was carefully assessed before proceeding to data processing and statistical analysis. Two analytical batches of placental tissue were collected and analyzed over a period of two years. The first batch was analyzed in 2016 and the second batch was subsequently analyzed in 2018 using the same instrumental platform. Importantly, aliquots of the same QC from first batch of samples was analyzed in every run across both sample batches when using MSI-CE-MS. **Figure 5.2(c)** depicts a control chart for the second analytical batch analyzed, which demonstrates that good technical precision was obtained (*CV*= 4.6%, *n*=76) over two consecutive days of analysis based on the normalized ion responses for a recovery standard (F-Phe) added to all placental extracts. Overall, acceptable technical precision was evident for F-Phe with few

outliers exceeding warning limits (± 3s). However, between-batch effects were nonetheless evident due to long-term system drift (*CV* > 20%) for certain metabolites as highlighted in **Figure S5.1(a)**. To correct for this systematic bias that was compound dependent, a batch-correction algorithm based on an empirical Bayesian framework was applied when relying on QC samples analyzed in each serial injection run by MSI-CE-MS (DiBattista et al. 2019). Indeed, control charts highlight considerable improvements in long-term technical precision following a QC-based batch correction algorithm as shown in **Figure S5.1(b)**. Importantly, **Figure S5.1(c)** also demonstrates that batch adjustment did not impact the underlying data structure as related to the natural biological variance of the murine placental metabolome.

5.4.3 Sex-specific Metabolic Adaptations in the Placenta with Gestation

We next aimed to determine sexual dimorphic differences in murine metabolomes from placental extracts associated with male (*n*=14) and female (*n*=14) fetuses. An overview of the batch-corrected placental metabolome is depicted in **Figure 5.3(a)** when using a 2D PCA scores plot that confirms good technical precision was achieved (median *CV* = 12%, *n*=12) based on repeated analysis of QCs as compared to the larger biological variation between individual murine placentae (median CV = 58%, *n*=28) after normalization to total dried weight. A 2D heat map using hierarchical clustering analysis (HCA) is also shown in **Figure 5.3(b)**, which highlights the relationship among 120 intracellular metabolites measured between sex-paired placentae from the same dam fed a normal diet. Overall metabolic profiles between male and female placentae show modest separation when using supervised multivariate analysis based on a partial least squares-discriminate analysis (PLS-DA) as shown in **Figure S5.2**. Also, a variables of importance in projection (VIP ≥ 2.0) lists six top-ranked metabolites that were largely responsible for sex-dependent differences in murine placental metabolomes, including uric acid, succinic acid, acetylcarnitine and several medium-chain acylcarnitines.

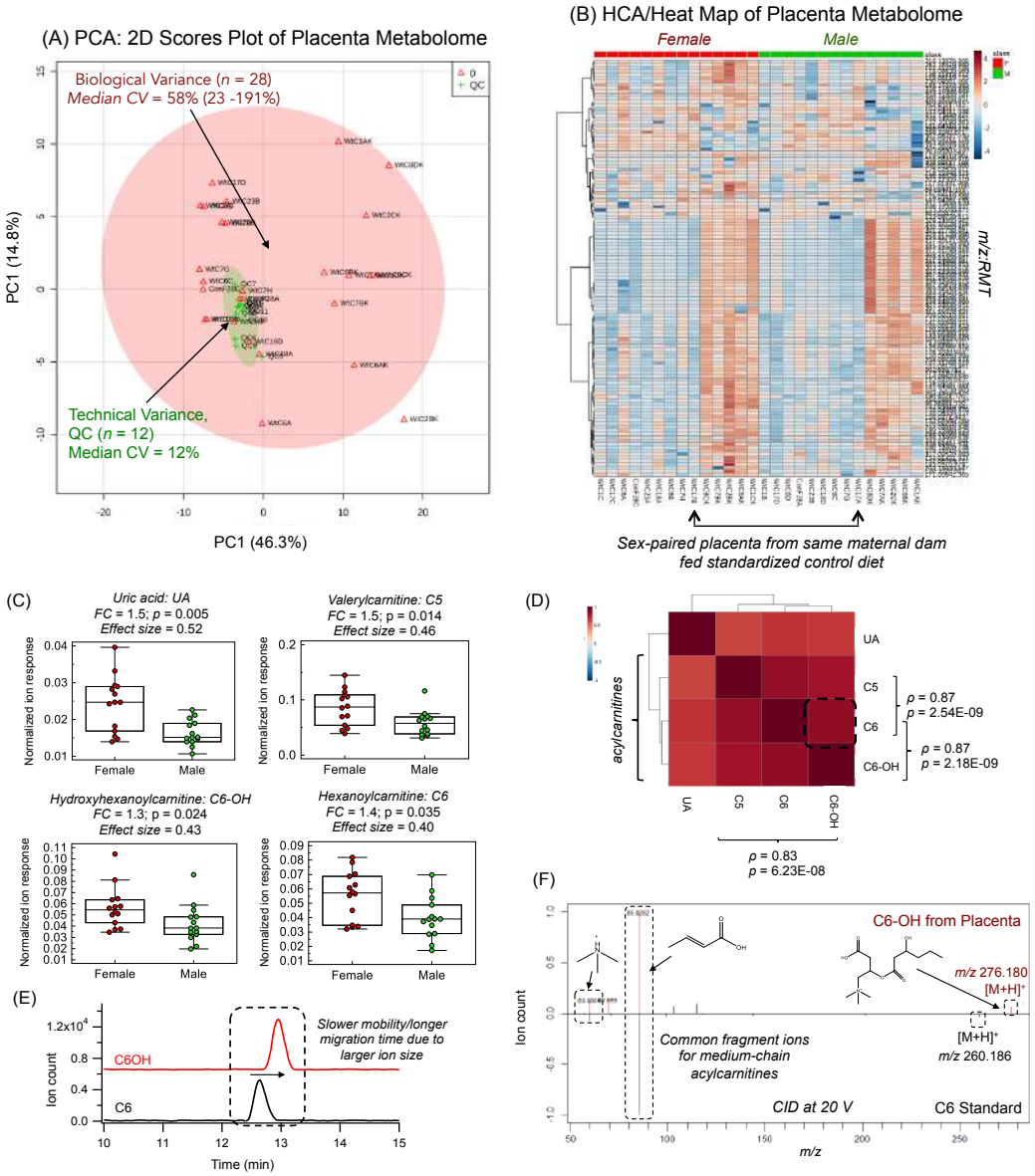

Figure 5.3: An overview of the murine placental metabolome in the form of **a** 2D PCA scores plot and **b** 2D heat map with HCA derived from maternal dams fed a standardized control diet prior to gestation. Metabolite ion responses were normalized to total dried weight (mg), batch-corrected, glog-transformed and autoscaled prior to multivariate statistical analysis. **c** Box-whisker plots of top-ranked placental metabolites showing sex-specific differences ($p < 0.05$) based on Mann-Whitney U test. **d** Spearman rank correlation analysis of the top-ranked placental metabolites demonstrating strong co-linearity among medium-chain acylcarnitines, C5, C6 and C6-OH ($\rho > 0.80$, $p < 1.0E-7$, n=28). **e** Extracted ion electropherograms overlay illustrating a slower positive mobility/longer migration time shift of a putatively unknown ion, C6OH as compared to C6 from a pooled placental tissue extract. **f** Mirror plot comparing MS/MS spectra acquired with a collision energy at 20 V for an unknown ion, tentatively identified as C6-OH based on comparison to a similar chemical standard analog, C6. Both spectra depict two common diagnostic product ions at m/z 85 and m/z 60 consistent with these medium-chain acylcarnitines, whereas their protonated molecular ion [M+H$^+$] are offset by m/z 16 due to hydroxyl substituent.

Table 5.1: Top-ranked placental metabolites showing sex-specific differences in female and male placentae derived from maternal dam fed standardized, control diets prior to and during gestation

m/z:RMT:mode	Compound ID	*p*-value[a]	*q*-value[b]	Effect size[c]	FC[d]
167.0211:0.960:n	Uric acid	0.005	0.37	0.52	1.48
246.1700:0.843:p	Valerylcarnitine	0.014	0.58	0.46	1.48
276.1789:0.889:p	Hydroxyhexanoylcarnitine	0.024	0.74	0.43	1.34
260.1856:0.857:p	Hexanoylcarnitine	0.035	0.86	0.40	1.39

[a] *Two-tailed exact p-values based on Mann-Whitney U test,*
[b] *q-value based on False Discovery Rate (FDR) using Benjimini-Hochberg procedure*
[c] *Effect size r values estimated from z-scores*
[d] *Fold-change (FC) based on the measured ion response ratio of female relative to male placentae*

Univariate statistical analysis was then applied to these top-ranked placental metabolites, which confirmed that four compounds were significantly different between female and male placentae following gestation when using a Mann-Whitney *U* test as summarized in **Table 5.1**. Similarly, **Figure 5.3(c)** depicts box-whisker plots for placental-derived uric acid and three medium-chain acylcarnitines ($p < 0.05$, effect size > 0.40), which however did not satisfy a False Discovery Rate (FDR) adjustment ($q > 0.05$). As expected, there was a strong positive correlation among all three medium-chain acylcarnitines ($\rho > 0.80$, $p < 0.001$, n=28) as depicted in the Spearman correction matrix in **Figure 5.3(d)**. Overall, increases in uric acid ($p = 0.005$), a known purine catabolite, was measured consistently within female placentae as compared to males with similar trends found for medium-chain acylcarnitines, namely valerylcarnitine ($p = 0.014$, C5), hexanoylcarnitine ($p = 0.035$, C6) and an unknown cation ($p = 0.024$, $[M+H]^+$). This unknown ion (276.179:0.899:p) was tentatively identified (*level 2*) as 3-hydroxyhexanoylcarnitine (C6-OH) as shown in **Figure 5.3(e)** based on its characteristic electrophoretic mobility shift as compared to its closest chemical analog commercially available, hexanoylcarnitine (C6) that lacks its substituted hydroxyl group. Also, high resolution MS/MS spectra confirms the detection of two diagnostic product ions (*m/z* 85; *m/z* 60) generated from collision-induced dissociation experiments when comparing C6-OH (from pooled placental extract)

with C6 (as authentic standard) as highlighted in **Figure 5.3(f)**. Furthermore, *in silico* fragmentation using MetFragWeb (Ruttkies et al. 2016) confirmed excellent spectral matching with experimental MS/MS spectra consistent with a hydroxylated medium-chain acylcarnitine.

5.5 Discussion

To date, there have been several metabolomics studies on both human and murine maternal placental tissue samples (Chi et al. 2014; Korkes et al. 2014; Austdal et al. 2015; Mumme et al. 2016; Walejko et al. 2018). In most cases however, multiple analytical platforms, including GC-MS, UPLC-MS and/or NMR were needed to achieve adequate coverage due to the chemical diversity of the placental metabolome, which ranges from polar/hydrophilic amino acids to hydrophobic long-chain fatty acids. To the best of our knowledge, this is the first study examining sex-specific metabolic adaptations on a murine placental model during normal gestation and feeding. MSI-CE-MS offers a high throughput platform for metabolomics with stringent QC that enables unambiguous identification and authentication of metabolites from murine placental extracts. Importantly, multiplexed separations using a QC-based batch correction algorithm (DiBattista et al. 2019; Saoi et al. 2019) allows for robust batch adjustment to metabolomic data since two independent batches of placental extracts were analyzed intermittently over a period of two years. A major finding of this work was that there was a 1.5-fold increase in uric acid within female as compared to male murine placentae. Uric acid is the terminal end-product of the purine (ATP) degradation pathway, catalyzed by xanthine dehydrogenase (XDH) or xanthine oxidase (XO) in the placenta (Bainbridge & Roberts 2008). Previous studies have reported deleterious impacts on placental vascular development, structure and function, most notably in cases of preeclampsia (Martin & Brown 2010). Interestingly, uric acid exhibits antioxidant properties in circulation (Sautin & Johnson 2008) by scavenging oxidizing agents (*i.e.,* reactive oxygen species, nitric oxide, transition metals),

whereas it may also contribute to oxidative stress and placental inflammation at elevated concentrations (hyperuricemia) upon formation of insoluble uric acid crystals resulting in fetal growth restriction and adverse pregnancy outcomes (Brien et al. 2017; Mulla et al. 2013). Indeed, treatment of pregnant mice with the xanthine oxidase inhibitor, allopurinol was shown to reduce placental uric acid levels that prevented placental insufficiency due to dietary fructose with improved fetal birth weights (Asghar et al. 2016). A trend towards a higher GSSG/GSH ratios and mixed oxidized disulfides (*e.g.,* CysGly-CysSS) in female as compared to male placentae may also indicate that female placentae are more susceptible to oxidative stress. Therefore our findings of elevated uric acid levels in female placentae likely indicates a greater need for its antioxidant properties for maintaining redox homeostasis relative to males, which have been previously reported to have higher antioxidant capacities in lean women with greater activity of superoxide dismutase and glutathione peroxidase (Evans & Myatt 2017). However, this same metabolic adaptation within female placentae may become liability to fetal development with excessive uric acid in responses to acute or chronic inflammation during gestation.

Interestingly, female placentae also demonstrated greater mitochondrial activity as reflected by higher levels of three medium-chain acylcarnitines (C5, C6, C6-OH) as compared to males during gestation. Carnitine and acylcarnitines play key roles in mitochondrial fatty acid beta-oxidation to fulfill energetic demands for fetal growth and development, especially in later stages of gestation (Holland et al. 2017). Previous studies in rodent models (Borum 2015; Ruoppolo et al. 2018) have reported sex-specific differences in intra-cellular acylcarnitines among other tissues (*i.e.,* heart, liver, skeletal muscle); however, the role of fatty acid metabolism remains poorly understood within placenta despite its association with pre-eclampsia, fetal fatty acid disorders and maternal liver diseases in pregnancy (Perazzolo et al. 2017; Shekhawat et al. 2003). The observed increase in medium-chain acylcarnitines within female placentae may be indicative of fatty acid beta-

oxidation as a preferred energetic fuel as compared to male placentae during normal gestation in the absence of adverse environmental stimuli. For instance, the placentae of obese women have been reported to have fewer mitochondria with lower acylcarnitine concentrations corresponding to reduced fatty acid oxidation capacity than lean women as an adaptive mechanism to restrict excessive fetal adiposity (Calabuig-Navarro et al. 2017). Similarly, chronic oxidative stress has been shown to impair placental fatty acid oxidation, lipid storage and ATP production leading to pregnancies at risk for fetal growth restriction (Thomas et al. 2018). Indeed, a modest trend towards increases in acetylcarnitine ($p = 0.070$; effect size = 0.34; $FC = 1.31$) and succinic acid ($p = 0.094$; effect size = 0.32; $FC = 1.25$) in our work highlight consistent trends towards an upregulation in fatty acid and oxidative metabolism within female as compared to male placentae. However, there were no sex differences measured in the uptake of all major saturated, monounsaturated and polyunsaturated (non-esterified) fatty acids in female and male placentae for mice fed a standardized diet, including essential omega-3 polyunsaturated fatty acids that are important for fetal nutrition in brain and retinal development (Cetin et al. 2009), such as DHA (**Table S5.2**).

Consequently, sexual dimorphism contributes to subtle differences in placental metabolism that likely reflects adaptive responses elicited by the fetus to maximize fitness for optimal growth while ensuring normal development. Elevated intracellular uric acid measured within female placentae may reflect a counter-balance to compensate for greater oxidative stress from higher mitochondrial activity due to medium-chain acylcarnitine utilization as compared to male placentae. While this work provided novel insights into sex-specific metabolic adaptations during normal gestation, nontargeted metabolite profiling was limited to placental tissue. Future metabolomics studies should also include analysis of maternal blood and fetal cord blood/tissues as complementary biospecimens to better elucidate the interactions between fetus and mother and their impact on

placental function that is modulated by dietary exposures (Gohir et al. 2019). By correlating metabolite changes in the placenta to circulatory measurements in maternal and fetal blood, a more comprehensive understanding of the impact of sexual dimorphism on fetal development may be realized. The integration of other "-omics" approaches with metabolomics can further validate our findings as related to sex-specific metabolic adaptations within placenta during fetal development, including the microbiome. Due to the significant biological variance between murine placentae, a larger sample size is also required to improve study power in future investigations. Future studies will examine the impact of maternal nutrition on long-term health outcomes in offspring, including sex-dependent risks for obesity and metabolic syndrome.

5.6 Conclusions

In summary, this is the first study to apply a robust and high throughput metabolomics platform for comprehensive metabolite profiling of placental extracts using minimal amounts of freeze-dried placental tissue (≈ 1-2 mg). Also, this quantitative approach to metabolic phenotyping used a rigorous data workflow for authenticating and identifying unknown metabolites while implementing stringent quality control measures to minimize false discoveries, including a batch-correction algorithm to correct for long-term signal drift. Over 120 polar/hydrophilic and lipid metabolites were reliably detected over a wide dynamic range in murine placental tissue extracts when normalized to dried weight. Complementary multivariate and univariate statistical methods revealed modest differences in placental metabolic profiles among paired male and female placentae from pregnant mice fed a standardized diet six weeks prior to and during gestation. Intracellular uric acid and three medium-chain acylcarnitines were consistently elevated in female placenta as compared to males, indicative of sex-specific differences in placental fatty acid beta-oxidation activity and antioxidant capacity. Specifically, our work demonstrated that female placentae showed a preference

towards increased lipid oxidation to fulfill energetic requirements that may require higher uric acid as an anti-oxidant to maintain redox homeostasis during gestation. Overall, this work provides deeper insights to the role of sex on metabolic adaptations within placenta that is critical to prevent fetal growth restriction and adverse birth outcomes early in life, as well as maternal health during pregnancy.

5.7 Acknowledgements

P.B.M. acknowledges funding support from the Natural Sciences and Engineering Research Council of Canada and Genome Canada. D.M.S acknowledges funding support by the Canada Research Chairs Program. M.S. also acknowledges support in the form of an Ontario Graduate Scholarship, and K.M.K was supported by a Farncombe Digestive Health Research Institute Student Fellowship.

5.8 References

Al-Qaraghouli. M., & Fang, Y. M. V. (2017) Effect of fetal sex on maternal and obstetric outcomes. *Frontiers of Pediatrics 5,* 144.

Asghar, Z. A., Thompson, A., Chi, M., Cusumano, A., Scheaffer, S., Al-Hammadi, N., et al. (2016). Maternal fructose drives placental uric acid production leading to adverse fetal outcomes. *Scientific Reports*, *6,* e25091.

Austdal, M., Thomsen, L. C. V., Tangerås, L. H., Skei, B., Mathew, S., Bjørge, L., et al. (2015). Metabolic profiles of placenta in preeclampsia using HR-MAS MRS metabolomics. *Placenta*, *36*, 1455–1462.

Azab, S., Ly, R., & Britz-McKibbin, P. (2019). Robust method for high throughput screening of fatty acids by multisegment injection-nonaqueous capillary electrophoresis-mass spectrometry with stringent quality control. *Analytical Chemistry*, *91*, 2329–2336.

Bainbridge, S. A., & Roberts, J. M. (2008). Uric acid as a pathogenic factor in preeclampsia. *Placenta*, *29*, Suppl A: S67-S72.

Borum, P. R. (2015). Variation in tissue carnitine concentrations with age and sex in the rat. *Biochemical Journal*, *176*, 677–681.

Brien, M.-E., Duval, C., Palacios, J., Boufaied, I., Hudon-Thibeault, A.-A., Nadeau-Vallée, M., et al. (2017). Uric acid crystals induce placental inflammation and alter trophoblast function via an IL-1–dependent pathway: Implications for fetal growth restriction. *The Journal of Immunology*, *198*, 443–451.

Calabuig-Navarro, V., Haghiac, M., Minium, J., Glazebrook, P., Ranasinghe, G. C., Hoppel, C., et al. (2017). Effect of maternal obesity on placental lipid

metabolism. *Endocrinology*, *158*, 2543–2555.
Cetin. I., Alvino, G., Cardellicchio, M. (2009) Long chain fatty acids and dietary fats in fetal nutrition. *Journal of Physiology 587,* 3441–3451.
Chen, S., Hoene, M., Li, J., Li, Y., Zhao, X., Häring, H.-U. U., et al. (2013). Simultaneous extraction of metabolome and lipidome with methyl tert-butyl ether from a single small tissue sample for ultra-high performance liquid chromatography/mass spectrometry. *Journal of Chromatography. A*, *1298*, 9–16.
Chi, Y., Pei, L., Chen, G., Song, X., Zhao, A., Chen, T., et al. (2014). Metabonomic profiling of human placentas reveals different metabolic patterns among subtypes of neural tube defects. *Journal of Proteome Research*, *13*, 934-945.
Chong, J., Soufan, O., Li, C. Caraus, I. , Li, S. Bourque, G., Wishart, D. S., Xia, J. (2018) MetaboAnalyst 4.0: Towards more transparent and integrative metabolomics analysis. *Nucleic Acids Res. 46,* W486–W494.
Clifton, V. L. (2010). Review: Sex and the human placenta: Mediating differential strategies of fetal growth and survival. *Placenta*, *31*, S33–S39.
Dearden, L., Bouret, S. G., & Ozanne, S. E. (2018). Sex and gender differences in developmental programming of metabolism. *Molecular Metabolism*, *15*, 8–19.
DiBattista, A., McIntosh, N., Lamoureux, M., Al-Dirbashi, O. Y., Chakraborty, P., & Britz-Mckibbin, P. (2019). Metabolic signatures of cystic fibrosis identified in dried blood spots for newborn screening without carrier identification. *Journal of Proteome Research*, *18*, 841–854.
DiBattista, A., McIntosh, N., Lamoureux, M., Al-Dirbashi, O. Y., Chakraborty, P., & Britz-McKibbin, P. (2017). Temporal signal pattern recognition in mass spectrometry: A method for rapid identification and accurate quantification of biomarkers for inborn errors of metabolism with quality assurance. *Analytical Chemistry*, *89*, 8112–8121.
DiBattista, A., Rampersaud, D., Lee, H., Kim, M., & Britz-McKibbin, P. (2017). High throughput screening method for systematic surveillance of drugs of abuse by multisegment injection-capillary electrophoresis-mass spectrometry. *Analytical Chemistry*. *89*, 11853–11861.
Dunn, W. B., Brown, M., Worton, S. A., Davies, K., Jones, R. L., Kell, D. B., & Heazell, A. E. P. P. (2012). The metabolome of human placental tissue: Investigation of first trimester tissue and changes related to preeclampsia in late pregnancy. *Metabolomics*, *8*, 579–597.
Dunn, W. B., Erban, A., Weber, R. J. M., Creek, D. J., Brown, M., Breitling, R., et al. (2013). Mass appeal: Metabolite identification in mass spectrometry-focused untargeted metabolomics. *Metabolomics*, *9*, 44–66.
Evans, L. S., & Myatt, L. (2017). Sexual dimorphism in the effect of maternal obesity on antioxidant defense mechanisms in the human placenta. *Placenta*, *51*, 64–69.
Fattuoni, C., Mandò, C., Palmas, F., Anelli, G. M., Novielli, C., Parejo Laudicina,

E., et al. (2018). Preliminary metabolomics analysis of placenta in maternal obesity. *Placenta*, *61*, 89-95.

Gabory, A., Ferry, L., Fajardy, I., Jouneau, L., Gothié, J. D., Vigé, A., et al. (2012). Maternal diets trigger sex-specific divergent trajectories of gene expression and epigenetic systems in mouse placenta. *PLoS ONE*, *7*, e47986.

Gabory, A., Roseboom, T. J., Moore, T., Moore, L. G., & Junien, C. (2013). Placental contribution to the origins of sexual dimorphism in health and diseases: Sex chromosomes and epigenetics. *Biology of Sex Differences*, *4*, 5.

Gohir, W., Kennedy, K. M., Wallace, J. G., Saoi, M., Bellissimo, C. J., Britz-McKibbin, P., et al. (2019). High-fat diet intake modulates maternal intestinal adaptations to pregnancy and results in placental hypoxia, as well as altered fetal gut barrier proteins and immune markers. *Journal of Physiology*, *597,* 3029–3051.

Holland, O., Dekker Nitert, M., Gallo, L. A., Vejzovic, M., Fisher, J. J., & Perkins, A. V. (2017). Review: Placental mitochondrial function and structure in gestational disorders. *Placenta*, *54*, 2–9.

King, J. H., Kwan, S. T. C., Yan, J., Klatt, K. C., Jiang, X., Roberson, M. S., & Caudill, M. A. (2017). Maternal choline supplementation alters fetal growth patterns in a mouse model of placental insufficiency. *Nutrients*, *9*, E765.

Korkes, H. A., Sass, N., Moron, A. F., Câmara, N. O. S., Bonetti, T., Cerdeira, A. S., et al. (2014). Lipidomic assessment of plasma and placenta of women with early-onset preeclampsia. *PLoS ONE*, *9*, e110747.

Lorente-Pozo, S., Parra-Llorca, A., Torres ,B., Torres-Cuevas, I., Nuñez-Ramiro, A., Cernada, M., García-Robles, A., Vento M. (2018) Influence of sex on gestational complications, fetal-to-neonatal transition, and postnatal adaptation. *Frontiers of Pediatrics, 6,* 63.

Mahieu, N. G., & Patti, G. J. (2017). Systems-level annotation of a metabolomics data set reduces 25 000 features to fewer than 1000 unique metabolites. *Analytical Chemistry*, *89*, 10397–10406.

Maples, K. R., & Mason, R. P. (1988). Free radical metabolite of uric acid. *Journal of Biological Chemistry*, *263*, 1709–1712.

Martin, A. C., & Brown, M. A. (2010). Could uric acid have a pathogenic role in pre-eclampsia? *Nature Reviews Nephrology*, *6*, 744–748.

Mulla, M. J., Salmon, J. E., Chamley, L. W., Brosens, J. J., Boeras, C. M., Kavathas, P. B., & Abrahams, V. M. (2013). A role for uric acid and the Nalp3 inflammasome in antiphospholipid antibody-induced IL-1β production by human first trimester trophoblast. *PLoS ONE*, *8*, e65237.

Mumme, K., Gray, C., Reynolds, C. M., Vickers, M. H., Harrison, C. J., Stanley, J. L., et al. (2016). Maternal-fetal hepatic and placental metabolome profiles are associated with reduced fetal growth in a rat model of maternal obesity. *Metabolomics*, *12*, 83.

Nori de Macedo, A., Mathiaparanam, S., Brick, L., Keenan, K., Gonska, T., Pedder, L., et al. (2017). The sweat metabolome of screen-positive cystic fibrosis infants: Revealing mechanisms beyond impaired chloride transport.

ACS Central Science, *3*, 904–913.
Patti, G. J., Yanes, O., & Siuzdak, G. (2012). Innovation: Metabolomics: the apogee of the omics trilogy. *Nature reviews. Molecular Cell Biology*, *13*, 263–269.
Perazzolo, S., Hirschmugl, B., Wadsack, C., Desoye, G., Lewis, R. M., & Sengers, B. G. (2017) The influence of placental metabolism on fatty acid transfer to the fetus. *Journal of Lipid Research*, *58*, 443–454.
Rosenfeld, C. S. (2015). Sex-specific placental responses in fetal development. *Endocrinology*, *156*, 3422-3434.
Rossant, J., & Cross, J. C. (2001). Placental development: Lessons from mouse mutants. *Nature Reviews Genetics*, *2*, 538–548.
Ruoppolo, M., Caterino, M., Albano, L., Pecce, R., Di Girolamo, M. G., Crisci, D., et al. (2018). Targeted metabolomic profiling in rat tissues reveals sex differences. *Scientific Reports*, *8*, 4663.
Ruttkies, C., Schymanski, E. L., Wolf, S., Hollender, J., & Neumann, S. (2016). MetFrag relaunched: Incorporating strategies beyond in silico fragmentation. *Journal of Cheminformatics*, *8*, 3.
Saoi, M., Percival, M., Nemr, C., Li, A., Gibala, M. J., & Britz-McKibbin, P. (2019). Characterization of the human skeletal muscle metabolome for elucidating the mechanisms of bicarbonate ingestion on strenuous interval exercise. *Analytical Chemistry*, *91*, 4709–4718.
Sautin, Y. Y., & Johnson, R. J. (2008). Uric acid: The oxidant-antioxidant paradox. *Nucleosides, Nucleotides and Nucleic Acids*. *27*, 608–619.
Shekhawat, P., Bennett, M. J., Sadovsky, Y., Nelson, D. M., Rakheja, D., & Strauss, A. W. (2003). Human placenta metabolizes fatty acids: implications for fetal fatty acid oxidation disorders and maternal liver diseases. *American Journal of Physiology-Endocrinology and Metabolism*, *284*, E1098–1105.
Simic, M. G., & Jovanovic, S. V. (1989). Antioxidation mechanisms of uric acid. *Journal of the American Chemical Society*, *111*, 5778–5782.
Thomas, M. M., Haghiac, M., Grozav, C., Minium, J., Calabuig-Navarro, V., O'Tierney-Ginn, P. (2018) Oxidative stress impairs fatty acid oxidation and mitochondrial function in the term placenta. *Reproduction Science,* doi: 10.1177/1933719118802054.
Walejko, J. M., Chelliah, A., Keller-Wood, M., Gregg, A., & Edison, A. S. (2018). Global metabolomics of the placenta reveals distinct metabolic profiles between maternal and fetal placental tissues following delivery in non-labored women. *Metabolites*, *8*, E10.
Wehrens, R., Hageman, , J. A., van Eeuwijk, F., Kooke, R., Flood, P. J., Wijnker, E. et al.
(2016) Improved batch correction in untargeted MS-based metabolomics. *Metabolomics, 12,* 88.
Yamamoto, M., Ly, R., Gill, B., Zhu, Y., Moran-Mirabal, J., & Britz-McKibbin, P. (2016). Robust and high throughput method for anionic metabolite profiling: Preventing polyimide aminolysis and capillary breakages under

alkaline conditions in capillary electrophoresis-mass spectrometry. *Analytical Chemistry*, *88*, 10710–10719.

5.9 Supporting Experimental

5.9.1 MSI-CE-MS Instrumentation and Workflow

The TOF-MS was performed in full-scan mode over a mass range of 50-1700 *m/z* at an acquisition rate of 500 ms/spectrum. The ESI conditions were Vcap = 2000 V, nozzle voltage = 2000 V, nebulizer gas = 10 psi, sheath gas = 3.5 L/min at 195 °C, drying gas 8 L/min at 300 °C, whereas, the MS voltage settings were fragmentor = 120 V, skimmer = 65V and Oct1 RF= 750 V. As part of quality assurance practices, the TOF-MS system was calibrated each day using an Agilent tune mixture to ensure mass ranges did not exceed 0.30 ppm. Additionally, daily cleaning of the CE electrode and ion source with 50% *vol* isopropanol with a lint free cloth was performed to minimize sample carryover and salt buildup. At the start of each day, a standard mixture followed by pooled QCs with blank were injected to equilibrate the CE-MS system while ensuring instrumental performance was adequate. At the end of each day, the capillary was flushed with 10 min with de-ionized water and air dried for 10 min.

5.9.2 Tandem Mass Spectrometry for Unknown Identification

Tandem mass spectrometry (MS/MS) was utilized in this study for structural elucidation and tentative identification of unknown placental metabolites that significantly differed between sexes. All Targeted MS/MS experiments were performed on an Agilent G7100A CE system (Agilent Technologies Inc., Mississauga, ON, Canada) equipped with a coaxial electrospray ionization (ESI) source coupled to an Agilent 6550 iFunnel QTOF-MS. A pooled placenta tissue extract was injected hydrodynamically at 100 bar for 20 sec followed by a BGE spacer at 100 mbar for 5 sec. Precursor ions were selected for collisional induced dissociation (CID) experiments at 10, 20 and 40 V. The ESI conditions were Vcap = 3500 V, nozzle voltage = 2000 V, nebulizer gas = 8 psi, drying gas 14L/min at 225 °C, whereas, the MS voltage settings were fragmentor = 380 V and Oct1 RF= 750 V. For structural elucidation, the METLIN database (Smith et al. 2005)

accessed through the MassHunter Personal Compound Database and Library (PDCL) manager was used. Since no authentic standards were used to confirm via co-migration with spiking, *in silico* fragmentation using MetFragWeb was employed for MS/MS spectral comparison (Ruttkies et al. 2016).

5.10 Supporting References

Ruttkies, C., Schymanski, E.L., Wolf, S., Hollender, J., & Neumann, S. (2016). MetFrag relaunched: Incorporating strategies beyond in silico fragmentation. *Journal of Cheminformatics*, *8,* 3.

Smith, C.A., O'Maille, G., Want, E.J., Qin, C., Trauger, S.A., Brandon, T.R., Custodio, D.E., Abagyan, R., Siuzdak, G. (2005). METLIN: A metabolite mass spectral database. *Therapeutic Drug Monitoring*, *27*, 747-751.

Table S5.1: Comprehensive list of 106 polar metabolites reliably measured in pooled placental tissue extracts by MSI-CE-MS. Metabolites were annotated based on their accurate mass (*m/z*), relative migration time (RMT), mode of ion detection (p or n), most likely molecular formula and mass error. Absolute concentrations for a majority of placental metabolites are also summarized based on calibration curves acquired from authentic standards.

***m/z*:RMT:mode**	**Compound ID**	**Chemical Formula**	**Mass Error (ppm)**	**Concentration (mmol/kg d.w.)**
76.0393:0.731:p	Glycine	$C_2H_5NO_2$	15.3	5.83±0.03
76.0757:0.582:p	Trimethylamine-*N*-oxide	C_3H_9NO	13.3	0.06±0.02
90.0550:0.652:p	β-Alanine	$C_3H_7NO_2$	6.6	--
90.0550:0.782:p	Alanine	$C_3H_7NO_2$	10.1	8.86±0.31
104.0706:0.782:p	GABA*[a,b]	$C_4H_9NO_2$	1.6	0.053±0.000
104.0706:0.851:p	BAIBA*[a,b]	$C_4H_9NO_2$	0.9	--
104.0706:0.943:p	Dimethylglycine (DMG)	$C_4H_9NO_2$	0.9	0.08±0.01
104.1075:0.605:p	Choline	$C_5H_{14}NO$	1.5	3.13±0.12
106.0499:0.860:p	Serine	$C_3H_7NO_3$	4.1	2.62±0.11
110.0270:1.483:p	Hypotaurine*	$C_2H_7NO_2S$	0.4	--
114.0662:0.648:p	Creatinine	$C_4H_7N_3O$	0.4	0.10±0.04
116.0706:0.917:p	Proline	$C_5H_9NO_2$	1.1	3.14±0.05
118.0611:0.725:p	Guanidoacetic acid*	$C_3H_7N_3O_2$	2.2	--
118.0863:0.852:p	Valine[a]	$C_5H_{11}NO_2$	0.4	1.99±0.45
118.0863:0.960:p	Betaine	$C_5H_{11}NO_2$	6.6	29.6±0.4
120.0655:0.899:p	Threonine	$C_4H_9NO_3$	-2.9	4.83±0.15
120.1020:0.661:p	*Unknown*	$C_5H_{13}NO_2$	0.4	--
122.0270:0.953:p	Cysteine	$C_3H_7NO_2S$	8.0	0.43±0.07
126.0219:1.615:p	Taurine[b]	$C_2H_7NO_3S$	0.2	6.25±0.05
131.1176:0.457:p	*N*-Acetylputrescine*[b]	$C_6H_{14}N_2O$	-5.8	--
132.0655:1.018:p	Hydroxyproline	$C_5H_9NO_3$	2.1	--
132.0768:0.769:p	Creatine	$C_4H_9N_3O_2$	2.1	7.87±0.26
132.1019:0.863:p	Isoleucine[b]	$C_6H_{13}NO_2$	-0.04	--
132.1019:0.873:p	Leucine[b]	$C_6H_{13}NO_2$	-0.04	--
133.0608:0.899:p	Asparagine	$C_4H_8N_2O_3$	-3.8	1.06±0.00
133.0972:0.613:p	Ornithine	$C_5H_{12}N_2O_2$	-8.4	0.11±0.06
134.0448:0.976:p	Aspartic Acid	$C_4H_7NO_4$	0.1	2.88±0.12

137.0458:1.083:p	Hypoxanthine	$C_5H_4N_4O$	1.1	0.37±0.03
137.0709:0.651:p	*N*-Methylnicotinamide*	$C_7H_8N_2O$	-2.7	--
141.0657:0.722:p	*Unknown*	$C_6H_8N_2O_2$	0.9	--
142.0264:1.506:p	*O*-Phosphoethanolamine[b]	$C_2H_8NO_4P$	-1.4	--
146.1181:0.712:p	Deoxycarnitine	$C_7H_{16}NO_2$	-4.4	0.12±0.14
146.1652:0.413:p	Spermidine	$C_7H_{19}N_3$	-1.0	--
147.0764:0.921:p	Glutamine	$C_5H_{10}N_2O_3$	0.3	417.66±0.02
147.1128:0.613:p	Lysine	$C_6H_{14}N_2O_2$	-1.4	3.18±1.66
148.0604:0.933:p	Glutamic Acid	$C_5H_9NO_4$	-0.5	13.0±0.9
150.0583:0.908:p	Methionine	$C_5H_{11}NO_2S$	-1.7	0.92±0.21
151.0431:0.511:p	*Unknown*	$C_5H_{11}O_3S$	-6.2	--
156.0768:0.653:p	Histidine	$C_6H_9N_3O_2$	-0.3	0.64±0.38
160.1330:0.738:p	*Unknown*	$C_8H_{17}NO_2$	0.01	--
162.1125:0.746:p	Carnitine	$C_7H_{15}NO_3$	3.5	12.0±1.2
166.0863:0.933:p	Phenylalanine	$C_9H_{11}NO_2$	-1.5	1.50±0.29
170.0924:0.668:p	Methylhistidine	$C_7H_{11}N_3O_2$	-1.0	0.24±0.19
175.1190:0.634:p	Arginine	$C_6H_{14}N_4O_2$	-0.7	0.83±0.16
176.1030:0.944:p	Citrulline	$C_6H_{13}N_3O_3$	-4.5	0.49±0.27
179.0481:0.804:p	Cysteinylglycine*	$C_5H_{10}N_2O_3S$	-1.3	--
182.0812:0.961:p	Tyrosine	$C_9H_{11}NO_3$	-2.4	10.6±0.1
188.1757:0.565:p	*N*-Acetylspermidine*	$C_9H_{21}N_3O$	-0.9	--
189.1346:0.638:p	Homoarginine	$C_7H_{16}N_4O2$	15.3	--
189.1598:0.635:p	Trimethyllysine	$C_9H_{20}N_2O_2$	-15.1	--
203.1503:0.676:p	Asymmetric dimethylarginine	$C_8H_{18}N_4O_2$	3.5	0.04±0.01
203.1503:0.687:p	Symmetric dimethylarginine	$C_8H_{18}N_4O_2$	-1.1	--
203.2230:0.410:p	Spermine	$C_{10}H_{26}N_4$	-4.9	0.16±0.14
204.1230:0.787:p	Acetylcarnitine	$C_9H_{17}NO_4$	1.5	4.13±0.21
205.0972:0.933:p	Tryptophan	$C_{11}H_{12}N_2O_2$	9.2	366±18
209.0921:0.891:p	Kynurenine	$C_{10}H_{12}N_2O_3$	-4.8	--
218.1387:0.808:p	Propionylcarnitine	$C_{10}H_{19}NO_4$	-0.8	0.05±0.05
230.0958:1.404:p	Ergothioneine*	$C_9H_{15}N_3O_2S$	-0.03	--
232.1543:0.820:p	Isobutyrylcarnitine[a]	$C_{11}H_{21}NO_4$	-0.01	--

232.1543:0.827:p	Butyrylcarnitine[a]	$C_{11}H_{21}NO_4$	-0.01	0.04±0.02
242.5621:0.883:p	CysGly-GSH*	$C_{15}H_{25}N_5O_9S_2$	-1.2	--
243.0737:1.044:p	*Unknown*	$C_9H_6N_8O$	-2.9	--
244.0991:0.848:p	*Unknown*	$C_{11}H_{17}NO_3S$	2.7	--
246.1700:0.837:p	Isovalerylcarnitine[a]	$C_{12}H_{24}NO_4$	-1.1	--
246.1700:0.843:p	Valerylcarnitine[a]	$C_{12}H_{24}NO_4$	-1.4	--
248.1492:0.852:p	Hydroxybutyrylcarnitine	$C_{11}H_{21}NO_5$	-0.2	--
258.1097:1.592:p	Glycerophosphoylcholine*[b]	$C_8H_{20}NO_6P$	-0.1	--
260.1856:0.857:p	Hexanoylcarnitine	$C_{13}H_{25}NO_4$	0.4	--
262.1647:0.869:p	*Unknown*	$C_{12}N_{23}NO_5$	-1.3	--
268.1040:0.871:p	Adenosine	$C_{10}H_{13}N_5O_4$	-1.9	--
269.0878:1.528:p	Inosine[b]	$C_{10}H_{12}N_4O_5$	-1.0	--
276.1551:0.833:p	*Unknown*	$C_{12}H_{17}N_7O$	8.1	--
276.1789:0.889:p	Hydroxyhexanoycarnitine	$C_{13}H_{25}NO_5$	-5.7	--
284.0989:1.149:p	Guanosine	$C_{10}H_{13}N_5O_5$	-3.2	--
298.0526:0.828:p	Cysteinylglycine cysteine mixed disulfide *	$C_8H_{15}N_3O_5S_2$	39.5	--
298.0959:0.883:p	Methylthioadenosine*	$C_{11}H_{15}N_5O_3S$	-4.4	--
307.0833:1.030:p	Oxidized glutathione disulfide	$C_{20}H_{32}N_6O_{12}S_2$	0.9	1.40±0.46
308.0911:1.108:p	Reduced glutathione	$C_{10}H_{17}N_3O_6S$	0.3	4.87±0.71
427.0952:0.990:p	Cysteinylglutathione mixed disulfide	$C_{13}H_{22}N_4O_8S_2$	-1.0	0.23±0.11
89.0244:1.155:n	Lactic acid	$C_3H_6O_3$	7.3	18.9±1.8
96.9696:1.720:n	Inorganic phosphate	H_3O_4P	0.2	12.6±0.1
103.0401:1.023:n	3-Hydroxybutyric acid	$C_4H_8O_3$	-0.01	3.77±2.74
103.0401:1.048:n	2-Hydroxybutyric acid	$C_4H_8O_3$	-0.3	0.11±0.02
117.0193:1.906:n	Succinic acid	$C_4H_6O_4$	1.4	3.27±1.84
128.0353:1.019:n	Oxoproline	$C_5H_7NO_3$	-8.7	0.38±0.04
133.0142:1.927:n	Malic acid	$C_4H_6O_5$	-1.1	--
167.0211:0.960:n	Uric acid	$C_5H_4N_4O_3$	4.4	0.88±0.02
171.0064:1.305:n	Glycerol 3-phosphate	$C_3H_9O_6P$	9.6	--
175.0252:0.911:n	Ascrobic Acid*	$C_6H_8O_6$	2.1	--
179.0561:0.568:n	Glucose	$C_6H_{12}O_6$	19.3	--
180.9520:1.720:n	*Unknown*	$C_6H_2N_2OS_2$	1.8	--

187.0426:1.155:n	*Unknown*	$C_8H_{12}O_3S$	0.9	--
191.0197:2.106:n	Citric acid/Isocitric acid	$C_6H_8O_7$	-6.6	--
195.0510:0.879:n	Gluconic acid	$C_6H_{12}O_7$	14.7	--
218.1034:0.823:n	Pantothenic acid	$C_9H_{17}NO_5$	0.9	0.05±0.01
259.0224:1.058:n	Glucose-6-phosphate[b]	$C_6H_{13}O_9P$	-6.6	0.39±0.01
264.9520:1.782:n	1,3-Bisphosphoglycerate*	$C_3H_8O_{10}P_2$	1.7	--
338.9888:1.534:n	Fructose-1,6-bisphosphate	$C_6H_{14}O_{12}P_2$	-5.3	0.62±0.07
346.0558:1.006:n	AMP	$C_{10}H_{14}N_5O_7P$	-2.2	1.27±0.08
347.0398:1.027:n	IMP[b]	$C_{10}H_{13}N_4O_8P$	-8.6	0.31±0.04
426.0221:1.176:n	ADP	$C_{10}H_{15}N_5O_{10}P_2$	0.0	0.33±0.03
482.9613:1.306:n	UTP[b]	$C_9H_{15}N_2O_{15}P_3$	-20.6	0.60±0.38
505.9885:1.220:n	ATP	$C_{10}H_{16}N_5O_{13}P_3$	-1.3	1.44±0.44
521.9834:1.196:n	GTP[b]	$C_{10}H_{16}N_5O_{14}P_3$	0.03	1.02±0.77
558.0644:0.916:n	ADP-Ribose*	$C_{15}H_{23}N_5O_{14}P_2$	0.2	--
662.1024:0.705:n	NAD^+	$C_{21}H_{28}N_7O_{14}P_2$	-5.7	0.70±0.04

[a] *Metabolites are prone to isobaric/isomeric interference with partial overlapping peaks using MSI-CE-MS.*
[b] *Not included in final study matrix.*
** Tentatively identified based on MS/MS spectral matching to public databases.*

Table S5.2: Summary of 29 acidic lipid metabolites reliably measured in pooled placental tissue extracts by MSI-NACE-MS. Metabolites are annotated based on their accurate mass (m/z), relative migration time (RMT), mode of ion detection (p or n), most likely molecular formula and mass error.. Absolute concentrations for placental lipid metabolites are also summarized based on calibration curves from authentic standards if available.

***m/z*:RMT:mode**	**Compound ID**	**Chemical Formula**	**Mass Error (ppm)**	**Concentration (mmol/kg d.w.)**
199.1703:1.032:n	Lauric acid (C12:0)[b]	$C_{12}H_{24}O_2$	-2.8	0.13±0.09
227.2017:1.004:n	Myristic acid (C14:0)	$C_{14}H_{28}O_2$	-3.0	0.44±0.15
241.2173:0.990:n	Pentadecanoic acid (C15:0)	$C_{15}H_{30}O_2$	-2.4	0.33±0.08
253.2173:0.985:n	Palmitoleic acid (C16:1n-7)	$C_{16}H_{30}O_2$	-1.7	1.54±0.47
255.2329:0.981:n	Palmitic acid (C16:0)	$C_{16}H_{32}O_2$	4.3	20±2
267.2330:0.975:n	Heptadecenoic acid (C17:1)	$C_{17}H_{32}O_2$	-0.8	
269.2486:0.966:n	Heptadecanoic acid (C17:0)	$C_{17}H_{34}O_2$	-2.1	0.104±0.067
277.2173:0.983:n	γ-Linolenic acid (C18:3n-6)[a]	$C_{18}H_{30}O_2$	-2.9	
277.2173:0.981:n	α-Linolenic acid (C18:3n-3)[a]	$C_{18}H_{30}O_2$	-2.3	
279.2330:0.967:n	Linoleic acid (C18:2n-6)	$C_{18}H_{32}O_2$	0.4	8.7±2.3
281.2486:0.961:n	Oleic acid (C18:1n-9)	$C_{18}H_{34}O_2$	0.8	9.1±2.3
283.2642:0.954:n	Stearic acid (C18:0)	$C_{18}H_{36}O_2$	2.6	48±4
297.2799:0.942:n	Nonadecanoic acid (C19:0)	$C_{19}H_{38}O_2$	-20.5	
301.2173:0.981:n	Eicosapentaenoic acid (20:5n-6)	$C_{20}H_{30}O_2$	59.5	0.88±0.28
303.2330:0.978:n	Arachidonic acid (20:4n-6)	$C_{20}H_{32}O_2$	2.4	12±3
305.2486:0.953:n	Eicosatrienoic acid (20:3n-6)	$C_{20}H_{34}O_2$	-0.3	
307.2642:0.942:n	Eicosadienoic acid (C20:2n-6)	$C_{20}H_{36}O_2$	-3.6	
309.2799:0.937:n	Eicosenoic acid (C20:1)	$C_{20}H_{38}O_2$	-6.7	
311.2955:0.931:n	Arachidic acid (C20:0n-6)	$C_{20}H_{40}O_2$	-3.4	
327.2330:0.988:n	Docosahexaenoic acid (C22:6n-3)	$C_{22}H_{32}O_2$	1.3	6±1
329.2486:0.982:n	Docosapentaenoic acid (C22:5n-3)	$C_{22}H_{34}O_2$	11.8	
331.2643:0.939:n	Docosatetraenoic acid (C22:4n-6)	$C_{22}H_{36}O_2$	-0.3	
337.3112:0.918:n	Erucic acid (C22:1n-9)	$C_{22}H_{42}O_2$	10.9	
339.3269:0.913:n	Docosanoic acid (C22:0)	$C_{22}H_{44}O_2$	-0.8	
365.3425:0.901:n	Nervonic acid (C24:1n-9)	$C_{24}H_{46}O_2$	-3.2	
367.3582:0.898:n	Tetracosanoic acid (C24:0)	$C_{24}H_{48}O_2$	-3.0	

407.2803:0.951:n	Cholic acid	$C_{24}H_{40}O_5$	7.5
448.3068:0.987:n	Glycochenodeoxycholic acid	$C_{26}H_{43}NO_5$	-6.9
565.5211:0.958:n	*Unknown*	$C_{36}H_{69}O_4$	-9.4

[a] *Partially resolved isobaric/isomeric fatty acids integrated as total of both isomers*
[b] *Not included in the final data matrix*

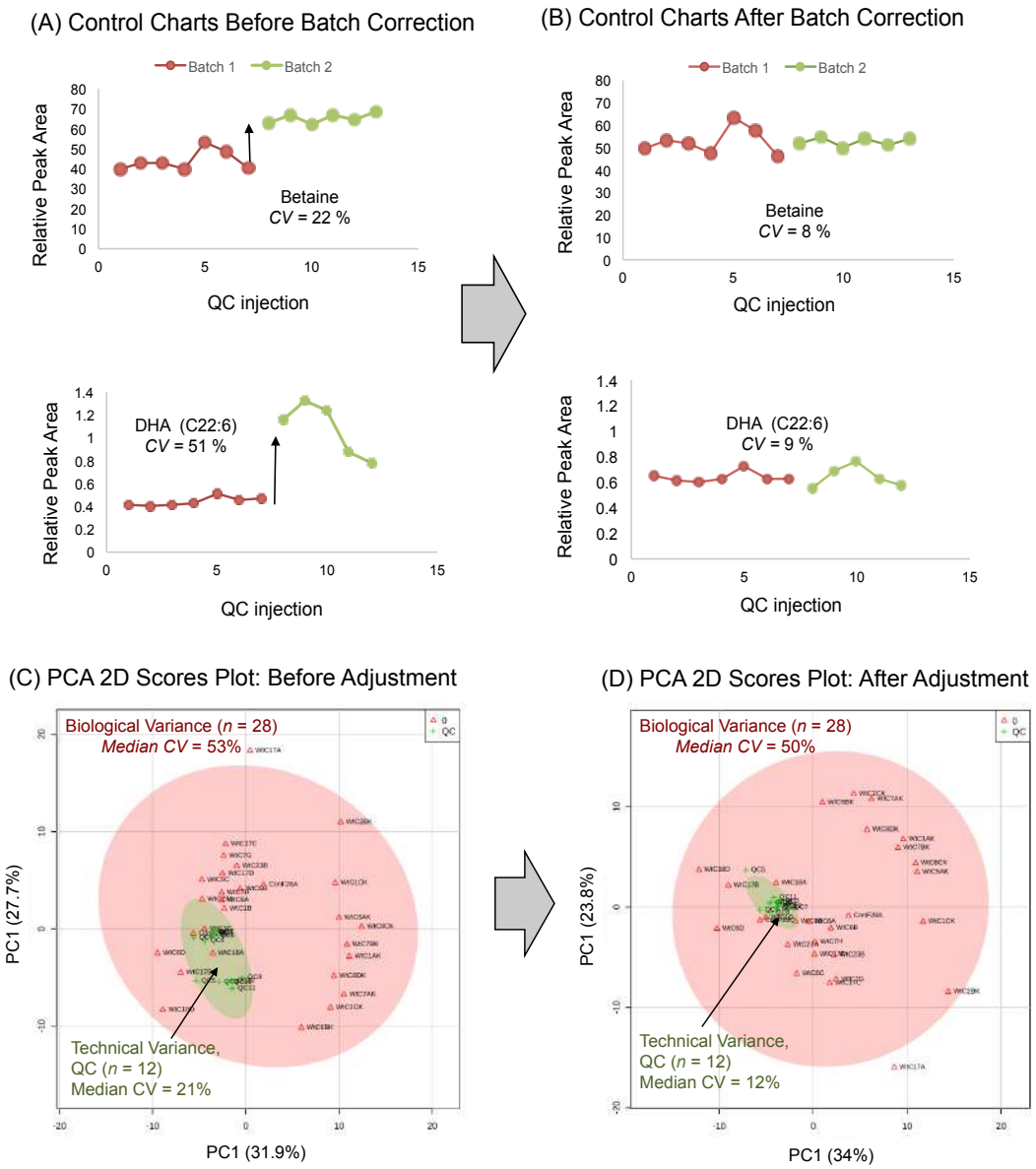

Figure S5.1: Control charts of placental QCs of betaine (118.0863:0.960:p) and docosahexaenoic acid (327.2330: 0.988:n) **a** before and **b** after batch correction was used to correct for signal drift in ESI-MS thereby improving technical precision when both analytical batches were combined. The red lines represent batch 1 analyzed in 2016, while the green lines represent batch 2 analyzed in 2018. Two 2D scores plots using PCA **c** before and **d** after application of QC based batch-correction algorithm, where overall technical variance significantly decreased from 21% to 12% without changing natural biological variance based on 120 metabolites reliably measured in the placental QCs (*n*=12).

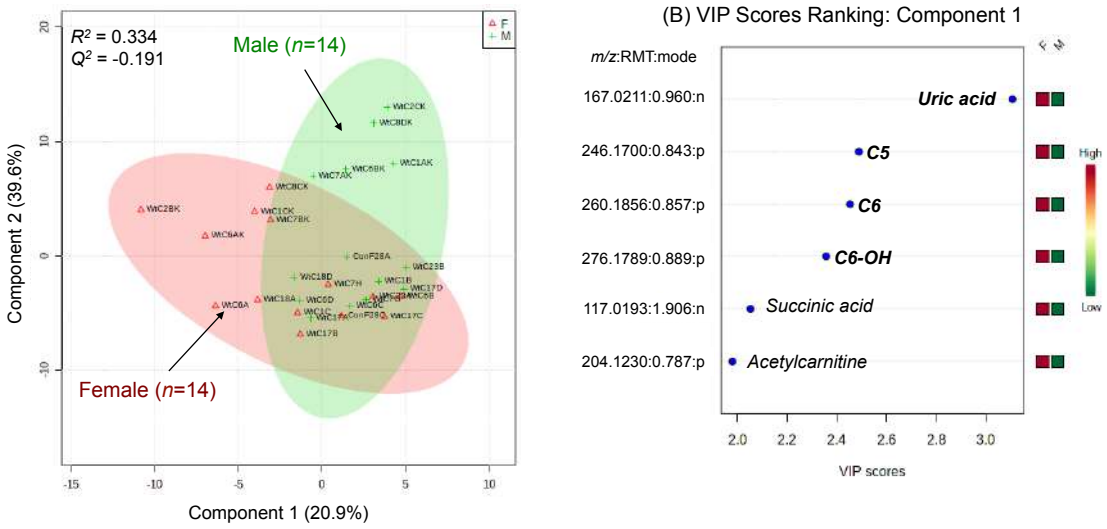

Figure S5.2: a A 2D PLS-DA scores plot showing sex-dependent differentiation of the murine placental metabolome of control-fed dams. Metabolite ion responses were normalized to an internal standard and dry weight (mg), and then autoscaled and batch-corrected when using a perturbation test. **b** Variance in Projection (VIP) plot along component 1 which lists the top-ranked metabolites discriminating between sex from placentae along the first component. Bolded metabolites are significant ($p < 0.05$) when using a Mann Whitney *U* test.

Chapter VI:
Future Directions in Tissue Metabolomics in Human Health Interventions and Clinical Research

Chapter VI: Future Directions in Tissue Metabolomics in Human Health Interventions and Clinical Research

6.1 Overview of major thesis contributions

The work presented in this thesis has contributed to new advancements in biomarker discovery using multiplexed separations with novel data workflows, including: (1) validating a high throughput screening platform for targeted analysis of a panel of serum γ-glutamyl dipeptides to allow for better risk assessment in non-alcoholic steatohepatitis (NASH) patients that complements classic liver enzyme tests and tissue histopathology, and (2) elucidating adaptive responses in the plasma metabolome due to abrupt physical inactivity as a diagnostic screening tool for early detection of sarcopenia in high risk older persons who are susceptible to frailty. Currently, there is an urgent need for population based-screening tools, such as non-invasive biomarkers, for preventing liver disease progression in non-alcoholic fatty liver disease (NAFLD) while also validating better prognostic indicators that predict liver-associated morbidity and/or mortality. Similarly, reliable screening tools must also be implemented to prevent sarcopenia in ageing populations across developed countries while also validating innovative lifestyle interventions for its effective prevention. Metabolomics offers a systemic approach for identifying clinically relevant biomarkers that also provide deeper insights to underlying disease pathophysiology. Biomarker discovery using metabolomics based on MSI-CE-MS have primarily focused on non-invasive human blood samples (*e.g.,* serum or plasma), which are widely used specimens for routine screening in a clinical setting. However, biofluids are non-organ specific and reflect numerous metabolic processes within the body that complicate biochemical interpretations. Therefore, it is imperative to assess metabolite changes localized within tissues, as they are the direct site and origin of most disease processes as a way to obtain more robust and specific biomarkers. This motivated the work presented in the second half of this thesis where new advancements in tissue metabolomics studies were developed, including (3) characterization of the human skeletal muscle metabolome from a

cohort of recreationally-active males undergoing a strenuous exercise regimen after ingestion of high oral dosages of bicarbonate as a way to provide new insights of acute alkalosis in preserving muscle function during interval exercise, and (4) comprehensive characterization of the murine placental metabolome derived from maternal dams fed a controlled diet prior to and during pregnancy to elucidate the influence of sex on placental adaptations that may influence fetal development and birth outcomes later in life.

Chapter I of this thesis provided a comprehensive review of tissue metabolomic studies in clinical research with a focus on biomarker discovery using complementary instrumental methods based on high efficiency separations coupled to high resolution mass spectrometry, as well as high field NMR methods. Recent trends and new advances for tissue metabolomics studies are highlighted while also discussing current limitations to be addressed in future research. *Chapter II* introduces multiplexed electrophoretic separations using multisegment injection-capillary electrophoresis-tandem mass spectrometry (MSI-CE-MS/MS) for targeted analysis of sixteen serum γ-glutamyl dipeptides from a cohort of overweight Japanese NASH patients using a multiplexed data workflow with stringent quality control. Rigorous method optimization and validation was performed to demonstrate the utility of this workflow as required in large-scale metabolomics studies with good technical precision, accuracy and robustness while reducing analysis times as compared to conventional single injection separation methods.[1] Importantly, unsupervised multivariate pattern recognition revealed two distinct NASH patient sub-groups (*i.e.,* low-risk *vs.* high-risk) based contrasting differences in serum γ-glutamyl dipeptide concentration profiles despite having similar clinical phenotypes and liver histopathology parametrics. Moreover, serum γ-glutamyl dipeptide concentrations were inversely correlated with GGT activity, which inferred that impairments in the glutathione salvage pathway among high-risk NASH patients with elevated oxidative stress who likely have poor clinical

prognosis. This study revealed the crucial role of the γ-glutamyl cycle in the pathophysiology and disease progression in advanced stages of NASH especially since patients often suffer from several other co-morbidies (*e.g.,* diabetes, hypertension). This research paves the way for developing better risk assessment tools to complement routine liver enzyme tests and histopathology, which will need to be further validated in a longitudinal study involving NASH patients when evaluating the predictive accuracy of serum γ-glutamyl dipeptides for potential clinical use.

In *Chapter III*, nontargeted metabolite profiling by MSI-CE-MS was performed in fasting plasma specimens collected from a cohort of prediabetic, older adults participating in two weeks of short-term step reduction (< 1000 steps/day) followed by two weeks of recovery, returning to normal ambulatory activity. We sought out to determine adaptive metabolic responses to acute periods of physical inactivity associated with metabolic dysregulation and muscle wasting at three time intervals during the intervention trial. Our findings revealed that two weeks short-term step reduction elicited a myriad of adaptive metabolic changes that did not return to baseline after two weeks of recovery. Increased levels in plasma metabolites associated with muscle energy metabolism, including circulating concentrations of glutamine, creatine, carnitine and deoxycarnitine, which were evident after step reduction and correlated with deceases in myofibrillar protein biosynthesis.[2] An unexpected finding in this study was that acute inactivity elicited a decrease in plasma uremic toxins (*e.g.,* indoxyl sulfate and hippuric acid), as well as changes in glutathione precursors (oxoproline and methionine). Among these panel of plasma metabolites, glutamine was the most significant biomarker associated with physical inactivity that was independent of sex and extent of step reduction as potential confounders. This apparent increase in plasma glutamine may suggest an increased efflux to circulation from the muscle as a result of increased protein catabolism from prolonged muscle disuse.[3,4] Our findings revealed

fundamental metabolic pathways to advance our understanding of the pathogenesis of early stages sarcopenia, which may provide a convenient way for therapeutic monitoring of the efficacy of lifestyle interventions that promote healthy ageing in geriatric populations. However, a major limitation of the study was that access to muscle tissue biopsies was not available in order to corroborate changes in circulatory metabolism with adaptive metabolic responses within skeletal muscle tissue following acute inactivity.

Chapter IV represents the first metabolomics study to characterize the human skeletal muscle metabolome from mass-restricted tissue biopsies (≈ 2 mg dried mass) with matching fasting plasma samples when using nontargeted profiling of polar/ionic metabolites by MSI-CE-MS together with targeted analysis of major electrolytes using CE with indirect UV.[5] Rigorous optimization of a quantitative tissue microextraction procedure achieved high metabolite recoveries (> 90%) while minimizing artifactual oxidation and hydrolysis (< 8%) among labile metabolites. Over 80 polar/ionic metabolites were reliably characterized in the majority of muscle tissue specimens collected from a cohort of recreationally-active males participating in standardized interval training with bicarbonate pretreatment in a double-blind, placebo-controlled cross-over study. In this case, dynamic changes in metabolites including in glycolytic metabolites (lactic acid), amino acids (alanine, glutamic acid) and acylcarnitines (acetylcarnitine) were identified as biomarkers of strenuous exercise in both muscle tissue and plasma specimens. Importantly, this study revealed that bicarbonate ingestion prior to strenuous interval exercise elicited perturbations in ionic homeostasis that attenuated potassium efflux from contacting muscle together with lower oxidative and energetic stress as reflected by lower intramuscular concentrations of GSH-Cys-SS, uric acid and anserine, which is a histidine-containing dipeptide from carnosine identified for the first time in human skeletal muscle using high resolution MS/MS. Overall, our findings revealed underlying molecular mechanisms associated with

acute bicarbonate ingestion and strenuous exercise on muscle metabolism, which may prove useful to design safe yet effective dietary interventions that inhibit fatigue. Although this work demonstrated the utility of tissue metabolomics to provide deeper biochemical insights that cannot always be inferred from circulatory metabolism, metabolome coverage was limited to polar/ionic metabolites.

Finally, in *Chapter V* nontargeted metabolomics was performed on murine placental tissue (≈ 2 mg dried mass) in mice fed a standardized, control diet to examine the impact of sex on the placental metabolome during gestation.[6] This was the first study to apply MSI-CE-MS to expand metabolome coverage beyond polar/ionic metabolites, such as long-chain fatty acids that are important mediators of inflammation and mitochondrial energy/function. Characterization of the murine placental metabolome resulted in over 120 placental metabolites reliably detected in placental tissue extracts over a wide dynamic range. Modest differences in metabolic profiles were observed between male and female placenta derived from the same control-fed maternal mice. Importantly, a panel of short-chain acylcarnitines (C5, C6, C6OH) were significantly increased in females compared to males, indicating a sex-dependent increase in lipid oxidation prevalent in females to fulfill energetic requirements during gestation. Interestingly, increases in placenta uric acid, a known antioxidant, were also measured in females to maintain redox homeostasis to compensate for lowered antioxidant capacities as compared to males. For the first time, our findings revealed novel insights into mechanisms dictating sex-specific metabolic adaptations in normal, uncomplicated murine pregnancies, which have important implications in the developmental origins of health and disease relevant to human health outcomes early in life.

6.2 Further validation of the role of γ-glutamyl dipeptides in liver biopsies for NASH risk assessment

To date, most tissue metabolomics studies on liver specimens have aimed to determine diagnostic markers in more severe forms of chronic liver diseases including hepatocellular carcinoma (HCC)[7,8] and cirrhosis,[9] where irreversible liver damage often results.[10] However, there have been far fewer studies focusing on NASH patient populations, who are at higher risk for liver-associated morbidity and/or mortality.[10] Therefore future metabolomics studies on paired liver biopsy and serum specimens in a larger, more diverse cohort of NASH patients is necessary in order to validate the role of γ-glutamyl dipeptides for NASH risk assessment. A major limitation highlighted in *Chapter II* was limited access to liver tissue biopsies to correlate intracellular γ-glutamyl dipeptides changes with those observed in the serum. This is imperative in order to gain an overall mechanistic understanding of how the γ-glutamyl-cycle leads to impairments in the glutathione salvage pathway in high-risk NASH patients, predisposing them to increased oxidative stress/inflammation and thus, lower life expectancies and poor prognosis.[11] Ideally, sample analysis by MSI-CE-MS should be performed using the data workflow proposed in *Chapter II* with stringent quality control. Moreover, expanding metabolome coverage to other polar and lipid metabolites, we can potentially discover tissue-derived makers that correlate with histopathology grading for NASH diagnosis.[12] These markers can then be validated for routine screening and prognostic testing to complement classic liver enzyme tests that often lack specificity,[10] as well as routine histopathology, which is prone to observer bias[12] and require longer turn-around times (*e.g.,* days to weeks) in clinical settings.

6.3 Examining the influence of sex on bicarbonate treatment responses following interval exercise

As discussed in *Chapter IV*, bicarbonate ingestion prior to strenuous interval exercise elicited modest treatment effects in metabolic pathways associated with

ionic homeostasis, purine degradation and oxidative stress. However, this study employed a small cohort of recreationally active men. Recently, there has been increasing evidence that sex influences skeletal muscle adaptations in response to exercise.[13] For instance Scalzo *et al*. observed higher mitochondrial protein synthesis in recreationally activity in males after training compared to females with similar baseline fitness. Higher rates of mitochondrial protein synthesis in males were due to an increase in 127 mitochondrial proteins.[14] Additionally, a recent study by Cardinale *et al*.[15] revealed that women had lower mitochondrial content compared to men due to lower oxygen affinity. Based on these preliminary findings, future studies are required to examine the dependence of biological sex in skeletal muscle adaptations in response to exercise as well as nutraceuticals, such as sodium bicarbonate. While numerous studies have explored the effects acute alkalosis through ingestion of alkalizing agents (*e.g.,* sodium bicarbonate, sodium citrate) in males on muscle metabolism as well as exercise performance, there is a lack of studies performed in recreationally active females due to challenges in recruitment when relying on highly invasive tissue biopsy procedures. Of these studies, the effects of acute alkalosis remain unclear.[16] Therefore, future studies involving a larger and more diverse cohort of recreationally-active participants should be performed in order to examine sex-dependent metabolic adaptations associated with dietary interventions and/or interval exercise. This will confirm the preliminary findings reported in *Chapter IV* while providing new insights to the underlying metabolic pathways that may differentially impact women as compared to men.

6.4 Characterizing metabolomes of fetal tissues for sex-specificity

In *Chapter V*, nontargeted metabolomics was performed using MSI-CE-MS on murine placental tissue for polar metabolites as well as fatty acids. The unique data workflow with stringent quality control adopted in this work can be applied to other mass-restricted tissue specimens for to achieve wide metabolite coverage without

the need for multiple analytical platforms,[17–19] which is often costly and impractical in many academic research settings. Sex-specific metabolic adaptations were observed between male and female placenta derived from the same maternal dam fed a controlled diet prior to and during gestation. A key finding from our study showed increased levels of short-chain acylcarnitines in female placenta compaed to males in uncomplicated, maternal pregnancies. This suggested a shift towards higher placental β-oxidation compared to males. While these findings provided preliminary insights to the influence of sex on the placental metabolome during gestation, future studies should also incorporate paired maternal and/or fetal tissues in order to gain a more comprehensive understanding of the impact of sex differences on maternal-fetal interactions during pregnancy. For instance, Mumme *et al.,*[19] employed a rodent model to examine the influence of maternal diet (control-fed, 4% salt, high fat, high fat +4% salt) on the placenta as well as maternal and fetal liver tissues. The authors were able to examine global metabolic changes in both the mother and offspring as a result of environmental insults *in utero* elicited by maternal diet. Moreover, access to paired tissues for future studies can be used to also examine how the role of biological sex plays on placental adaptations that impact subsequent birth outcomes, such as obesity and metabolic syndrome. More studies are urgently needed to investigate the influence of sex during early stages of fetal development and how these adaptations can differentially impact health outcomes later in childhood.

6.5 General Conclusions

In conclusion, this thesis presents unique applications of multiplexed separations using MSI-CE-MS for the discovery of putative, non-invasive blood-based biomarkers to identify high risk adults prone to NASH progression as well as inactivity-induced losses in muscle mass and function in older adults. Additionally, the second half of this thesis presented two unique tissue metabolomics studies. The first study involved the first comprehensive characterization of the human skeletal

muscle with paired matching plasma specimens from recreationally active men participating in standardized exercise trials following bicarbonate pre-treatment. Metabolite coverage was expanded using MSI-NACE-MS to include fatty acids and intact lipids in the second study, where murine placental metabolome characterization was achieved to examine sex-specific adaptations during gestation. Overall, this thesis paves way for routine metabolite profiling in tissues in order to gain deeper insights to pathophysiology and functionality in organs, which is the direct site of where metabolite changes owing to a disease take place.

6.6 References

(1) Hirayama, A.; Igarashi, K.; Tomita, M.; Soga, T. Development of Quantitative Method for Determination of γ-Glutamyl Peptides by Capillary Electrophoresis Tandem Mass Spectrometry: An Efficient Approach Avoiding Matrix Effect. *J. Chromatogr. A* **2014**, *1369*, 161–169.

(2) McGlory, C.; Von Allmen, M. T.; Stokes, T.; Morton, R. W.; Hector, A. J.; Lago, B. A.; Raphenya, A. R.; Smith, B. K.; McArthur, A. G.; Steinberg, G. R.; et al. Failed Recovery of Glycemic Control and Myofibrillar Protein Synthesis with 2 Wk of Physical Inactivity in Overweight, Prediabetic Older Adults. *Journals Gerontol. - Ser. A Biol. Sci. Med. Sci.* **2018**, *73*, 1070-1077.

(3) Meynial-Denis, D. Glutamine Metabolism in Advanced Age. *Nutr. Rev.* **2016**, *74,* 225-236

(4) Mosoni, L.; Patureau Mirand, P.; Houlier, M. .; Arnal M. Age-Related Changes in Protein Synthesis Measured in Vivo in Rat Liver and Gastrocnemius Muscle. *Mech Ageing Dev* **1993**, *68* (1–3), 209–220.

(5) Saoi, M.; Percival, M.; Nemr, C.; Li, A.; Gibala, M. J.; Britz-Mckibbin, P. Characterization of the Human Skeletal Muscle Metabolome for Elucidating the Mechanisms of Bicarbonate Ingestion on Strenuous Interval Exercise. *Anal. Chem.* **2019**, *91*, 4709-4718.

(6) Gohir, W.; Kennedy, K. M.; Wallace, J. G.; Saoi, M.; Bellissimo, C. J.; Britz-McKibbin, P.; Petrik, J. J.; Surrette, M. G.; Sloboda, D. M. High-fat Diet Intake Modulates Maternal Intestinal Adaptations to Pregnancy and Results in Placental Hypoxia, as Well as Altered Fetal Gut Barrier Proteins and Immune Markers. *J. Physiol.* **2019**, https://doi.org/10.1113/JP277353.

(7) Lin, Y.; Ma, C.; Bezabeh, T.; Wang, Z.; Liang, J.; Huang, Y.; Zhao, J.; Liu, X.; Ye, W.; Tang, W. 1 H NMR-Based Metabolomics Reveal Overlapping Discriminatory Metabolites and Metabolic Pathway Disturbances between Colorectal Tumor Tissues and Fecal Samples. *Int. J. Cancer* **2019**, doi: 10.1002/ijc.32190

(8) Wang, Z.; Cui, B.; Zhang, F.; Yang, Y.; Shen, X.; Li, Z.; Zhao, W.; Zhang, Y.; Deng, K.; Rong, Z. Development of a Correlative Strategy to Discover Colorectal Tumor Tissue Derived Metabolite Biomarkers in Plasma Using Untargeted Metabolomics. *Anal. Chem.* **2019**, *91*, 2401-2408.

(9) Schofield, Z.; Reed, M. A. C.; Newsome, P. N.; Adams, D. H.; Günther, U. L.; Lalor, P. F. Changes in Human Hepatic Metabolism in Steatosis and Cirrhosis. *World J. Gastroenterol.* **2017**, *23*, 2685-2695.

(10) Angulo, P. Nonalcoholic Fatty Liver Disease. *N. Engl. J. Med.* **2002**, *346*, 1221–1231.

(11) Dowman, J. K.; Tomlinson, J. W.; Newsome, P. N. Pathogenesis of Non-Alcoholic Fatty Liver Disease. *Q J Med* **2010**, *103*, 71–83.

(12) Kleiner, D. E.; Brunt, E. M.; Van Natta, M.; Behling, C.; Contos, M. J.; Cummings, O. W.; Ferrell, L. D.; Liu, Y. C.; Torbenson, M. S.; Unalp-Arida, A.; et al. Design and Validation of a Histological Scoring System for Nonalcoholic Fatty Liver Disease. *Hepatology* **2005**, *41*, 1313–1321.

(13) Skelly, L. E.; Gibala, M. J. Skeletal Muscle Mitochondrial Bioeneretics in Humans: Does Sex Matter? *Exp. Physiol.* **2019**, *104*, 460–462.

(14) Scalzo, R. L.; Peltonen, G. L.; Binns, S. E.; Shankaran, M.; Giordano, G. R.; Hartley, D. A.; Klochak, A. L.; Lonac, M. C.; Paris, H. L. R.; Szallar, S. E.; Greater Muscle Protein Synthesis and Mitochondrial Biogenesis in Males Compared with Females during Sprint Interval Training. *FASEB J.* **2014**, *28*, 2705-2714.

(15) Cardinale, D. A.; Larsen, F. J.; Schiffer, T. A.; Morales-Alamo, D.; Ekblom, B.; Calbet, J. A. L.; Holmberg, H. C.; Boushel, R. Superior Intrinsic Mitochondrial Respiration in Women than in Men. *Front. Physiol.* **2018**, *9*, 1133

(16) Carr, A. J.; Hopkins, W. G.; Gore, C. J.; Carr, A.J., Hopkins, W.G., Gore, C. J. Effects of Acute Alkalosis and Acidosis on Performance: A Meta-Analysis. *Sport. Med.* **2011**, *41*, 801–814.

(17) Dunn, W. B.; Brown, M.; Worton, S. A.; Davies, K.; Jones, R. L.; Kell, D. B.; Heazell, A. E. P. P. The Metabolome of Human Placental Tissue: Investigation of First Trimester Tissue and Changes Related to Preeclampsia in Late Pregnancy. *Metabolomics* **2012**, *8*, 579–597.

(18) Chi, Y.; Pei, L.; Chen, G.; Song, X.; Zhao, A.; Chen, T.; Su, M.; Zhang, Y.; Liu, J.; Ren, A. Metabonomic Profiling of Human Placentas Reveals Different Metabolic Patterns among Subtypes of Neural Tube Defects. *J. Proteome Res.* **2014**, *13*, 934-945.

(19) Mumme, K.; Gray, C.; Reynolds, C. M.; Vickers, M. H.; Harrison, C. J.; Stanley, J. L.; Ruggiero, K.; Villas-Bôas, S. G.; Baker, P. N.; Sulek, K. Maternal-Fetal Hepatic and Placental Metabolome Profiles Are Associated with Reduced Fetal Growth in a Rat Model of Maternal Obesity. *Metabolomics* **2016**, *12*, 83.